Latvijas Universitātes Cietvielu Fizikas Institūts

Dr. Phys. Uldis Rogulis

DEFEKTU ELEKTRONISKĀS STRUKTŪRAS NOTEIKŠANA AR EPR OPTISKĀS DETEKCIJAS METODĒM IZOLATORU MATERIĀLOS

Kopsavilkums par darbu ciklu habilitācijai cietvielu fizikā

Rīga 1999

SATURS

IEVADS

Defektu un procesu pētījumos svarīga problēma ir defektu centru optisko īpašību korelācija ar struktūras pētījumu metožu datiem. Tradicionāli defektu struktūru pēta galvenokārt ar elektronu paramagnētiskās rezonanses (EPR) metodēm un optiskās īpašības, praktiski nesaistīti, ar optiskām (absorbcijas, luminescences) metodēm. Šo korelāciju problēmu tieši vislabākajā veidā izdodās risināt ar optiski detektējamās elektronu paramagnētiskās rezonanses (OD EPR) metožu palīdzību [1*-7*].

Darbā OD EPR metodikas attīstītas Latvijā, Latvijas Universitātes Cietvielu fizikas institūtā un no 1988. gada sākti OD EPR pētījumi. Izveidojās ļoti laba sadarbība ar Paderbornas Universitātes Fizikas fakultāti, Prof. Dr. J.-M. Špēta laboratoriju (Vācija), liela daļa no pētījumiem veikta šīs sadarbības rezultātā.

Darba koncepcija bija- zinot vai atrodot EPR defekta pamatstāvoklī, ar OD EPR mērījumiem noskaidrot defekta absorbcijas magnētiskā cirkulārā dihroisma (MCDA) un absorbcijas vai luminescences joslas; ja iespējams, tad iegūt jaunu informāciju par defektu elektronisko struktūru un enerģētiskajiem stāvokļiem. Tādejādi pētījumi veikti jaunā zinātniskajā virzienā- defektu optisko īpašību saistības ar EPR noskaidrošana ar EPR optiskās detekcijas metodēm.

Darbā ar OD EPR metodēm pētīta defektu elektroniskā un ģeometriskā struktūra.

Darba mērķis bija izpētīt defektu elektronisko struktūru ar OD EPR metožu palīdzību.

Konkrētie darba uzdevumi bija:

- noskaidrot defektu optisko (absorbcijas, luminescences) un EPR īpašību saistību, tai skaitā praktiski svarīgos rentgena atmiņas ekrānu un scintilatoru materiālos;
- noskaidrot defektu mijiedarbības procesus un fotostimulētās luminescences mehānismus rentgena atmiņas ekrānu materiālos;
- iegūt informāciju par autolokalizēto eksitonu (ALE) ierosinātajiem stāvokļiem NaBr kristālā un Li_2GeO_3 kristālā.

Pirmā pētījumu grupa attiecās uz defektu struktūras pētījumiem un tiešas korelācijas noteikšanu ar to optiskajām (absorbcijas, magnētiskā cirkulārā dihroisma) īpašībām. Noskaidrotas jaunas V_K centru MCDA joslas virknē sārmu metālu halogenīdu (SMH) kristālu, kā arī H centru MCDA spektra joslu novietojums KBr un KI kristālos. Noteikts H centru g

tenzora parametrs $g_{\perp} = 2.08$ KI kristālā. Ar OD EPR (MCDA- detektētā EPR) metodi izdalītas jaunas MCDA joslas Tl^{2+} centriem virknē SMH kristālu, pie tam jodīdu kristālos novērtēti arī EPR parametri, kuri agrāk nebija zināmi. Noskaidroti 3 dažādi ar Cd saistīti defekti un to optiskās īpašības BaF_2 scintilatora kristālā. Atrastas un izpētītas jaunas PO_4^{2-} un PO_3^{2-} radikāļu defektu absorbcijas (MCDA) joslas kalcija fosfāta stiklā sarkanajā un infrasarkanajā spektra diapazonā. Šādas joslas iespējamas arī šiem radikāļu centriem optisko gaismas vadu stiklos. Izpētīts molibdenu saturoša defekta struktūras modelis $CdWO_4$ scintilatoru kristālā, kurš pēc audzēšanas ieguvis zilganu nokrāsu.

Otrajā grupā pētīti Frenkeļa defektu pāru F un H centru mijiedarbība ar krosrelaksācijas OD EPR metodi. Šie dati ļāvuši novērtēt attālumu starp F un H centriem KBr kristālā. Ar MCDA-detektētā EPR metožu palīdzību noskaidrots fotostimulētās luminescences mehānisms un identificēts aktīvais caurumu ķērājcentrs kā Tl^{2+} centrs RbI:Tl kristālā. Ar MCDA un OD EPR pētīti ar In saistītie radiācijas defekti KBr:In kristālā. Novērots t.s. gaismassummu atjaunošanās efekts, ko neizdodas izskaidrot vienkārša F - In^{2+} defektu rekombinācijas modeļa ietvaros.

Trešā pētījumu grupa attiecās uz autolokalizēto eksitonu ierosināto stāvokļu izpēti ar OD EPR metodi. Pirmo reizi reģistrēts I tipa autolokalizētā eksitona OD EPR spektrs NaBr kristālā. Identificēti autolokalizēto eksitonu tripleta ierosinātie stāvokļi Li_2GeO_3 kristālā, noteikti sīkstruktūras mijiedarbības galveno asu virzieni un vērtības.

No darbā iegūtajiem galvenajiem rezultātiem noformulētas *Habilitācijas darba tēzes.*

Darbu cikla kopsavilkumā ir izmantoti divu veidu apzīmējumi citētai literatūrai- ar zvaigznīti un bez tās. Ar zvaigznīti apzīmētas (piem. [2*]) atsauksmes uz tiem darbiem, kuru aprakstītajos pētījumos nav piedalījies habilitācijas darba autors. Bez zvaigznītes (piem. [3]) atzīmētas atsauksmes uz tiem darbiem, kuros aprakstītajos pētījumos ir piedalījies habilitācijas darba autors. Darbu cikla kopsavilkuma beigās ir atbilstoši divi citētās literatūras saraksti.

Darbu cikla kopsavilkuma Pielikums ir atsevišķs sējums, kurā ir visu šajā kopsavilkumā citēto habilitācijas darba autora publikāciju kopijas. Publikāciju kopijas pielikumā ievietotas tādā secībā, kāda ir atsauksmes darbu cikla kopsavilkuma tekstā.

1. OPTISKI DETEKTĒJAMĀ EPR (OD EPR) METODES UN PAMATPRINCIPI

Platzonas materiālos (šeit- materiāli ar aizliegtās zonas platumu lielāku par 3 eV) izolētu defektu optiskās absorbcijas joslas pārsvarā atrodās aizliegtajā zonā (zīm. 1.a). EPR pārsvarā gadījumu tiek pētīts defekta pamatstāvoklī un sniedz daudz informāciju par defekta ģeometrisko struktūru, spinu stāvokli un simetriju. Tradicionālie optiskie- absorbcijas, luminescences pētījumi noris gandrīz nesaistīti ar EPR un saistība nospiedošā vairumā gadījumu paliek neskaidra, vai labākajā gadījumā tiek pievestas netiešas korelācijas.

EPR optiskās detekcijas metodēs mēra luminescences gaismu, vai arī izdala tās cirkulāro polarizāciju [1*] un pēta EPR ierosinātajā elektroniskajā stāvoklī. EPR optiskajā detekcijā izmanto arī absorbcijas magnētisko cirkulāro dihroismu (MCD, lai uzsvērtu absorbciju, lieto paplašinātu saīsinājumu MCDA [2*]). Optiskajai detekcijai var pielietot arī spina atkarīgo rekombināciju (tuneļluminescenci) [3*,4*]. Šīs metodes, kā arī to rezultāti ir aprakstītas pārskatos [1*-7*].

Mūsu darbā šīs EPR optiskās detekcijas metodes mēs pielietojām dažādu defektu centru EPR un optisko īpašību saistības izpētei platzonu materiālos, tai skaitā arī ar praktisko pielietojumu- fotostimulēto rentgena atmiņas ekrānu materiālu un scintilatoru materiālu defektu un procesu izpētei.

Lielā mērā šajā darbā pārsvarā pielietota MCDA- detektētā EPR metodika un šeit mēs to īsumā ilustrēsim uz t.s. "sārmu metāla atoma" modeļa [8*] piemēra, kas attēlots zīm. 1.b. Pamatstāvoklī ir s^1 elektroniskā konfigurācija ar termu $^2S_{1/2}$ un optiski ierosinātajā stāvoklī elektroniskā konfigurācija p^1 ar termiem $^2P_{1/2}$ un $^2P_{3/2}$ kas ir sašķēlušies spinorbitālās mijiedarbības dēļ. Magnētiskajā laukā, Zēmana efekta dēļ, termu elektronisko līmeņu deģenerācija tiek noņemta, zīm. 1.b parādīti attiecīgie magnētiskā momenta projekcijas m_j stāvokļi. Pārejas var būt dažādi cirkulāri polarizētas (CP), ja $\Delta m_j = \pm 1$. Tā piemēram, no pamatstāvokļa $m_j = \pm 1/2$ uz $m_j = \pm 1/2$ ierosinātajā stāvoklī var būt divas CP pārejas. Tā kā pamatstāvokļa līmeņu apdzīvotība (spinu polarizācija) atšķirās, tad pārejas ar dažādu CP ir ar dažādu intensitāti, pie tam, jo zemāka temperatūra, jo šī atšķirība ir lielāka. Platzonas materiālos, kuriem dominē jonu saite, defektu absorbcijas joslas ir platas un joslu pusplatumi ir stipri lielāki

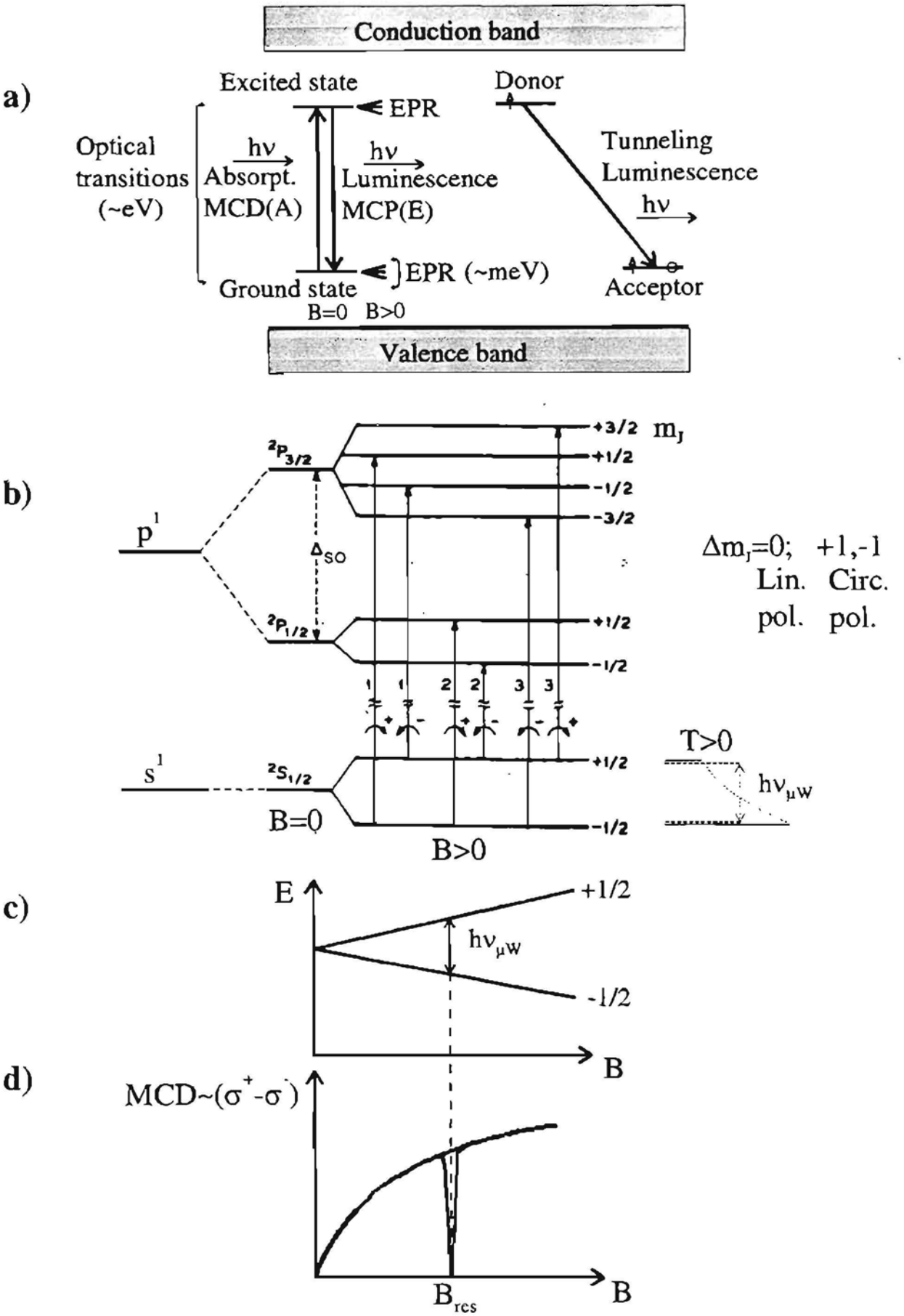

1. zīm. a) ilustrācija OD EPR metodēm;
b) OD EPR metodes principa ilustrācija uz t.s. "sārmu metāla atoma" modeļa piemēra;
c) un d) OD EPR rezonanses brīdī pamatstāvokļa līmeņu apdzīvotība tiecās izlīdzināties un MCDA efekts tiecās uz nulli.

par Zēmana sašķelšanos. Cirkulāri polarizēto pāreju intensitāšu starpība pie viena konkrēta viļņa garuma (pēc normēšanas, skat. [2*]) tiek saukta par magnētisko cirkulāro dihroismu (MCDA).

OD EPR rezonanses brīdī (zīm. 1.c) līmeņu apdzīvotības tiecās izlīdzināties un MCDA amplitūda tiecās uz nulli (teorētiski, zīm.1.d). Praktiski OD EPR efekts ir dažu vai dažu desmitu procentu līmenī. Līdzīgā veidā, rezonanses brīdī mainot spinu polarizāciju un līdz ar to arī optisko pāreju intensitāti, darbojas visi EPR optiskās detekcijas varianti. Optimāla OD EPR signāla iegūšanai tiek izmantotas zemas (4.2K līdz 1.5K) temperatūras, stipri magnētiskie lauki (līdz 6T) un augstas mikroviļņu starojuma frekvences (24GHz līdz 95GHz). Šie OD EPR metožu aparatūras aspekti labi aprakstīti pārskatos (skat., piemēram, [1*-5*]) un mēs dotajā Kopsavilkumā tos sīkāk neaplūkosim, bet turpmākajās nodaļās aplūkosim darbā iegūtos galvenos rezultātus.

2. DEFEKTU STRUKTŪRAS UN OPTISKO ĪPAŠĪBU PĒTĪJUMI

Šajā nodaļā aprakstīti pētījumu rezultāti, kuros pētīts EPR defektu pamatstāvoklī, zināma EPR gadījumā mērīts OD EPR pēc MCDA signāla izmaiņām. Vairākos gadījumos iegūti jauni dati par defektu elektronisko struktūru un optisko pāreju dabu.

2.1. V_K un H centru magnetooptisko īpašību pētījumi [1,2]

V_K centriem un H centriem SMH bija labi zināms gan EPR [9*,10*], gan optiskā absorbcija [10*,11*], taču šo spektru tieša saistība nebija noteikta ar OD EPR metodēm. V_K un H centru ģeometriskā struktūra parādīta zīm. 2 (augšā). Šīs V_K un H centru struktūras noskaidrotas ar EPR, un tās ir: viena X_2^- molekula 2 anjona mezglos (V_K centrs) un viena X_2^- molekula vienā anjona mezglā (H centrs).

Mēs mērījām MCDA KBr kristālā (un arī citos SMH kristālos ar NaCl struktūru) un tad, pēc zināmajiem šo centru EPR parametriem, meklējām V_K un H centriem atbilstošos OD EPR spektrus. Pārsvarā OD EPR spektros redz perpedikulāri pret magnētiskā lauka virzienu orientētu

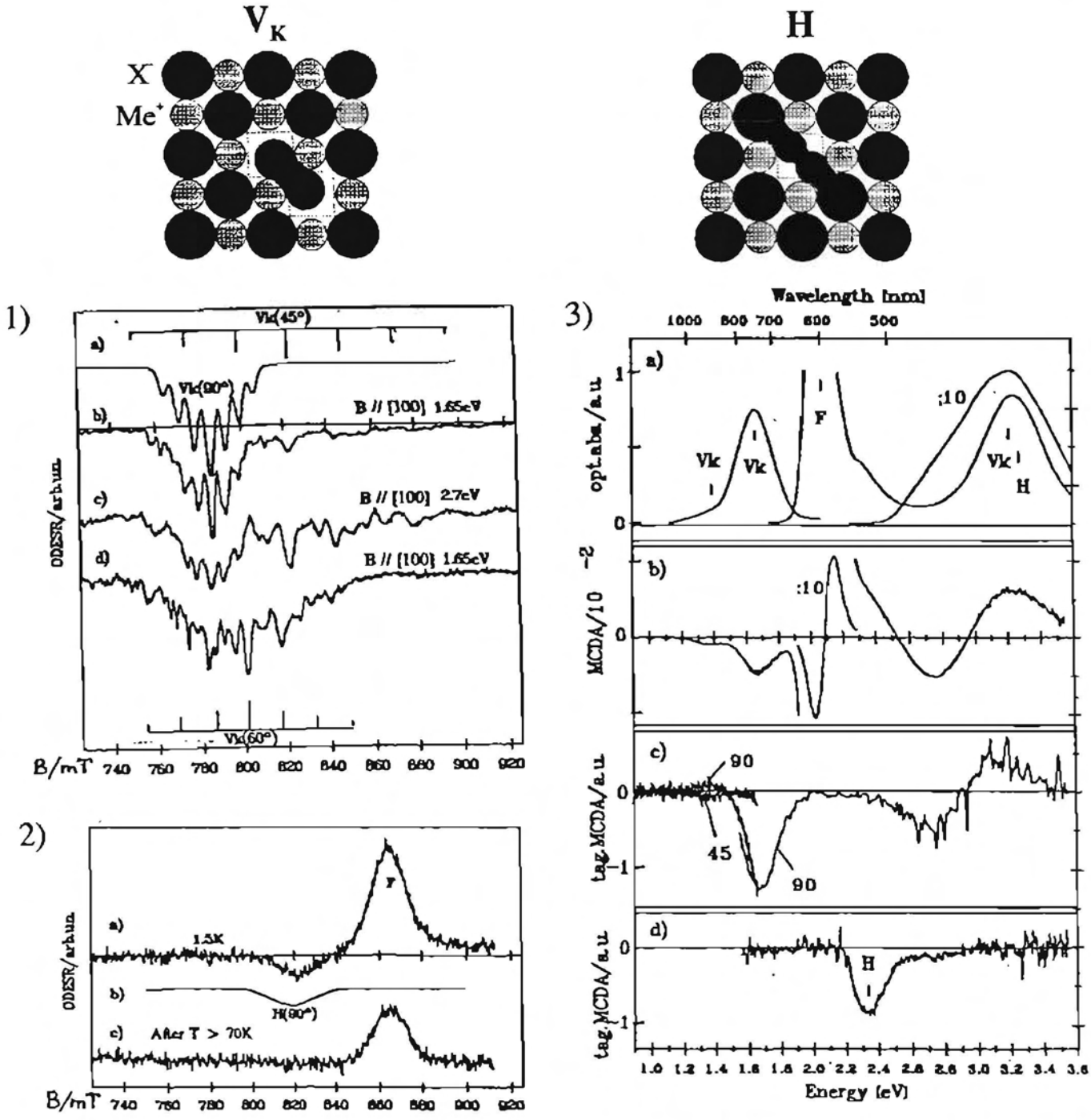

2. zīm. 1) x- apstarota KBr kristāla OD EPR spektri:

a) 90^0 V_K centru izrēķinātais spektrs;

b), c), d) OD EPR spektri divās MCDA joslās dažādi orientētiem V_K centriem [1].

2) F un H centru OD EPR spektri pie 4.2K ar x- apstarotā KBr kristālā:

a) OD EPR 2.4 eV MCDA joslā;

b) 90^0 orientētu H centru aprēķinātais spektrs;

c) OD EPR 2.4 eV MCDA joslā pēc H centru termiskās sagraušanas.

3) a) x- apstarota KBr kristāla optiskās absorbcijas dati (skat. atsauces [1]);

b) MCDA pie B=2T un T=1.5K, F, H un V_K centriem KBr kristālā pēc x- apstarošanas pie 4.2K;

c) V_K centru "tagged MCDA" spektri;

d) H centru "tagged MCDA" spektrs.

centru rezonanses līnijas [12*]. Šīs rezonanses mēs atradām KBr kristālā V_K centriem (zīm. 2.1) un KBr kristālā H centriem (zīm. 2.2)[1].

Zinot šīm rezonansēm atbilstošās magnētiskā lauka vērtības, mēs atradām OD EPR ierosmes spektrus (jeb kā tos sauc arī par "tagged MCDA" [2*,5*]) un selektīvi izdalījām no summārā MCDA spektra tikai V_K un H centriem atbilstošās MCDA joslas (zīm. 2.3). V_K centra gadījumā katrai centru orientācijai pret magnētiskā lauka virzienu ir iespējama citāda MCDA zīme.

V_K centru MCDA joslām ultravioletajā spektra diapazonā ir atvasinājuma forma un tās centrs nevienā SMH nesakrīt ar zināmo $^2\Sigma_u^+ \leftrightarrow {}^2\Sigma_g^+$ absorbcijas joslu (zīm. 3.1 [2]). Lai izskaidrotu šīs V_K centru UV MCDA joslas, tika ņemts vērā, ka X_2^- molekulārajā modelī $^2\Sigma_u^+ \leftrightarrow {}^2\Pi_u$ pāreja ir pēc grupu teorijas aizliegta. Teorētiskā analīze [2] rādīja, ka ja V_K centru uzskata par dinamisku sistēmu, kas reāli var būt asimetriska (necentrāla) tad simetrija pazeminās līdz C_{2v} un tad pēc grupu teorijas reāli šīs pārejas kļūst daļēji atļautas (zīm. 3.2). Šāda hipotēze bija izteikta jau darbā [11*], lai izskaidrotu V_K centru papildus absorbcijas joslu KI kristālā. Optiskās absorbcijas spektros šīs pārejas parādās varbūt tikai pleca veidā blakus intensīvajai $^2\Sigma_u^+ \leftrightarrow {}^2\Sigma_g^+$ absorbcijas joslai, bet MCDA spektros ir vienas no galvenajām novērojamajām V_K centru pārejām.

Noteiktos V_K centru un H centru MCDA spektrus un OD EPR rezonanses mēs izmantojām F un H centru krosrelaksācijas procesu pētījumos (nodaļa 3.1) un procesu fotostimulējamajos rentgena atmiņas ekrānu materiālos pētījumos ar magnetooptiskājām metodēm (nodaļa 3.2).

2.2. Tl^{2+} caurumu ķērājcentru centru magnetooptiskās īpašības SMH kristālos [3-5]

Tl^{2+} aktivatora caurumu centri (uz Tl^+ piejaukuma saķerts caurums) var spēlēt būtisku lomu ar Tl aktivētos fotostimulējamos rentgena atmiņas ekrānos [13*,14*]. Šajos fotostimulējamos atmiņas ekrānos notiekošos procesus ir perspektīvi un informatīvi pētīt ar MCDA metodēm.

Tl^{2+} centru EPR vairākos SMH kristālos bija zināms [15*,16*]. Mēs ar OD EPR metodi atradām zināmajos gadījumos Tl^{2+} centriem atbilstošās EPR rezonanses (zīm. 4.a). Arī jodīdos mēs atradām Tl^{2+} centru OD EPR rezonanses, kaut gan šeit Tl^{2+} EPR *spinhamiltoniāna* parametri nebija no literatūras zināmi. Mēs šos EPR parametrus (g faktoru un Tl hipersīkstruktūras

1)

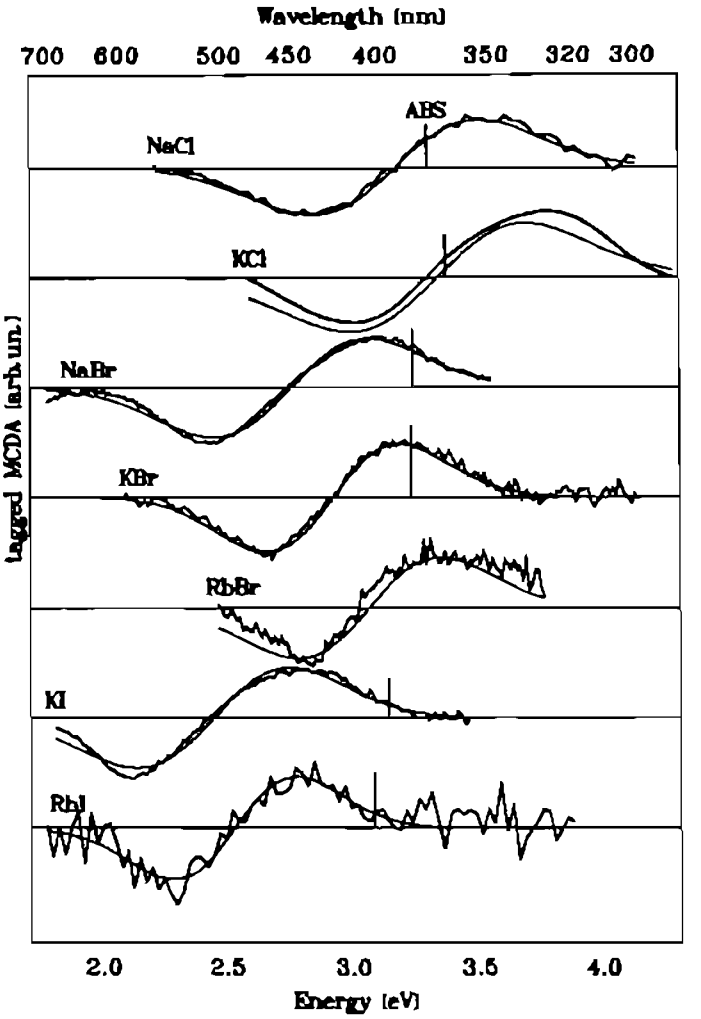

2)

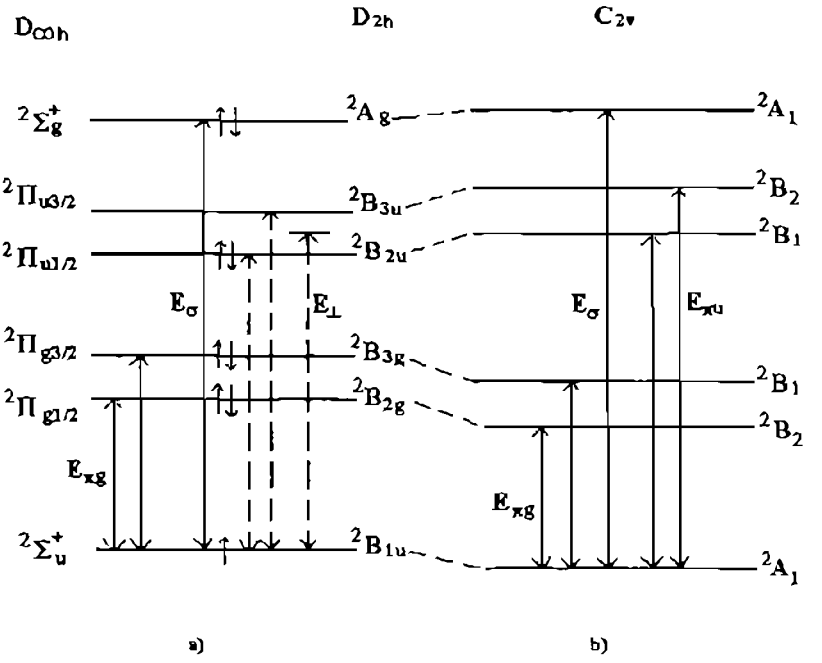

3. zīm. 1) V_K centru UV pāreju "tagged MCDA" spektri septiņos SMH kristālos. Atzīmēts UV absorbcijas joslu novietojums.

2) Enerģijas līmeņu izmaiņu shematisks attēlojums X_2^- molekulārajā modelī, ko var radīt V_K centra lēna aksiāla oscilācija [2]:
a) "on- centre" X_2^- (D_{2h});
b) "off- centre" X_2^- (C_{2v}).

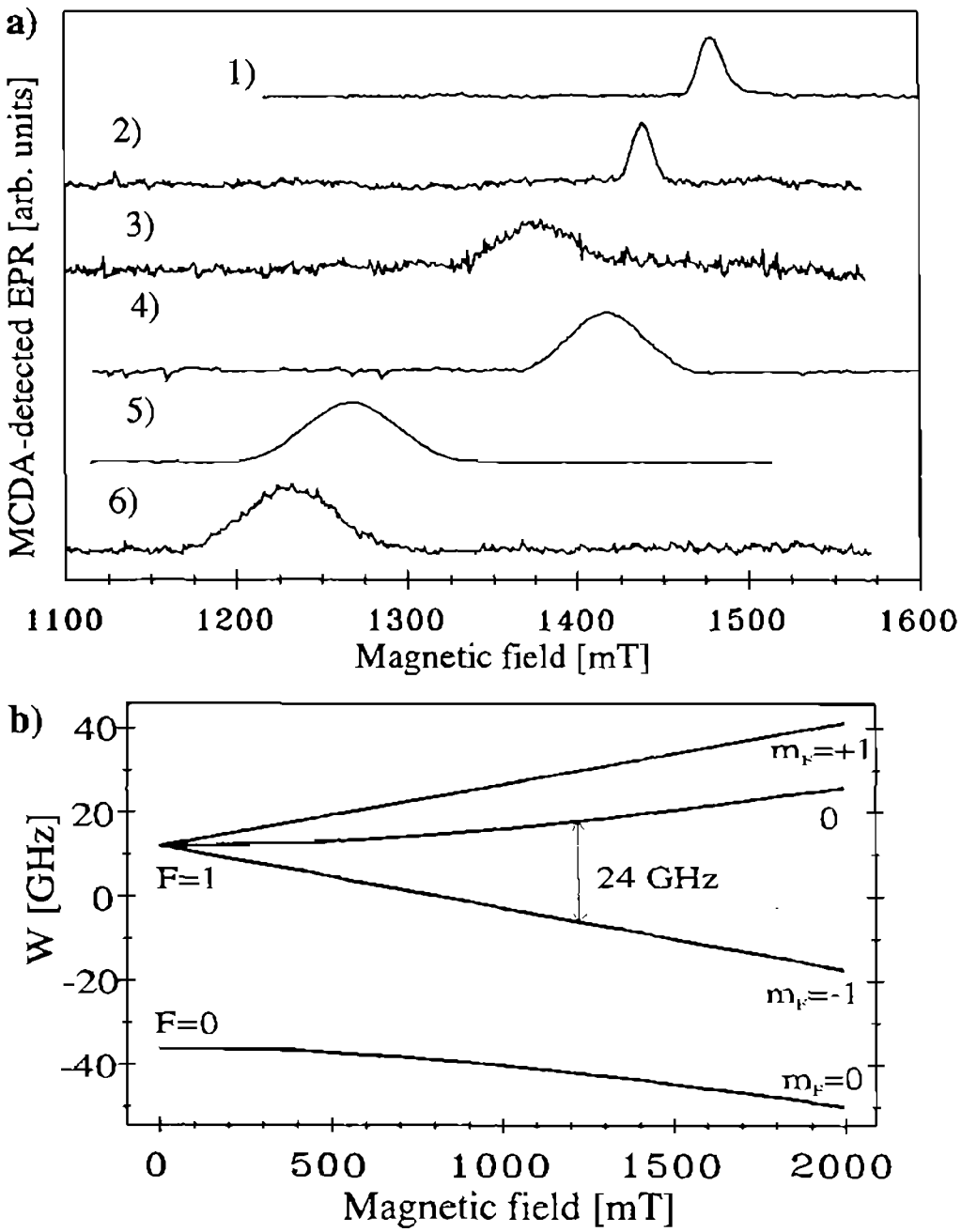

4. zīm. a) Tl^{2+} centru MCDA- detektētā EPR spektri sešos SMH kristālos. T=1.5K un B ll [100]. Mikroviļņu diapazons 24 GHz [3].

b) Breita- Rabi enerģijas līmeņu diagramma Tl^{2+} centriem RbI:Tl kristālā [3].

mijiedarbības konstanti A) novērtējām, kaut gan abi parametri nevarēja sākotnēji tikt viennozīmīgi noteikti, jo novērojama bija tikai viena rezonanses līnija. Uzzinot precīzi vienu no šiem parametriem, vai arī novērojot vēl kādu papildus rezonanses līniju, EPR parametri jodīdu kristāliem varētu tikt koriģēti. Tl^{2+} centriem ir ļoti liela s^1 elektrona hipersīkstruktūras (*hss*) mijiedarbība ar Tl kodola spina magnētisko momentu. OD EPR pārejas Tl^{2+} centru elektroniskajā pamatstāvoklī attēlotas zīm. 4.b, t.s. Breita- Rabi shēmā, parādīta pāreja $|0> \leftrightarrow |1>$, kuru mēs novērojām 24 GHz mikroviļņu diapazonā.

Zinot šīs OD EPR rezonanses, mēs selektīvi izdalījām no visa MCDA spektra tās MCDA joslas, kuras atbilst tieši Tl^{2+} centriem virknē SMH kristālu, un tās ir parādītas zīmējumā 5.a. Daudzas no šīm joslām agrāk absorbcijas mērījumos nebija novērotas, vai arī to korelācija ar Tl^{2+} centriem bija atzīmēta ar jautājuma zīmi.

Tl^{2+} centriem atbilstošo MCDA joslu ir vairāk (jodīdos pavisam 7 joslas), nekā tas bija aplūkots līdz šim literatūrā aplūkotajā modelī $[TlX_6]$ kompleksam. Lielo joslu daudzumu mēs izskaidrojām [3,4] ar lādiņa pārneses joslu $t_{1u} \leftrightarrow a_{1g}$ spinorbitālo sašķelšanos (zīm. 5.b). Tas izskaidroja 6 no 7 novērojamajām MCDA joslām. Vienas MCDA joslas izskaidrošanai bija nepieciešams atrast kādas papildus pārejas, to arī spāņu kolēģi [4] izskaidroja $[TlX_6]$ modeļa ietvaros kā pāreju no t_{2u} - līmeņa, kura var būt daļēji atļauta.

Šīs zināšanas par Tl^{2+} centru MCDA joslām mēs izmantojām nodaļā 3.2, lai izpētītu fotostimulētās luminescences mehānismu rentgena atmiņas ekrāna materiālā RbI:Tl [16].

2.3. Trīs ar Cd piejaukumu saistītu defektu optiskās īpašības BaF_2 scintilatoru kristālā [6,7]

Cd piejaukums BaF_2 kristālos var tikt ievadīts, lai cīnītos ar skābekļa nekontrolējamo piejaukumu kristāla audzēšanas procesā.

Cd_c^+ centri regulārā režģa katjona mezglā bija jau zināmi no EPR pētījumiem literatūrā [19*], to EPR spektrs γ- apstarotam BaF_2 kristālam (I tips, skat. [6]), salīdzinājumam, attēlots zīmējumā 6.b. Mēs BaF_2 kristālos novērojām vēl vienu EPR spektru [6], kurš ir parādīts zīm. 6.a. To mēs interpretējam kā perturbētu Cd_c^+ centru, kaut gan perturbācijas daba mums paliek

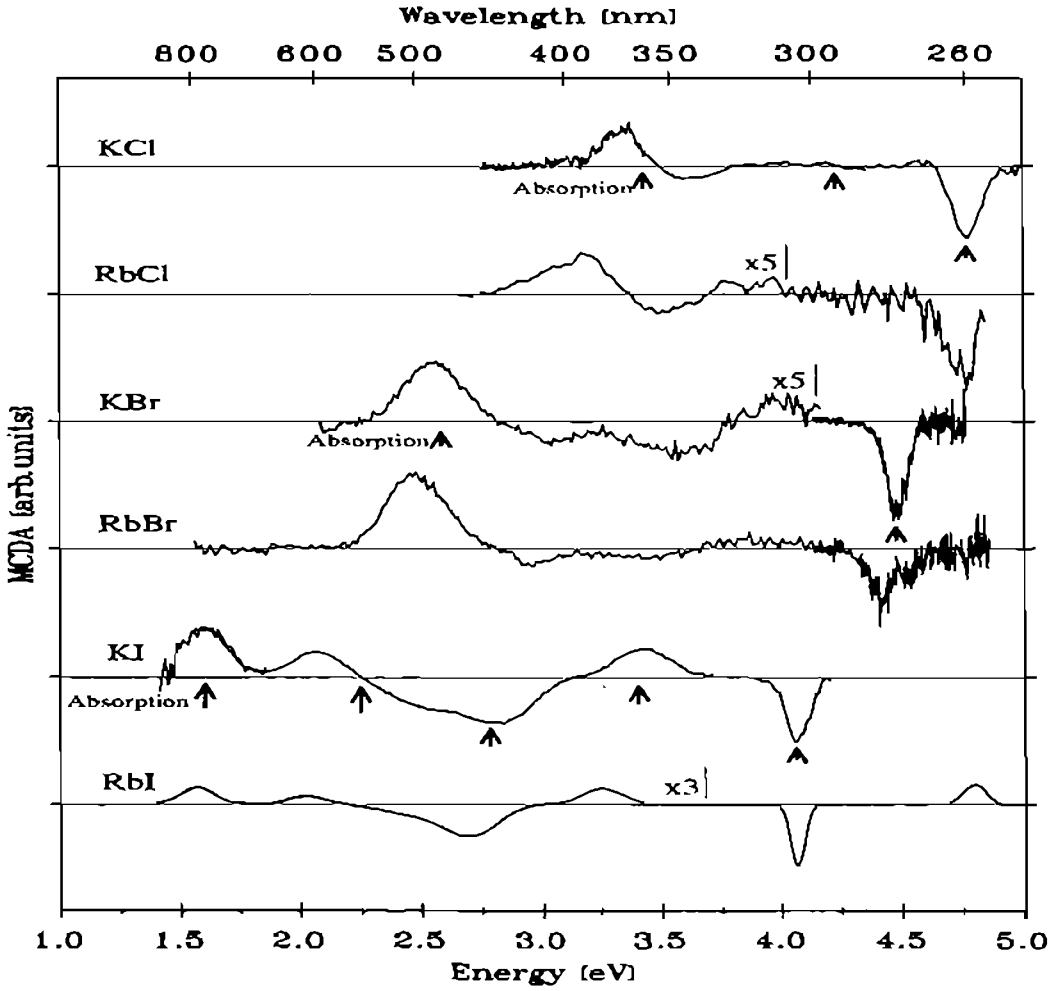

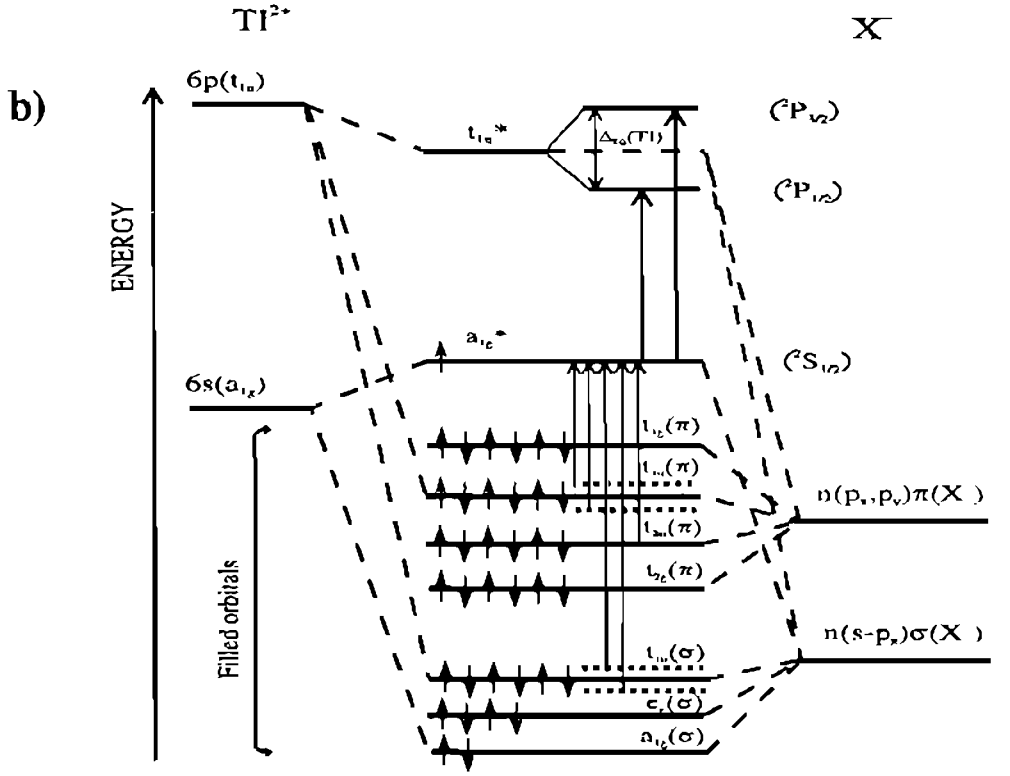

5. zīm. a) Tl^{2+} centru "tagged MCDA" spektri sešos SMH kristālos [3].

b) kvalitatīva [TlX_6] oktaedrāla kompleksa enerģijas līmeņu shēma (pēc [17*,18*,3,4]).

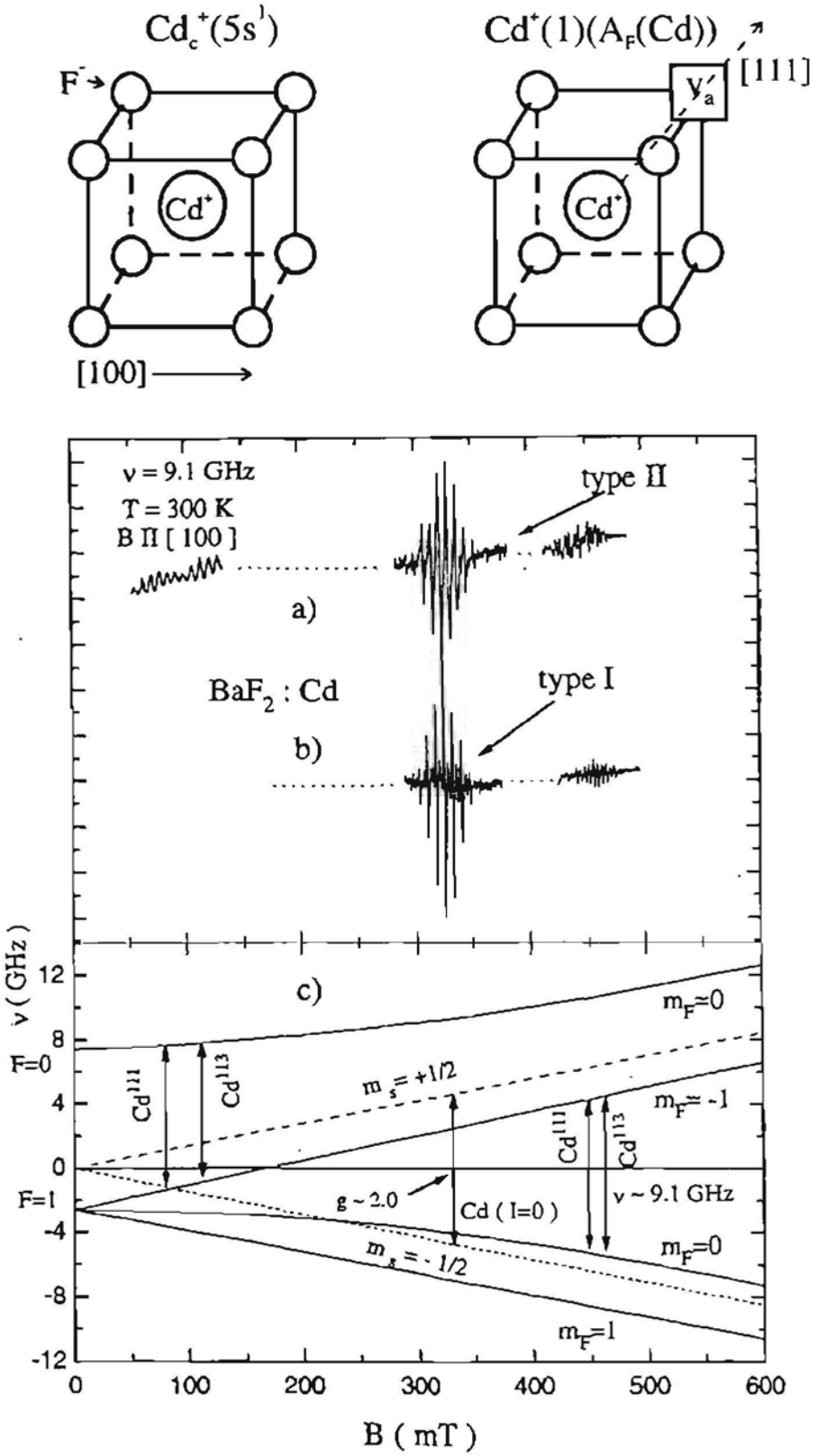

6. zīm. Cd centru struktūras modeļi BaF_2 kristālā.

a) II tipa BaF_2:Cd kristāla EPR spektrs 9 GHz mikroviļņu diapazonā;

b) salīdzinājumam- literatūrā [19*] zināmā Cd_c^+ centra EPR spektrs;

c) II tipa parauga EPR spektram atbilstošā Breita- Rabi enerģijas līmeņu diagramma.

nezināma. Šim perturbētajam Cd_c^+ centram hipersīkstruktūras mijiedarbība nesapārotā s^1 elektrona spinam (S=1/2) ar Cd kodola spinu I=1/2 (diviem Cd izotopiem) ir mazāka nekā neperturbētajam Cd_c^+ centram. Tādēļ 3cm (9 GHz) mikroviļņu diapazona EPR spektros var novērot arī līniju grupu zemos magnētiskajos laukos (zīm. 6.a). Atbilstošās EPR pārejas ir attēlotas zīm. 6.c, Breita- Rabi enerģijas līmeņu diagrammā.

Pēc MCDA signāla optiski detektētā EPR spektri γ- apstarotos BaF_2 kristālos attēloti zīm. 7.1. Cd_c^+ centram OD EPR spektros ir novērojama lielāka *hss* sašķelšanās mijiedarbībā ar Cd kodola spina magnētisko momentu (zīm. 7.1, līkne a). Perturbētajam Cd_c^+ centram ir mazāka *hss* sašķelšanās vērtība (zīm. 7.1, līknes b). Zīm 7.2 parādīts kopējais BaF_2 kristāla inducētās absorbcijas spektrs, kā arī MCDA spektri dažādajiem ar Cd piejaukumu saistītajiem defektiem [6,7]. A_F(Cd) centra (skat. zīm. 6, augšā) MCDA spetra interpretēšanu mēs veicām pēc analoģijas ar darba [20*] pētījumu rezultātiem.

Tādejādi mēs, kombinējot EPR un MCDA un MCDA- detektētā EPR pētījumus, konstatējām 3 ar Cd piejaukumu saistītu defektu iespējamību ar γ– apstarotos BaF_2 scintilatoru kristālos UV spektra diapazonā. Ar optiskajiem mērījumiem vien nebija iespējams noteikt ar Cd saistīto defektu absorbcijas joslas BaF_2 kristālā, jo sevišķi tādēļ, ka pēc mūsu novērojumiem, citi nekontrolējamie piejaukumi var dot absorbcijas joslas, kuras spektrāli pārklājas ar Cd defektu joslām.

2.4. Molibdenu saturoša defekta struktūras modelis $CdWO_4$ scintilatoru kristālā [8]

$CdWO_4$ kristāli tiek plaši izmantoti kā scintilatoru materiāli. Mēs pētījām $CdWO_4$ kristālu EPR spektrus un atradām, ka paraugā, kurš pēc audzēšanas ieguvis "zilganu" nokrāsu, novērojams zīmējumā 8.a parādītais EPR spektrs. Mēs šajā spektrā novērojam *hss* sašķelšanos uz Mo piejaukuma kodola izotopiem ar spinu I=5/2. Tas viennozīmīgi pierāda, ka defekta sastāvā ietilpst Mo, kaut gan paraugos šis piejaukums speciāli ievadīts netika. Pārējās *hss* sašķelšanās bija iespējams izskaidrot kā nesapārotā elektrona spina S=1/2 mijiedarbību ar divām dažādām W kodolu grupām, aprēķinātais spektrs šajā gadījumā ir attēlots zīmējumā 8.b.

1)

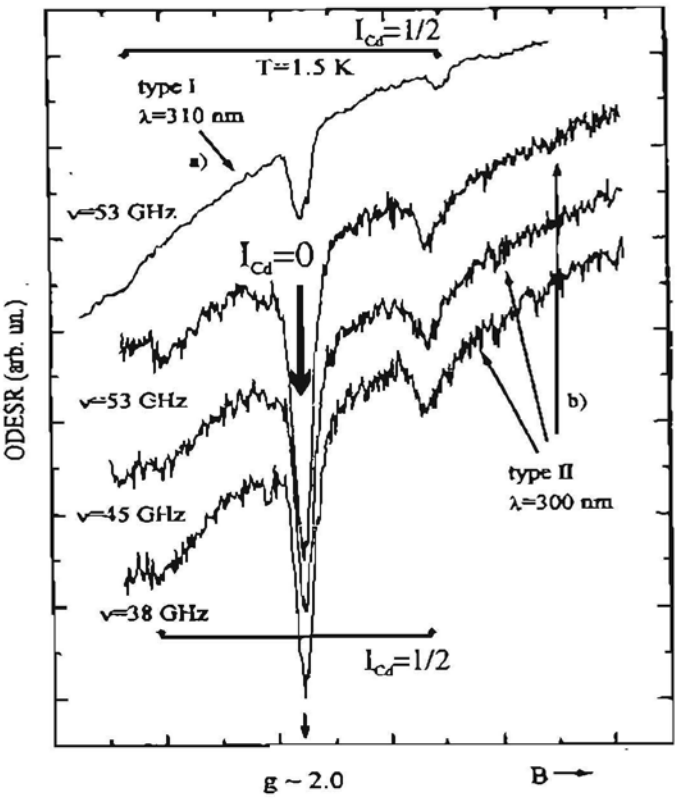

2)

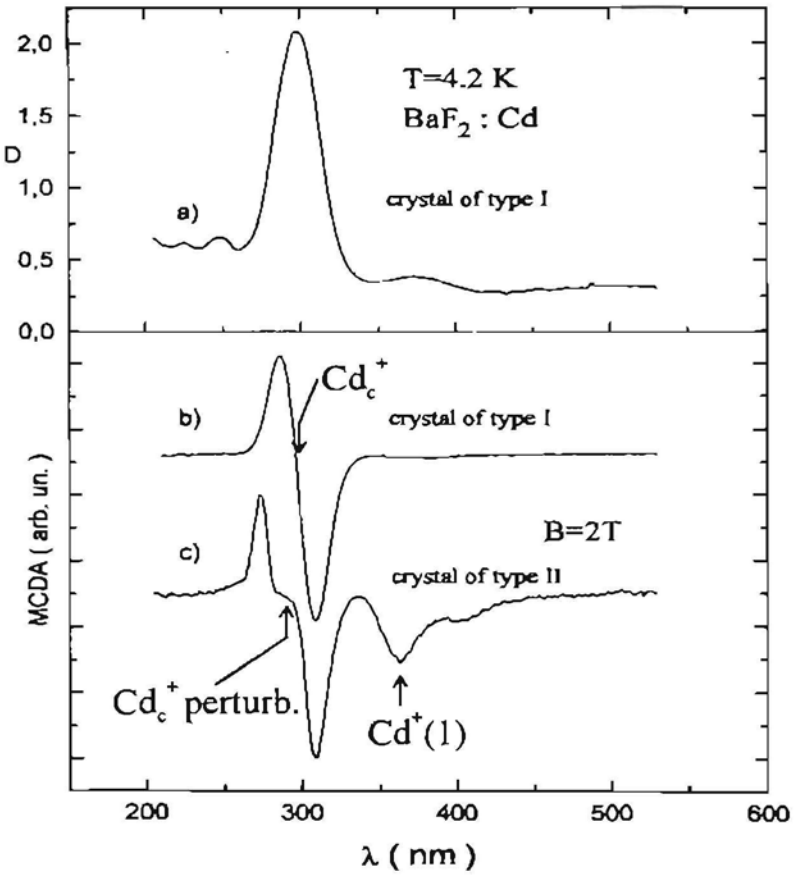

7. zīm. 1) a) I tipa BaF_2:Cd kristāla OD EPR spektrs, detektēts 310 nm MCDA joslā;
b) II tipa BaF_2:Cd kristāla OD EPR spektrs, detektēts 300 nm MCDA joslā;
2) a) γ- apstarota I tipa BaF_2:Cd (0.02 at.%) kristāla inducētās absorbcijas spektrs;
b) I tipa kristāla MCDA spektrs; c) II tipa kristāla MCDA spektrs; parādītas Cd defektiem atbilstošās MCDA joslas.

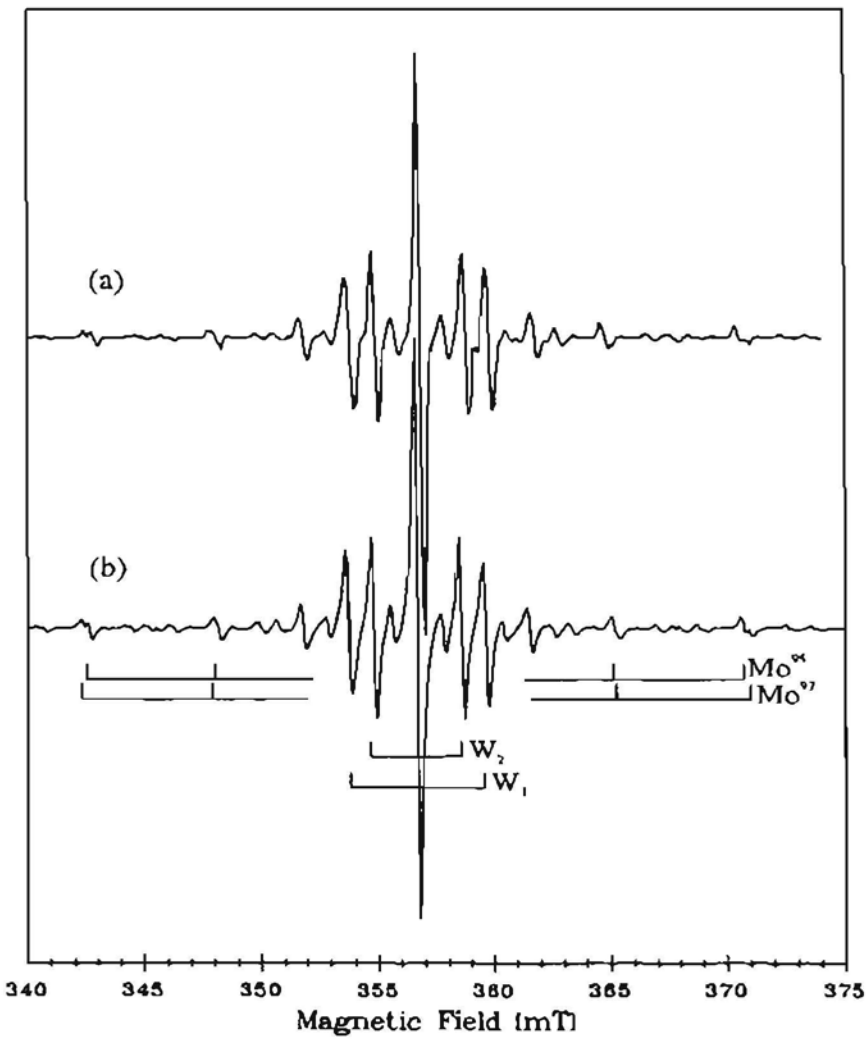

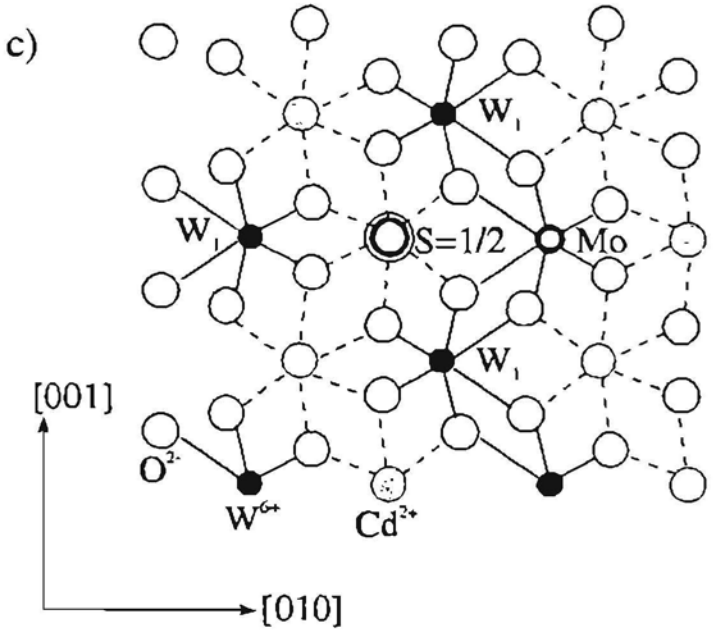

8. zīm. a) eksperimentālais $CdWO_4$ kristāla EPR spektrs, T=20K, B||[010], mikroviļņu frekvence 9.08 GHz;
b) izrēķinātais EPR spektrs [8];
c) molibdenu saturošā defekta nesapārotā spina S=1/2 iespējamais novietojums $CdWO_4$ kristāla struktūrā.

Piedāvātais molibdenu saturošā defekta struktūras modelis attēlots zīmējumā 8.c ($CdWO_4$ kristāla struktūras attēlojums pēc [21*,22*]). Tiek uzskatīts, ka molibdens aizvieto vienu no volframa kaimiņu atomiem. Nesapārotā elektrona spins ir 1/2 , un tas atrodas Cd režģa mezgla pozīcijā. Taču, tas nevar būt lokalizēts uz Cd kodola, jo nenovērojam papildus sašķelšanās uz šāda centrālā Cd kodola. Patreizējā laika momentā vēl nav izdevies šo EPR spektru tieši saistīt ar MCDA spektru vai novērot to pēc luminescences detektētajā OD EPR.

2.5. PO_4^{2-} un PO_3^{2-} defektu optisko īpašību pētījumi kalcija fosfāta stiklā [9]

Uz mūsu darba sākumu bija zināma PO_4^{2-} un PO_3^{2-} radikāļu centru veidošanās [23*-25*] ar rentgenu apstarotos fosfātu stiklos, tai skaitā kalcija fosfāta stiklā, kā arī literatūrā izvirzīti to struktūras modeļi. Bija zināmi šo radikāļu centru EPR signāli un absorbcijas josla, ar maksimumu ap 2.4 eV, bija ar netiešām korelāciju metodēm noteikta kā PO_4^{2-} centram atbilstoša absorbcijas josla [24*,25*].

Zīmējumā 9.1 parādīti pēc MCDA optiski detektētā EPR spektri, kuros norādītas gan PO_4^{2-}, gan PO_3^{2-} radikāļu centriem atbilstošās *hss* sašķelšanās [23*-25*], ko nosaka centru nesapārotā spina *hss* mijiedarbība ar P kodola spinu I = 1/2.

Zīmējumā 9.2 parādīti inducētās absorbcijas spektri (līkne a), kā arī summārais ar rentgenu apstarota kalcija fosfāta stikla MCDA spektrs (līkne b). Zinot zīmējumā 9.1 parādītajos OD EPR spektros PO_4^{2-} un PO_3^{2-} centriem atbilstošās rezonanses lauku vērtības, mēs selektīvi izdalījām to MCDA spektrus (zīm. 9, līknes c un d). Bez jau zināmās 2.4 eV joslas, kura pēc mūsu rezultātiem tiešām atbilst PO_4^{2-} radikāļiem, mēs atradām, ka šī josla daļēji atbilst arī PO_3^{2-} radikāļiem. Mēs noskaidrojām papildus, ka abiem radikāļiem ir MCDA joslas arī spektra infrasarkanajā daļā, ko jāņem vērā praktiskajos pielietojumos, ja šie radikāļu centri veidojās citos oksīdu (kvarca) optisko viļņvadu materiālos.

1)

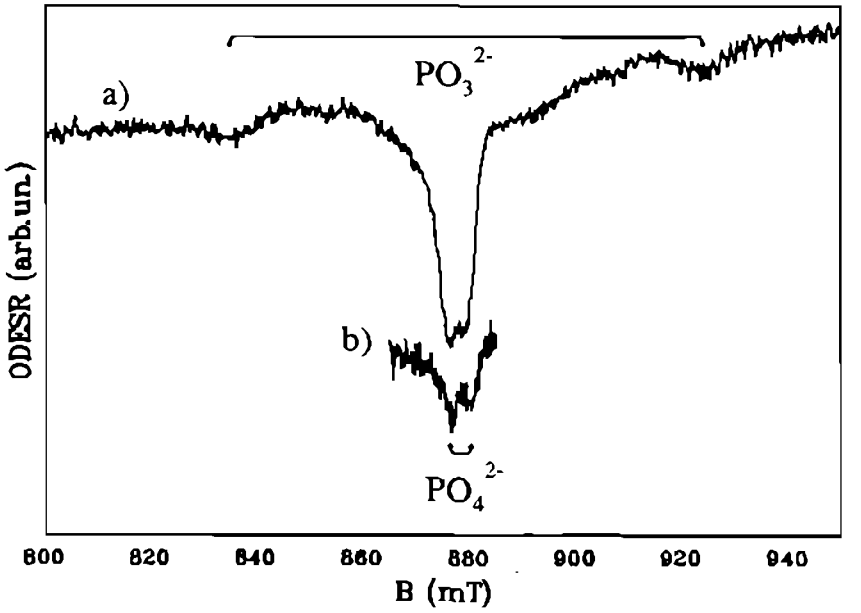

2)

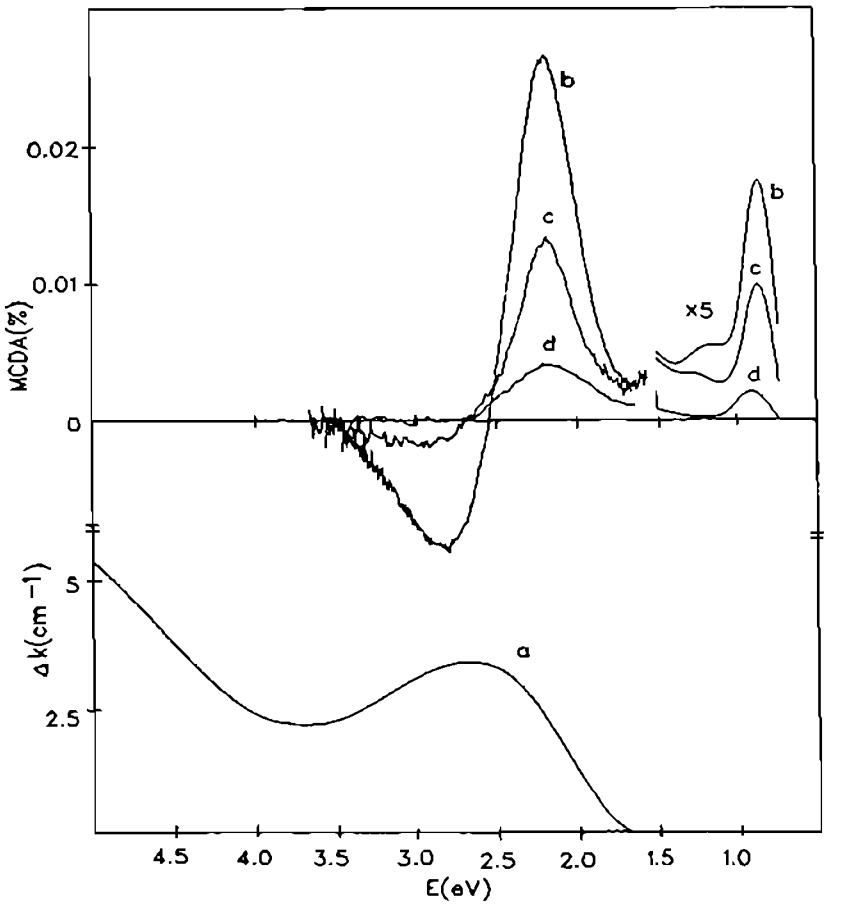

9. zīm. 1) x- apstarota $CaO-P_2O_5$ stikla OD EPR spektri, mērīti 2.2 eV MCDA joslā pie T=1.5K (līkne a) un T=4.2K (līkne b); mikroviļņu frekvence 24.1 GHz;
2) a) x- apstarota $CaO-P_2O_5$ stikla inducētās absorbcijas spektrs;
b) MCDA spektrs;
c) PO_4^{2-} centru "tagged MCDA" spektrs, mērīts pie B=875 mT, T=1.5K;
d) PO_3^{2-} centru "tagged MCDA" spektrs, mērīts pie B=835 mT.

3. DEFEKTU MIJIEDARBĪBAS PROCESU PĒTĪJUMI SMH KRISTĀLOS

Šajā nodaļā aprakstītajos pētījumos OD EPR un MCDA dati izmantoti, lai izpētītu krosrelaksācijas mijiedarbību starp F un H centriem, kā arī, lai izpētītu fotostimulētās luminescences mehānismu uz SMH fristāliem bāzētos rentgena atmiņas ekrānu materiālos.

3.1. F un H Frenkeļa defektu pāru mijiedarbības pētījumi ar krosrelaksācijas OD EPR metodi KBr kristālā [10-13]

Frenkeļa defektiem F un H ir fundamentāla nozīme defektu ģenerācijas procesos SMH kristālos (skat., piemēram, pārskatu [26*]).

Mūsu darba nodaļā 2.1 aprakstītajos pētījumos bija noteikts H centru MCDA spektrs (zīm. 2.3.d) un atbilstošais OD EPR spektrs (zīm. 2.2.a) KBr kristālā. Tādejādi, zinot F centra un H centru OD EPR un MCDA (zīm. 10.1, attiecīgi līknes (1) un (2)) spektrus, mēs varējām pētīt Frenkeļa defektu F un H mijiedarbību. Mērot MCDA F centru joslā, bet ieslēdzot un izslēdzot mikroviļņu jaudu pie magnētiskā lauka vērtībām, kas atbilst H centru pamatstāvokļa EPR vērtībām (zīm. 10.2.a) varējām novērot F centru MCDA amplitūdas izmaiņas. Tas nozīmē, ka šajā eksperimentā, izmaiņas H centra pamatstāvokļa spinu polarizācijā spēja izsaukt izmaiņas F centra spinu līmeņu apdzīvotībā, t.s. krosrelaksācijas mijiedarbības rezultātā. Krosrelaksācijas efekta lielums atkarībā no rezonanses magnētiskā lauka vērtībām attēlots zīm. 11.1, bet atbilstošā enerģijas līmeņu shēma- zīm. 11.2.

Tādejādi mūsu eksperimentos konstatēts, ka F un H centru spinu sistēmas KBr kristālā pēc rentgenapstarošanas zemās temperatūrās (4.2 K) ir saistītas un iespējams arī novērtēt attālumu kādā F un H centriem jāatrodas, lai būtu iespējama krosrelaksācijas mijiedarbība [10-13].

1)

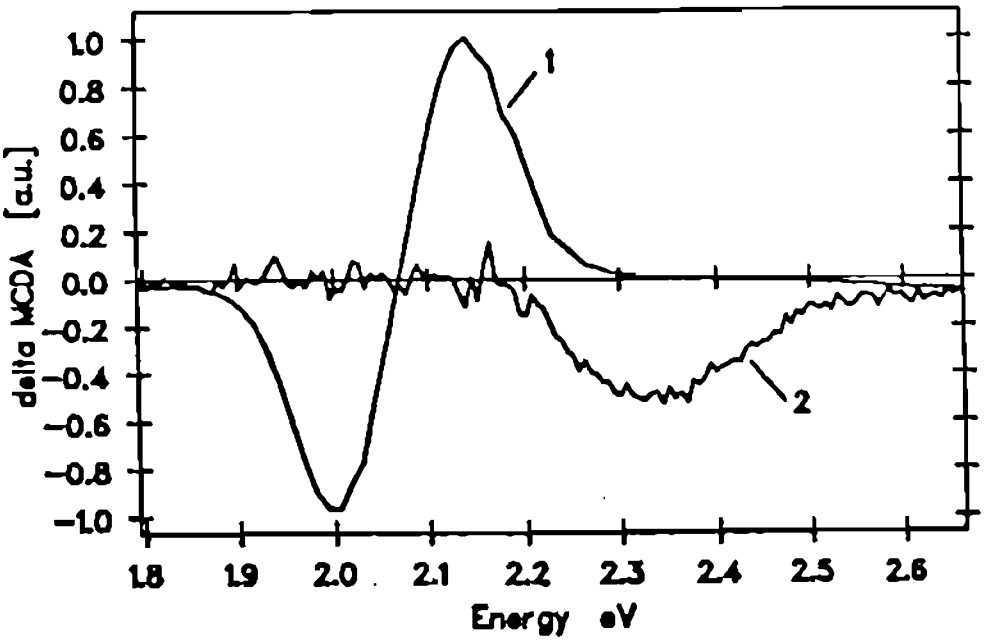

2)

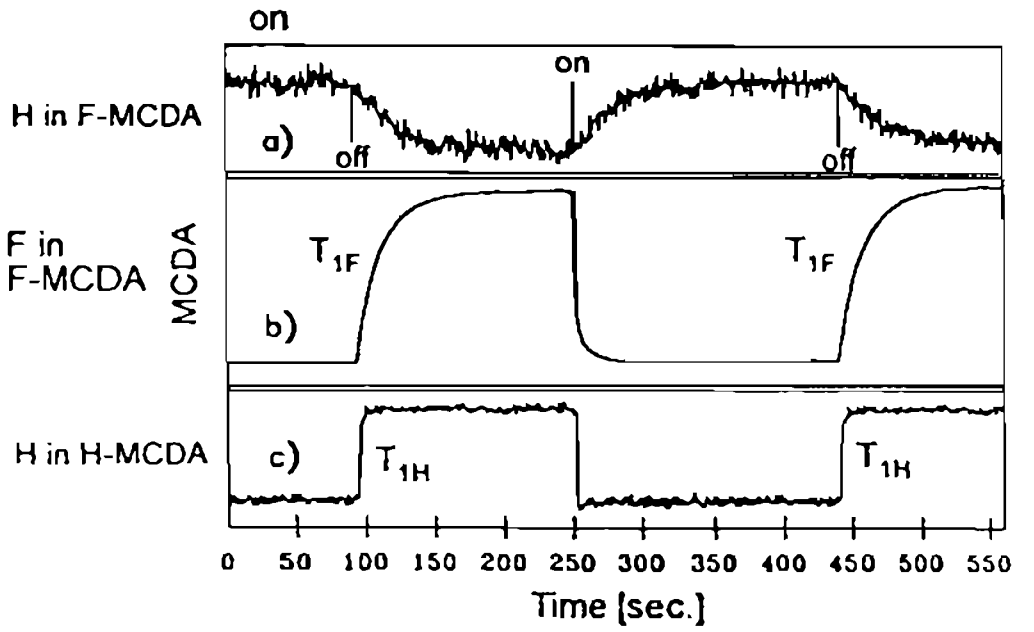

10. zīm. 1) pie 4.2K x- apstarota KBr kristāla F centru (1) un H centru (2) "tagged MCDA" spektri;
2) OD EPR efektu kinētika, ieslēdzot un izslēdzot mikroviļņu starojumu:
a) F centru MCDA joslas kinētika, inducējot H centru EPR (krosrelaksācijas efekts);
b) F centru MCDA joslas kinētika, inducējot F centru EPR;
c) H centru MCDA joslas kinētika, inducējot H centru EPR.

1)

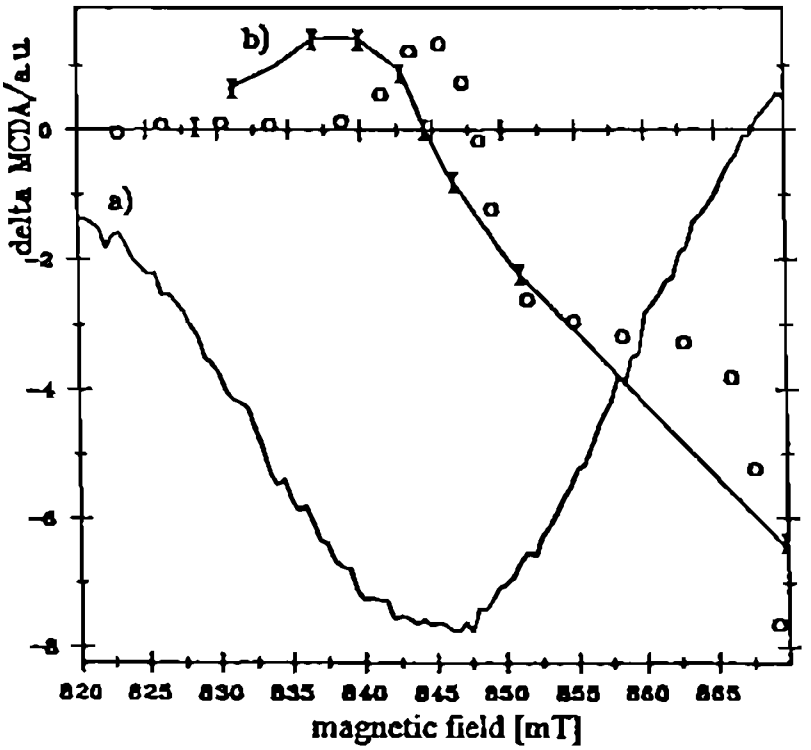

2)

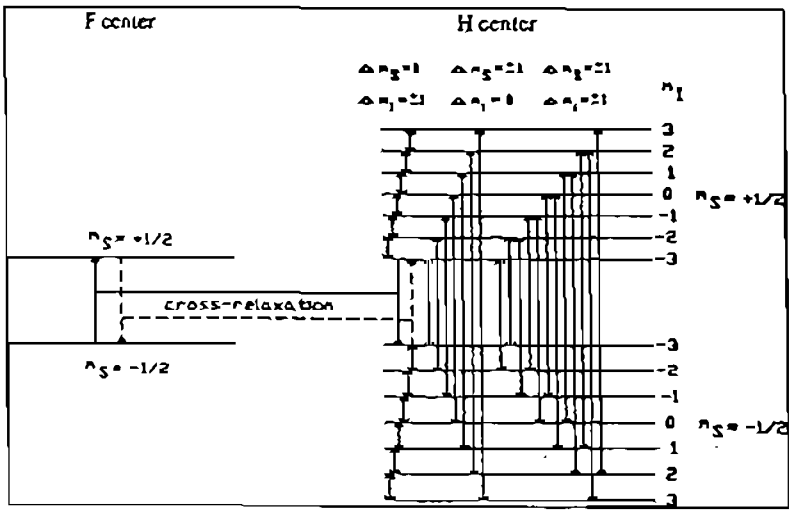

11. zīm. 1) F un H centru krosrelaksācijas efekts KBr kristālā:
a) H centru OD EPR spektrs KBr;
b) I- izmērītais krosrelaksācijas efekts F centru MCDA joslā;
o- aprēķinātais krosrelaksācijas efekta spektrs [10];
2) enerģijas līmeņu shēma F un H centru krosrelaksācijai KBr kristālā [10].

3.2. Caurumu ķērājcentru identifikācija un fotostimulētās luminescences mehānisma izpēte RbI-Tl kristālā [14]

Lai izpētītu ķērājcentru dabu un fotostimulētās luminescences (FSL) mehānismu rentgena atmiņas ekrānu materiālos, nepieciešams identificēt un sekot elektronu un, jo sevišķi, caurumu ķērājcentru uzvedībai ar iespējami tiešām metodēm. Pētījumos ļoti noderīgas izrādījās magnetooptiskās (MCDA un OD EPR) metodes.

Uz mūsu darba sākuma periodu, literatūrā bija izteikta hipotēze, ka RbI:Tl kristālā FSL aktīvais caurumu ķērājcentrs varētu būt V_{KA}, t.i. pie Tl^+ piejaukuma saķerts V_K centrs [27*]. Mūsu mērījumos ar ar MCDA un OD EPR metodēm, bez jau agrāk literatūrā identificētajām F centra pārejām (skat. [8*]), varējām identificēt arī Tl^{2+} centru MCDA un OD EPR spektrus (skat. nodaļu 2.2). F un Tl^{2+} centru MCDA- detektētā EPR spektri parādīti zīmējumā 12.1 un attiecīgie MCDA spektri attēloti zīmējumā 12.2.

Zinot visu defektu šo centru MCDA joslas, mēs sekojām centru MCDA amplitūdu izmaiņām pēc rentgenizācijas zemās temperatūrās (T= 4.2K-80K). Novērojām caurumu centru V_K dominējošu rašanos, kā arī redzējām, kā pēc V_K centru termiskās delokalizācijas notiek caurumu pārlāde uz Tl^{2+} centriem (zīm. 12.3.a). Netika konstatēta caurumu saķeršana par V_{KA}, kā bija teikts literatūrā izteiktajā hipotēzē [27*]. Papildus mēs konstatējām, ka gaismojot ar monohromatisku gaismu jebkurā no Tl^{2+} absorbcijas joslām, izdodas caurumus no Tl^{2+} centriem daļēji pārlādēt atpakaļ par V_K centriem (zīm 12.3.b). Pēc atkārtotas parauga uzsildīšanas virs V_K centru delokalizācijas temperatūras, varējām atkal caurumu pārlādēt uz Tl^+ aktivatora, veidojot Tl^{2+} centru, t.i. reakcija ir atgriezeniska: $V_K \leftrightarrow Tl^{2+}$. Šādi MCDA metodes mums atļāva tieši un selektīvi sekot caurumu centru lokalizācijai, ko RbI:Tl kristālā ar absorbcijas metodēm precīzi un selektīvi būtu grūti izdarīt.

MCDA un OD EPR mērījumu rezultātā, kombinācijā ar EPR un luminescences mērījumiem, mums izdevās konstatēt FSL intensitātes tiešu korelāciju ar Tl^{2+} centru MCDA amplitūdu, un noteikt, ka RbI:Tl kristāla fotostimulētajā luminescencē darbojas vienkāršais F* --- Tl^{2+} centru pāru modelis [14].

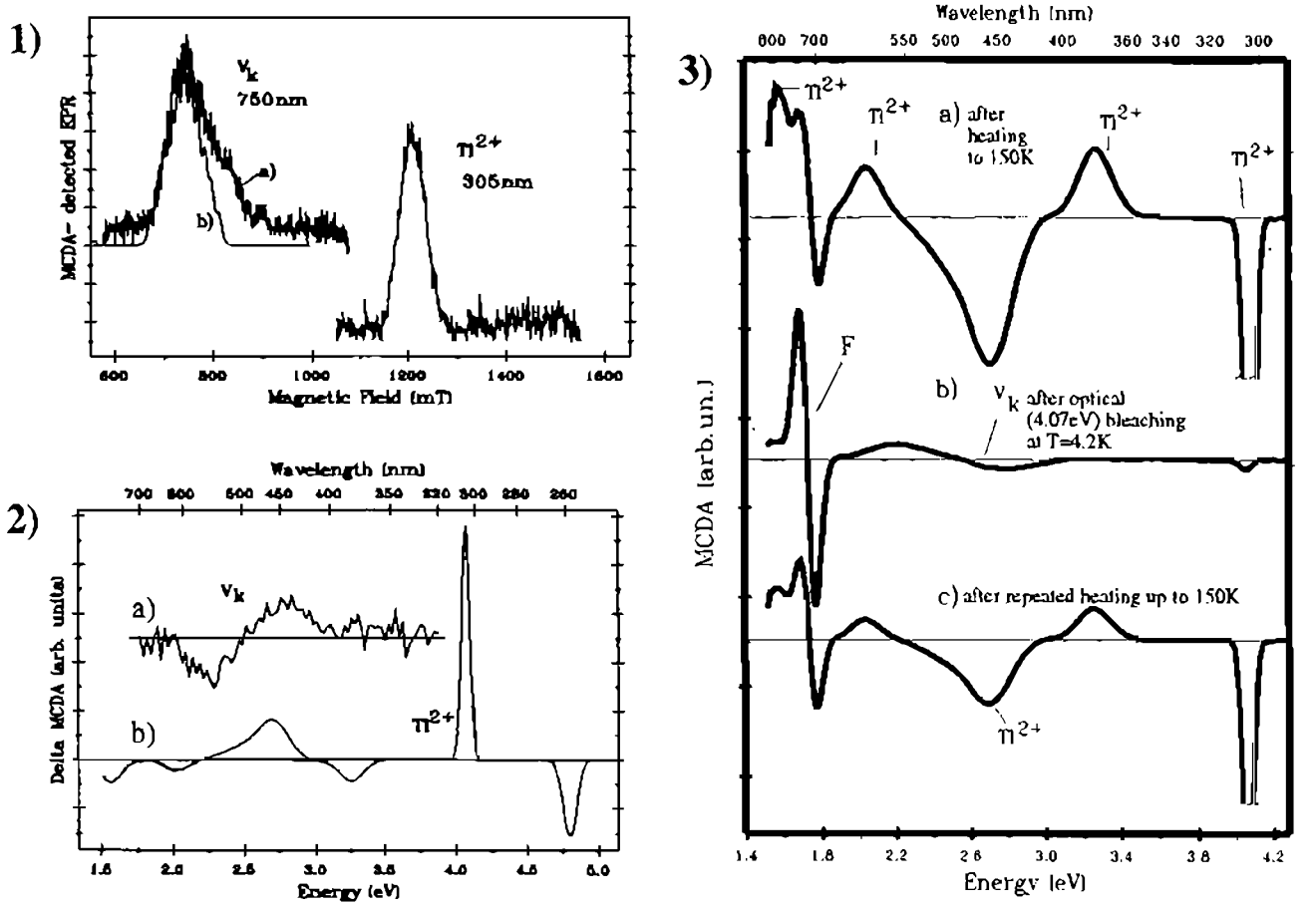

12. zīm. 1) MCDA- detektētā EPR spektri RbI:Tl kristālā:

a) V_K centriem, mērīts pie 1.56 eV;

b) Tl^{2+} centriem, mērīts 4.07 eV MCDA joslā;

2) V_K centru (a) un Tl^{2+} centru (b) "tagged MCDA" spektri RbI:Tl kristālā;

3) RbI:Tl kristāla MCDA spektri pēc x- apstarošanas pie 80K, mērīti pie 4.2K:

a) pēc izkarsēšanas līdz 150K;

b) pēc optiskās (4.07 eV) gaismošanas pie T=4.2K;

c) pēc atkārtotas karsēšanas līdz 150K.

Literatūrā bija aprakstīts viedoklis, ka KBr:In kristāla FSL izskaidrojama ar vienkāršo F* --- In^{2+} centru pāru modeli [28*]. Tomēr, mūsu OD EPR mērījumos novērotais In^{2+} centrs FSL nepiedalījās [15-17]. Otrkārt, mēs novērojām t.s. FSL "gaismassummu atjaunošanās" efektu, kuru nebija iespējams izskaidrot ar vienkāršo defektu pāru modeli [16]. RbBr:Ga kristāla jaunākajos pētījumos, tika konstatēta divu Ga^{2+} tipa caurumu ķērājcentru eksistence, no kuriem viens korelē ar FSL intensitāti, bet otrs nē [18].

Pētījumu rezultāti parāda, ka identificējot defektus ar OD EPR un MCDA metodēm, iespējams sekot defektiem un procesiem atmiņas ekrānu materiālos. Šādu informāciju iegūt, izmantojot tikai absorbcijas metodes un luminescences metodes, nebija iespējams.

4. AUTOLOKALIZĒTO EKSITONU OPTISKI DETEKTĒJAMĀ EPR (OD EPR) PĒTĪJUMI

4.1. Pirmā tipa autolokalizētā eksitona OD EPR pētījumi NaBr kristālā [19,20]

SMH kristālos autolokalizētie eksitoni (ALE) pirmajā tuvinājumā ir V_K (X_2^-) centri ar saķertu elektronu [29*]. Tomēr, analizējot ALE ierosinātos stāvokļus un luminescenci, konstatēts, ka ALE ierosinātie stāvokļi var būt vai nu gandrīz simetriski ("on-centre", jeb I tipa, novērojami NaBr un NaI kristālos), arī vairāk vai mazāk nesimetriski ("off-centre", jeb II un III tips, novērojami vairumā pārējo SMH kristālu ar NaCl struktūru) [30*]. Uz mūsu darba sākumu OD EPR spektri bija reģistrēti vairākos "off-centre" (pārsvarā III tipa) ALE, bet I tipa autolokalizētajiem eksitoniem šādi ODEPR spektri reģistrēti nebija [29*].

Mēs izmērījām I tipa ALE OD EPR spektru NaBr kristālā [19]. Sākotnēji mēs plato OD EPR joslu ar plato tā vidusdaļā saistījām ar samērā nelielu ALE tripleta stāvokļa sašķelšanos nulles laukā vērtību [19]. Vēlākos gados, japāņu autori [31*] izmērīja OD EPR spektru citā mikroviļņu diapazonā un, kopā ar mūsu iegūto rezonanses līniju, nonāca pie secinājuma, ka NaBr kristālā ALE tripleta stāvokļa parametram D jābūt stipri lielākam, un ka mēs sākotnēji bijām novērojuši tikai vienu no tripleta stāvoklim iespējamajām atļautajām OD EPR rezonanses pārejām. Mēs šo

interpretāciju pārbaudījām un secinājām, ka D parametra vērtībai tiešām jābūt stipri lielākai, bet dinamisku efektu dēļ rezonanses joslas *hss* komponentēm amplitūdu sadalījums var atšķirties no statistiski sagaidāmā [20].

4.2. Autolokalizēto eksitonu OD EPR pētījumi Li_2GeO_3 kristālā [21]

Li_2GeO_3 kristāla struktūra sastāv no GeO_4 tetraedru ķēdēm un Li joni izvietojas starp šīm ķēdēm ([32*], zīm. 13.a). Mūsu darba sākumā bija zināma šī kristāla, ar rentgena vai UV starojumu ierosinātā luminescence, par kuru domāja, ka tā varētu būt saistīta ar autolokalizētā eksitona luminescenci [22].

Mēs šīs luminescences ierosināto stāvokļu izpētei pielietojām OD EPR metodi, detektējot to rentgenluminescences laikā un ieguvām zīmējumā 13.b attēlotos OD EPR spektrus. Šīs rezonanses ir anizotropas, t.i., atkarīgas no leņķa starp ārējā magnētiskā lauka virzienu un kristāla asīm, rezonanses līniju leņķa atkarība ir attēlota zīmējumā 14.a. Līniju leņķiskās atkarības mēs varējām aprakstīt ar tripleta sistēmām raksturīgo *spin- hamiltoniāna* operatoru [7*,29*]:

$$H = \mu_B \mathbf{B} g \mathbf{S} + D[S_z^2 - 1/3S(S+1)] + E(S_x^2 - S_y^2)$$

kur D un E ir sīkstruktūras mijiedarbību (sašķelšanos nulles laukā) raksturojošie parametri. Zemajos magnētiskajos (ap 310 mT) novērotās rezonanses līnijas ir gandrīz izotropas un tās var aprakstīt ar "aizliegto" pāreju ar $|\Delta m_S|=2$ (zīm. 14.a,b), bet no leņķa atkarīgo rezonanšu grupu, kura centrējās ap 770 mT, mēs varējām aprakstīt ar t.s. "atļautajām" pārejām $|\Delta m_S|=1$.

Lai aprakstītu visas novērotās rezonanses līnijas un to leņķisko atkarību, mums bija jāpieņem divu tripleta stāvokļu eksistence Li_2GeO_3 kristālā. Abu tripleta stāvokļu sīkstruktūras (kristāliskā lauka) galvenās ass virzieni (apzīmēts ar *FS*) ir ļoti tuvi *Ge--netiltiņa skābekļa* ass virzienam, kā parādīts zīmējumā 14.c [21].

Tādejādi, mūsu OD EPR dati kopā ar luminescences polarizācijas mērījumiem, luminescences dzīves laiku un to temperatūras atkarību pētījumu rezultātiem, palīdzēja noskaidrot autolokalizēto eksitonu ierosināto stāvokļu īpašības Li_2GeO_3 kristālā [21].

a)

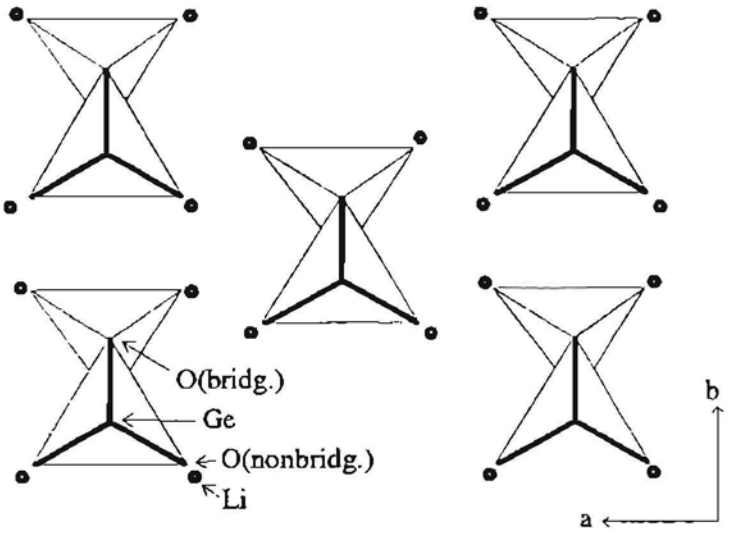

b)

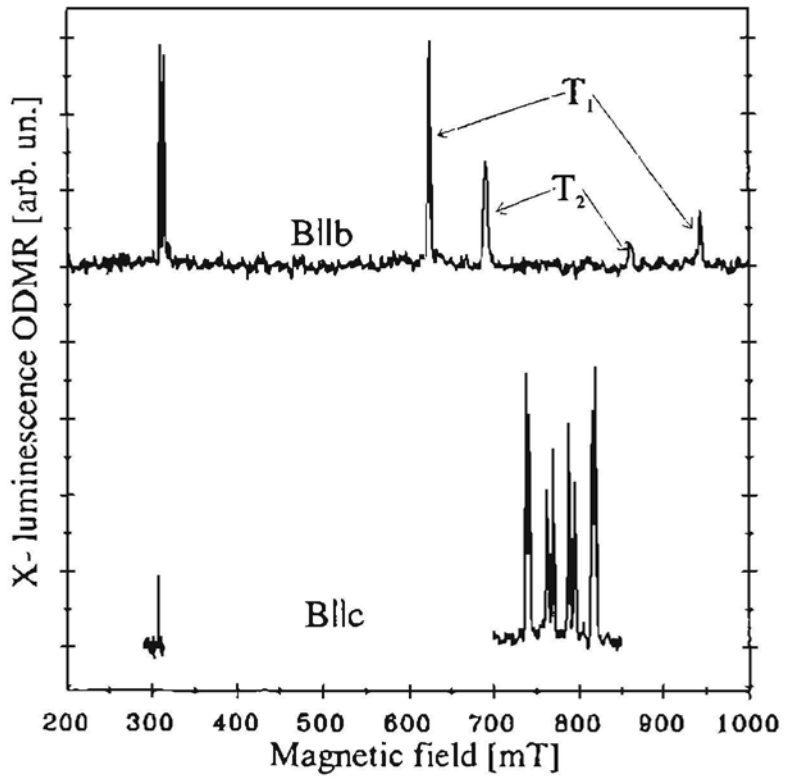

13. zīm. a) Li_2GeO_3 kristāla struktūra a-b plaknē (pēc [32*]);

b) pēc Li_2GeO_3 kristāla rentgenluminescences detektētā OD EPR spektri 24 GHz mikroviļņu diapazonā, pie T=4,2K.

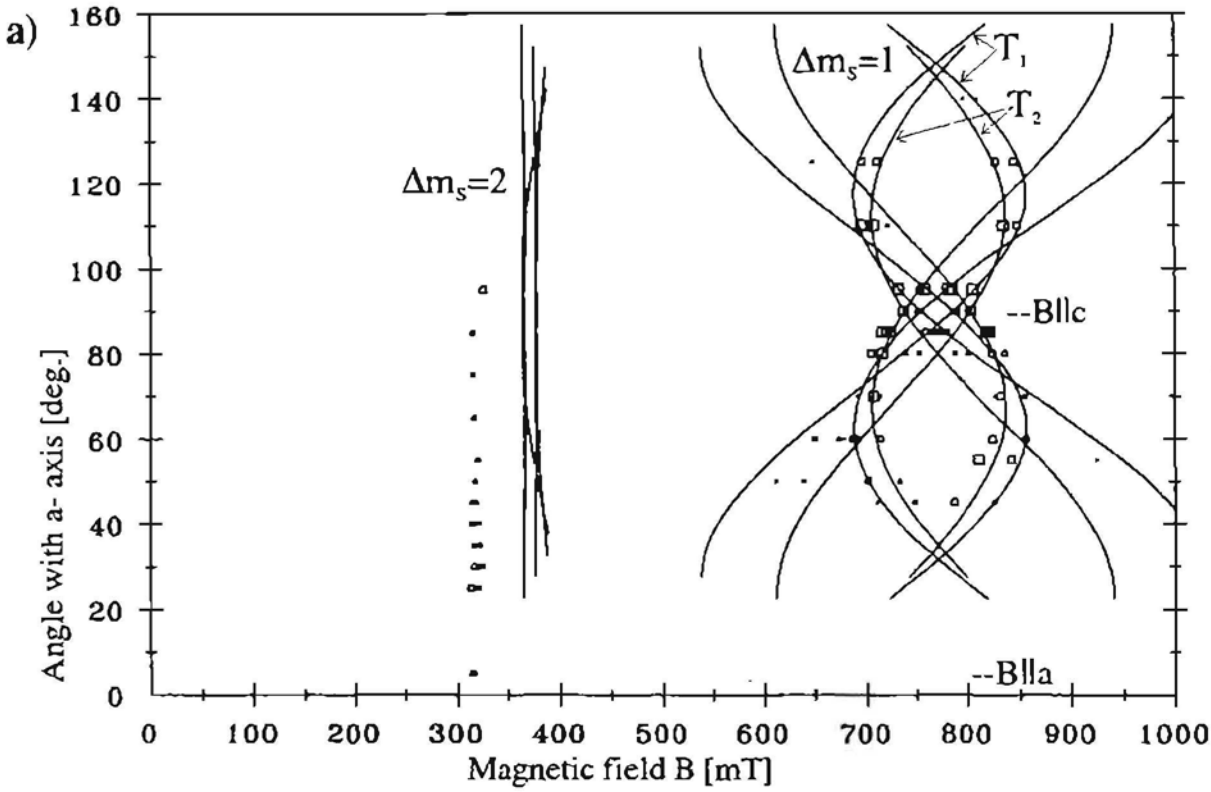

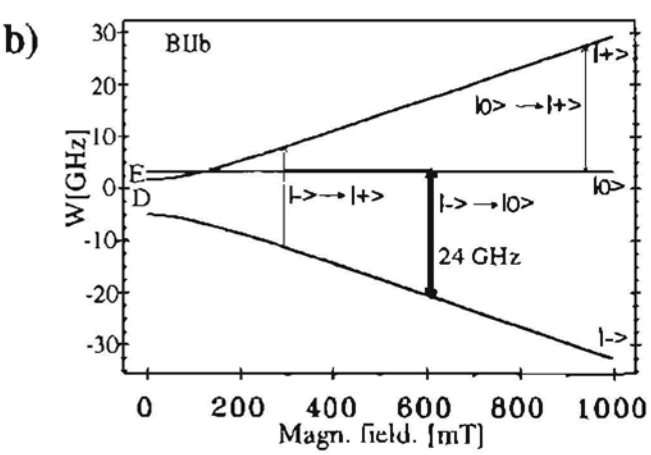

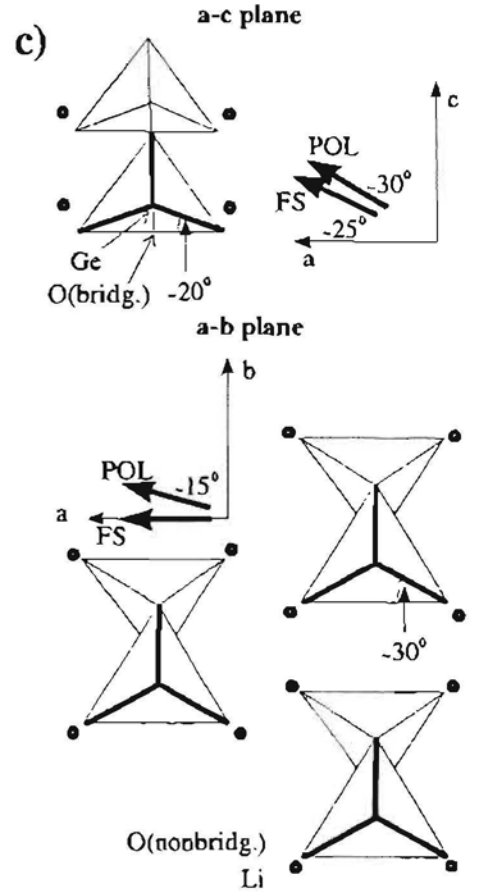

14. zīm. a) OD EPR līniju leņķiskā atkarība Li_2GeO_3 kristāla a-c plaknē. Ar kvadrātiņiem atzīmēta eksperimentālā līniju pozīcija, nepārtrauktās līnijas ir aprēķinātā rezonanses līniju leņķiskā atkarība;

b) tripleta stāvokļu enerģijas līmeņu shēma magnētiskajā laukā;

c) tripleta stāvokļu sīkstruktūras mijiedarbības tenzora galvenās ass (FS) un polarizācijas mērijumos noteiktās ass (POL) leņķiskais novietojums Li_2GeO_3 kristāla a-c un a-b plaknēs.

5. HABILITĀCIJAS DARBA TĒZES

1. Defektu absorbcijas magnētiskā cirkulārā dihroisma (MCDA) pētījumos kombinācijā ar elektroniskā pamatstāvokļa EPR selektīvi izdalītas konkrētiem defektiem atbilstošās absorbcijas joslas platzonas materiālos:

- V_K centriem sārmu metālu halogenīdu (SMH) kristālos MCDA spektros UV spektra diapazonā parādās daļēji atļautas $^2\Sigma_u^+ \leftrightarrow {}^2\Pi_u$ pārejas.
- Tl^{2+} defektu centriem SMH kristālos MCDA spektros var tikt novērotas līdz 7 optiskajām pārejām. Tl^{2+} defektu garo viļņu MCDA joslas SMH izskaidrojamas ar $t_{1u} \leftrightarrow a_{1g}$ lādiņa pārneses joslu spinorbitālo sašķelšanos.
- BaF_2 scintilatoru kristālos iespējami trīs ar Cd piejaukumu saistīti defekti ar absorbcijas joslām UV spektra diapazonā: regulārā Cd^+ mezglā saķerta elektrona centrs Cd_c^+, ar nezināmu perturbāciju perturbēts Cd_c^+ centrs un ar anjona vakanci perturbēts $Cd^+(1)$ centrs.
- Konstatēta molibdenu saturoša defekta klātbūtne $CdWO_4$ scintilatoru kristālā, kurš pēc audzēšanas ieguvis zilganu nokrāsu. Piedāvātajā defekta struktūras modelī nesapārotais elektrons atrodas Cd režģa mezgla pozīcijā un Mo jons aizvieto vienu no apkārtējo W kaimiņu joniem.
- PO_4^{2-} un PO_3^{2-} radikāļu defektiem ar rentgenu apstarotos kalcija fosfāta stiklos novērotas agrāk nezināmas šo defektu MCDA (absorbcijas) joslas optiskajos viļņvados izmantojamajā infrasarkanajā spektra diapazonā.

2. EPR optiskās detekcijas (OD EPR) pētījumos identificēti mijiedarbībās iesaistītie defekti:

- Atrasti tieši eksperimentāli pierādījumi par Frenkeļa defektu, F un H centru, telpisko korelāciju pēc to ģenerācijas zemās temperatūrās KBr kristālos. Krosrelaksācijas mijiedarbības rezultātā, H centra magnētiskās rezonanses brīdī novērotas izmaiņas F centra pamatstāvokļa spinu līmeņu apdzīvotībā.
- Ar rentgenu apstarota RbI:Tl kristāla fotostimulētajā luminescencē aktīvais caurumu ķērājcentrs ir Tl^{2+} cauruma centrs un fotostimulācijas procesā darbojas vienkāršais $\{F^*...Tl^{2+}\}$ pāru modelis.

3. Li_2GeO_3 kristālā, pēc OD EPR datiem, autolokalizētajiem eksitoniem ir divi tripleta elektroniskie ierosinātie stāvokļi. Abiem tripleta stāvokļiem sīkstruktūras mijiedarbības (sašķelšanās nulles laukā) galvenās ass virziens ir ļoti tuvs *Ge--netiltiņa skābekļa* saites virzienam.

6. NOBEIGUMS

Darba galvenos uzdevumus kopumā ir izdevies izpildīt, daudzos gadījumos OD EPR pētījumos platzonas materiālos izdevies iegūt informāciju par defektu optisko un EPR raksturlielumu savstarpējo saistību, ko atsevišķi EPR vai optiskajos mērījumos iegūt nav iespējams, kā arī OD EPR eksperimentos iegūto informāciju izmantot procesu pētījumos rentgena atmiņas ekrānu materiālos. Šādus OD EPR pētījumus joprojām perspektīvi turpināt citos perspektīvos atmiņas ekrānu un scintilatoru materiālos, kā arī citos platzonas materiālos.

Darba praktiskā nozīme Latvijā un Baltijas reģiona mērogā ir tā, ka pirmoreiz attīstītas un pētījumos ieviestas OD EPR metodikas. Starptautiskā mērogā nozīmīgi ir sistemātiski OD EPR pētījumi plašākā platzonu materiālu klasē, ar uzsvaru uz caurumu ķērājcentru optisko īpašību sistemātisku identificēšanu un pētījumiem praktiski svarīgos rentgena atmiņas ekrānu un scintilatoru materiālos.

Darbs veikts Latvijas Universitātes Cietvielu fizikas institūtā, ciešā sadarbībā ar Paderbornas Universitātes Fizikas fakultāti (Vācija).

Habilitācijas darba rezultāti publicēti 22 publikācijās zinātniskos žurnālos un 16 starptautisko konferenču tēzēs. Autora ieguldījums darbos, kas veikti kopā ar citiem kolēģiem, ir MCDA un OD EPR spektru mērījumi, spektru parametrizācija un kvalitatīva interpretācija.

Autors izsaka pateicību LU Cietvielu fizikas institūta, bet jo sevišķi Kristālu fizikas daļas kolēģiem un vad. Prof. I. Tālem par ilggadēju atbalstu darbā veiktajiem pētījumiem.

Autors izsaka pateicību Paderbornas Universitātes Fizikas fakultātes Prof.Dr. J.-M. Špēta laboratorijas kolēģiem par iespēju veikt lielu daļu no darbā veiktajiem zemo temperatūru OD EPR un MCDA pētījumiem, bet jo sevišķi Prof. J.-M. Spētam par ilggadēju sniegto atbalstu, diskusijām un motivāciju OD EPR pētījumu virzienā.

Par atbalstu grūtajā darba sākuma periodā, CFI izveidojot OD EPR mēriekārtu eksperimentiem šķidrā hēlija temperatūrās, esmu pateicīgs Prof. A. Siliņam, Prof. J. Kļavam, Dr. Hab. phys. M. Springim, Dr. Hab. phys. L. Čugunovam, Prof. A. Truhinam, Dr. Hab. phys. D. Milleram.

Esmu ļoti pateicīgs CFI Jauno zinātnieku perspektīvo pētījumu grupas, tagadējās Magnetooptikas grupas agrākajiem un tagadējiem kolēģiem, bet jo sevišķi Dr. phys. J. Trokšam, Dipl. phys. D. Bricim, bez kuru entuziasma nebūtu iedomājama OD EPR mēriekārtas izveide.

Esmu pateicīgs Prof. K.S. Songam un Prof. M. Moreno par diskusijām un sadarbību MCDA joslu dabas teorētiskā noskaidrošanā.

Saviem pirmajiem zinātnisko darbu vadītājiem Doc. V. Grabovskim un Prof. I. Vītolam esmu pateicīgs par pieredzi optisko un zemo temperatūru eksperimentu jomā.

Pateicos savai dzīvesbiedrei Mag. Phys. A. Rogulei par atbalstu un pacietību visā dotā darba veikšanas laikā.

CITĒTĀ LITERATŪRA

1*. S. Geschwind, in *Electron Paramagnetic Resonance* (Ed. By S. Geschwind, New York: Plenum Press) 1972, pp. 233-425.

2*. J.-M. Spaeth, J.R. Niklas and R.H. Bartram. *Structural Analysis of Point Defects in Solids, Springer Series in Solid State sciences 43* (Heidelberg: Springer) 1992.

3*. P.G. Baranov, Bull. Acad. Sci. USSR, Phys. Ser., 1981, vol. 45, p. 23.

4*. N.G. Romanov, Bull. Acad. Sci. USSR, Phys. Ser., 1985, vol. 47, p. 2054.

5*. J.-M. Spaeth and F. Lohse. J. Phys. Chem. Solids, 1990, vol. 51, p.861.

6*. W.B. Lynch and D.W. Pratt, Magn. Reson. Rev, 1985, vol. 10, p.111.

7* I.Y. Chen, *Triplet State ODMR Spectroscopy* (Ed. R.H. Clark, New York: Willey), 1982.

8*. W.B. Fowler, *The Physics of Color Centers* (Ed. W.B. Fowler, New York: Academic Press) 1968.

9*. T.G. Castner and W. Känzig, J. Phys. Chem. Solids, 1957, vol.3, p.178.

10*. D. Schoemaker, Phys. Rev., 1973, vol. B7, p.786.

11*. C.J. Delbecq, W. Hayes and P.H. Yuster, Phys. Rev., 1961, vol. 121, p. 1043.

12*. J.-M. Spaeth, W. Meise and K.S. Song, J. Phys.: Condens. Matter, 1994, vol. 6, p.1801.

13*. G. Blasse, J. Alloys Compd., 1993, vol. 192, p.17.

14*. J.-M. Spaeth, Th. Hangleiter, F.-K. Koschnick and Th. Pawlik, Radiat. Eff. Defects Solids, 1995, vol. 135, p. 499.

15*. W. Dreybrodt and D. Silber, Phys. Status Solidi, 1967, vol. 20, p. 337.

16*. S.V. Nistor, D. Schoemaker and I. Ursu, Phys. Status Solidi (b), 1994, vol. 185, p. 9.

17*. C.J. Ballhausen and H.B. Gray, *Molecular Orbital Theory* (New York: Benjamin), 1965, p.103.

18*. M. Moreno, J.Phys.C.: Solid State Physics, 1979, vol. 12, L921.

19*. V.F. Krutikov, N.I. Silkin and V.G. Stepanov, Sov. Phys. Sol. State, 1976, vol.18, p.2958.

20*. N.G. Romanov, V.V. Dyakonov, V.A. Vetrov and P.G. Baranov, Phys. Stat. Sol. (b), 1988, vol.147, K171.

21*. R.W.G. Wyckoff, Crystal Structures (2nd edn., New York: Interscience), 1965, vol. 3, pp.42-43.

22*. A. Watterich, G.J. Edwards, O.R. Gilliams, L.A. Kappers, D.P. Madecsi, K. Raksanyi and R. Voszka, J. of Phys. Chemistry of Solids, 1991, vol.52, p.449-455.

23*. G.O. Karapetyan, A.K. Sherstyuk and D.M. Yudin, Opt. Spektrosk., 1967, vol.22, p.443.

24*. T.V. Bocharova, G.O. Karapetyan and O.A. Yaschurschinskaya, Sov. Phys. Chem. of Glasses, 1985, vol.11, p. 677.

25*. M.N. Vilchinskaya, A.V. Dmitryuk, E.G. Ignatyev, G.O. Karapetyan and G.T. Petrovskii, Sov. Phys.- Dokl., 1984, vol. 274, p.158.

26*. N. Itoh, Advances in Physics, 1981, vol. 31, p. 491.

27*. M. Thoms, H. von Seggern and A. Winnacker, J. Appl. Phys., 1994, vol. 76, p. 1800.

28*. P.F. Braslavets, A. Kalnins, I. Plavina, A.I. Popov, B.I. Rapoport and A. Tale, Phys. Stat. Sol. (b), 1992, vol. 170, p. 395.

29*. K.S. Song and R.T. Williams, *Self- Trapped Excitons, Springer Series in Solid State Sciences 105* (Heidelberg: Sprienger), 1993.

30*. K. Kan'no, T. Tanaka and T. Hayhashi, Rev. Sol. State Sci., 1990, vol. 4, p. 383.

31*. K. Kan'no, M. Shirai, M. Matsumoto and I. Akimoto, Proc. 13th ICDIM (Wake Forest University), 1996.

32*. H. Wöllenkle, A. Wittmann, Monatshefte für Chemie, 1968, vol. 99, p. 244.

CITĒTĀS HABILITĀCIJAS DARBA AUTORA PUBLIKĀCIJAS

1. U. Rogulis, W. Meise and J.-M. Spaeth, Optically detected magnetic resonance of V_K and H centers in KBr and KI crystals. In: Defects in Insulating Materials, ed. by O. Kanert, J.-M. Spaeth, World Scientific, Singapore, 1993, vol.1, pp. 468-470.

2. U. Rogulis, K.S. Song and J.-M. Spaeth, Magneto-optical properties of the UV absorption bands of V_K centers in alkali halides. Journal of Physics: Condensed Matter, 1995, vol.7, pp. 7699-7708.

3. U. Rogulis, J.-M. Spaeth, I. Cabria, M. Moreno, J. Aramburu and M.T. Bariusso, Optical properties of Tl^{2+} hole centres in alkali halides. Part I: Investigation with optical detection of paramagnetic resonance, Journal of Physics: Condensed Matter, 1998, vol. 10, pp. 6473-6479.

4. I. Cabria, M. Moreno, J. Aramburu, M.T. Bariusso, U. Rogulis and J.-M. Spaeth, Optical properties of Tl^{2+} hole centres in alkali halides. Part II: MS-Xα calculations. Journal of Physics: Condensed Matter, 1998, vol. 10, pp. 6481- 6490.

5. J.-M. Spaeth and U. Rogulis, Optical properties of Tl^{2+} hole centres in alkali halides investigated with optical detection of paramagnetic resonance. Rad. Eff. and Def. in Solids, 1998 (in press).

6. U. Rogulis, J.Trokšs, Ā.Veispāls, I.Tāle, P.Kūlis and M.Spriņģis, ODMR of Cd impurity centers in γ- irradiated BaF_2 crystals. Radiation Effects and Defects in Solids, 1995, vol.135, pp. 361-365.

7. M.Spriņģis, Ā.Veispāls, P.Kūlis, U.Rogulis, I.Tāle and J.Trokšs, Optical and spectral properties of the Cd-containing BaF_2. Proceedings of Int. Conf. on Inorganic Scintillators and Their Applications SCINT'95, Delft, 1996, Delft Univ. Press, Netherlands, pp. 403-406.

8. U. Rogulis, EPR of Molybdenum-related Defect in $CdWO_4$. Radiation Measurements, 1998, vol. 29, No 3-4, pp. 287-289.

9. D. Brics, J. Ozols, U. Rogulis, J. Trokss, W. Meise and J.-M. Spaeth, Magnetic circular dichroism of the optical obsorption and optically detected ESR of X- irradiated Tb^{3+} doped and undoped $CaO-P_2O_5$ glasses. Solid State Communications, 1992, vol. 81, pp. 745-748.

10. W. Meise, U. Rogulis, F.K. Koschnick, J.-M. Spaeth. Direct experimental evidence for the spatial correlation of F and H centers in alkali halides after their generation at low temperatures, In: Defects in Insulating Materials, ed.by O.Kanert, J.-M.Spaeth, World Scientific, Singapore, 1993, vol.2, pp. 1078- 1081.

11. F.K. Koschnick, W. Meise, U. Rogulis, J.-M. Spaeth, R.S. Eachus. Spatial correlation of radiation- induced defects in BaFBr and KBr studied by cross- relaxation ODMR

spectroscopy. In: Defects in Insulating Materials, ed.by O.Kanert, J.-M.Spaeth, World Scientific, Singapore, 1993, vol.1, pp. 252- 266.

12. J.-M.Spaeth, F.K.Koschnick, W.Meise and U.Rogulis, Cross relaxation in magnetic resonance as a tool to study spatial correlations between defects in insulators. Nuclear Instruments and Methods in Physics Research, 1994, B91, pp. 175-182.

13. W.Meise, U. Rogulis, F.K. Koschnick, K.S. Song and J.-M. Spaeth, Experimental evidence for spatial correlation between F and H centres formed by exciton decay at low temperatures in KBr. Journal of Physics: Condensed .Matter, 1994, vol.6, pp. 1815- 1824.

14. U. Rogulis, C. Dietze, Th. Pawlik, Th. Hangleiter and J.-M. Spaeth, Identification of the hole- trapping sites and the mechanism of the photostimulated luminescence of the X- ray storage phosphor RbI:Tl^+. Journal of Applied Physics, 1996, vol.80, pp. 2430-2435.

15. U.Rogulis, J.-M.Spaeth, I.Tale and E.Ruzha, ODEPR of indium colour centres in the X-irradiated storage phosphor KBr-In. Radiation Effects and Defects in Solids, 1995, vol.134, pp. 471-475.

16. U.Rogulis, I.Tāle, Th.Hangleiter and J.-M.Spaeth, The photostimulation process in the X-ray storage phosphor KBr-In. Journal of Physics: Condensed Matter, 1995, vol.7, pp.3129-3137.

17. Th. Hangleiter, U.Rogulis, C.Dietze, J.-M.Spaeth, P.Willems, L.Struye and P.J.R.Leblans, The X-ray storage phosphors RbI:Tl^+ and KBr:In^+ and other In^+ and Ga^+ doped alkali halides. Proceedings of Int. Conf. on Inorganic Scintillators and Their Applications SCINT'95, Delft, 1996, Delft Univ. Press, Netherlands, pp. 452- 455.

18. U. Rogulis, S. Schweizer, S. Assmann, and J.-M. Spaeth, Ga^{2+} hole centers and photostimulated luminescence in the X-ray storage phosphor RbBr:Ga^+. J. of Applied Physics, 1998, vol. 84, No 8, pp. 1-6.

19. U. Rogulis, J.- M. Spaeth and K.S. Song, Optically detected magnetic resonance of the STE in NaBr. Journal of Physics: Condensed Matter, 1995, vol.7, pp. 4939-4947.

20. U. Rogulis, F.K. Koschnick, J.-M. Spaeth and K.S. Song, Zero Field Splitting and Line Shape of the ODMR of Self-Trapped Excitons in NaBr. Journal of Physics: Condensed Matter, 1997, vol. 9, pp.1-13.

21. U. Rogulis, A. Trukhin, J.-M. Spaeth and M. Springis, ODMR of triplet states of the self-trapped excitons in Li_2GeO_3 crystals. Materials Science Forum, 1997, vols. 239-241, pp.577-580.

22. A.N. Truhin, U. Rogulis, M. Springis, Self-trapped excitons in Li_2GeO_3. J. Luminescence 1997, vol.72-74, pp. 890-892.

Institute of Solid State Physics
University of Latvia

Dr. Phys. Uldis Rogulis

DETERMINATION OF THE ELECTRONIC STRUCTURE OF DEFECTS IN INSULATOR MATERIALS BY OPTICAL DETECTION OF EPR

Summary of the Habilitation Thesis

Riga 1999

CONTENTS

INTRODUCTION

An important problem in the investigations of defects and defect interaction processes in wide-band gap materials such as insulators is the determination of the correlation between the optical properties of the defect centres and the data obtained by structure sensitive investigation techniques like electron paramagnetic resonance (EPR). Traditionally, the structure of defects has been investigated mainly by means of EPR techniques and the optical properties of defects (in practice - separately from the EPR) - by means of optical techniques (absorption, luminescence). The best and direct solution of this problem is to use optically detected EPR (ODEPR) techniques.

During the present work ODEPR techniques have been introduced to Latvia, in the Institute of Solid State Physics (ISSP), University of Latvia, and since 1988 ODEPR investigations have been started. In the course of this work a very good and fruitful cooperation has been developed with the research group of Prof. Dr. J.-M. Spaeth in the Department of Physics, University of Paderborn (Germany). A great deal of these investigations are due to this collaboration and continuous support.

The main *concept* of this work was: by taking into account the published data or our recently obtained data on the EPR of a defect ground state, to determine the defect's magnetic circular dichroism of the absorption (MCDA) and the absorption or luminescence bands by means of the ODEPR measurements; if it was possible also to get new information about the defect's electronic structure and energy states. Thus, the investigations have been performed in a new scientific area, *i. e.*, the investigations of the correlation between the defect's optical and EPR properties by means of the ODEPR techniques.

The *aim* of this work was: the investigation of the defect's electronic structure and optical properties by means of ODEPR techniques. The actual and particular tasks were:

- to find out the relations between the optical (absorption, luminescence) and EPR properties of the defects in several insulating materials (including X-ray storage phosphor and scintillator materials);
- to ascertain the defect interaction processes and the photostimulated luminescence mechanisms in X-ray storage materials;
- to obtain information about excited states of the self-trapped excitons (STE's) in NaBr and Li_2GeO_3 crystals.

The *first* group of investigations is related to the studies of the structure of defects and to the determination of the direct correlation with their optical (absorption, magnetic circular dichroism (MCDA)) properties. Several new MCDA bands of the V_K centres have been found in a series of alkali halide (AH) crystals, as well as the spectral positions of the MCDA bands of H centres in KBr and KI crystals. The parameters of the g-tensor have been determined to be $g_\perp = 2.08$ in KI crystals. By using the ODEPR (MCDA-detected EPR) technique several new MCD bands have

been determined for the Tl^{2+} centres in several AH crystals. Previous unknown parameters of the ODEPR and EPR of the Tl^{2+} centres in iodide crystals have been determined.

Three different Cd impurity-related defects have been found in BaF_2 scintillator crystals and their optical properties have been determined. New absorption (MCDA) bands of the PO_4^{2-} and PO_3^{2-} radical defects have been detected and investigated in calcium phosphate glass in the red and infrared spectral regions. These radical defects may have such bands in the optical waveguide glasses. The molybdenum impurity-related defect structure model in the $CdWO_4$ scintillator crystal ('blue colored' after the crystal growth) has been investigated.

The *second* group of investigations is related to the studies of the interaction between the Frenkel defect pairs like F and H centres by detection of the cross-relaxation effects in ODEPR. These data allowed to estimate the distance between the F and H centres in the {F...H} pair in KBr at low temperatures after their generation. By means of the MCDA-detected EPR techniques the mechanism of the photostimulated luminescence (PSL) has been investigated and the actual hole trap centre - the activator centre Tl^{2+} - has been identified in RbI:Tl crystals. By means of the MCDA and ODEPR techniques In impurity-related radiation-induced defects have been investigated in KBr crystals doped with In as an activator. The so-called, 'replenishment' effect of the PSL in KBr:In has been observed, which can not be explained by the simple defect pair $\{F^*...In^{2+}\}$ recombination model in contrast to earlier assumptions made in the literature.

The *third* group of investigations is related to the studies of the excited states of the self-trapped excitons (STE) by ODEPR techniques. For the first time, the ODEPR spectrum of the type I STE in NaBr crystals has been detected. The triplet excited states of the STE have been investigated and identified in Li_2GeO_3 crystals, the principal directions and values of the crystalline field gradients have been determined.

The contribution of the author of this Thesis in his papers published in cooperation with other colleagues is: the measurements of the MCDA and ODEPR spectra, the quantitative analysis of the spectra and their qualitative interpretation.

The main results obtained in this work are presented in the *Abstract of Habilitation Thesis.*

In this Summary of the Thesis, two kinds of references to the literature have been used: marked with an asterisk or without it. The references to the other authors and research groups have been marked with an asterisk (for example [2*]). The references of the author's papers are not marked. In accordance with this, two lists of references are presented.

The supplement of the summary of the Habilitation Thesis is a separate volume, including the reprints of the author's papers as well as a list of all published papers and abstacts. The reprints in the supplement have been presented in the same sequence as they have been referred to in the summary of the Habilitation Thesis.

1. PRINCIPLES OF OPTICAL DETECTION OF EPR (OD EPR)

The energy levels of isolated defects are positioned generally in the forbidden gap of wide-band gap materials between which absorption bands are observed schematically shown in Fig. 1.a. Mostly, EPR has been investigated in the electronic ground state of defects and provided a lot of information about the microscopic structure of the defects. Traditionally optical investigations (absorption, luminescence) have been carried out unrelated to EPR investigations and correlations between both data mostly remained unclear, or only indirect correlations could be suggested.

For one way of optical detection of EPR the luminescence emission or its circular polarisations are separated under the influence of magnetic field and microwave radiation are measured [1*]. In this case the EPR of the optically excited electronic state can be investigated. Also the magnetic circular dichroism of the optical absorption (MCDA [2*]) is used for optical detection of the EPR. The spin- dependent recombination (tunnelling luminescence) can also be used [3*,4*]. All these techniques as well as the main research results obtained with them have been reported in several reviews [1*-7*].

In our work, we used these techniques to determine the direct correlation between EPR and optical spectra of different defect centres in wide-band gap insulator materials. From a practical aspect of applications, we studied defects and their interactions in photostimulable X-ray storage phosphor screen materials and scintillators.

Mostly we used EPR optically detected via the MCDA, and schematically we illustrate this technique for the example of the, so-called 'alkali-metal atom' model [8*], as shown in Fig. 1.b. In this model, the electronic configuration of the ground state is s^1 in the state $^2S_{1/2}$, and in the optically excited state the electronic configuration is p^1 with the spin-orbit split states $^2P_{1/2}$ and $^2P_{3/2}$. In an external magnetic field, due to the Zeeman effect, the degeneracy of the electronic levels is removed, the resulting projections of the magnetic moment m_j are shown. The optical transitions can have different circular polarisations (CP) if $\Delta m_j = \pm 1$. One or two CP transitions are allowed from each of the ground state Zeeman levels with $m_j = \pm 1/2$ to the excited Zeeman and spin-orbit split states with $m_j = \pm 1/2, \pm 3/2$. The populations of the ground state Zeeman levels in the magnetic field are different, the different transitions have different intensities, and this difference greatly enhances at low temperatures. In the wide-band gap materials, the halfwidth of the defect absorption bands is much larger than the Zeeman splitting. Therefore the transitions with different circular polarizations are generally not spectrally resolved. They become resolved by larger splittings of the levels as, for example, by a large spin-orbit splitting.

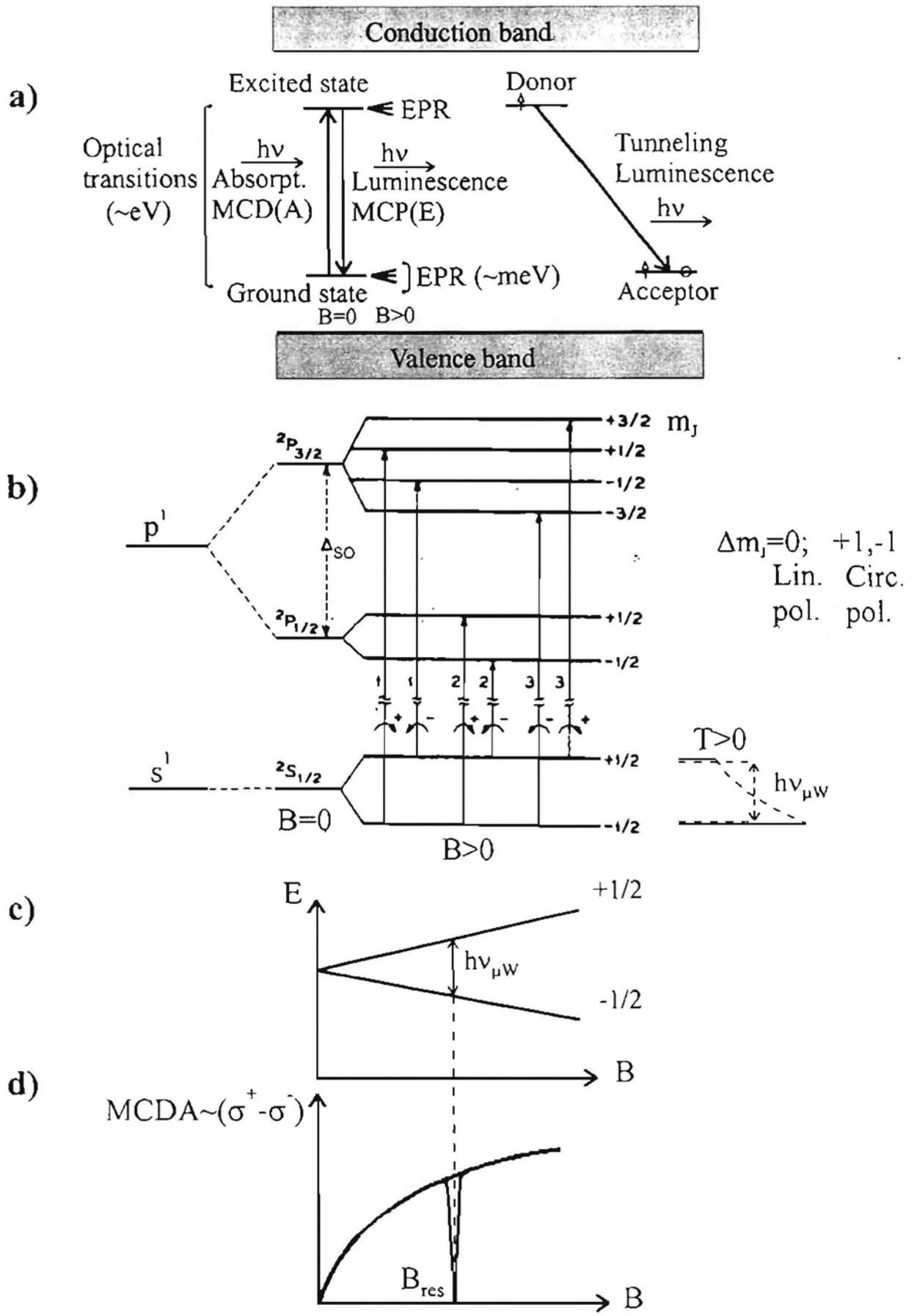

Fig. 1. a) Schematic representation of the optical detection of the EPR via the magnetic circular dichroism of the absorption;
b) The 'alkali-metal atom' model to illustrate the principle of the MCDA- EPR method;
c) and d) At the moment of the saturation of EPR resonance of the ground state, populations of the Zeeman levels tend to become equal and the MCDA tends to zero.

The difference of the absorption coefficients of the circular dichroic transitions (after some scaling, see [2*]) is called the magnetic circular dichroism (MCDA). Due to the induction of the ODEPR resonance (Fig. 1.c.) the populations of the ground state Zeeman levels tend to equalize and the MCDA signal tends to zero (Fig. 1.d.). In practical measurements the ODEPR effect is in the range from several percents to several tens of percents.

All kinds of optical detection of EPR follow a similar principal scheme, i.e. in the moment of resonance the spin polarisation of the Zeeman levels is changed and therefore the intensity of the optical transitions changes. In order to reach an optimal ODEPR signal intensity, the ODEPR is usually measured at low temperatures (at 1.5 K to 4.2 K) as well as at high magnetic fields (up to 6 T) and at high microwave frequencies (from 24 GHz to 95 GHz). These experimental aspects have all been described well in several reviews (see, for example, [1*-5*]) and we do not discuss them again in the present Summary. The next chapters are devoted to review the main results of the investigations related with the Habilitation Thesis.

2. INVESTIGATIONS OF DEFECT STRUCTURE AND OPTICAL PROPERTIES

In this chapter, the results of the investigations are presented and discussed, in which the EPR of the ground state of a defect has been investigated. In several cases, when the EPR was known, ODEPR via the MCDA has been studied. In some cases, new data about the electronic structure of defects and the nature of the optical transitions have been obtained.

2.1. Investigations of the Magnetooptical Properties of V_K and H centres [1,2]

There are well-known data about the EPR [9*,10*] and optical absorption spectra [10*,11*] of the V_K centres and H centres in alkali halide crystals. The microscopic structures of V_K and H centres in most of the AH crystals with NaCl structure are shown in Fig. 2 (top). Their structures have been established by EPR: a X_2^- molecule located on two anion sites (V_K centre) and a X_2^- molecule located on one anion site (H centre).

We measured the MCDA in a KBr crystal (and also in several other AH crystals with NaCl structure) and searched for the corresponding ODEPR spectra of the V_K and H centres by taking into account the known EPR parameters for these centres. We found the ODEPR resonances for the V_K centre (Fig. 2.1) and for the H centre in KBr (Fig. 2.2). In the ODEPR spectra mainly the

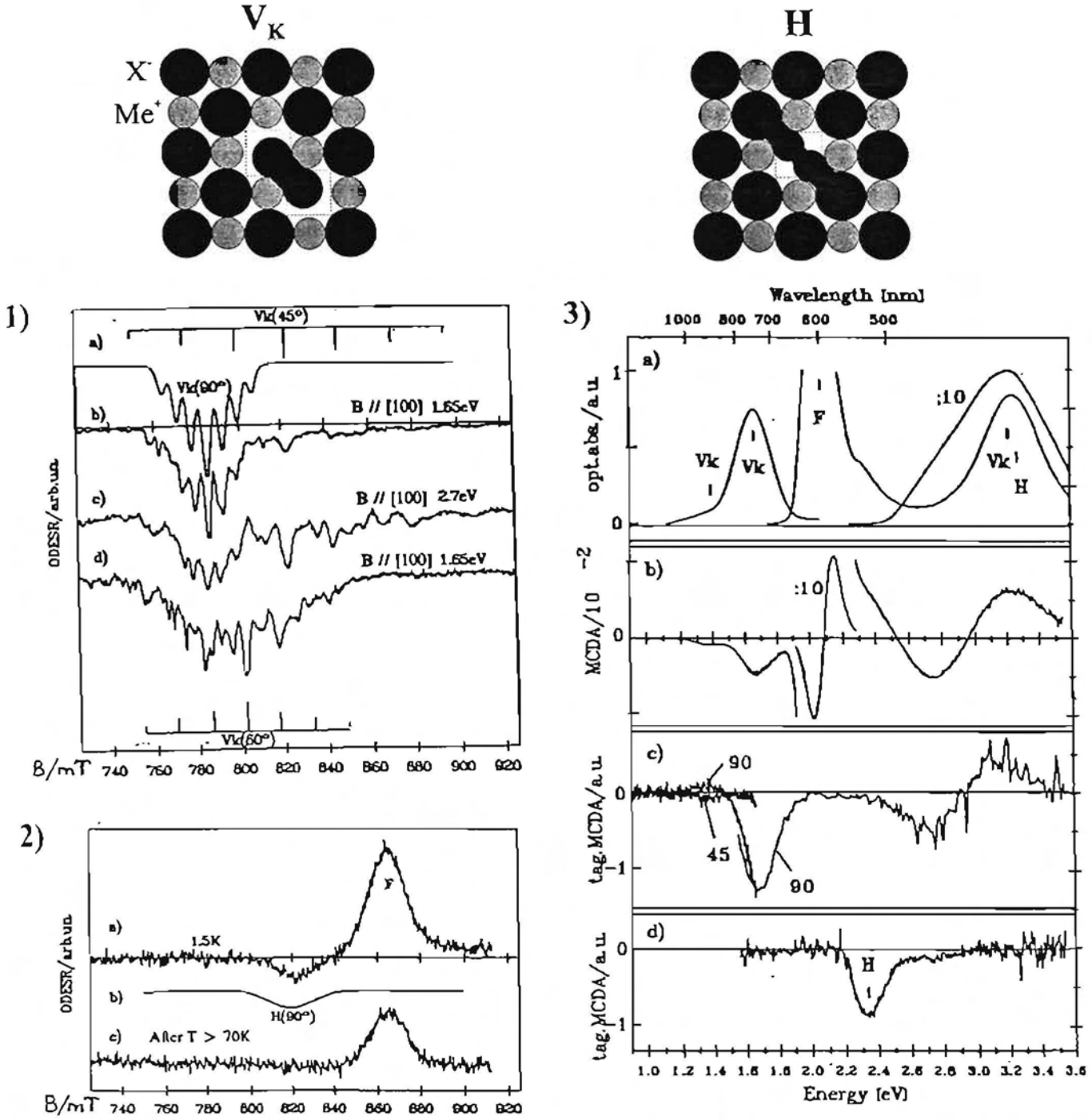

Fig. 2. 1) ODEPR spectra of a KBr crystal x- irradiated at 4.2 K:
a) Simulation of 90° oriented V_K centres;
b), c), d) ODEPR measured in the two MCDA bands at 2.7 eV and 1.65 eV of 90°, 60° and 45° oriented V_K centres [1].

2) ODEPR of F and H centres in KBr x- irradiated at 4.2 K:
a) ODEPR in the MCDA at 2.4 eV;
b) Simulated EPR spctrum of 90° oriented H centres;
c) ODEPR in the MCDA band at 2.4 eV after annealing the H centres to 70 K.

3) a) Optical absorption literature data of x- irradiated KBr (see ref. in [1]);
b) MCDA at B = 2 T and T= 1.5 K of F, H and V_K centres in KBr x- irradiated at 4.2 K;
c) 'Tagged MCDA' of V_K centres;
d) 'Tagged MCDA' of H centres.

resonances of the centres having their molecular axes perpendicular to the external magnetic field are seen [12*].

We measured the excitation spectra of the MCDA of these ODEPR lines (so-called 'tagged MCDA' [2*,5*]) and selected from the total MCDA spectra the MCDA bands corresponding to the V_K and H centres (Fig. 2.3). For the V_K centres, each orientation of the centre with respect to the magnetic field may have a different sign of the MCDA (positive or negative).

The MCDA band of the V_K centres in the UV spectral region has a derivative lineshape and its centre does not coincide with the peak of the well-known UV absorption band from the transition $^2\Sigma_g^+ \leftrightarrow {}^2\Sigma_u^+$ in an AH crystal (Fig. 3.1. [2]).

The $^2\Sigma_g^+ \leftrightarrow {}^2\Pi_u$ transition, which would be MCDA- active, is forbidden in the X_2^- molecular model in accordance with group theory because of symmetry. A theoretical analysis [2] showed that if the V_K centre is considered as a dynamical system, the symmetry is lowered to C_{2v} and this transition becomes partially allowed (Fig. 3.2). This hypothesis was used already earlier by [11*] in order to explain the additional absorption shoulder observed in KI crystals. This transition would be seen as a small low energy shoulder below the strong $^2\Sigma_g^+ \leftrightarrow {}^2\Sigma_u^+$ absorption band. It is the 'characteristic' V_K transition in the MCDA spectra, where the $^2\Sigma_g^+ \leftrightarrow {}^2\Sigma_u^+$ transition is not seen. The theoretical analysis also showed that the MCDA of V_K and H centres with their axes parallel to the external magnetic field is zero explaining why mainly the perpendicular centres have been measured.

The MCDA spectra of the V_K and H centres have been used in Ch. 3.1 to investigate the processes of cross-relaxation between F and H centres, and in Ch. 3.2 to investigate the processes in the photostimulated X-ray storage phosphors.

2.2. Magnetooptical Properties of Tl^{2+} Hole Trapped Centres in Alkali Halide Crystals [3-5]

Photostimulable X-ray storage phosphor materials contain, as rule, an activator ion, the luminescence of which is detected in the information read-out process [13*,14*]. One of such activator ions is Tl^+ and therefore we investigated Tl^+- trapped hole centres Tl^{2+} by use of the MCDA technique in alkali halide crystals.

The EPR data of the Tl^{2+} centres are known for several AH crystals [15*,16*]. By using the MCDA- detected EPR we measured the ODEPR spectra of the Tl^{2+} centres in 6 AH crystals (Fig. 4.a.) and compared their hyperfine (*hf*) structure with the known *hf* data from EPR: they agree

1)

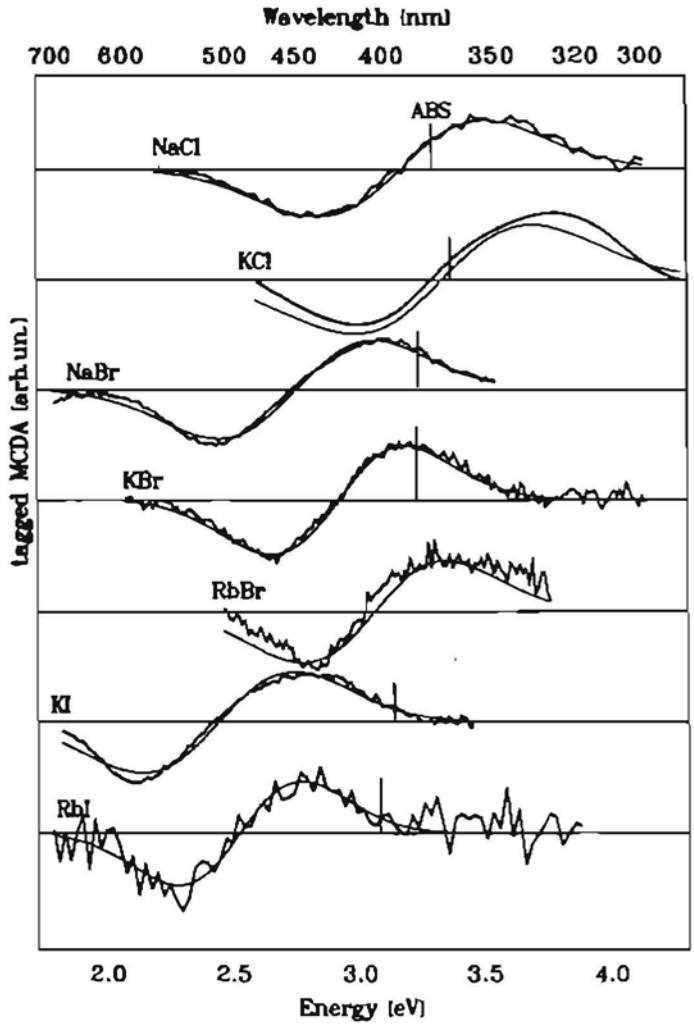

2)

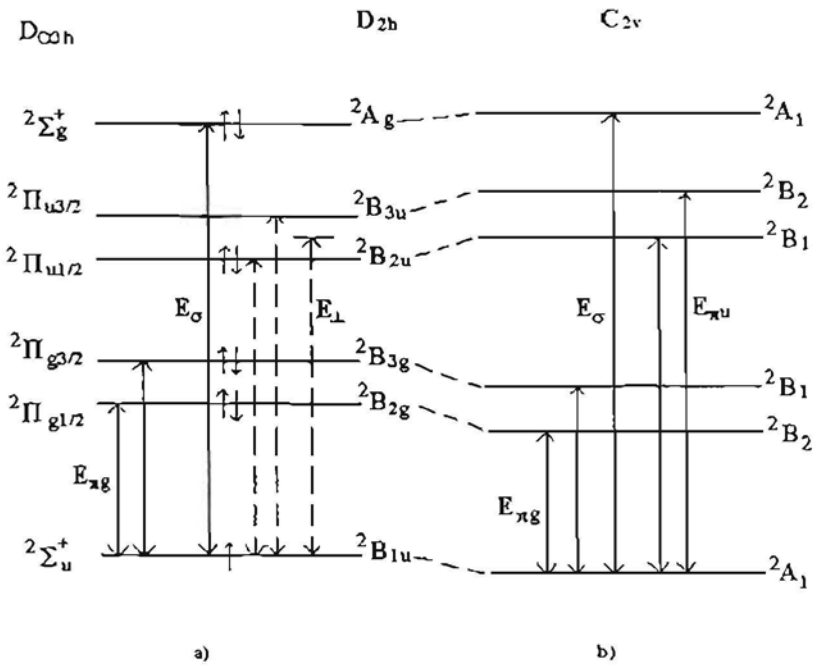

Fig. 3. 1) ' Tagged MCDA' spectra of the UV transitions of V_K centres in seven alkali halides. The positions of the UV absorption bands are indicated by bars.

2) Schematic representation of the energy levels for theregular X_2^- molecular model (a) and assuming a slow axial centre oscillation (b) [2]:

a) 'on- centre' X_2^-, symmetry D_{2h};

b) 'off- centre' X_2^-, symmetry C_{2v}.

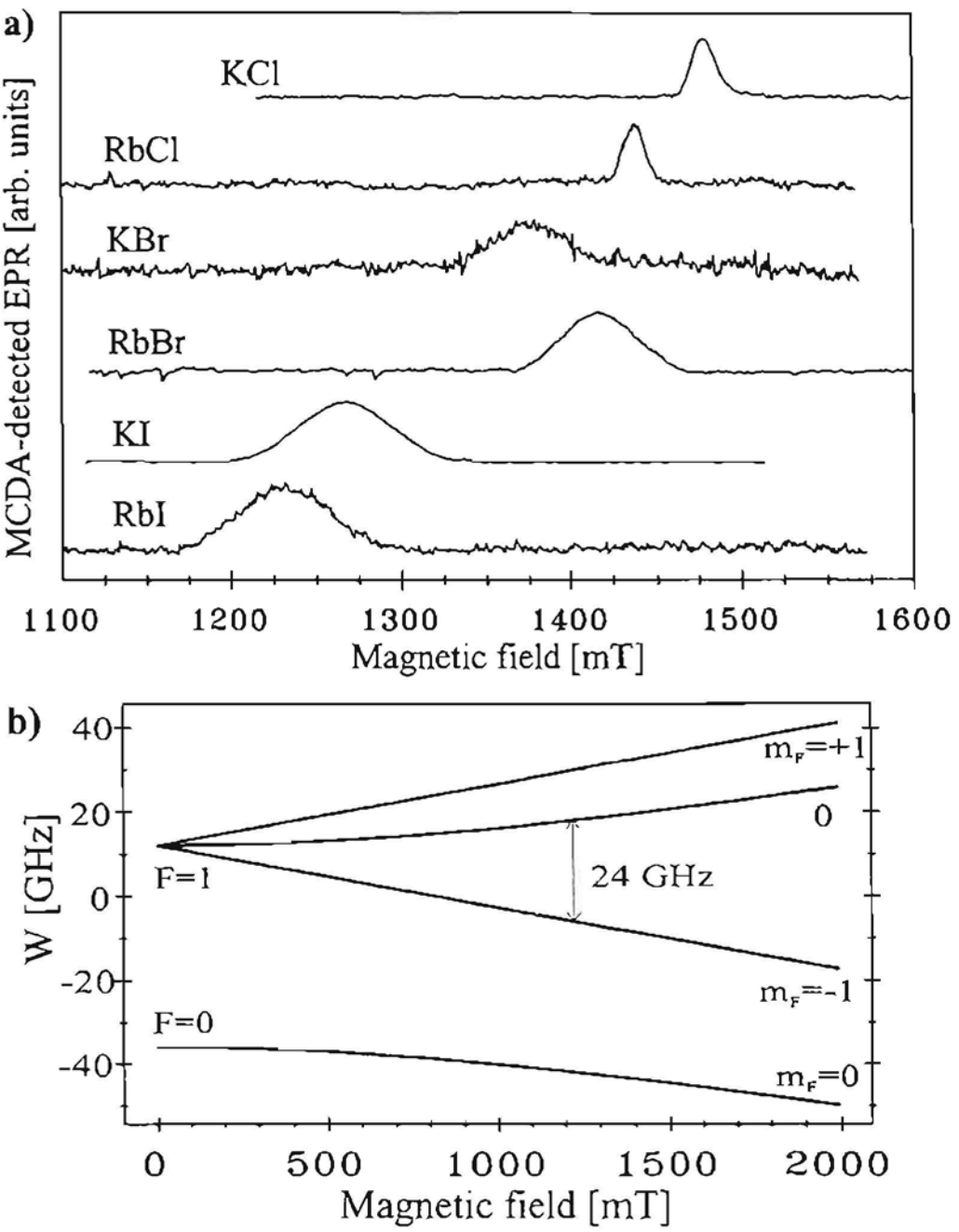

Fig. 4. a) MCDA- detected EPR spectra of the Tl^{2+} centres in six alkali halides. T = 1.5 K and B ll [100], microwave frequency range 24 GHz [3].

b) Breit- Rabi diagram for Tl^{2+} centres in RbI:Tl [3].
($I(^{203}Tl, ^{205}Tl) = 1/2$; the small difference in g_N is not resolved)

very well [3]. No EPR *spin-Hamiltonian* parameters (g- factor or Tl- *hf* interaction constant A) were known for the Tl^{2+} centres in KI and RbI. We observed only one resonance transition in each of the two iodides. We could not determine both parameters (g and A) from only one resonance line and therefore assumed the g- value to be a little bit larger as in the bromides. If additional resonance data become available, these parameters should be corrected. The Tl^{2+} centre has a very large hyperfine interaction of the s^1 electron with the nuclear magnetic moment of the Tl nucleus. The ODEPR transition $|0> \leftrightarrow |1>$ (which we observed in the 24 GHz microwave range) is shown for the ground state of the Tl^{2+} centre in the Breit-Rabi diagramm (Fig. 4.b, the two isotopes with similar g_N factors ^{203}Tl and ^{205}Tl could not be resolved).

After determination of the ODEPR resonances we found all MCDA bands of the Tl^{2+} centres by measuring the excitation spectra of the resonance lines. These 'tagged' MCDA bands are shown in Fig. 5.a for several AH crystals with the NaCl structure. Most of these bands were not known previously from absorption measurements or their relation to the Tl^{2+} centres has been questioned. It turned out that the Tl^{2+} centres have more MCDA bands than absorption bands previously discussed in the literature [16*,18*] for the $[TlX_6]$ complex model (for iodides altogether 7 bands). We interpreted [3,4] these MCDA bands as spin - orbit - split charge transfer transitions $t_{1u} \leftrightarrow a_{1g}$ (Fig. 5.b.). This explains 6 from 7 observed MCDA transitions in the iodides. To explain the 'extra' MCDA band it was necessary to find the additional allowed transitions. The extra transition was explained [4] as a transition from the t_{2u} - level, which may be partially allowed.

We used these data on the MCDA bands of the Tl^{2+} centres in section 3.2., to investigate the mechanism of the photostimulated luminescence in the x- ray storage phosphor RbI:Tl [16].

2.3. Optical Properties of Three Cd Impurity-Related Defect Centres in BaF_2 Scintillator Crystals [6,7]

Cd- impurity doping can be used in the synthesis of BaF_2 scintillator crystals to diminish the oxygen contamination during the crystal growth.

The EPR of the Cd_c^+ centres has previously been reported (Cd_c^+ is placed on a regular cation lattice site) [19*]; the EPR spectrum of the γ- irradiated BaF_2 crystal (crystal of type I, see [6]) is shown, for comparison, in Fig. 6.b. We observed in the γ- irradiated BaF_2 crystals another EPR spectrum [6] which is shown in Fig. 6.a. We related this spectrum to a perturbed Cd_c^+ centre. However, the nature of the perturbation remains unknown as yet. For this perturbed Cd_c^+ centre,

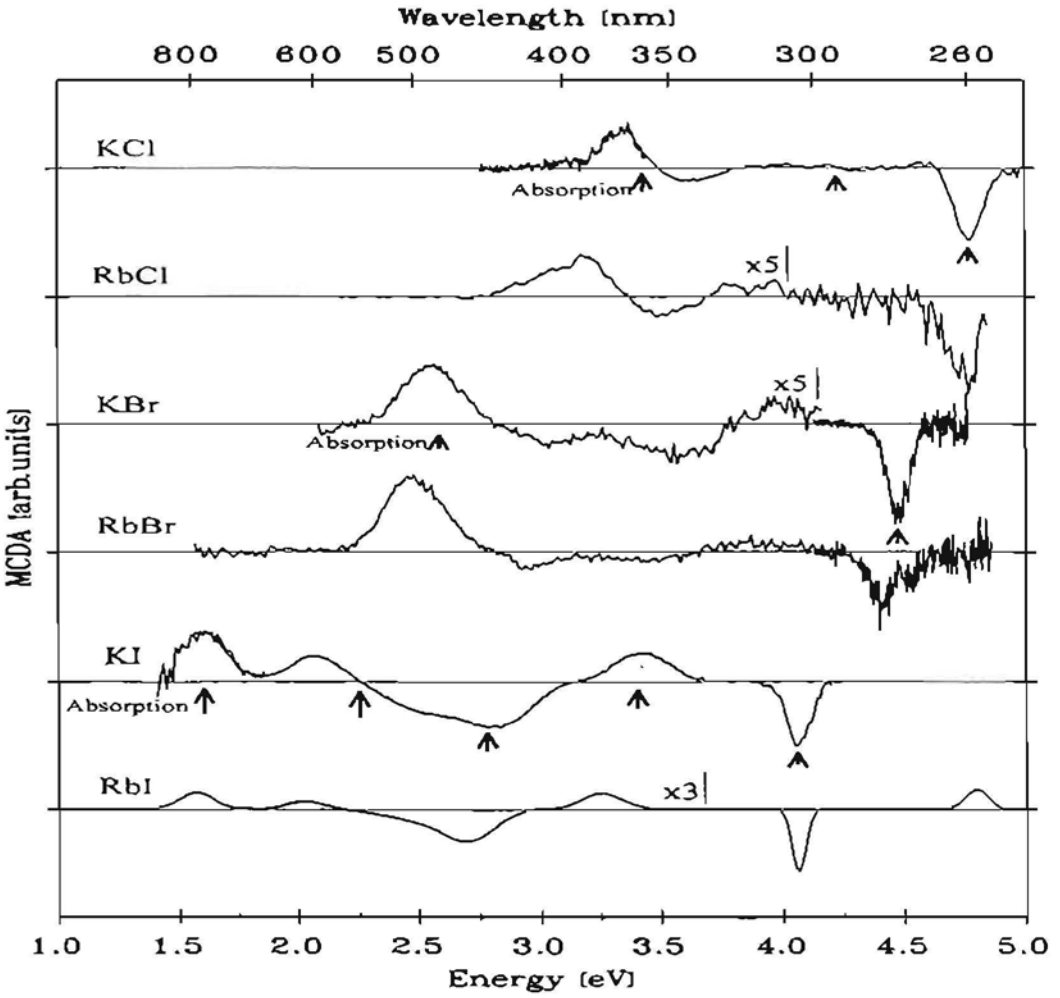

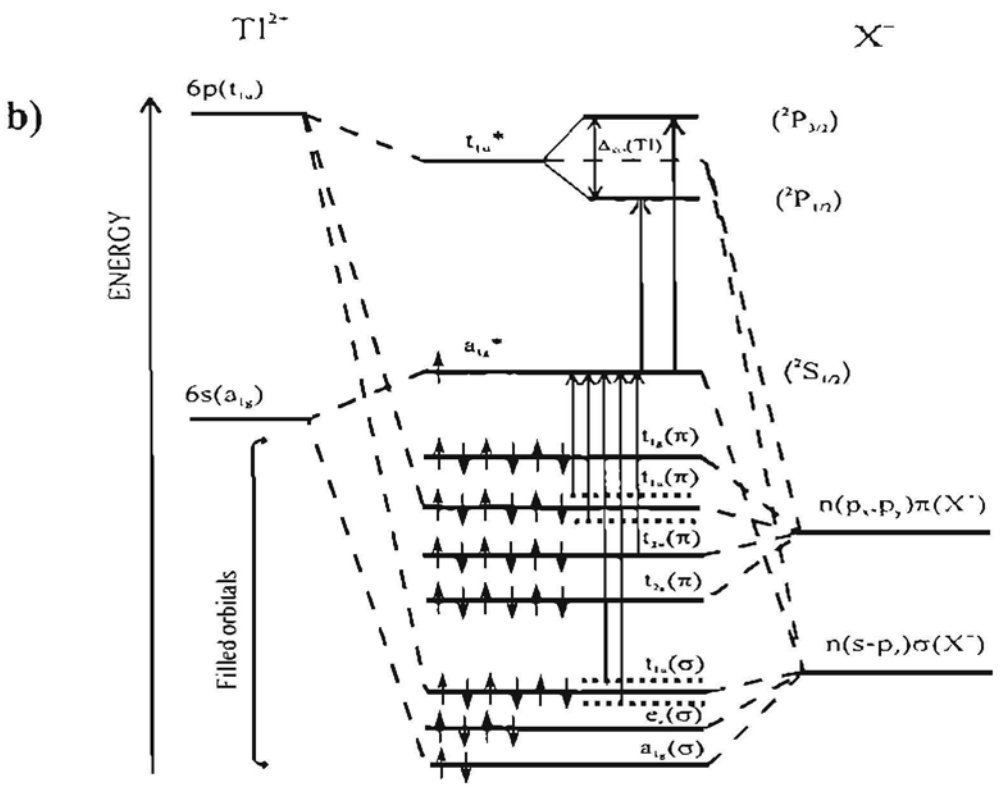

Fig. 5. a) Spectra of the 'tagged MCDA' of the Tl^{2+} centres in six alkali halide crystals [3].
b) Qualitative energy level diagram of a $[TlX_6]^{4-}$ octahedral complex (after [17*,18*,3,4]).

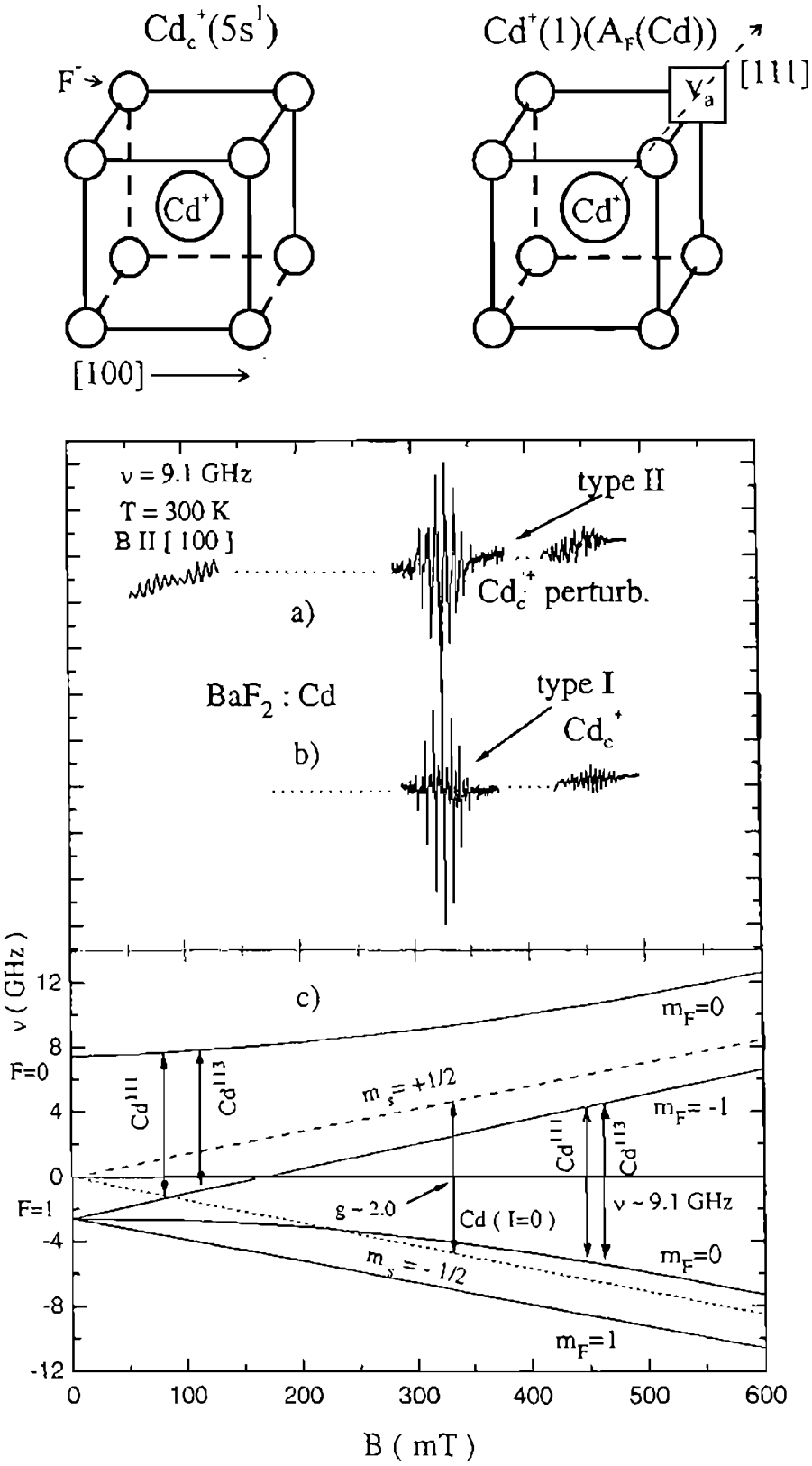

Fig. 6. Structure models of the Cd- related defects in BaF_2 crystals.

a) EPR spectrum of the perturbed Cd_c^+ centre in BaF_2:Cd crystal of type II. (Crystals of type II contained more uncontrolled impurities);

b) For comparison, the EPR spectrum of the known Cd_c^+ centre [19*];

c) Breit- Rabi diagram for the EPR spectrum of the perturbed Cd_c^+ centre.

the *hf*- interaction of the unpaired electron s^1 (S=1/2) with the Cd nuclear spins (two isotopes with spin I=1/2) is smaller than that of the unperturbed Cd_c^+ centre. Therefore it is possible to observe the low field group of the EPR lines in the 3 cm (9 GHz) microwave band (Fig. 6.a). The corresponding EPR transitions are shown in the Breit- Rabi energy diagram in Fig. 6.c.

The MCDA-EPR spectra are shown in Fig. 7.1 for γ- irradiated BaF_2:Cd crystals. The *hf*- splitting in the ODEPR spectrum of the Cd_c^+ centre is larger (Fig. 7.1, spectrum a) than the *hf*- splitting of the perturbed Cd_c^+ centre (Fig. 7.1, spectra b). In Fig. 7.2 the MCDA spectra are shown for different Cd impurity - related defects [6,7] as well as optical absorption spectra. The interpretation of the so-called A_F(Cd) centre we made in analogy with ref. [20*]. (The A_F(Cd) centre is a Cd_c^+ with a next nearest anion vacancy according to [20*]).

From the EPR and MCDA and MCDA- detected EPR investigations we estimated in the UV spectral region the presence of three Cd impurity - related defects in γ- irradiated BaF_2 scintillator crystals (Cd_c^+ , Cd_c^+ perturbed, Cd_c^+(1), Fig. 7.2.b,c). From the absorption measurements only it was impossible to identify the Cd impurity-related absorption bands since according to our experience other uncontrolled impurities can have absorption bands in the UV as well.

2.4. Model of the Molybdenum-Related Defect in $CdWO_4$ Scintillator Crystals |8|

$CdWO_4$ crystals are widely used as scintillators. We investigated the EPR in $CdWO_4$ crystals (which were 'coloured blue' after the crystal growth) at low temperatures. The EPR spectrum is shown in Fig. 8.a. The spectrum shows splittings which are positioned symmetrically about the intense central line. Splittings are found to be nearly isotropic and are caused by the superhyperfine (*shf*) interactions of the unpaired spin with several sets of equivalent neighbour nuclei. Only one EPR spectrum for an arbitrary orientation of the crystal could be observed, no site splitting due to non-equivalent centre orientations were present. We found the *shf* splittings due to Mo impurity isotopes with I = 5/2 (natural abundance 15.9% for Mo^{95} and 9.6% for Mo^{97}). We concluded that a Mo impurity is involved in the defect present. The crystals were not specially doped with Mo, but Mo is known to be a common uncontrollable impurity in $CdWO_4$ crystals.

In addition to Mo- splittings we see two additional pairs of *shf* lines. It was possible to take two alternative sets of *shf* parameters, which explained these additional *shf* lines. The first set of the parameters involves two different *shf* interactions W_1 and W_2 with three (W_1) and four (W_2)

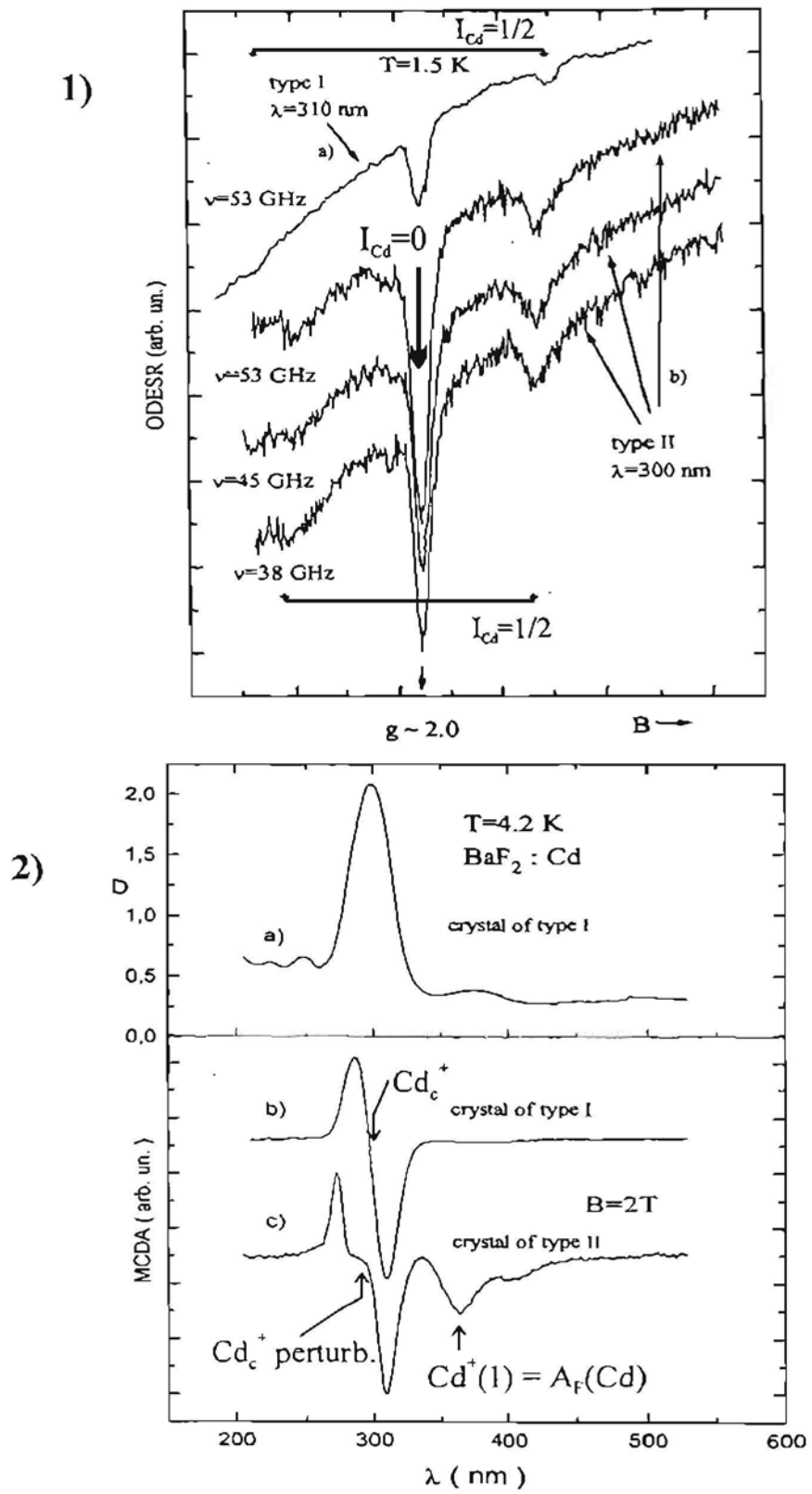

Fig. 7. 1) a) MCDA-EPR spectrum of the BaF_2:Cd (0.02 at.%) in crystals of type I, detected in the 310 nm MCDA band ;

b) MCDA-EPR spectra of the BaF_2:Cd in crystals of type II, detected in the 300 nm MCDA band. Spectra measured at different microwave frequencies are normalized to g = 2;

2) a) Spectrum of the γ ray-induced absorption of the BaF_2:Cd crystal of type I;

b) MCDA spectrum of the BaF_2:Cd crystal of type I;

c) MCDA spectrum of the BaF_2:Cd crystal of type II. The MCDA bands of the Cd- related defects are shown.

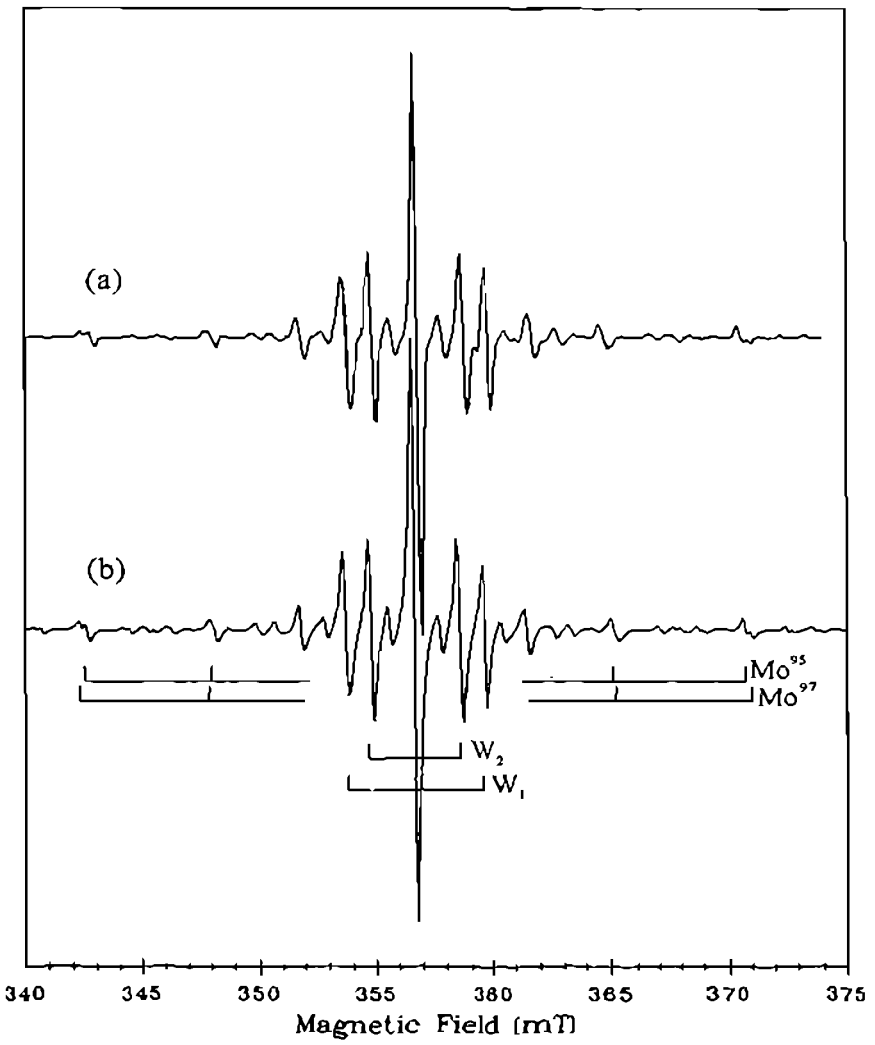

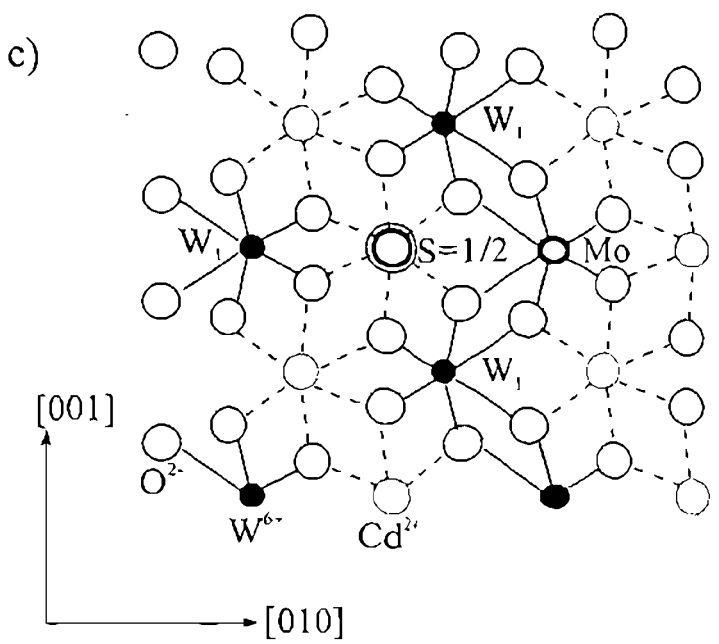

Fig. 8. a) EPR spectrum of a $CdWO_4$ crystal, measured at T = 20 K for B ∥ [010] applying a microwave frequency of 9.08 GHz;
b) Simulated EPR spectrum assuming *shf* interactions with one Mo nucleus and two sets of equivalent W nuclei [8];
c) Possible structural position of the unpaired spin S = 1/2 of the Mo- containing defect shown for the plane (100) of $CdWO_4$.

equivalent tungsten nuclei W^{183} (I = ½ with a natural abundance 14.3%). The simulated spectrum with this set of parameters is shown in Fig. 8.b, all details of the EPR spectrum are well reproduced, even the relative intensities of the main *shf* lines.

The second alternative set of parameters involves, besides the Mo *shf* interaction, involves two different *shf* interactions with two pairs of equivalent Cd neighbours (^{111}Cd has I = ½ with a natural abundance 12.8% and ^{113}Cd has I = ½ with a natural abundance 12.2%) and two additional W nuclei [8]. In this case the relative intensities of the main *shf* lines could not be reproduced exactly enough, such that we preferred in [8] the first set of the parameters as shown in Fig. 8.b.

The proposed model of the molybdenum - related defect is shown in Fig. 8.c (the structure of the $CdWO_4$ crystal is shown according [21*,22*]). We propose that Mo replaces one of the neighbour W atoms in one of the two existing W neighbour sets (one of the W sets is placed above and another one- below the Cd- site along the [100] axis). The unpaired electron has an electron spin S=1/2 and would be localised on a Cd site. However, it is not localized on a Cd ion, because we do not observe large additional splittings from such a central Cd nucleus (since the *shf* splittings are nearly isotropic, the spin density at the central nucleus should be high, which would lead to a large *shf* interaction). At present no relation of this EPR spectrum to the MCDA spectrum or to the EPR detected in luminescence could be found.

2.5. Investigations of the PO_4^{2-} and PO_3^{2-} Defects in Calcium Phosphate Glasses [9]

At the beginning of our present investigations of the x- irradiated phosphate glasses, the formation of the PO_4^{2-} and PO_3^{2-} radical centres had been established [23*-25*], as well as some structural models had been proposed. The EPR signals of the radical defects were known and in the case of the PO_4^{2-} radical also the induced absorption band at 2.4 eV had been attributed to this radical by indirect correlation methods [24*,25*].

The spectra of the EPR detected via MCDA of the X-ray irradiated calcium phosphate glasses are shown in Fig. 9.1. The *hf* splittings corresponding to the PO_4^{2-} as well as to the PO_3^{2-} radical defects have been identified. They are caused by the *hf* interaction of the unpaired spin of the centres with the ^{31}P nuclear spin I = ½ [23*-25*].

In the Fig. 9.2 the spectra of the induced optical absorption (spectrum a), and the MCDA spectrum (b) are shown for the X-ray irradiated calcium phosphate glass. By using the resonance field values of the ODEPR of the radical defects, the MCDA bands (corresponding to the PO_4^{2-}

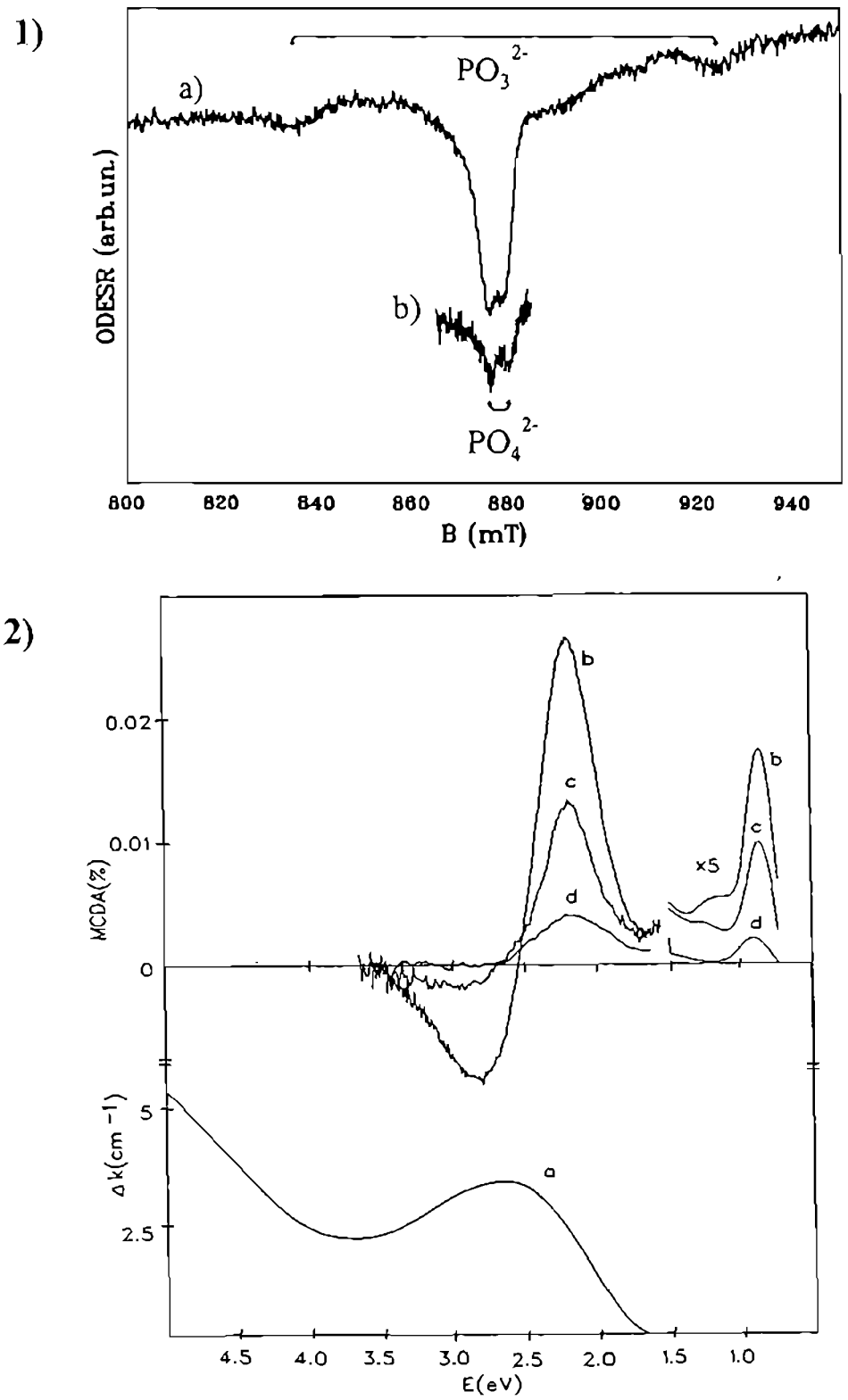

Fig. 9. 1) MCDA-EPR spectra of undoped $CaO-P_2O_5$ glass measured at 2.2 eV for T = 1.5 K (curve a) and T = 4.2 K (curve b);
2) a) Radiation-induced change of the optical absorption of a $CaO-P_2O_5$ glass after x-ray irradiation at 300 K;
b) MCDA spectrum of the x-ray irradiated $CaO-P_2O_5$ glass;
c) 'Tagged MCDA' spectra of the PO_4^{2-} centre, measured at B = 875 mT;
d) 'Tagged MCDA' spectra of the PO_3^{2-} centre, measured at B = 835 mT.

and PO_3^{2-} defects) could be separated (Fig. 9.2, spectra c and d). We concluded that the known absorption band at 2.4 eV indeed is related to the PO_4^{2-} radicals, but at these wavelengths partially also the MCDA of the PO_3^{2-} radicals overlaps. We found out that both of the radical defect centres have MCDA bands in the red and infrared spectral regions. These bands may be important considering the absorption of such radical defects in P- doped silicon dioxide optical waveguide materials.

3. INVESTIGATIONS OF DEFECT INTERACTION PROCESSES IN ALKALI HALIDES

In this chapter ODEPR and MCDA data have been used to investigate the cross-relaxation interaction between F and H centres as well as to study the mechanism of the photostimulated luminescence in some X-ray storage phosphor materials based on the AH crystals containing activators.

3.1. Investigation of the Interaction between Frenkel Pairs (F and H Centres) in KBr Crystals by Cross-Relaxation ODEPR Techniques [10-13]

Frenkel pairs play a fundamental role in the defect formation processes in AH crystals (see, for example, references in [26*]).

In section 2.1. we described the MCDA spectrum (Fig. 2.3.d) and the ODEPR spectrum (Fig. 2.2.a) of the H centre in KBr crystals. Therefore we knew the ODEPR spectra of F and H centres and the corresponding MCDA spectra of F and H centres (Fig. 10.1, curves 1 and 2, resp.) at low temperature (4.2 K) in X- irradiated KBr crystals. We observed the interaction between H and F centres as changes in the MCDA amplitude of the F centres, if we switched 'on' and 'off' the microwaves at the resonance magnetic fields of the H centre. These changes are shown in Fig. 10.2. We concluded that the changes in the spin polarization of the H centre ground state cause changes in the Zeeman level population of the F centre. These data were interpreted as the so - called cross-relaxation interaction between the spin systems of F and H centres. The magnetic field dependence of the cross-relaxation effect is shown in Fig. 11.1 and the corresponding energy level scheme in Fig. 11.2.

1)

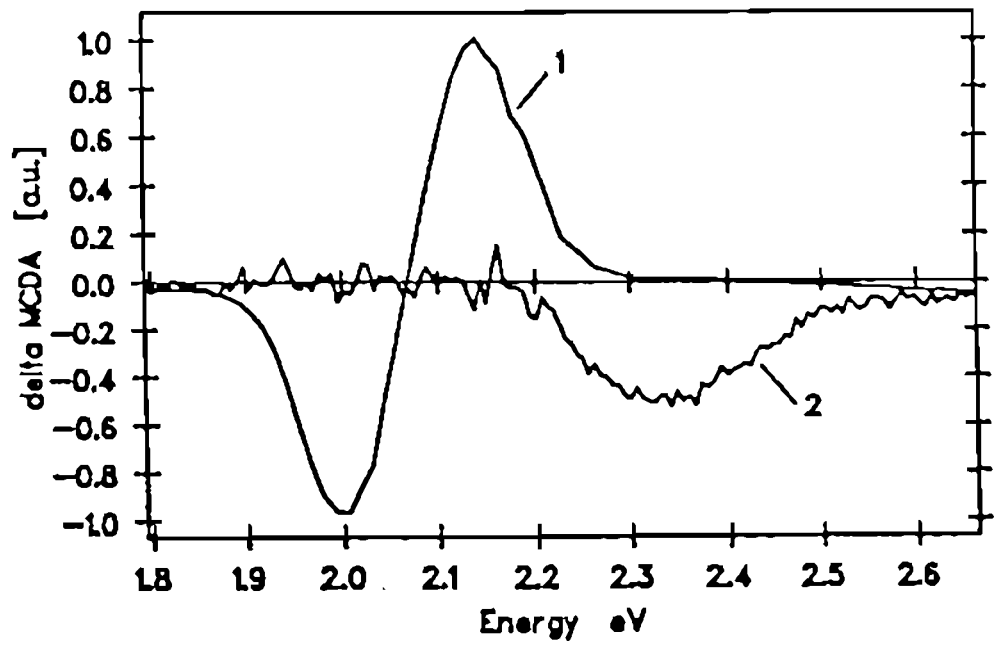

2)

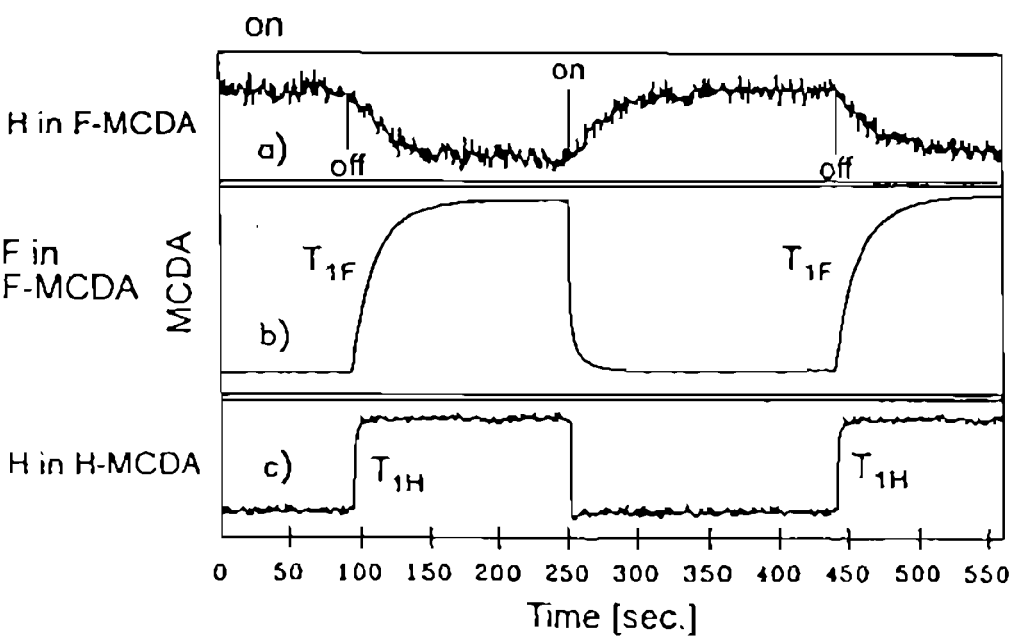

Fig. 10. 1) 'Tagged MCDA' spectra of F centres (1) and H centres (2) in KBr x-ray irradiated at 4.2 K;

2) Time-resolved measurements of the ODEPR effect after switching 'on' and 'off' microwaves:

a) Behaviour of the MCDA of the F centres when inducing the H- centre EPR (CR);

b) Behaviour of the MCDA of the F centres when inducing the F- centre EPR (T_{1F});

c) Behaviour of the MCDA of the H centres when inducing the H- centre EPR (T_{1H}).

1)

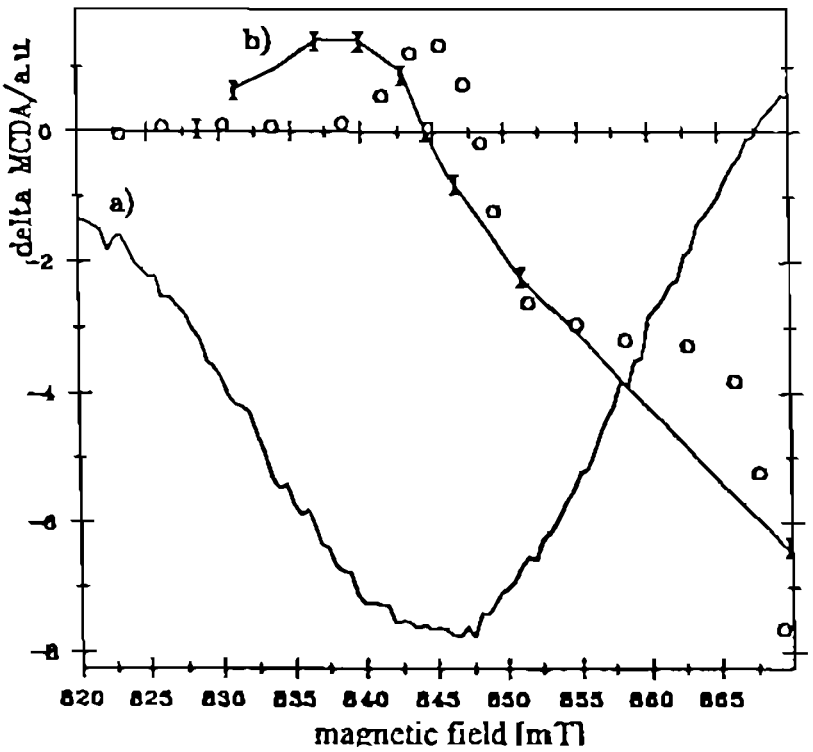

2)

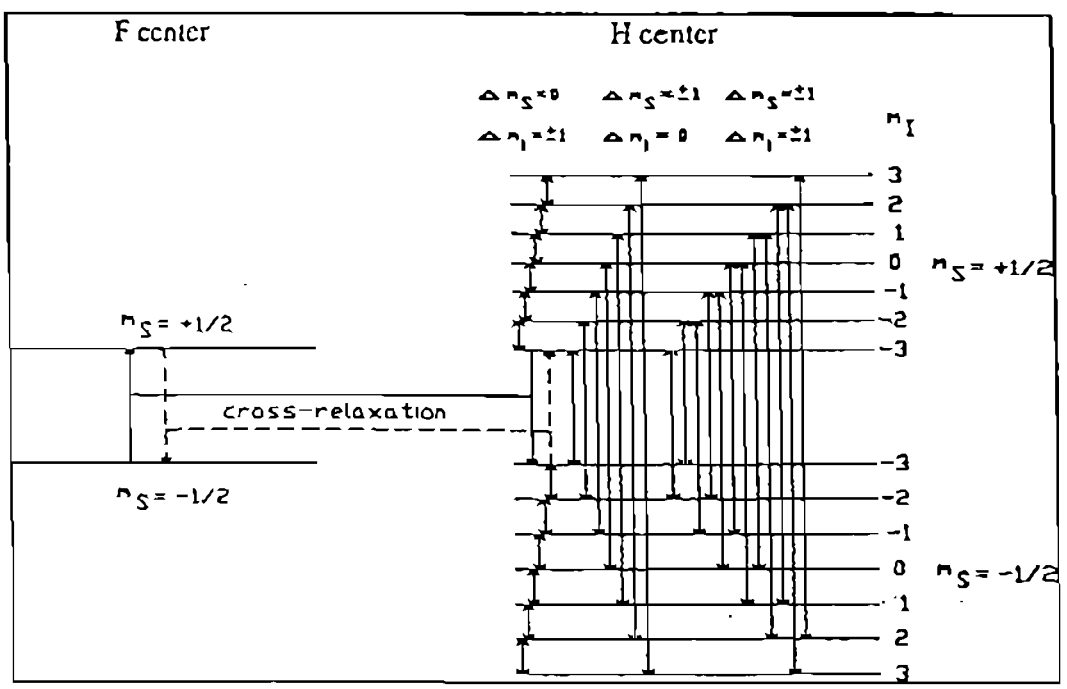

Fig. 11. 1) Cross-relaxation effect between F and H centres in KBr:
a) OD EPR spectrum of H centres in KBr;
b) I- measured cross-relaxation effect in the MCDA of the F centres;
o- calculated cross-relaxation effect [10];
2) Energy level-scheme for the cross-relaxation between F and H centres in KBr [10].

We showed that the spin systems of F and H centres are coupled in KBr crystals after X-irradiation at LHeT (4.2 K) and that the minimal distance between the F and H centres, for which a stable pair of F and H centres is formed upon exciton decay can be determined [10-13] to be 4 lattice spacings along a [110] direction. At shorter separations F and H centres recombine.

3.2. Investigation of the Photostimulated Luminescence Mechanism and Identification of the Hole-Trap Centres in the X-Ray Storage Phosphor RbI:Tl [14]

In order to investigate the processes in X-ray storage phosphor materials, it is necessary to identify the electron and, especially, hole trap centres with some 'direct' techniques, such as magnetooptical (MCDA and ODEPR) techniques.

At the beginning of our work, a hypothesis has been found in the literature [27*] that the V_{KA} centres (V_K centres trapped at a Tl^+ impurity) may act as the hole trap centre in RbI:Tl crystals. The position of the F centre MCDA band was known (see [8*]), and we previously identified the MCDA of the Tl^{2+} centres (section 2.2.) and of the V_K centres (section 2.1.) by using ODEPR. The ODEPR spectra of the Tl^{2+} and V_K centres are shown in Fig. 12.1, and the corresponding MCDA bands in Fig. 12.2.

The changes of the MCDA bands after X-ray irradiation of a RbI:Tl crystal at low temperatures (T = 4.2 K to 80 K) are shown in Fig. 12.3. Immediately after the low temperature X-ray irradiation holes are mostly trapped as V_K centres and after thermal delocalisation of the V_K centres holes are mostly retrapped by Tl^+ forming the Tl^{2+} centres (Fig. 12.3.a). No retrapping of the holes to form V_{KA} centres (as proposed in [27*]), have been observed. We found, that holes can partially be retrapped back to V_K centres by bleaching with monochromatic light in any of the absorption (MCDA) bands of the Tl^{2+} centres (Fig. 12.3.b.). After repeated heating of the sample above the thermal delocalization temperature of the V_K centres, it was possible to retrap again the holes at Tl^+ forming Tl^{2+} centres (Fig. 12.3.c), i.e. the reaction is reversible $V_K \leftrightarrow Tl^{2+}$. Therefore, the MCDA measurements allowed us to sensitively follow the localization and retrapping of the holes in RbI:Tl crystals. To perform such investigations only with absorption measurements would not be sensitive and selective enough.

As a result of MCDA, ODEPR, EPR and luminescence measurements we could determine the direct correlation of the photostimulated luminescence intensity of RbI:Tl crystals with the MCDA- amplitude of the Tl^{2+} centres. We stated that the photostimulated luminescence of RbI:Tl crystal can be explained by a simple {F* -- Tl^{2+}} centre recombination model [14].

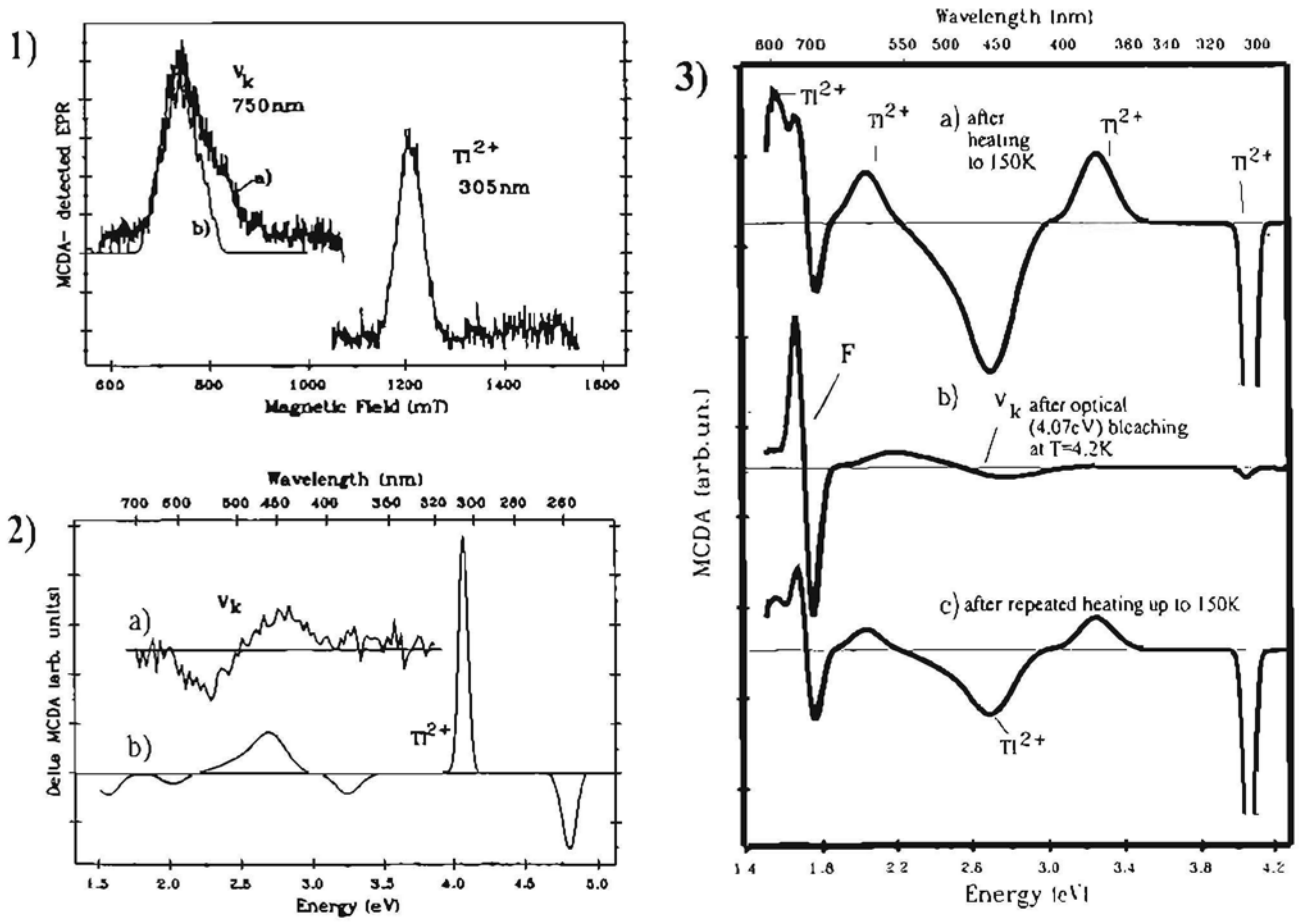

Fig. 12. 1) MCDA- detected EPR spectra in RbI:Tl crystal:
a) of V_K centres, measured at 1.56 eV;
b) of Tl^{2+} centres, measured at 4.07 eV;

2) 'Tagged MCDA' spectra of the V_K centres (a) and of Tl^{2+} centres (b) in RbI:Tl;

3) MCDA spectra of the RbI:Tl crystal, measured at T = 4.2 K and B= 2 T after x-ray irradiation at T = 80 K:
a) after heating to T = 150K;
b) after optical (4.07 eV) bleaching at T = 4.2 K;
c) after repeated heating to T = 4.2 K.

For the crystal KBr:In a similar simple pair model was proposed in [28*], but our ODEPR and MCDA investigations did not confirm this. At first, the MCDA of the In^{2+} centre, which we found in RT X-irradiated KBr:In, did not correlate with the PSL [15-17]. Secondly, the so - called 'replenishment' of the PSL has been found. It is not possible to explain the 'replenishment' effect in the simple {F* -- In^{2+}} pair model [16]. In recent investigations of the X-ray storage phosphor material RbBr:Ga [18], which will be continued, it was found, that there exist two Ga^{2+} type centres: one of them is found to correlate with the PSL, but the second Ga^{2+} centre does not.

Thus, the magnetooptical (MCDA, ODEPR) technique was helpful to investigate defects and processes in X-ray storage phosphor materials on the basis of AH crystals doped with activators.

4. INVESTIGATIONS OF THE ODEPR OF SELF- TRAPPED EXCITONS

4.1. ODEPR of Type I Self-Trapped Excitons in NaBr Crystals [19,20]

Self-trapped excitons (STE) in AH crystals are V_K (X_2^-) centres with a trapped electron in a first approximation [29*]. The radiative excited states of the STE's may be nearly symmetric ('on- centre' STE, or type I, in NaBr, NaI crystals) or more or less asymmetric ('off- centre' or types II, III for other AH with NaCl structure) [30*]. At the beginning of our work, the ODEPR spectra had been detected for several 'off- centre' (mostly type III) STE's, but not for the STE of the type I ('on- centre') [29*].

We measured the ODEPR spectrum of the STE in a NaBr crystal [19]. At the beginning we suggested that the broad ODEPR band with a plateau in the central part of the band is caused by the two transitions of the STE triplet state and that the zero field splitting parameter D of the STE in the NaBr crystal is very small [19]. Later, Japanese researchers [31*] measured the ODEPR of the STE of NaBr crystal with another microwave frequency. They interpreted their ODEPR resonance together with our ODEPR spectrum and concluded that the zero-field parameter D of the STE in NaBr crystal has to be much larger [31*]. According to their work we observed in our first experiments only one of the two triplet state resonance transitions. We verified this interpretation and confirmed that, indeed, the zero-field value D may be very large [20]. The line shape of the ODEPR transitions is affected by different dynamical effects of the nuclear substates and therefore the amplitude of the *hf-* transitions may significantly differ from the expected

statistical occupation values of these states [20]. This explained the 'flat' line shape observed in ODEPR which first led to the wrong interpretation of the spectrum.

4.2. Investigations of the ODEPR of the Self-Trapped Excitons in Li_2GeO_3 Crystals [21]

The structure of a Li_2GeO_3 crystal consists of GeO_4 tetrahedron chains with Li ions between them (Fig. 13.a [32*]). The luminescence spectrum of Li_2GeO_3 crystals was known under X-ray or UV excitation [22]. It has been suggested that this luminescence may be caused by the excited state of the STE.

We investigated this luminescence with ODEPR techniques under the X-ray excitation and observed the ODEPR resonances which are shown in Fig. 13.b. The resonance line positions are generally dependent on the angle between the crystal axis and the direction of the external magnetic field. The angular dependence for rotation in the plane a-c is shown in Fig. 14.a. We described these angular dependent resonance spectra by the conventional *spin- Hamiltonian* for a triplet spin systems [7*,29*]:

$$H = \mu_B \mathbf{B} g \mathbf{S} + D[S_z^2 - 1/3S(S+1)] + E(S_x^2 - S_y^2)$$

where D and E are zero-field splitting parameters.

The low field resonances at about 310 mT are nearly isotropic and have been attributed to so - called 'forbidden' transitions $|\Delta m_S| = 2$ (Fig. 14.a,b.). The angle- dependent groups of lines positioned around the field values of 770 mT was attributed to the 'allowed' transitions with $|\Delta m_S| = 1$.

We had to assume the existence of two triplet states T_1 and T_2 in the Li_2GeO_3 crystal to explain all of the observed ODEPR lines. Both triplet states have very similar values of the angles of the principal axes of the zero-field splitting (fine-structure interaction) tensors. These directions are noted by *FS* in Fig. 14.c and they are very close to the *Ge--nonbridging oxygen* bond directions [21].

Therefore, the ODEPR data together with the luminescence polarization measurements, photoluminescence life-time and temperature dependence measurements allowed us to detrmine the model of the STE triplet excited states in Li_2GeO_3 crystal [21].

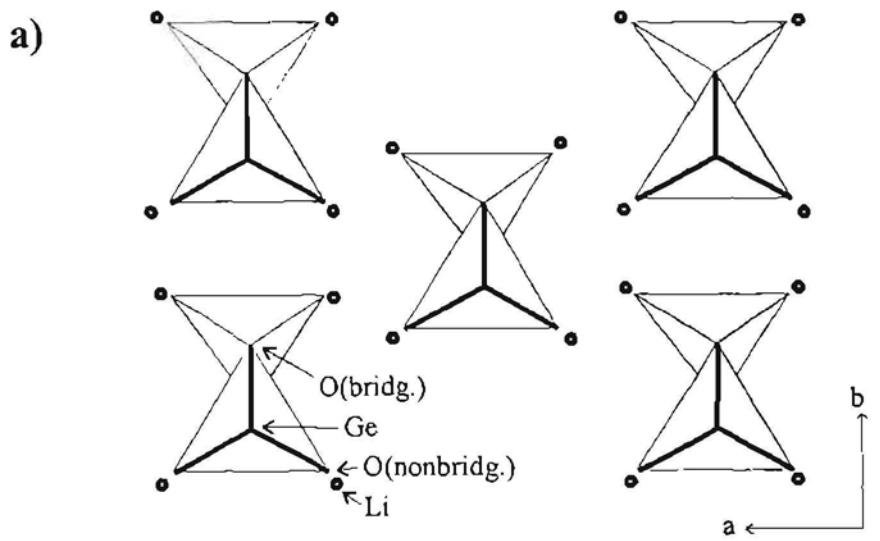

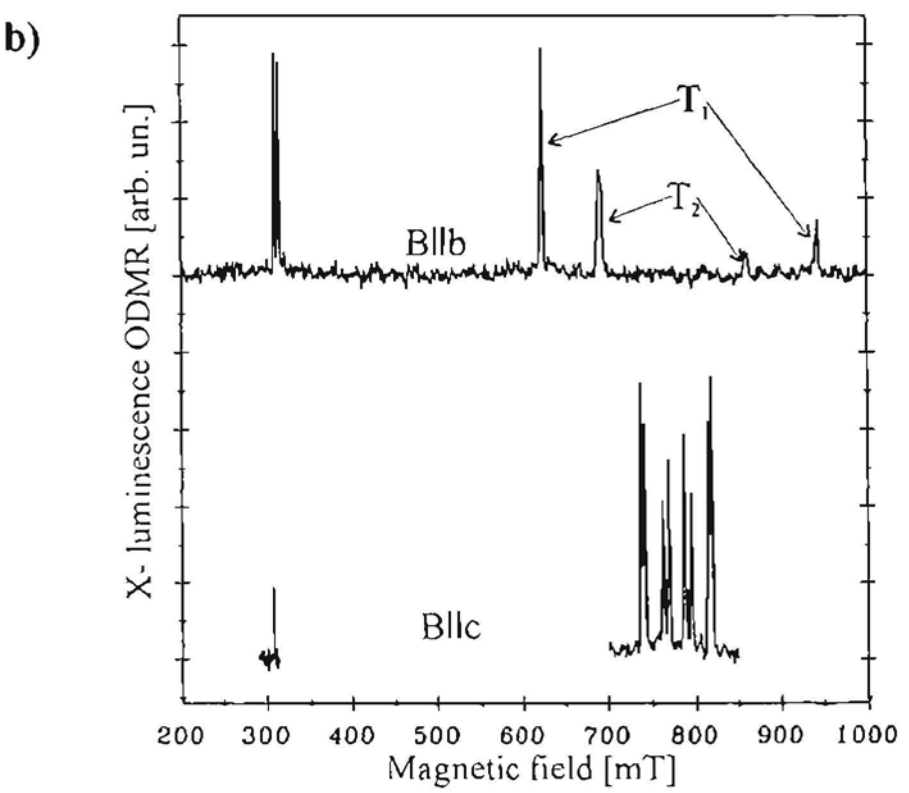

Fig 13. a) Li_2GeO_3 structure in the a-b plane (after [32*]);
b) ODEPR detected in the x-ray induced luminescence of Li_2GeO_3 at 1.5 K as a change in total luminescence intensity (K- band, 24 GHz).

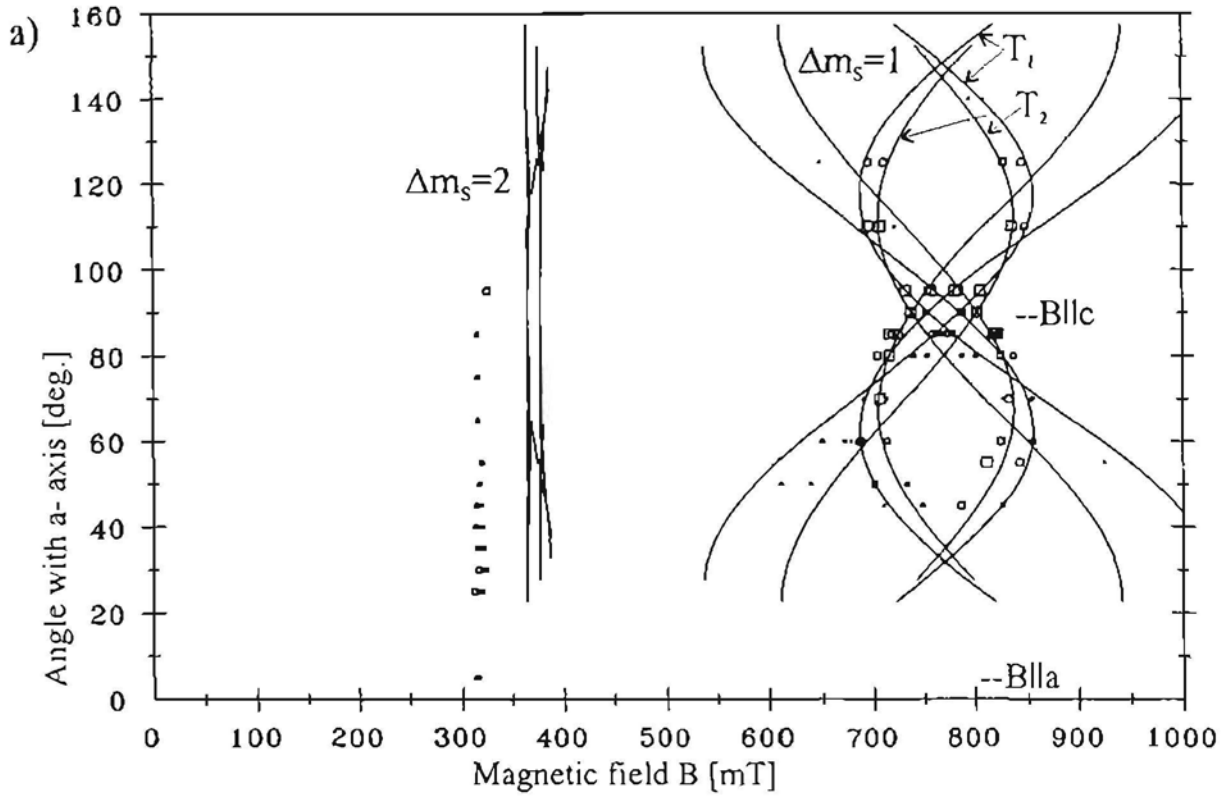

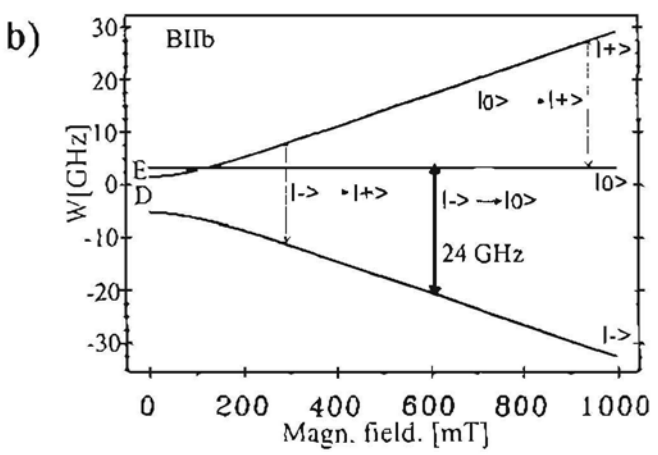

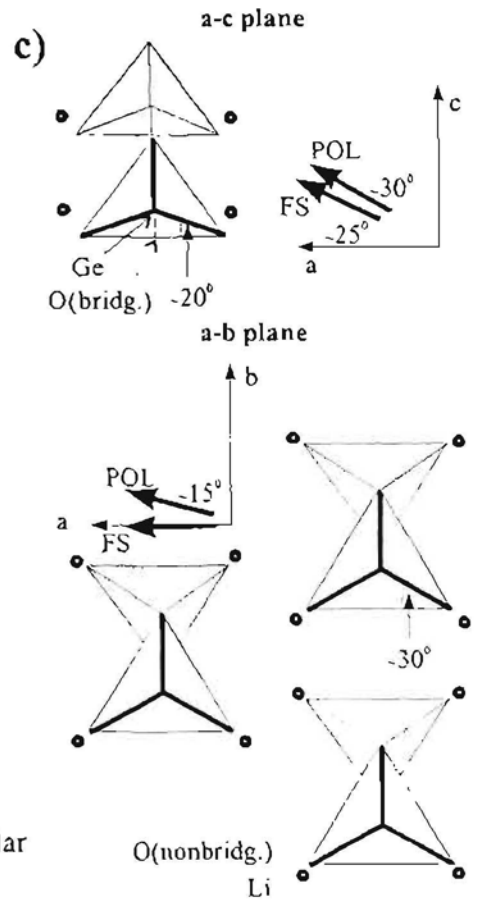

Fig. 14. a) OD EPR- angular dependence in the a-c plane of the Li_2GeO_3. Squares mark the line positions, solid lines are calculated for two parameter sets T_1 and T_2;

b) The energy level scheme of the triplet state for the magnetic field, perpendicular to the principal axis of the D tensor;

c) The angular positions of the FS and polarization (POL) axes in the a-c and a-b planes of the Li_2GeO_3 crystal.

5. ABSTRACT OF HABILITATION THESIS

1. With investigations of the optical absorption, magnetic circular dichroism (MCDA) in combination with the EPR of the electronic ground state, the following absorption bands related to definite defects have been detected and singled out in insulator materials:

- The partially allowed transitions $^2\Sigma_u^+ \leftrightarrow {}^2\Pi_u$ appeared in the MCDA spectra of V_K centres in alkali- halide (AH) crystals.
- Up to 7 optical transitions can be observed in the MCDA spectra of Tl^{2+} defects in AH crystals. The long-wavelength MCDA bands of the Tl^{2+} defects in AH are explained as spin-orbit split charge transfer transitions involving the neighbour halogens.
- Three Cd- impurity- related defects are possible in BaF_2 scintillator crystals with absorption bands in the UV spectral region: an electron trapped on a Cd^{2+} ion in a regular cation site (Cd_c^+ centre), a Cd_c^+ centre perturbed by an unknown perturbation and an anion vacancy perturbed $Cd^+_c(1)$ centre.
- The presence of a molybdenum-related defect is determined in $CdWO_4$ scintillator crystals which are 'coloured blue' after crystal growth. In the proposed structure model an unpaired electron is situated on a Cd-site and a Mo ion replaces one of the neighbour W ions.
- New MCDA (absorption) bands of the PO_4^{2-} and PO_3^{2-} radical defects are observed in X-ray irradiated calcium phosphate glasses in the infrared spectral region (used for optical waveguides).

2. Some defects involved in interactions have been identified in the optically detected EPR experiments:

- Direct experimental evidence has been found for spatial correlation of Frenkel pairs (F and H centres) after their generation at low temperature in KBr crystals. Changes in spin-population of the F centre ground state have been observed due to the cross-relaxation interaction when inducing magnetic resonance of the H centres.
- The Tl^{2+} hole centre acts as an active hole centre in the photostimulated luminescence of the X-ray irradiated RbI:Tl crystal, and the simple pair $\{F^*\text{--}Tl^{2+}\}$ model describes the photostimulation process.

3. The self- trapped excitons in a Li_2GeO_3 crystal have two excited triplet states, according to the ODEPR data. For both triplet states the direction of the principal axes of the zero-field interaction tensors are very close to the direction of the *Ge--nonbridging oxygen* bond.

6. EPILOGUE

The main results of the work have been in many cases obtained by optical detection of the EPR which gives the direct information about the relation between the optical and EPR characteristics of a defect. It would be impossible to get such an information from separate optical or EPR measurements. There is a still perspective to continue the ODEPR investigations for X-ray storage phosphor and scintillator materials, as well as for other materials.

The practical role of this work for Latvia and the Baltic region is that, for the first time, ODEPR techniques have been developed and used in this region. From an international point of view, the systematic ODEPR investigations in this work in several classes of the wide-band gap materials are remarkable, with a main trend which is the systematic determination and identification of the hole trap centres and their optical properties and the investigation of some materials with a practical use for the X-ray memory screens and scintillators.

This work was performed in the Institute of Solid State Physics, University of Latvia, in very close collaboration with continuous support from the Department of Physics, University of Paderborn, Germany.

About 22 published papers are related to the topics of this Thesis. The main results of this research were reported at nine scientific conferences and symposiums. The contribution of the author of this Thesis in his papers published in cooperation with other colleges is: the MCDA and ODEPR spectra measurements, the quantitative analysis of the spectra and, in most cases, their qualitative interpretation.

The author expresses gratitude to colleagues from the Institute of Solid State Physics, University of Latvia, but especially to the Department of Crystal physics and the Head of the Department Prof. I. Tale for the support of this work during many years.

The author is very grateful to the colleagues of the research group of Prof. Dr. J.-M. Spaeth, University of Paderborn, for the opportunity to do a great part of the MCDA and ODEPR investigations at liquid helium temperatures, and especially to Prof. Dr. J.-M. Spaeth for the continuous support during many years, many fruitful discussions and the motivation to continue these investigations.

For support in the period of the building of the equipment for the MCDA and ODEPR investigations in the ISSP, at the beginning of the work, the author thanks Prof. A. Silins, Prof. J. Kliava, Dr. hab. Phys. M. Springis, Dr. Hab. Phys. L. Chugunov, Prof. A. Trukhin and Dr. hab. Phys. D. Millers.

The author is much oblidged to recent colleagues of the group of the perspective research of the ISSP and especiallly to Dr. Phys. J. Trokss and Dipl. Phys. D. Brics without whose enthusiasm the functioning of the ODEPR equipment in ISSP would be impossible.

The author thanks Prof. K.S. Song and Prof. M: Moreno for discussions and cooperation to explain theoretically the origin of the MCDA bands.

The author is obliged to his first scientific supervisors Doc. V. Grabovskis and Prof. I. Vitols for an experience in optical and low temperature techniques.

Special thanks I give to my wife Mag. Phys. A. Rogule for her continuous support and patience during the course of the whole work.

REFERENCES

1*. S. Geschwind, in *Electron Paramagnetic Resonance* (Ed. By S. Geschwind, New York: Plenum Press) 1972, pp. 233-425.

2*. J.-M. Spaeth, J.R. Niklas and R.H. Bartram. *Structural Analysis of Point Defects in Solids, Springer Series in Solid State sciences 43* (Heidelberg: Springer) 1992.

3*. P.G. Baranov, Bull. Acad. Sci. USSR, Phys. Ser., 1981, vol. 45, p. 23.

4*. N.G. Romanov, Bull. Acad. Sci. USSR, Phys. Ser., 1985, vol. 47, p. 2054.

5*. J.-M. Spaeth and F. Lohse. J. Phys. Chem. Solids, 1990, vol. 51, p.861.

6*. W.B. Lynch and D.W. Pratt, Magn. Reson. Rev, 1985, vol. 10, p.111.

7* I.Y. Chen, *Triplet State ODMR Spectroscopy* (Ed. R.H. Clark, New York: Willey), 1982.

8*. W.B. Fowler, *The Physics of Color Centers* (Ed. W.B. Fowler, New York: Academic Press) 1968.

9*. T.G. Castner and W. Känzig, J. Phys. Chem. Solids, 1957, vol.3, p.178.

10*. D. Schoemaker, Phys. Rev., 1973, vol. B7, p.786.

11*. C.J. Delbecq, W. Hayes and P.H. Yuster, Phys. Rev., 1961, vol. 121, p. 1043.

12*. J.-M. Spaeth, W. Meise and K.S. Song, J. Phys.: Condens. Matter, 1994, vol. 6, p.1801.

13*. G. Blasse, J. Alloys Compd., 1993, vol. 192, p.17.

14*. J.-M. Spaeth, Th. Hangleiter, F.-K. Koschnick and Th. Pawlik, Radiat. Eff. Defects Solids, 1995, vol. 135, p. 499.

15*. W. Dreybrodt and D. Silber, Phys. Status Solidi, 1967, vol. 20, p. 337.

16*. S.V. Nistor, D. Schoemaker and I. Ursu, Phys. Status Solidi (b), 1994, vol. 185, p. 9.

17*. C.J. Ballhausen and H.B. Gray, *Molecular Orbital Theory* (New York: Benjamin), 1965, p.103.

18*. M. Moreno, J.Phys.C.: Solid State Physics, 1979, vol. 12, L921.

19*. V.F. Krutikov, N.I. Silkin and V.G. Stepanov, Sov. Phys. Sol. State, 1976, vol.18, p.2958.

20*. N.G. Romanov, V.V. Dyakonov, V.A. Vetrov and P.G. Baranov, Phys. Stat. Sol. (b), 1988, vol.147, K171.

21*. R.W.G. Wyckoff, Crystal Structures (2nd edn., New York: Interscience), 1965, vol. 3, pp.42-43.

22*. A. Watterich, G.J. Edwards, O.R. Gilliams, L.A. Kappers, D.P. Madecsi, K. Raksanyi and R. Voszka, J. of Phys. Chemistry of Solids, 1991, vol.52, pp.449-455.

23*. G.O. Karapetyan, A.K. Sherstyuk and D.M. Yudin, Opt. Spektrosk., 1967, vol.22, p.443.

24*. T.V. Bocharova, G.O. Karapetyan and O.A. Yaschurschinskaya, Sov. Phys. Chem. of Glasses, 1985, vol.11, p. 677.

25*. M.N. Vilchinskaya, A.V. Dmitryuk, E.G. Ignatyev, G.O. Karapetyan and G.T. Petrovskii, Sov. Phys.- Dokl., 1984, vol. 274, p.158.

26*. N. Itoh, Advances in Physics, 1981, vol. 31, p. 491.

27*. M. Thoms, H. von Seggern and A. Winnacker, J. Appl. Phys., 1994, vol. 76, p. 1800.

28*. P.F. Braslavets, A. Kalnins, I. Plavina, A.I. Popov, B.I. Rapoport and A. Tale, Phys. Stat. Sol. (b), 1992, vol. 170, p. 395.

29*. K.S. Song and R.T. Williams, *Self- Trapped Excitons, Springer Series in Solid State Sciences 105* (Heidelberg: Sprienger), 1993.

30*. K. Kan'no, T. Tanaka and T. Hayhashi, Rev. Sol. State Sci., 1990, vol. 4, p. 383.

31*. K. Kan'no, M. Shirai, M. Matsumoto and I. Akimoto, Proc. 13th ICDIM (Wake Forest University), 1996.

32*. H. Wöllenkle, A. Wittmann, Monatshefte für Chemie, 1968, vol. 99, p. 244.

AUTHOR'S PUBLICATIONS

1. U. Rogulis, W. Meise and J.-M. Spaeth, Optically detected magnetic resonance of V_K and H centers in KBr and KI crystals. In: Defects in Insulating Materials, ed. by O. Kanert, J.-M. Spaeth, World Scientific, Singapore, 1993, vol.1, pp. 468-470.

2. U. Rogulis, K.S. Song and J.-M. Spaeth, Magneto-optical properties of the UV absorption bands of V_K centers in alkali halides. Journal of Physics: Condensed Matter, 1995, vol.7, pp. 7699-7708.

3. U. Rogulis, J.-M. Spaeth, I. Cabria, M. Moreno, J. Aramburu and M.T. Bariusso, Optical properties of Tl^{2+} hole centres in alkali halides. Part I: Investigation with optical detection of paramagnetic resonance, Journal of Physics: Condensed Matter, 1998, vol. 10, pp. 6473-6479.

4. I. Cabria, M. Moreno, J. Aramburu, M.T. Bariusso, U. Rogulis and J.-M. Spaeth, Optical properties of Tl^{2+} hole centres in alkali halides. Part II: MS-Xa calculations. Journal of Physics: Condensed Matter, 1998, vol. 10, pp. 6481- 6490.

5. J.-M. Spaeth and U. Rogulis, Optical properties of Tl^{2+} hole centres in alkali halides investigated with optical detection of paramagnetic resonance. Rad. Eff. and Def. in Solids, 1998 (in press).

6. U. Rogulis, J.Trokss, A.Veispals, I.Tle, P.Kulis and M.Springis, ODMR of Cd impurity centers in γ- irradiated BaF_2 crystals. Radiation Effects and Defects in Solids, 1995, vol.135, pp. 361-365.

7. M.Springis, A.Veispals, P.Kulis, U.Rogulis, I.Tale and J.Trokss, Optical and spectral properties of the Cd-containing BaF_2. Proceedings of Int. Conf. on Inorganic Scintillators and Their Applications SCINT'95, Delft, 1996, Delft Univ. Press, Netherlands, pp. 403-406.

8. U. Rogulis, EPR of Molybdenum-related Defect in $CdWO_4$. Radiation Measurements, 1998, vol. 29, No 3-4, pp. 287-289.

9. D. Brics, J. Ozols, U. Rogulis, J. Trokss, W. Meise and J.-M. Spaeth, Magnetic circular dichroism of the optical obsorption and optically detected ESR of X- irradiated Tb^{3+} doped and undoped $CaO-P_2O_5$ glasses. Solid State Communications, 1992, vol. 81, pp. 745-748.

10. W. Meise, U. Rogulis, F.K. Koschnick, J.-M. Spaeth. Direct experimental evidence for the spatial correlation of F and H centers in alkali halides after their generation at low temperatures, In: Defects in Insulating Materials, ed.by O.Kanert, J.-M.Spaeth, World Scientific, Singapore, 1993, vol.2, pp. 1078- 1081.

11. F.K. Koschnick, W. Meise, U. Rogulis, J.-M. Spaeth, R.S. Eachus. Spatial correlation of radiation- induced defects in BaFBr and KBr studied by cross- relaxation ODMR

spectroscopy. In: Defects in Insulating Materials, ed.by O.Kanert, J.-M.Spaeth, World Scientific, Singapore, 1993, vol.1, pp. 252- 266.

12. J.-M.Spaeth, F.K.Koschnick, W.Meise and U.Rogulis, Cross relaxation in magnetic resonance as a tool to study spatial correlations between defects in insulators. Nuclear Instruments and Methods in Physics Research, 1994, B91, pp. 175-182.

13. W.Meise, U. Rogulis, F.K. Koschnick, K.S. Song and J.-M. Spaeth, Experimental evidence for spatial correlation between F and H centres formed by exciton decay at low temperatures in KBr. Journal of Physics: Condensed .Matter, 1994, vol.6, pp. 1815- 1824.

14. U. Rogulis, C. Dietze, Th. Pawlik, Th. Hangleiter and J.-M. Spaeth, Identification of the hole- trapping sites and the mechanism of the photostimulated luminescence of the X- ray storage phosphor RbI:Tl^+. Journal of Applied Physics, 1996, vol.80, pp. 2430-2435.

15. U.Rogulis, J.-M.Spaeth, I.Tale and E.Ruzha, ODEPR of indium colour centres in the X-irradiated storage phosphor KBr-In. Radiation Effects and Defects in Solids, 1995, vol.134, pp. 471-475.

16. U.Rogulis, I.Tale, Th.Hangleiter and J.-M.Spaeth, The photostimulation process in the X-ray storage phosphor KBr-In. Journal of Physics: Condensed Matter, 1995, vol.7, pp.3129-3137.

17. Th. Hangleiter, U.Rogulis, C.Dietze, J.-M.Spaeth, P.Willems, L.Struye and P.J.R.Leblans, The X-ray storage phosphors RbI:Tl^+ and KBr:In^+ and other In^+ and Ga^+ doped alkali halides. Proceedings of Int. Conf. on Inorganic Scintillators and Their Applications SCINT'95, Delft, 1996, Delft Univ. Press, Netherlands, pp. 452- 455.

18. U. Rogulis, S. Schweizer, S. Assmann, and J.-M. Spaeth, Ga^{2+} hole centers and photostimulated luminescence in the X-ray storage phosphor RbBr:Ga^+. J. of Applied Physics, 1998, vol. 84, No 8, pp. 1-6.

19. U. Rogulis, J.- M. Spaeth and K.S. Song, Optically detected magnetic resonance of the STE in NaBr. Journal of Physics: Condensed Matter, 1995, vol.7, pp. 4939-4947.

20. U. Rogulis, F.K. Koschnick, J.-M. Spaeth and K.S. Song, Zero Field Splitting and Line Shape of the ODMR of Self-Trapped Excitons in NaBr. Journal of Physics: Condensed Matter, 1997, vol. 9, pp.1-13.

21. U. Rogulis, A. Trukhin, J.-M. Spaeth and M. Springis, ODMR of triplet states of the self-trapped excitons in Li_2GeO_3 crystals. Materials Science Forum, 1997, vols. 239-241, pp.577-580.

22. A.N. Truhin, U. Rogulis, M. Springis, Self-trapped excitons in Li_2GeO_3. J. Luminescence 1997, vol.72-74, pp. 890-892.

Latvijas Universitātes Cietvielu Fizikas Institūts

Dr. Phys. Uldis Rogulis

DEFEKTU ELEKTRONISKĀS STRUKTŪRAS NOTEIKŠANA AR EPR OPTISKĀS DETEKCIJAS METODĒM IZOLATORU MATERIĀLOS

PIELIKUMS

Kopsavilkumā citēto habilitācijas darba autora publikāciju kopijas

Rīga, 1999

OPTICALLY DETECTED MAGNETIC RESONANCE OF V_k AND H CENTERS IN KBr AND KI CRYSTALS

U.Rogulis*, W.Meise, J.-M.Spaeth
Universität-GH Paderborn, FB Physik, Postfach 1621, D-4790 Paderborn
**Institute of Solid State Physics, University of Latvia, 19 Raina Bulvaris, 226098, Riga, Latvia*

Magnetooptical investigations on the fundamental hole centers, V_k and H, in the alkali halide crystals KBr and KI are presented to show the direct correlation between the optical absorption bands and the electron spin resonance (ESR) of these defects. Conventionally measured ESR data as well as optical absorption data of these centers are well known from the literature [1-7].

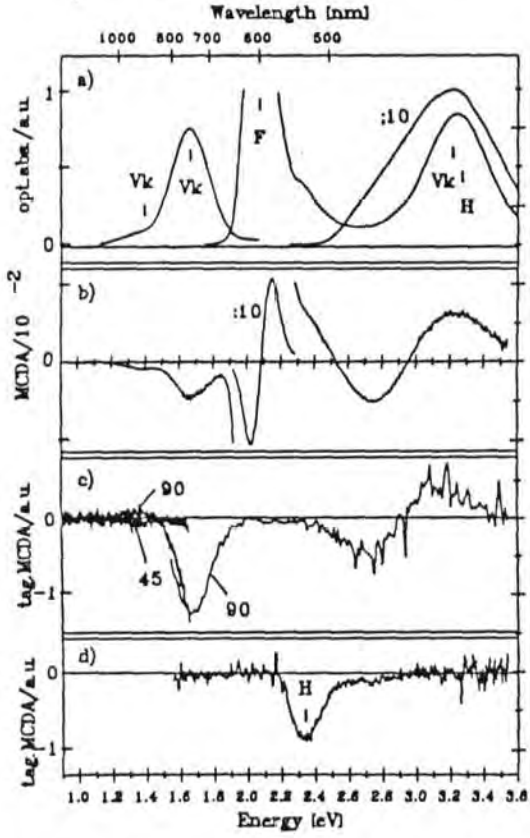

Fig. 1: a) optical absorption, literature data [1-7]. b) MCDA at B = 2T and T=1.5K of F, H and V_k centers in KBr x-irradiated at 4.2K, c) tagged MCDA of V_k centers, d) tagged MCDA of H centers.

Pure and Tl-activated KBr and KI crystals were used for the present investigations. The apparatus for the optically detected electron spin resonance (ODEPR) using the magnetic circular dichroism of the absorption (MCDA) is the same as that described in [8].

For the first time the magnetooptical transitions as well as ODEPR spectra of H and V_k centers are measured. Fig.1.b. shows the MCDA spectrum of a KBr crystal x-irradiated at 4.2K, containing F, V_k and H centers. For comparison, in Fig.1.a., the maxima of the absorption bands of V_k, F and H centers (from the literature) are presented.

The ODEPR spectra of V_k centers in the KBr crystal detected in the MCDA peaks at 2.7eV and 1.65eV are presented in Fig.2(b-d).

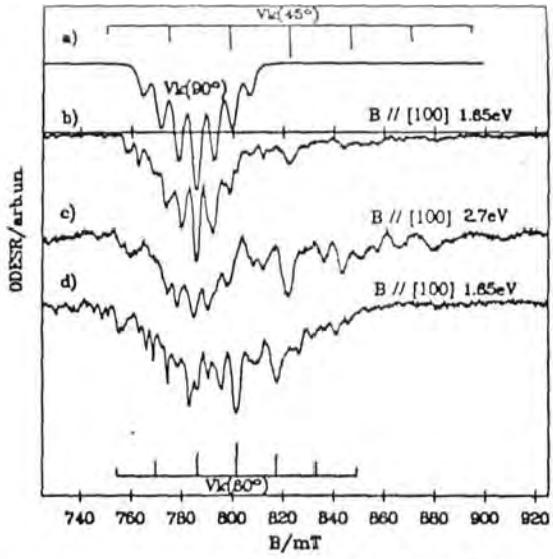

Fig.2: ODEPR spectra of a KBr crystal x-ray irradiated at 4.2K. a) simulation of 90° oriented V_k centers, b) c) d) ODEPR in the two MCDA bands at 2.7eV and 1.65eV of 90°, 60° and 45° oriented V_k centers.

We find in the ODEPR spectra mainly 90°, 60° and 45° oriented V_k centers.

Thus, using the method of "MCDA tagged by ESR" [8] we can separate out the MCDA from the V_k centers (Fig.1.c.).

In Fig.3.a. the broad unresolved ODEPR signal, centred at B=820 mT of pure KBr X-irradiated at 4.2K is shown, which we attribute to the H centers in KBr. The corresponding "tagged MCDA" spectrum is shown in Fig.1.d. In the absorption region of 2.2-2.5 eV we find the MCDA of the H centers.

This MCDA of H centers vanishes after annealing the crystal to 70K, where H centers are thermally destroyed. The MCDA and ODEPR spectra of the V_k centers in KI crystals have similar properties as those in KBr crystals with parameters changes, accordingly.

Using the ODEPR method we were able to detect the ODEPR spectrum in Fig.4.b.which we attribute to H center in KI. The parameter $g_\perp$ of the ESR spectrum for the H center is $g_\perp=2.08\pm0.01$. In contrast to previous estimates of the hyperfine parameters [2] that $A_\perp=0$ for H centers in KBr, we estimate the following hyperfine parameters for H centers in this crystal from an ESR line simulation: $A_\perp\approx5$mT. This value optimises the simulated ODEPR spectrum (Fig.3.b.). The linewidth $\Delta B_{1/2}$ of the single hf transitions is taken to be 5mT.

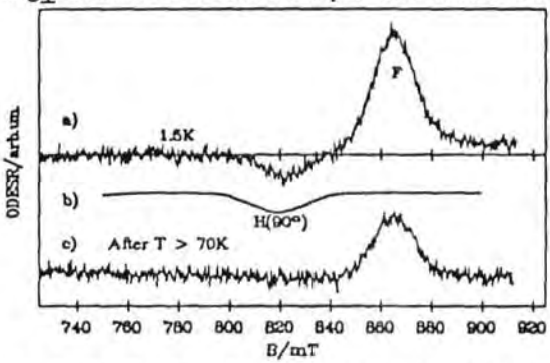

Fig.3: ODEPR of F and H centers in KBr x-ray irradiated at 4.2K. a) ODEPR in the MCDA at 2.4eV, b) simulated EPR spectrum of 90° oriented H centres, c) ODEPR in the MCDA band at 2.4eV after annealing the crystal to 70K. H centers are destroyed.

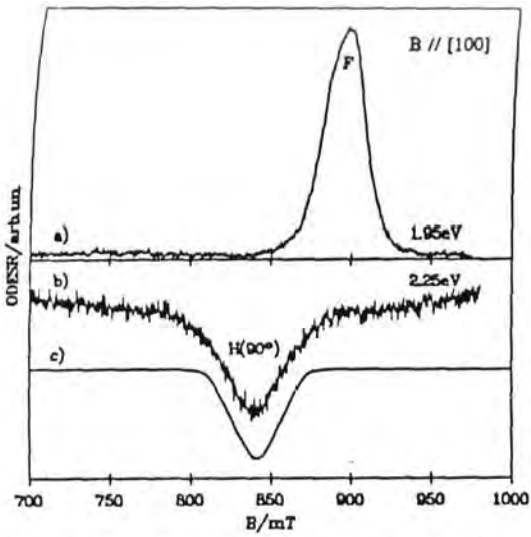

ODEPR of F and H centers in KI x-ray irradiated at 4.2K.
a) ODEPR of F centers measured in the F center MCDA band located at 1.95eV
b) ODEPR of H centers measured in the H center MCDA band located at 2.25eV
c) simulated EPR spectrum of H centers

The parameters for the ESR of the H center in KI are also about $A_{\perp}$=7mT, $\Delta B_{1/2}\approx$5mT. We note that for both V_k and H centers the ODEPR spectra of the 90° oriented centers with respect to the magnetic field are always dominant, while we do not detect the ODEPR of 0° oriented V_k and H centers.

Using the wave functions of the usual molecular ion model for V_k and H centers [3], the UV transition is fully σ-polarised ($\sigma_g \Rightarrow \sigma_u$) and there should be no MCDA at all in agreement with the failure to observe centers with their axis parallel to the magnetic field. The fact that we do see an MCDA and a ODEPR spectrum of perpendicular centers is due to the effect of the spin orbit interaction. Details of a corresponding calculation will be published elsewhere [9].

References.
1.)T. G.Castner and W. Kanzig, J. Phys. Chem. Solids 3 (1957) 178.
2.)W. Kaenzig and T. O. Woodruf, J. Phys. Chem. Solids 9 (1958) 70.
3.)D. Schoemaker, Phys. Rev. B7 (1973) 786.
4.)C. J. Delbecq, W. Hayes and P .H. Yuster, Phys. Rev. 121 (1961) 1043.
5.)J. D. Konitzer and H. N. Hersh, J. Phys. Chem. Solids 27 (1966) 771.
6.)B. J. Faraday and W. D. Compton, Phys. Rev. 138 (1965) A893.
7.)D. Schoemaker, Phys. Rev. 174 (1968) 1060.
8.)F. J. Ahlers, F. Lohse, J.-M. Spaeth and L. F. Mollenauer, Phys. Rev. B28 (1983) 1249.
9.)U. Rogulis, W. Meise, J. -M. Spaeth, K.S.. Song, to be published

THE $(F_2^+)_H$ CENTER ENERGY STRUCTURE IN ALKALI HALIDES

V.N. Salomatov, T.G. Yuriyeva
Irkutsk State University, 20 Gagarin Boulevard, SU-664003, Irkutsk, Russia

1. Introduction

Alkali halides containing F_2^+-like centers are well known to be worth-while laser materials[1-4]. At present the $F_2^+(O^{2-})$ model[1-4] is generally recognized to be ascribed to laser-active $(F_2^+)_H$ colour centers in alkali halides containing oxygen. But in the interpretation of results[1-4] it is ignored that in the case of extra-charged O^{2-} impurity ion perturbance F_2^+ center spectra shifts should be more significant than those observed during the experiment (hundredth parts of electron-volt). Therefore it is of interest to estimate the $(F_2^+)_H$ center energy parameters in $F_2^+(O^-)$ model (perturbance is realized by O^- impurity ion) for NaCl, KCl and KBr crystals investigated experimentally in detail and also to determine the result of other anion impurities (H^-, homologous F^-, Cl^-, Br^-, J^-) influence on the F_2^+ center spectra characteristics in these crystals and in LiF:H^- as well.

2. Calculation Method

The calculation of the F_2^+ center energy parameters change caused by the impurity ions was carried out within the framework of Bartram-Stoneham-Gash method[5] in Alig·s modification[6]. The change of i-th electron state of F_2^+ center energy caused by the influence of an impurity ion was written as follows:

$$\Delta E_i = [(A_1 - A_-) + (B_1 - B_-)(E_i - U_1)]|\Phi_i(\bar{R}_1)|^2(1 - \sum_{\gamma \neq 1}^{N} B\gamma|\Phi_i(\bar{R}_1)|^2)^{-1}.$$

The pseudopotential coefficients $A\gamma$, $B\gamma$ were used for regular and the majority of impurity ions[5] including O^- and H^- ions[7]. The pseudopotential coefficients for J^- were calculated using formulae (3.6)-(3.8)[5] and J^- wave functions[8]. Obtained values are as follows: $B=314.3\ a_0^3$; $A_H=-194.21\ Ry\cdot a_0^3$ and $A_X=-16.96\ Ry\cdot a_0^3$, where A_H, A_X are A parameter components defined by Hartree and exchange interections, respectively, and a_0 is the Bohr radius. The symbols "1","_" in this expression are related to impurity and substituted regular anions. $U\gamma$ is the electron potential energy in the γ-th unit cell. $\bar{R}\gamma$ defines the γ-th unit cell position. $\Phi_i(\bar{R}\gamma)$ is pseudowave function value in γ-th unit cell. F_2^+ wave functions are taken from the paper[9].

3. Theoretical Results and Discussion

The results of calculation for $F_2^+(O^-)$ and $F_2^+(F^-, Cl^-, Br^-, J^-)$ centers in NaCl, KCl, KBr and experimental data[3] for comparison are given in Tables 1 and 2. ΔE is the shift of the zero-phonon line position (absorption spectrum maximum) of the $(F_2^+)_H$ center as compared with the F_2^+ center. Defect configurations involved are illustrated in Figure. The upper label of ΔE corresponds to a configuration number in Figure.

J. Phys.: Condens. Matter 7 (1995) 7699–7708. Printed in the UK

Magneto-optical properties of the UV absorption bands of V_K centres in alkali halides

U Rogulis†§, K S Song‡ and J-M Spaeth†

† Fachbereich Physik, Universität-GH Paderborn, Warburger Strasse 100, D-33098 Paderborn, Germany

‡ Department of Physics, University of Ottawa, Ontario, Canada K1N 6N5

Received 2 May 1995, in final form 21 July 1995

Abstract. A new UV absorption band below the original UV band has been discovered through the magnetic circular dichroism of the V_K centre absorption (MCDA) in seven alkali halide crystals. This new band is attributed to the transition $\Sigma_u \rightarrow \Pi_u$ which becomes dipole allowed as a result of a loss of inversion symmetry. We attribute this lowered symmetry to the slow axial oscillation along the V_K axis which results in a momentarily 'frozen' geometry of the species at the classical turning point. An approximate estimation of the coupling between the even and odd parity molecular orbitals of Σ and Π symmetry is made in KBr. From this it appears that the coupling between the even and odd parity states is not negligible. Observed experimental trends in the seven crystals are explained from this model.

1. Introduction

V_K centres in alkali halides are trapped hole centres, in which the hole is shared between two adjacent halogen ions along the ⟨110⟩ directions. They have been investigated intensively with optical spectroscopy and electron paramagnetic resonance (EPR) (see e.g. Fowler 1968). V_K centres are created by ionizing radiation and are only stable below room temperature. V_K centres are fundamental hole centres which play a key role in many luminescence processes, for example in scintillator crystals for the detection of x-ray radiation (see e.g. Spaeth *et al* 1994a for the system CsI:Tl). The optical absorption bands of V_K centres are found in the UV and in the IR spectral regions and are explained as $\Sigma_u \rightarrow \Sigma_g$ and $\Sigma_u \rightarrow \Pi_g$ transitions in an X_2^- (X = halogen) molecular model, respectively. Also the EPR of the V_K centres is explained with this model (Schoemaker 1973). There is the general view that V_K centres have a perfect D_{2h} symmetry, in which the halogens have inversion symmetry, i.e. have the same hole charge. Recently for V_K centres in KBr a second absorption band was identified in the UV by means of measuring the magnetic circular dichroism of the absorption (MCDA) and the MCDA-detected EPR spectrum (Spaeth *et al* 1994b). Its MCDA peaks at 2.7 eV, whereas the previously reported absorption band peaks at 3.22 eV (Delbecq *et al* 1961). Only for KI has a second UV transition peaking at 2.12 eV been reported previously by Delbecq *et al* (1961). This second UV transition cannot be explained with the conventional X_2^- molecular model. In KI it was tentatively attributed by Delbecq *et al* (1961) to a $\Sigma_u \rightarrow \Pi_u$ transition, which is forbidden in the X_2^- molecular

§ Permanent address: Institute of Solid State Physics, University of Latvia, 8 Kengaraga Street, LV-1063 Riga, Latvia.

0953-8984/95/397699+10$19.50

model because of the parity violation, but which could be allowed as a consequence of some distortion, which, however, remained unspecified in Delbecq *et al* (1961). It was speculated by Rogulis *et al* (1993) and Spaeth *et al* (1994b) that the loss of inversion symmetry might arise from a soft axial translational vibrational mode of the V_K centres. It was proposed that the very slow axial oscillations of the centre make the centre seem 'frozen' at the classical turning points during the optical transition, which would be equivalent to having a momentarily off-centre geometry making the $\Sigma_u \rightarrow \Pi_u$ transition allowed.

It is the purpose of this paper to examine whether the occurrence of this second UV absorption band is a common feature to all V_K centres in alkali halides of the NaCl structure.We therefore investigated V_K centres in seven alkali halides with the MCDA technique. We found that indeed the second UV transition is a common feature, which in many cases is only revealed by means of the MCDA and, therefore, has escaped previous investigations of the optical absorption. We tentatively explain the absorption assuming a soft axial translational vibrational mode of the V_K centres, i.e. by a dynamically broken inversion symmetry.

2. Experiment

The alkali halide crystals were grown with the Czochralski method and doped with NO_2^- (0.5 mol% in the melt for NaCl and KCl, 1 mol% for NaBr) or Tl (0.5 mol% in the melt for KBr, KI, RbBr and RbI) in order to facilitate the generation of V_K centres by x-irradiation. The crystals were irradiated with x-rays (50 kV, 5 mA) *in situ* in the MCDA spectrometer at 4.2 K for 1–2 hours. The MCDA and MCDA-detected EPR spectra were measured with a custom-built computer-controlled spectrometer working in the K band (24 GHz) between 1.5 K and room temperature in the spectral range between 220 nm and about 1000 nm. Most measurements were performed at 1.8 K.

3. Experimental results

In figure 1(a) the optical absorption and in figure 1(b) the MCDA of V_K centres in NaBr are shown. The UV absorption band does not have the spectral shape of a single Gaussian, but seems to be a superposition of two Gaussians peaking at 3.3 eV and at 2.6 eV. The decomposition into two Gaussians is indicated in figure 1(a). Figure 1(b) shows the MCDA which is the differential absorption of right and left circularly polarized light measured in a longitudinal static magnetic field. Several positive and negative peaks are resolved. When setting the MCDA to 1.58 eV and inducing microwave transitions (24.09 GHz), the MCDA-detected EPR spectrum of figure 2, curve a, is measured for $B_0 \parallel [100]$. This is the known EPR spectrum of V_K centres in NaBr for those centres which have their molecular axes perpendicular to the field orientation, superimposed on centres with axes under 45° with respect to the field orientation. The simulated spectrum using the g-factors and Br hyperfine (hf) interaction parameters known from conventional EPR experiments (Schoemaker 1973), and assuming a half width of 4 mT for each Br hf transition, is shown in figure 2(b). It agrees very well with the MCDA-detected EPR spectrum (the small isotope differences between ^{79}Br and ^{81}Br are not resolved). It has been shown previously that V_K centres with their axes parallel to the magnetic field have no MCDA and can thus not be detected by MCDA-detected EPR (Spaeth *et al* 1994b).

When measuring the excitation spectrum of the MCDA on setting the magnetic field at one V_K EPR line (e.g. 800 mT for the perpendicular V_K centres), i.e. measuring the

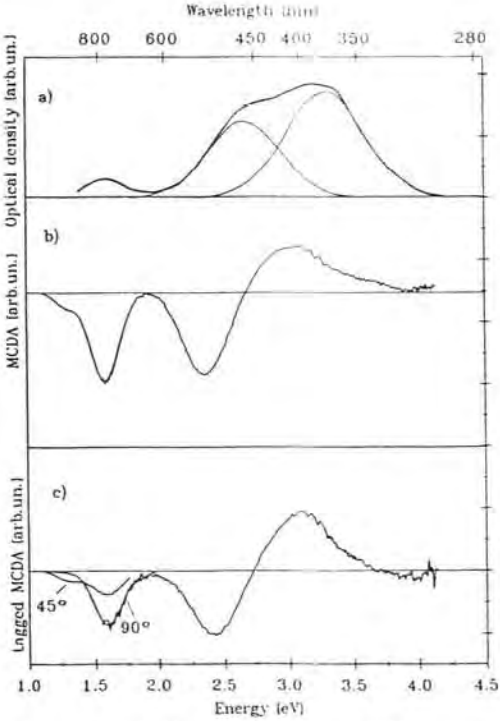

Figure 1. (a) Absorption spectrum of V_K centres in NaBr. (b) MCDA of the absorption spectrum of figure 1(a) measured at 1.8 K and $B = 3$ T. (c) Tagged MCDA of V_K centres with their axes perpendicular to the magnetic field (90°) measured at $B = 800$ mT and of V_K centres under 45° measured at 855 mT. Microwave frequency 24.1 GHz, $T = 1.8$ K, $B \parallel [100]$.

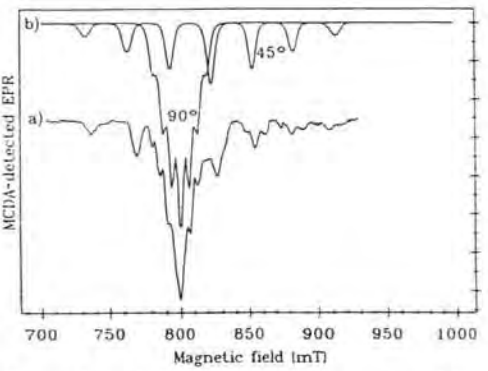

Figure 2. (a) MCDA-detected EPR spectrum of V_K centres in NaBr: $B_0 \parallel [100]$, $\nu = 24.09$ GHz measured at 1.58 eV and 1.8 K. (b) Simulated ESR spectrum of 90° and 45° V_K centres in NaBr using the known g-factors and Br hyperfine interaction parameters from conventional EPR (Schoemaker 1973). A Br line width of 4 mT was assumed; the slight difference between ^{79}Br and ^{81}Br is neglected.

so-called 'tagged' MCDA spectrum (see e.g. Spaeth *et al* 1992), the MCDA spectrum of figure 1(c) is obtained. The MCDA of figure 1(b) between 1 and 4 eV is reproduced. Thus, the MCDA peaks all belong to the V_K centres. The measurement of the tagged MCDA, when setting B_0 into an EPR line of those V_K centres which have an angle of 45° with respect to the field orientation (e.g. 855 mT), gives a slight difference in the IR MCDA (figure 1(c)).

Figure 3 shows the analogous results for NaCl. Also here the tagged MCDA for the 90° V_K centres reproduces the measured MCDA. The measurement of the tagged MCDA for the 45° V_K centres shows a slight shift of the IR MCDA band: its peak is lower by approximately 0.1 eV in energy compared to the perpendicular V_K centres.

From figure 4, representing the optical absorption (taken from Murray and Keller (1967)) and the tagged MCDA for the 90° V_K centres in RbI (measured at 830 mT), it becomes particularly apparent that the MCDA in the UV is measured predominantly from the low-energy side of the UV absorption and that it is very small, if not absent, where the UV absorption has its highest peak. In RbI it was difficult to measure the perpendicular centres

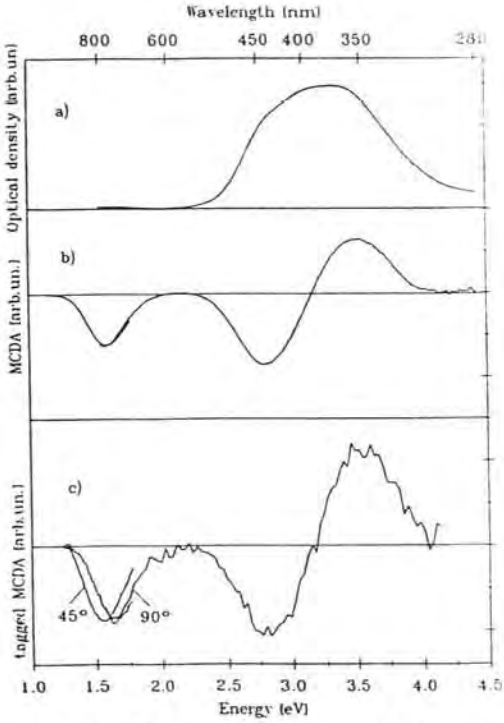

Figure 3. (a) Absorption spectrum of V_K centres in NaCl. (b) MCDA of the absorption spectrum of figure 3(a) measured at 1.8 K and $B = 3$ T. (c) Tagged MCDA of V_K centres with their axes perpendicular to the magnetic field (90°) measured at $B = 850$ mT and of V_K centres under 45° measured at 865 mT. Microwave frequency 24.06 GHz, $T = 1.8$ K, $B \parallel [100]$.

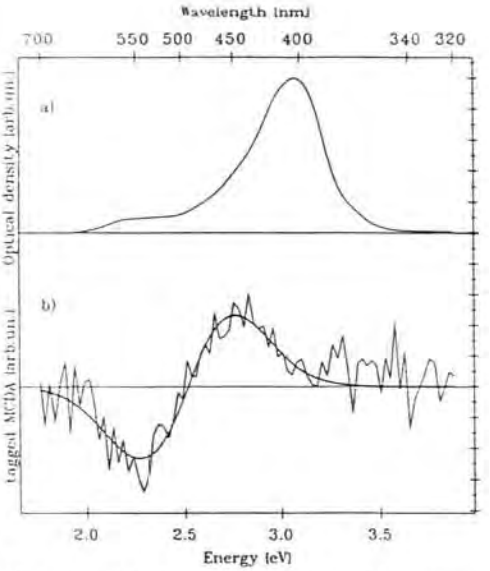

Figure 4. (a) Absorption spectrum of V_K centres in RbI. (b) Tagged MCDA of V_K centres with their axes perpendicular to the magnetic field (90°) measured at $B = 830$ mT. Microwave frequency 23.7 GHz, $T = 1.8$ K, $B \parallel [100]$. The smooth line is a simulation using a derivative of a Gaussian line shape.

due to the overlap with another ODEPR signal. However, as was seen for NaBr and NaCl, the tagged MCDA spectra of the 45° and 90° centres coincide in the UV band. The solid line in figure 4(b) is a simulation assuming a derivative-like spectral shape for the MCDA, being the derivative of a Gaussian absorption line.

In figure 5 a survey of the tagged MCDA spectra for the 90° V_K centres in the UV region is given for seven alkali halides. The vertical bars indicate the positions of the peaks of the UV absorption bands as measured in optical absorption. The solid lines represent simulations of line shapes assuming derivatives of Gaussian bands which describe the experiments rather well. Attempts to measure the MCDA spectra of V_K centres in KF and RbCl, both doped with Tl, failed. The signals were too weak.

In none of the alkali halides does the zero transition of the MCDA coincide with the peak position of the UV absorption band. In the bromides and more so in the iodides it is apparent that the MCDA is shifted towards lower energy and must originate in another optical transition than in the known UV (high-energy) absorption band. It thus seems to be a general feature of the V_K centres that they have two UV absorption bands. The high-

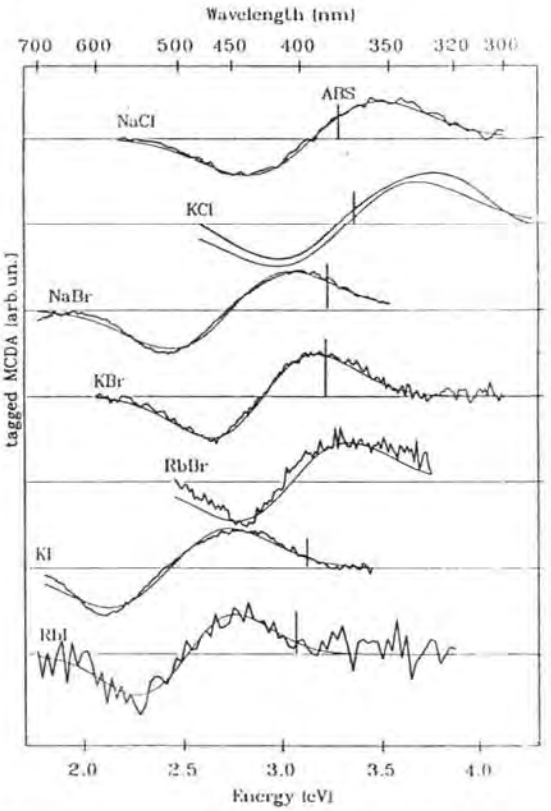

Figure 5. Tagged MCDA spectra of the UV transitions of V_K centres with their axes perpendicular to the magnetic field in seven alkali halides. The positions of the peaks of the UV absorption bands are indicated by vertical bars.

energy band shows no or only a very weak magnetic circular dichroism, while the band at lower energy, although having a comparatively weak absorption band, has a strong MCDA effect. The energy separation between the two UV bands, if one identifies the peak of the low-energy transition with the zero transition of the MCDA signal, increases from the chlorides through the bromides for the same alkali ions. On the other hand, it decreases with increasing alkali ions, for example from NaBr to RbBr or from KI to RbI.

In table 1 the positions of the UV absorption peaks ('ABS'), the zero transitions of the UV MCDAs (MCD_0) and the energy separation of the positive and negative MCDA peaks ($MCD_+ - MCD_-$) as well as $E_\perp$, the average energy separation between the Σ_u and Π_u levels, derived from EPR (Schoemaker 1973) are collected. The shifts between ABS and MCD_0 are also listed.

4. Discussion

Our experiments have shown that the second UV transition at lower energy compared to the known UV band must be a common feature to all V_K centres in the alkali halides. It therefore seems unlikely that its occurrence is attributable to a distortion by another defect as was tentatively proposed by Delbecq *et al* (1961) for their observation of this extra

Table 1. UV absorption and MCDA data of V_K centres in alkali halides (in eV). ABS = peak of the UV absorption band; MCD_0 is the zero transition of the MCDA bands, MCD_+, MCD_- are the energy positions of the positive and negative MCDA peaks; $E_\perp$ = average of the Σ_u–Π_u energy separation (after Schoemaker 1973).

		Na	K	Rb
Cl	ABS	3.28[a]	3.40[a]	
	MCD_0	3.17	3.35	
	ABS – MCD_0	0.11	0.05	
	$(MCD_+) - (MCD_-)$	0.7	0.75	
	$E_\perp$	2.28	2.42	
	ABS	3.22[b]	3.22[a]	
Br	MCD_0	2.75	2.91	3.06
	ABS – MCD_0	0.47	0.31	
	$(MCD_+) - (MCD_-)$	0.67	0.52	0.53
	$E_\perp$	1.95	2.19	2.23
	ABS		3.10[a]	3.06[c]
			2.12	2.21
I	MCD_0		2.43	2.50
	ABS – MCD_0		0.67	0.56
	$(MCD_+) - (MCD_-)$		0.66	0.55
	$E_\perp$		2.03	2.12

[a] Delbecq *et al* 1961.
[b] Schoemaker 1973.
[c] Murray and Keller 1967.

band in KI. The question arises, therefore, of what could be the reason for this additional UV band. In principle, one could think that it arises from a charge transfer transition from the neighbouring alkali ions into the X_2^- molecule. However, one would then expect a stronger dependence of the MCDA effects on the alkalis, which is not observed. The MCDA intensity, i.e. $I_+ - I_-$, is rather similar in all the alkali halides observed. Since the X_2^- molecular model has been successful so far in explaining the EPR results and other optical properties, it is tempting to seek explanation within this model. In order to explain a second UV band, it is necessary to find a 'mechanism' which would make the $\Sigma_u \rightarrow \Pi_u$ transition dipole allowed by removing the inversion symmetry. In our previous paper on MCDA measurements of V_K centres in KBr and KI, we suggested that there is a soft axial translational mode of vibration along the ⟨110⟩ directions and that this slow axial oscillation of the centre makes the centre seem 'frozen' at the classical turning points during the optical transition. This is equivalent to having a momentary off-centre geometry of the V_K centre, thereby making the Σ_u–Π_u transition allowed. Since the oscillation is fast compared to 10 GHz normally used in EPR, this symmetry breaking is not seen in the EPR experiments.

Regarding the nature of the 'frozen' motion at the classical turning points, we can offer the following qualitative comments. Considering that the V_K centre can be formed along the ⟨110⟩ axis at equally spaced intervals, it is to be expected that the soft axial mode would deviate from a simple harmonic potential as it approaches the mid-point to the next site. Indeed, an approximate calculation based on the CNDO code embedded in an ionic lattice suggests a flattening of the potential around 1 Å off the centre. This would enhance the 'freezing' effect near the classical turning points. The broad bandwidth (about 0.5 eV) of the new UV band (figure 1(a)) seems to indicate that the absorption is not between a pair

of vibronic states differing by one quantum of the axial mode phonon.

In the off-centre geometry, the two halogens will have unequal hole charges. In the on-centre position, both halogens are relaxed inwards. As a consequence of the axial motion (e.g. for the turning points), one halogen moves towards the halogen lattice site which has the full positive Madelung potential, which is repulsive for the hole, while the other moves further away from this repulsive potential. Consequently, the latter halogen will acquire more hole charge than the former. This can be formally expressed by mixing the Σ_g and Σ_u molecular orbitals. The electrostatic lattice potential thus causes a charge transfer between the two halogen components of the V_K centre for an 'asymmetric' position of the V_K centre. As will be discussed below, this makes the $\Sigma_u \rightarrow \Pi_u$ transition dipole allowed.

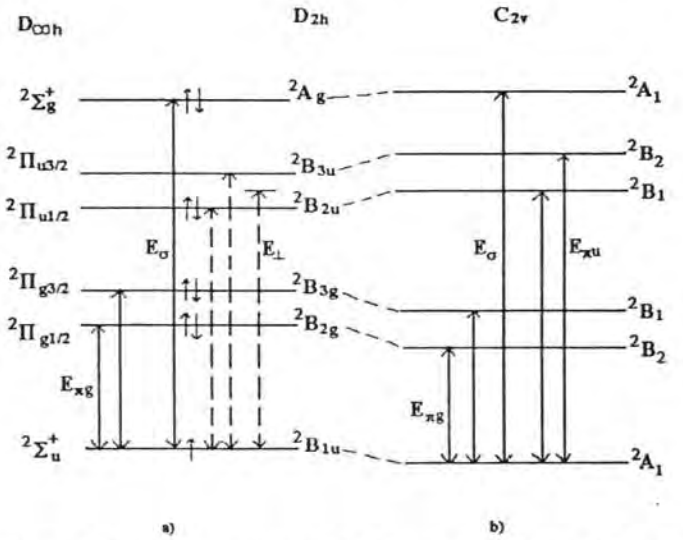

Figure 6. Schematic representation of the energy level changes for the X_2^- molecular model caused by the slow axial centre oscillation: (a) on-centre X_2^- (D_{2h}); (b) off-centre X_2^- (C_{2v}).

It is possible to give a general qualitative discussion on the MO energy levels as the inversion symmetry is broken. Figure 6 shows schematic changes, in particular the level repulsion between Σ_u and Σ_g, and Π_u and Π_g. This is the direct consequence of mixing of above pairs of states through the odd-parity potential term introduced by loss of inversion. It is likely that the effect is larger for the second than for the first. At static equilibrium, $\Sigma_u \rightarrow \Sigma_g$ and $\Sigma_u \rightarrow \Pi_g$ transitions are optically allowed and correspond, respectively, to the UV and IR bands. We propose that the new UV band observed by MCDA corresponds to $\Sigma_u \rightarrow \Pi_u$ transition which becomes allowed because of the loss of inversion symmetry at the classical turning point. It can be seen that the two UV band energies tend to be larger than in the on-centre geometry, while the IR band changes less. Such absorption energy changes have been noted in alkaline earth fluorides between the V_K and H centres, oriented respectively along the ⟨100⟩ and ⟨111⟩ axes (Parker *et al* 1981). It is therefore interesting to examine whether such variation is present in the data obtained in the present work by MCDA and earlier works by EPR (Schoemaker 1973). As shown in table 1, $E_\perp$ (the average of $\Sigma_u \rightarrow \Pi_u$), derived from the g shifts observed in EPR, is systematically smaller than the new UV band peaks, identified as the zero of the MCDA (MCD_0 in table 1). There are some interesting and systematic trends among the crystals studied. They are discussed

below.

Qualitatively, in this model one can also understand the trends we have observed in the various alkali halides. For example, the new band shifts to lower energy for the same halogen when the alkali ion becomes smaller, i.e. the lattice constant decreases (e.g. on going from RbBr to NaBr, it varies from 3.06 eV to 2.75 eV).

Since there is less space in NaBr than in RbBr for the off-centre motion, the Π_u level moves less upwards and Σ_u moves less downwards (see figure 6(b)). Therefore, the new UV band in NaBr peaks at lower energy than in RbBr.

The other trend, i.e. the lower energy of the new band, when varying the halogens from smaller to larger ones, can be understood as follows. Owing to the smaller size of Cl_2^- compared with those of Br_2^- or I_2^-, there is relatively more space in NaCl to induce larger off-centre axial motion. Several basic properties of the self-trapped excitons in alkali halides depend in a sensitive way on this geometric relation (Song and Williams 1993). Therefore, the effect of the off-centre motion, i.e. a higher energy for the $\Sigma_u \rightarrow \Pi_u$ transition, is less on going from the chlorides to the iodides in agreement with the observed trends.

In the ideal case of a single Gaussian absorption band, there are simple relations between the optical absorption and MCDA spectra (see e.g. Spaeth *et al* 1992). If the absorption coefficient α can be represented by a Gaussian: $\alpha_0 e(-(E - E_0)^2/W^2)$, the MCDA signal, which is proportional to the first derivative of α, consists of two parts, one negative and the other positive. The peak-to-peak energy separation is given by $W\sqrt{2}$ and equal to $0.85W_{1/2}$, where $W_{1/2}$ is the half-width. Also, the absorption band peak E_0 is given by the zero of MCDA, represented by MCD_0 in table 1. In an ideal case, the two parts of the MCDA signal are symmetrical, except for the signs. In the above discussion, W represents the absorption band width originating from electron–phonon coupling and we have assumed that it is larger than the splitting between $\Pi_{1/2}$ and $\Pi_{3/2}$.

One of the striking observations made in the present work is the absent or very weak MCDA signal from the strong UV band, and the much stronger MCDA from the generally weak lower-energy UV band. In the following, we present a qualitative discussion of this observation based on the assumption that the new lower-energy UV band originates from the $\Sigma_u \rightarrow \Pi_u$ transition, which becomes allowed as a result of the relaxation of the parity selection rule at the classical turning point of the axial oscillation along ⟨110⟩. Lifting of the inversion symmetry, without changing other symmetries, will promote mixing of Σ_u and Σ_g states as well as Π_u and Π_g states. This is described below:

$$|\Sigma_{u'}\rangle = |\Sigma_u\rangle + a|\Sigma_g\rangle \qquad |\Sigma_{g'}\rangle = |\Sigma_g\rangle - a'|\Sigma_u\rangle. \tag{1}$$

Because of the orthohogonality between $|\Sigma_{u'}\rangle$ and $|\Sigma_{g'}\rangle$, which now belong to the same irreducible representation, $a = a'$. This mixing coeficient is determined either by perturbation theory or by solving a secular determinant involving the pair of interacting states.

A semi-quantitative estimate of the mixing coefficients is made in the appendix. It shows that the mixing is not negligible and lends support to the model presented here to explain the observed results. The MCDA signal is obtained by calculating the difference of the left and right circularly polarized absorptions. From this it follows that

$$I_+ - I_- = (I_+^0 - I_-^0)(1 - a^2) \qquad a \leqslant 1. \tag{2}$$

Here, the I^0 are the intensities before mixing and have been shown to be non-zero for the V_K axis perpendicular to the static magnetic field (Spaeth *et al* 1994b, Meise 1993). It follows that the new MCDA signal is reduced by a factor $(1 - a^2)^2$ which is generally smaller than unity.

The MCDA signal associated with the new UV band can be analysed in a similar way after the perturbed states $|\Sigma_{u'}\rangle$ and $|\Pi_{u'}\rangle$ are described as

$$|\Sigma_{u'}\rangle = |\Sigma_u\rangle + a|\Sigma_g\rangle \tag{3}$$

$$|\Pi_{u'}\rangle = |\Pi_u\rangle + b|\Pi_g\rangle. \tag{4}$$

In this case, a is the same as a above, but b is unrelated to a. A simple consideration based on perturbation theory indicates that a and b are of the same sign, but b is expected to be larger than a. Using the above vectors, one can find

$$I_+ - I_- = a^2[I_+ - I_-]_1 + b^2[I_+ - I_-]_2 + 2ab[\text{cross terms}] \tag{5}$$

with

$$[I_+ - I_-]_1 = \left|\langle\Sigma_g|I_+|\Pi_u\rangle\right|^2 - \left|\langle\Sigma_g|I_-|\Pi_u\rangle\right|^2 \tag{6}$$

$$[I_+ - I_-]_2 = \left|\langle\Sigma_u|I_+|\Pi_g\rangle\right|^2 - \left|\langle\Sigma_u|I_-|\Pi_g\rangle\right|^2. \tag{7}$$

The second term (7) represents the MCDA due to the IR band, derived in Meise (1993), and does not vanish. The first term has not been completely derived and is expected not to vanish. The cross term is made of products of different matrix elements instead of squares of the same matrix as above. Although it is not simple to show that the sum of all three terms is large, it seems fair to say that generally it would not vanish.

When setting $a = 0$, a limiting case, we are left with the term of (7), of which we know that it does not vanish from the observation of an MCDA in the IR bands. Thus, with the assumption of the off-centre oscillation, one is able to explain both the appearance of the new UV band and the fact that it has an MCDA which is stronger than that of the UV band coming from the $\Sigma_u \rightarrow \Sigma_g$ transition.

Appendix. Mixing of even and odd parity states

Here, we present the results of a semi-quantitative estimation of the mixing coefficients coupling the even and odd parity states of the V_K centre which is realized by the soft translational mode Q_2. First, we studied the potential energy variation of the V_K centre in the KBr crystal. This was obtained by embedding a CNDO code in the point charge lattice, with Born–Mayer-type short-range interaction in the same way as in earlier studies of the self-trapped excitons. According to this approximate calculation, the translational motion is, indeed, very soft. For a shift of 0.8 Å, the energy rises by about 0.14 eV. We also observed that around 1 Å the potential flattens, suggesting a deviation from harmonic potential.

At several values of the axial shift Q_2, we have examined the variation of the even and odd parity molecular orbital (MO) energies. As expected, the energy difference between the even (gerade) and odd (ungerade) parity states increases for both Σ and Π MOs as a result of the coupling. We attribute the new UV band to the Σ_u–Π_u transition. Therefore, we consider the mixing in both states with their respective even parity MO. The example described below is at a shift of $Q_2 \cong 1.3$ Å. Following an aproach already used in an earlier study of the V_K and H centres in CaF_2 (Parker *et al* 1981), we solve a secular determinant of the following form for both Σ and Π states.

$$\begin{vmatrix} -\Delta - E & V \\ V & \Delta - E \end{vmatrix} = 0$$

As in Parker *et al* (1981), it is more convenient to express the Σ (or Π) MOs in terms of atomic bases z_1 and z_2 (or y_1 and y_2) on the pair of bromines. $2V$ gives the UV (or IR) transition energy at $Q_2 = 0$. 2Δ describes the potential (mostly the Madelung potential)

difference between the two atoms at finite Q_2. The two parameters Δ and V are deduced from the MO energies obtained from the CNDO calculation. The UV energy varies between 4.7 eV and 5.0 eV (and the IR between 0.42 to 0.56 eV) for the on-centre and off-centre geometries. (The UV energies are somewhat larger than the observed one around 3 eV and the IR smaller compared to 1.2 eV experimentally. The CNDO parameters used were fitted mainly to the equilibrium bond length and stretching mode frequency. Also, the above energies are one-electron energies.)

Finally, the new eigenvectors are obtained:

$$|\Sigma_{u'}\rangle = 0.96|\Sigma_u\rangle + 0.26|\Sigma_g\rangle$$
$$|\Pi_{u'}\rangle = 0.33|\Pi_g\rangle + 0.93|\Pi_u\rangle.$$

This shows that the mixing is not negligible around this region of Q_2. It is clear that the precise magnitude of the mixing depends on the amplitude of the low-frequency vibration. A more reliable determination of these parameters would be desirable, but is beyond the scope of this paper.

Acknowledgments

The authors are grateful to Professor N Itoh and Dr K Tanimura for supplying the samples of NaBr–NO_2^- and NaCl–NO_2^- including their absorption spectra and for helpful discussions.

References

Delbecq C J, Hayes W and Yuster P H 1961 *Phys. Rev.* **121** 1043

Fowler W B 1968 *The Physics of Color Centers* ed W B Fowler (New York: Academic) ch 2, 8

Meise W 1993 *Doctoral Thesis* Paderborn

Murray R B and Keller F J 1967 *Phys. Rev.* **153** 993

Parker S, Song K S, Catlow C R A and Stoneham A M 1981 *J. Phys. C: Solid State Phys.* **14** 4009

Rogulis U, Meise W and Spaeth J M 1993 *Proc. Int. Conf. on Defects in Insulating Materials (Nordkirchen, 1992)* vol 1, ed O Kanert and J M Spaeth (Singapore: World Scientific) p 468

Schoemaker D 1973 *Phys. Rev.* B **7** 786

Song K S and Williams R T 1993 *Self-trapped Excitons (Springer Series in Solid State Sciences 105)* (Heidelberg: Springer) ch 5

Spaeth J M, Meise W and Song K S 1994a *J. Phys.: Condens. Matter* **6** 3999

——1994b *J. Phys.: Condens. Matter* **6** 1801

Spaeth J M, Niklas J R and Bartram R H 1992 *Structural Analysis of Point Defects in Solids (Springer Series in Solid-State Sciences 43)* (Heidelberg: Springer)

J. Phys.: Condens. Matter 10 (1998) 6473–6479. Printed in the UK PII: S0953-8984(98)92183-X

Optical properties of Tl^{2+} hole centres in alkali halides: I. Investigation with optical detection of paramagnetic resonance

U Rogulis†‖, J-M Spaeth†, I Cabria‡, M Moreno‡, J A Aramburu‡ and M T Barriuso§

† Universität-Gesamthochschule Paderborn, Fachbereich Physik, Warburger Strasse 100, D-33098 Paderborn, Germany

‡ Departamento Ciencias de la Tierra y Física de la Materia Condensada, Facultad de Ciencias, Universidad de Cantabria, 39005 Santander, Spain

§ Departamento Física Moderna, Facultad de Ciencias, Universidad de Cantabria, 39005 Santander, Spain

Received 3 March 1998, in final form 22 April 1998

Abstract. The spectra of the magnetic circular dichroism of the absorption (MCDA) and of optically detected electron paramagnetic resonance (ODEPR) of Tl^{2+} hole centres have been investigated in a number of alkali halides. Several new absorption bands were found using excitation spectra of the Tl^{2+} ODEPR lines. The number of the MCDA transitions of Tl^{2+} in the bromides and especially in the iodides is larger than predicted by the molecular orbital picture discussed so far in the literature. An explanation will be given in part II by Cabria *et al* on the basis of MS–Xα calculations including the spin–orbit effects of the ligands.

1. Introduction

Tl^{+} activators in some x-ray storage phosphors such as RbI act as hole trap centres and form Tl^{2+} hole centres which, upon photostimulation, recombine with electrons liberated from the electron trap centres, i.e. F-centres (Rogulis *et al* 1996).

The microscopic structure of the Tl^{2+} hole centres was studied by electron paramagnetic resonance (EPR) in KCl by Dreybrodt and Silber (1967) and in KCl, RbCl and KBr by Frey *et al* (1975). Several optical absorption bands were reported for Tl^{2+} in KCl (Delbecq *et al* 1966), KBr (Roth and Halperin 1982) and KI (Hadley *et al* 1966, Hersh 1959, Kink 1968). The magnetic circular dichroism of the absorption (MCDA) of the UV absorption bands in KCl and KI have been measured by Beaumont *et al* (1973). They were interpreted as being due to s–p 'atomic-like' transitions, where the excited p orbitals of Tl^{2+} are split by the large spin–orbit interaction of thallium resulting in two resolved absorption bands. Several further absorption bands in the visible spectral region were observed in Tl^{2+} doped KI crystals (Hadley *et al* 1966, Hersh 1959), but no direct identification as being due to Tl^{2+} could be presented. Nistor *et al* (1994) reviewed the optical and EPR data available until 1994 as well as proposed models to explain the optical transitions of Tl^{2+} centres.

‖ Permanent address: Institute of Solid State Physics, University of Latvia, 8, Kengaraga Street, LV-1063 Riga, Latvia.

0953-8984/98/296473+07$19.50

In our previous work we reported on the identification of several MCDA bands of Tl^{2+} centres in RbI using the MCDA excitation spectra measured in the Tl^{2+} EPR transition ('MCDA tagged by EPR', see Spaeth *et al* 1992). In this work we present a systematic study of the MCDA and MCDA-detected EPR of Tl^{2+} centres in six alkali halides. We detected many more transitions than previously reported elsewhere, which can clearly be associated with Tl^{2+} according to the experimental method used, in particular in the iodides in the low energy ('red') spectral region. For an understanding the existing molecular orbital (MO) models had to be extended. A theoretical interpretation will be presented in part II of the paper, by Cabria *et al* (1998).

2. Experimental details

The alkali halide crystals were grown with the Czochralski method and doped with 0.5 mol% Tl in the melt. The crystals were irradiated with x-rays (50 kV, 5 mA) *in situ* in the MCDA spectrometer for 1–2 hours. After irradiation at low temperatures, the temperature was, as a rule, increased beyond the temperature of the thermal stability of the V_K centres for about 5 min in order to diminish the amount of V_K centres and to increase the amount of the Tl^{2+} centres. However, irradiation at higher temperatures up to 300 K did not change the observed spectra.

The MCDA and MCDA-detected EPR spectra were measured with a custom-built computer-controlled spectrometer working in the K band (24 GHz) between 1.5 K and room temperature in the spectral range between 220 nm and about 1000 nm. Most measurements were performed at 1.5 K (for the method see e.g. Spaeth *et al* 1992). The sign of the MCDA is calibrated using the MCDA of the F-centre (Paus 1980) and presented such that positive values mean a right circular polarization.

3. Experimental results

The MCDA-detected EPR spectra of several x-irradiated Tl-doped alkali halides are shown in figure 1(a). One broad structureless EPR line appears at magnetic fields well above those corresponding to $g = 2$ (~850 mT). The lines are attributed to the $|1,-1\rangle \rightarrow |1,0\rangle$ transition of the Tl^{2+} centre (Dreybrodt and Silber 1967) with the quantum numbers $F = 1$, $m_F = 0, \pm 1$ because of the large hyperfine (hf) interaction with the two magnetic isotopes ^{203}Tl (29.5% natural abundance) and ^{205}Tl (70.5% abundance) (see figure 1(b) for the level scheme). Both isotopes have $I = 1/2$ and very similar nuclear moments, such that they are not resolved in our MCDA-EPR spectra. No superhyperfine interactions with lattice neighbours could be resolved. The line positions are isotropic within experimental error. The second transition expected between $|1,0\rangle$ and $|1,+1\rangle$ has not been observed in the K band in the available magnetic field range up to 3.5 T.

The Tl hf coupling constants A determined from the spectra by diagonalization of the appropriate spin Hamiltonian (Dreybrodt and Silber 1967) are collected in table 1. For the determination of the Tl hf interaction from the spectra we had to assume the g factors, since only one of the two transitions could be measured. For KCl, RbCl and KBr we used the g factors known from conventional EPR measurements. Our hf coupling constants A thus determined agree very well with those determined previously with conventional EPR (see table 1). A possible variation with temperature seems only small (our experiments were done at 1.5 K, previous EPR at 77 K). This is in line with the observation in the analogous system Cd^+ (s^1 configuration) in alkali halides where the temperature variation of A between 77 K and 4 K is only about 10^{-2} (Toyotomi and Onaka 1973).

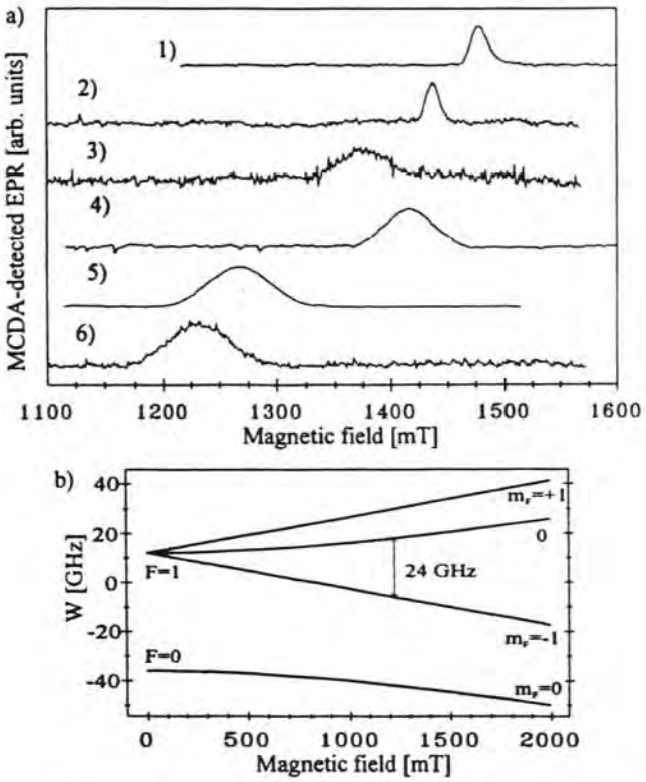

Figure 1. (a) MCDA-detected EPR spectra of the Tl^{2+} centres in six alkali halide crystals. The MCDA background has been subtracted. Measurements were made at $T = 1.5$ K and $B \parallel [100]$. Slightly different microwave frequencies were used: (1) KCl—23.9 GHz, (2) RbCl—23.7 GHz, (3) KBr—23.7 GHz, (4) RbBr—24.1 GHz, (5) KI—23.9 GHz, 6) RbI—23.7 GHz. (b) Breit–Rabi diagram for Tl^{2+} centre in RbI–Tl crystal with the g-factor of 2.1 and A (^{205}Tl) = 48 GHz.

For RbBr we used the same g factor as in KBr. According to the observation that g in KBr is larger than in KCl we assumed $g = 2.1$ in KI and RbI, a value somewhat larger than g in KBr. The resulting A values of Tl may have to be corrected, if better values of the g factors become available.

Figure 2 shows the MCDA bands obtained by measuring the MCDA excitation spectra of the Tl^{2+} resonance line shown in figure 1(a) for each alkali halide (in several cases the low energy bands were scaled up by a factor of 3 or 5 because of the low intensity of the original spectra). The peak positions of the MCDA bands measured are collected in table 2 together with those previously published and with the absorption band peaks. In all six alkali halide crystals we obtained a number of new MCDA bands besides the known bands in the UV. The largest number of bands (seven) was obtained in the iodides. All the bands are clearly due to Tl^{2+}, since in all bands the EPR of Tl^{2+} can be measured.

We observed an interesting feature of the lowest energy MCDA band in KI. The low energy MCDA band of the Tl^{2+} centre in KI at 1.6 eV is very similar in spectral shape and position to the MCDA band of the allowed 'red' transition of the V_K centre (Spaeth *et al* 1994). This similarity, however, seems to be fortuitous in view of the theoretical interpretation of the MCDA bands given by Cabria *et al* in part II.

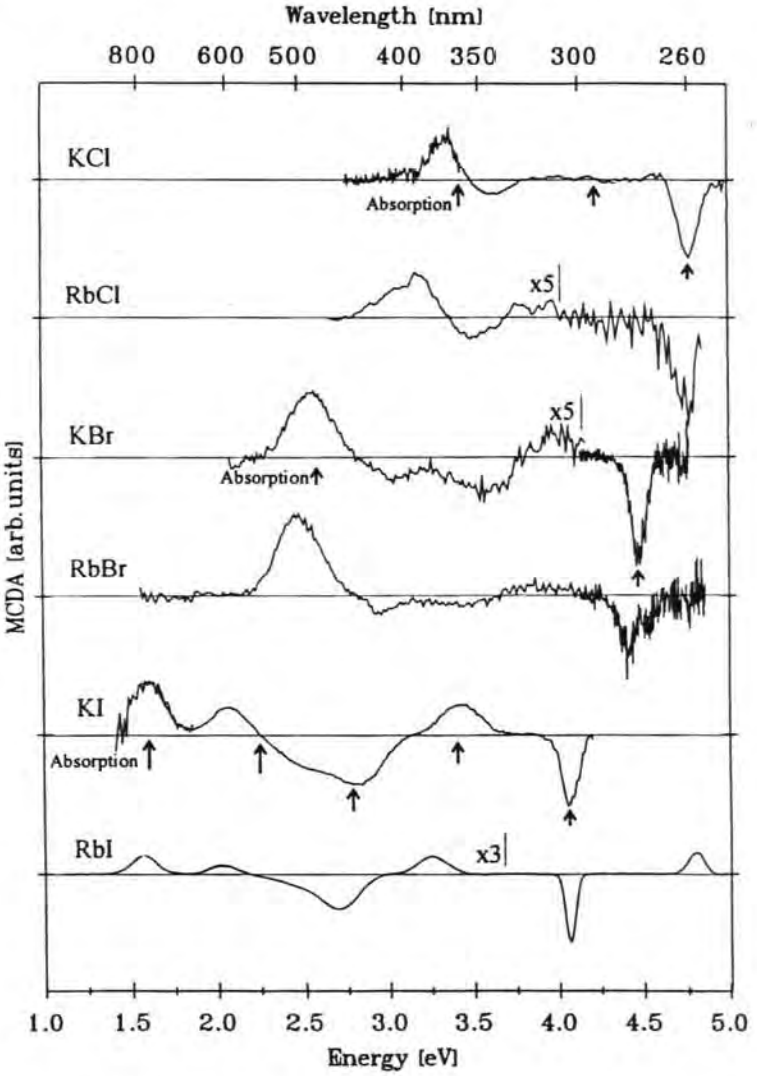

Figure 2. The spectra of the 'tagged MCDA' of the Tl^{2+} centres of six alkali halide crystals, measured at $T = 1.5$ K in the EPR lines of Tl^{2+}. For the RbCl, KBr and RbI crystals the low energy part of the spectra was scaled up.

4. Discussion

The electronic configuration of the Tl^{2+} centre is a $6s^1$ electron in an octahedral crystal field regarding the six nearest halogen neighbours: Tl^{2+} X_6^{6-}. The a_{1g} ground state is paramagnetic. The optical transition from the $^2S_{1/2}$ to the spin–orbit-split $^2P_{3/2}$ and $^2P_{1/2}$ excited states gives rise to the two UV transitions, of which except for RbI only the one with lower energy (to the $^2P_{1/2}$ state) is shown in figure 2. The reversal of signs in the MCDA bands in KI is typical for a spin–orbit-split excited state and has already been reported previously (Beaumont *et al* 1973). The splitting between the two UV transitions is 0.75 eV

Table 1. The ^{205}Tl hyperfine splitting parameters of the EPR and those obtained from the MCDA-EPR measurements for the Tl^{2+} centres of the alkali halides.

		g	A (Ghz)	Ref. for EPR
KCl	EPR	2.010	105.8	b,c
	MCDA-EPR	2.01[a]	110 ± 4	
RbCl	EPR	2.010	104.9	c
	MCDA-EPR	2.01[a]	103 ± 4	
Kbr	EPR	2.067	92.6	c
	MCDA-EPR	2.067[a]	93 ± 5	
RbBr	MCDA-EPR	2.067[a]	92 ± 5	
KI	MCDA-EPR	2.1[a]	52 ± 3	
RbI	MCDA-EPR	2.1[a]	48 ± 3	

[a] Assumption.
[b] Dreybrodt and Silber (1967).
[c] Frey *et al* (1975).

Table 2. Band positions of the MCDA bands and of the absorption bands of Tl^{2+} centres in six alkali halide crystals (values in eV).

KCl		
ABS	3.40; 4.22[a]	4.73; 5.63[a]
KCl		
MCDA	3.35; 3.6; 4.05 (v. weak)	4.73; 5.67[b]
RbCl		
MCDA	3.15; 3.50	4.75
KBr		
ABS	2.58[c]	4.46[c]
KBr		
MCDA	2.55; 3.05; 3.57; 4.0	4.48
RbBr		
MCDA	2.48; 2.95; approx. 3.45; 3.9	4.40
KI		
ABS	1.58; 2.25; 2.79; 3.42 [d–f]	4.06; 4.82 [d–f]
KI		
MCDA	1.60; 2.07; 2.45; 2.8; 3.43	4.05; 4.82 [b]
RbI		
MCDA	1.57; 2.03; approx. 2.35; 2.7; 3.25	4.07; 4.82

[a] Delbecq *et al* (1966).
[b] Beaumont *et al* (1973).
[c] Roth and Halperin (1982).
[d] Hadley *et al* (1966).
[e] Hersh (1959).
[f] Kink (1968).

in RbI and 0.9 eV in KCl, almost the reduced atomic value for the spin–orbit splitting of Tl (Beaumont *et al* 1973).

The question arises why one observes more transitions at lower energy. According to the model of Moreno (1979a, b) there are also hole transitions possible into the σ and π linear combinations of halogen p orbitals with t_{1u} symmetry (see figure 3) resulting in two further transitions. The MCDA spectra reveal changes of sign between the bands suggesting qualitatively that these two transitions are indeed four transitions because of transitions to spin–orbit-split σ and π linear combinations. For those one would expect a change of sign

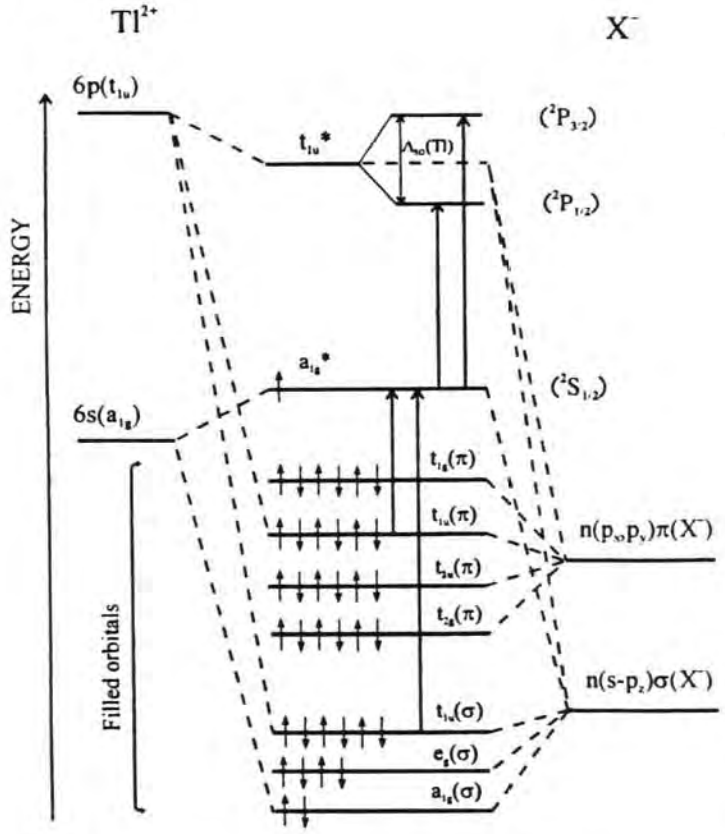

Figure 3. Qualitative energy level diagram of a $[TlX_6]$ octahedral complex (after Nistor *et al* 1994, Ballhausen and Gray 1965, Moreno 1979a, b).

(Fowler 1968). The energy splittings between the positive and negative bands decrease on going from the iodides to the bromides and are hardly visible in the chlorides. This supports their interpretation, since the halogen spin–orbit splitting decreases strongly from the iodides to the chlorides. However, the number of five additional transitions in the iodides (altogether seven transitions) is not explained by such an energy level scheme.

An explanation of the observed MCDA spectra is presented in part II of the paper, by Cabria *et al* (1998), using an MS–Xα calculation and including the ligand spin–orbit effects.

Acknowledgments

This work has been partially supported by the CICYT under project No PB95-0581. I Cabria is indebted to the Spanish Ministerio de Educacion y Ciencia for a postgraduate grant.

References

Ballhausen C J and Gray H B 1965 *Molecular Orbital Theory* (New York: Benjamin) p 103

Beaumont J H, Hayes W and Laiho R T S 1973 *J. Phys. C: Solid State Phys.* **6** L479

Cabria I, Moreno M, Aramburu J A, Barriuso M T, Rogulis U and Spaeth J-M 1998 *J. Phys.: Condens. Matter* **10** 6481

Delbecq C J, Ghosh A K and Yuster P H 1966 *Phys. Rev.* **151** 599
Dreybrodt W and Silber D 1967 *Phys. Status Solidi* **20** 337
Fowler W B 1968 *The Physics of Color Centers* ed W B Fowler (New York: Acdemic) ch 2, p 125
Frey W, Huss R, Seidel H and Werkmann E 1975 *Phys. Status Solidi* b **68** 257
Hadley W B, Polick S, Kaufman R G and Hersh H N 1966 *J. Chem. Phys.* **45** 2040
Hersh H N 1959 *J. Chem. Phys.* **31** 909
Kink R A 1968 *Doctoral Thesis* Tartu
Moreno M 1979a *J. Phys. C: Solid State Phys.* **12** L921
——1979b *Solid State Commun.* **29** 653
Nistor S V, Schoemaker D and Ursu I 1994 *Phys. Status Solidi* b **185** 9
Paus H J 1980 *Habilitationsschrift* Universität Stuttgart
Rogulis U, Dietze C, Pawlik Th, Hangleiter Th and Spaeth J M 1996 *J. Appl. Phys.* **80** 2430
Roth M and Halperin A 1982 *J. Phys. Chem. Solids* **43** 609
Spaeth J M, Meise W and Song K S 1994 *J. Phys.: Condens. Matter* **6** 1801
Spaeth J M, Niklas J R and Bartram B H 1992 *Structural Analysis of Point Defects in Solids (Springer Series in Solid State Sciences 43)* (Berlin: Springer)
Toyotomi Y and Onaka R 1973 *J. Phys. Soc. Japan* **34** 623

J. Phys.: Condens. Matter **10** (1998) 6481–6490. Printed in the UK PII: S0953-8984(98)92184-1

Optical properties of Tl^{2+} hole centres in alkali halides: II. MS–Xα calculations

I Cabria†, M Moreno†, J A Aramburu†, M T Barriuso‡, U Rogulis§‖ and J-M Spaeth§

† Departamento Ciencias de la Tierra y Física de la Materia Condensada, Facultad de Ciencias, Universidad de Cantabria, 39005 Santander, Spain

‡ Departamento Física Moderna, Facultad de Ciencias, Universidad de Cantabria, 39005 Santander, Spain

§ Universität-Gesamthochschule Paderborn, Fachbereich Physik, Warburger Strasse 100, D-33098 Paderborn, Germany

Received 3 March 1998

Abstract. MS–Xα calculations at different values of the metal–ligand distance, R, have been performed for TlX_6^{4-} units (X = Cl, Br, I) subjected to the electrostatic potential of KX lattices. The results confirm that the optical absorption bands peaked at 3.4 and 4.2 eV in KCl:Tl^{2+} can be associated with the $t_{1u}(\pi) \rightarrow a_{1g}^*$ and $t_{1u}(\sigma) \rightarrow a_{1g}^*$ charge transfer (CT) transitions respectively of the $TlCl_6^{4-}$ complex. Also, the systematic red shift experienced by such transitions on passing from KX to RbX is related to the increase of R induced by the host lattice change. The spin–orbit coupling in $t_{1u}(\pi)$ and $t_{1u}(\sigma)$ levels determines the sign of the magnetic circular dichroism of the optical absorption (MCDA) and it is shown that for bromides and iodides the two CT transitions can exhibit a different pattern as is experimentally observed. Also the non-existence of MCDA signal in the $t_{1u}(\sigma) \rightarrow a_{1g}^*$ region of KCl:Tl^{2+} is related to a practically zero value of the spin–orbit splitting. The existence of five CT peaks for iodides is explained through the γ_{8-} component of the $t_{2u} \rightarrow a_{1g}^*$ CT transition, whose oscillator strength increases following the ligand spin–orbit coefficient. As t_{2u} is always found to be located about 0.15 eV below $t_{1u}(\pi)$, this new component can also explain the asymmetry observed in the MCDA spectra of chlorides and bromides in the high energy side of the $t_{1u}(\pi) \rightarrow a_{1g}^*$ transition. In all these TlX_6^{4-} units, the unpaired electron is found to be located mainly on the X ligands, the charge on them increasing along the Cl → Br → I series. This is related to the corresponding decrease of the hyperfine constant for whose core polarization effects are calculated to be negligible. From the present results, the equilibrium Tl^{2+}–Cl^- distance would be close to 2.80 Å thus implying a 10% inwards relaxation with respect to the host lattice. To our knowledge these are the first calculations reported on heavy $6s^1$ impurities.

1. Introduction

Measurements of the magnetic circular dichroism of the optical absorption (MCDA) and the optically detected electron paramagnetic resonance (ODEPR) have been carried out on Tl^{2+} placed in the six KX and RbX lattices (X = Cl, Br, I). The experimental results are reported in part I of the paper (Rogulis *et al* 1998). The measurement of tagged MCDA spectra is relevant as it allows one to associate *unambiguously* the fine details observed through

‖ Permanent address: Institute of Solid State Physics, University of Latvia, 8, Kengaraga Street, LV-1063 Riga, Latvia.

0953-8984/98/296481+10$19.50

the MCDA technique with a centre well distinguished from others using EPR (Spaeth *et al* 1992). Therefore, a reasonable explanation of the main features displayed by the MCDA spectra clearly ascribed to Tl^{2+} (Rogulis *et al* 1996, 1998) is now attractive and, at the same time, necessary.

Apart from discussing the charge transfer (CT) origin proposed for the lowest bands in KCl:Tl^{2+} (Moreno 1979) and exploring the influence of *ligand* spin–orbit coupling upon the MCDA spectra of the whole series, special attention has to be paid to explain the following experimental facts:

(i) the *red shift* undergone by the first two bands on passing from KX:Tl^{2+} to RbX:Tl^{2+};

(ii) the sign of the circular dichroism for each of the involved bands;

(iii) the absence of MCDA signals for the absorption band peaked at 4.22 eV in KCl:Tl^{2+};

(iv) the existence of five bands in the iodides other than the two transitions coming from the atomic $6s \rightarrow 6p$ ($^2P_{3/2}$; $^2P_{1/2}$) transitions and

(v) the asymmetry of the MCDA spectra in the first absorption band of chlorides and bromides.

To gain a better insight into these problems, theoretical calculations on TlX_6^{4-} complexes (X = Cl, Br, I) placed in alkali halide lattices can be helpful. It is worth noting, for instance, that the first assignments of optical bands due to Tl^{2+}, Ag^0 or Pb^{3+} in alkali halides were made (Moreno 1979) using *only* the empirical optical electronegativity scale (Jørgensen 1970). Moreover, at variance with what is found for 3d impurities, little theoretical effort has been devoted up to now to understand the properties due to s^1 ions (Nistor *et al* 1994). Theoretical calculations have recently been carried out for Ag^0-doped KCl (Cabria *et al* 1997), while calculations on $6s^1$ ions (like Hg^+, Tl^{2+} or Pb^{3+}) placed in insulators have not yet been reported.

For the first calculation of Tl^{2+} in halides the relatively simple MS–Xα method was used as this method reasonably explains the charge transfer (CT) bands due to impurities like Cr^{3+} or Cu^{2+} placed in insulators (Aramburu *et al* 1996, Aramburu and Moreno 1997). Moreover, in the case of the $5s^1$-Ag^0-atom-doped KCl, MS–Xα and self-consistent charge extended Hückel calculations both have confirmed (Cabria *et al* 1997) the existence of a CT band in the ultraviolet region associated with the Ag^0 impurity.

Relevant details about the calculations are given in the next section, while in section 3 the present theoretical results are used for achieving a better insight into the experimental data of part I.

2. Computational details

In order to explain the *main trends* displayed by the experimental data on Tl^{2+} impurities in six alkali halides, MS–Xα calculations have been done for Tl^{2+} embedded in KX lattices (X = Cl, Br, I). Initially, calculations were done on TlX_6^{4-} units subjected to the electrostatic potential due to the rest of the lattice (Aramburu and Moreno 1997). Later, clusters like $(TlX_6K_{12}X_8)^0$ involving 27 ions have been used. As the main features are reproduced by both types of calculation, only the results on seven ion clusters are exposed.

To evaluate the importance of the core polarization contribution to the hyperfine constant, A, polarized MS–Xα calculations have also been carried out. As Tl^{2+} is a heavy ion the present MS–Xα calculations have been done including all relativistic corrections which are spin independent (Sakurai 1967, Wood and Boring 1978). The influence of spin–orbit coupling on relevant features displayed by optical and MCDA spectra is considered later.

As the equilibrium Tl^{2+}–X^- distance in the different host lattices is not experimentally known, the calculations have been performed at different values of the Tl^{2+}–X^- distance, called R. Taking into account the ionic radii of Pb^{2+} and Hg^{2+} we have tentatively varied R in the range 2.80 Å–3.00 Å for KCl:Tl^{2+} and around 3.0 Å and 3.25 Å for KBr:Tl^{2+} and KI:Tl^{2+}, respectively.

Similar to the procedure employed in previous work (Aramburu *et al* 1992, 1996) atomic sphere radii were chosen following Norman's criterion (Norman 1976) and the α values in the atomic regions taken from Schwarz (1972). Transition energies were considered through the Slater transition state procedure (Slater 1974).

3. Results and discussion

The ordering of significant one-electron orbitals in the ground state of TlX_6^{4-} units is depicted in figure 1. In all these calculations the unpaired electron is found to lie in the antibonding a_{1g}^* level partially related to the 6s level of free Tl^{2+}. A population analysis of this relevant level is presented later.

For testing the importance of relativistic corrections in the present results, firstly the value of the $5d \rightarrow a_{1g}^*$ transition corresponding to the $TlCl_6^{4-}$ complex was explored. When ignoring the relativistic corrections the value of such a transition is calculated to be 14.3 eV, while it becomes equal only to 11.7 eV when including the corrections. This result implies that also this transition is far beyond the optical region and is thus unimportant for the absorption in the optical range. The suppression of relativistic corrections also leads to changes of other properties like the charge distribution in the antibonding a_{1g}^* orbital.

When ignoring in a first approximation the spin–orbit coupling, only the three $a_{1g}^* \rightarrow t_{1u}^*$, $t_{1u}(\pi) \rightarrow a_{1g}^*$ and $t_{1u}(\sigma) \rightarrow a_{1g}^*$ transitions (described in figure 1) are compatible with electric dipole selection rules in O_h symmetry and the Pauli principle. The calculated energy of such transitions for $TlCl_6^{4-}$ is given in table 1. The results given therein strongly support that for KCl:Tl^{2+}, where the optical absorption bands peak at 3.40 eV and 4.22 eV, those transitions can in fact be associated with the CT transitions $t_{1u}(\pi) \rightarrow a_{1g}^*$ and $t_{1u}(\sigma) \rightarrow a_{1g}^*$ of the $TlCl_6^{4-}$ complex. This situation is thus rather different from that calculated at $R = 3.14$ Å for Tl^+ in KCl (Bramanti *et al* 1971) where the separation between $t_{1u}(\sigma)$ and a_{1g}^* levels was found to be 6.5 eV.

As has been found for Cu^{2+} or Cr^{3+} impurities in halides (Aramburu *et al* 1992, 1996) the energy (E) of CT transitions appears to be rather sensitive to changes in R. From table 1 $dE/dR \simeq -70$ meV pm^{-1} is found for both CT transitions of the $TlCl_6^{4-}$ complex. Using this figure, the 0.20 eV red shift experienced by the lowest CT transition on going from KCl:Tl^{2+} to RbCl:Tl^{2+} can reasonably be associated with an increase of the equilibrium Tl^{2+}–Cl^- distance $\Delta R_e = 3$ pm. It is worthwhile noting that this value is, as expected, positive but at the same time much smaller than $\Delta R_0 = 15$ pm corresponding to the increase experienced by the anion-cation distance of the perfect host lattice. This behaviour has been observed in the case of common impurities, where the impurity–ligand distance is only slightly dependent on the host lattice (Barriuso and Moreno 1984). As to the actual value of the equilibrium Tl^{2+}–Cl^- distance for KCl:Tl^{2+}, the results collected in table 1 indicate that R would be close to 2.80 Å, which thus implies an inwards relaxation of about 10% with respect to the cation–anion separation ($R = 3.14$ Å) of the perfect host lattice.

In table 2 the calculated energies of optical transitions for $TlBr_6^{4-}$, TlI_6^{4-} and also $TlCl_6^{4-}$ are presented. The calculations lead to a ~1.7 eV red shift of CT transitions on passing from $TlCl_6^{4-}$ to TlI_6^{4-} which is very close to that observed experimentally (part I, figure 2).

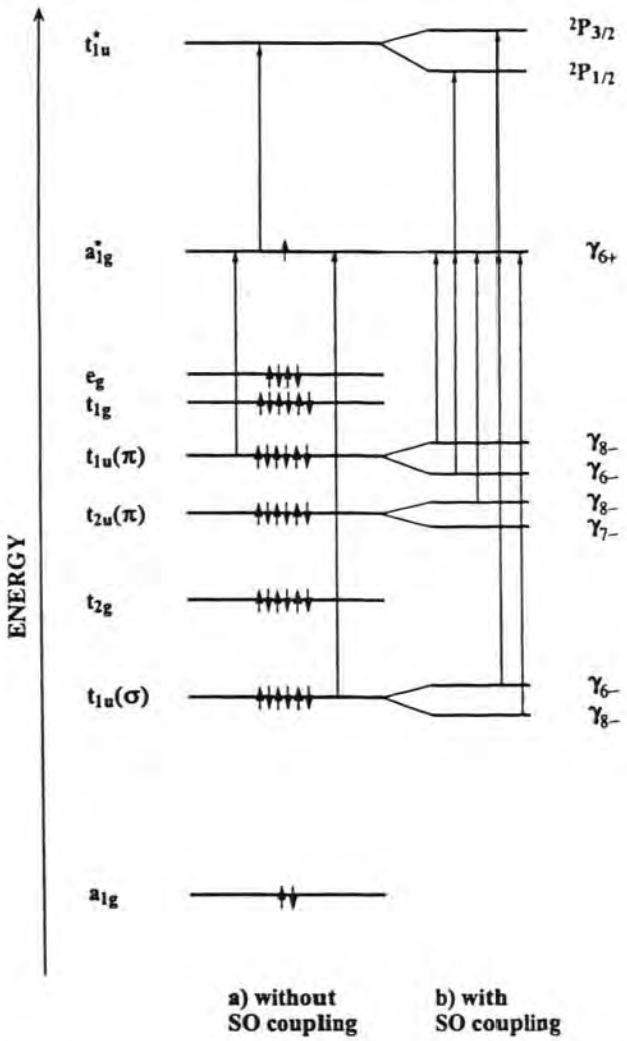

Figure 1. Molecular orbital diagram for octahedral TlX_6^{4-} units (X = Cl, Br, I) derived from the present MS–Xα calculations. In that diagram only the one-electron levels arising from the 6s and 6p levels of free Tl^{2+} and from n_{LP} levels (n_L = quantum number of the valence shell) of the six halogen ions involved in the complex are shown. The unpaired electron is located in the antibonding a_{1g}^* level and the six levels lying below are made mainly from n_{LP} levels of the ligands. In the figure the electric-dipole-allowed transitions for TlX_6^{4-} units are also shown. The expected transitions, when the spin–orbit coupling is present or absent, are both depicted. In the absence of spin–orbit coupling only the $a_{1g}^* \rightarrow t_{1u}^*$ and the two charge transfer transitions, $t_{1u}(\pi) \rightarrow a_{1g}^*$ and $t_{1u}(\sigma) \rightarrow a_{1g}^*$, are allowed, while when that coupling exists, seven transitions are permitted. Note that only the γ_{8-} component of the $t_{2u} \rightarrow a_{1g}^*$ transition becomes allowed as far as the ligand spin–orbit coupling increases.

It is worth noting that the corresponding experimental red shift for the $a_{1g}^* \rightarrow t_{1u}^*$ transition is only 0.7 eV and thus nearly half the value observed for CT transitions. This trend is also reproduced by the present calculations.

Table 1. Optical transition energies (in eV) calculated through the MS–Xα method for $TlCl_6^{4-}$ (first row) and $(TlCl_6K_{12}Cl_8)^0$ (second row) clusters at different values of the metal–ligand distance R (in Å). The results are compared to the experimental values in KCl:Tl^{2+} (Delbecq *et al* 1996). In the case of the $a_{1g}^* \rightarrow t_{1u}^*$ transition the theoretical value is compared to the centre of the gravity associated with the $^2P_{1/2}$ and $^2P_{3/2}$ states. Note that the transition energies are nearly independent of the cluster size.

	R				
Transition	2.75	2.80	2.85	2.90	Experimental
$a_{1g}^* \rightarrow t_{1u}^*$	5.34	5.48	5.69	5.79	5.33
	5.24	5.55	5.74	5.85	
$t_{1u}(\pi) \rightarrow a_{1g}^*$	3.57	3.26	2.89	2.58	3.40
	3.66	3.26	2.90	2.55	
$t_{1u}(\sigma) \rightarrow a_{1g}^*$	4.50	4.11	3.68	3.31	4.22
	4.60	4.13	3.69	3.29	

Table 2. Optical transition energies, E (in eV), calculated through the MS–Xα method for $TlCl_6^{4-}$, $TlBr_6^{4-}$ and TlI_6^{4-} complexes. The value (in Å) of the metal–ligand distance R, taken for each complex, is also given. The sensitivity, dE/dR (in meV pm^{-1}), to changes of R is also reported.

		$a_{1g}^* \rightarrow t_{1u}^*$		$t_{1u}(\pi) \rightarrow a_{1g}^*$		$t_{1u}(\sigma) \rightarrow a_{1g}^*$	
	R	E	dE/dR	E	E/dR	E	dE/dR
$TlCl_6^{4-}$	2.80	5.48	30	3.26	−66	4.11	−79
$TlBr_6^{4-}$	3.00	5.36	18	2.05	−50	3.00	−64
TlI_6^{4-}	3.25	4.94	8	1.45	−37	2.40	−50

The sensitivity dE/dR of different transition energies for $TlBr_6^{4-}$ and TlI_6^{4-} is also given in table 2, and the trends are similar to those obtained for $TlCl_6^{4-}$. As a salient feature, the 6s → 6p-like transition is calculated to be less sensitive to R changes than the CT transitions. This is again in agreement with what is experimentally observed (part I, figure 2), in particular for RbI:Tl^{2+} and KI:Tl^{2+}, where the two $^2P_{1/2}$ and $^2P_{3/2}$ components of the $a_{1g}^* \rightarrow t_{1u}^*$ transition are well observed. Therefore, the experimental dE/dR value can be used as an *additional* argument for distinguishing a CT transition from the 6s → 6p-like.

As to the electron density, the red shift undergone by the CT transitions on passing from KCl:Tl^{2+} to KI:Tl^{2+} should also imply an increase in the unpaired spin density on ligands. This idea is confirmed by the results on the charge distribution in the a_{1g}^* orbital given in table 3. Moreover, these results indicate that the unpaired electron is located more on the ligands than on the central ion. Also, the decrease followed by the charge on the Tl(6s) orbital along the Cl → Br → I series can be related to the decrease of the experimental hyperfine constant A. For instance, the experimental value for Tl in alkali chlorides is $A = 104$ GHz, while $A = 93$ GHz in the case of bromides. In recent experiments on Tl^{2+} in $PbCl_2$, where the co-ordination number is also six, the hyperfine constant has also been measured to be close to 100 GHz (Nistor *et al* 1995). As to the Tl(6s) charge (table 3), it decreases by about 10% on going from $TlCl_6^{4-}$ to $TlBr_6^{4-}$. This decrease is thus comparable to that experienced by A. Nevertheless, the reduction of A (part I, table 1) when passing from KBr:Tl^{2+} ($A = 93$ GHz) to KI:Tl^{2+} ($A = 52$ GHz) is higher than that corresponding

Table 3. Distribution of the electronic charge (in %) for the unpaired a_{1g}^* level obtained through the MS–Xα method for the indicated complexes. The value (in Å) of the metal–ligand distance R at which calculations have been carried out is also given.

	R	Tl (6s)	X (ns)	X (np)
$TlCl_6^{4-}$	2.80	39.9	7.2	52.9
$TlBr_6^{4-}$	3.00	34.1	4.4	61.5
TlI_6^{4-}	3.25	29.7	2.6	67.7

to the charge on the central ion. A clarification of this point requires a further study of the actual g factor associated with TlI_6^{4-}. A first analysis of the g factor using a perturbative scheme (Moreno 1980) suggests that g values around 2.5 are not unreasonable for TlI_6^{4-}.

It is worth noting that the $|a_{1g}^*\rangle$ wavefunction can be briefly expressed as

$$|a_{1g}^*\rangle = \alpha_M|Tl(6s)\rangle - \lambda_{p\sigma}|\phi_{p\sigma}\rangle - \lambda_s|\phi_s\rangle \tag{1}$$

where $|\phi_{p\sigma}\rangle$ and $|\phi_s\rangle$ signify linear combinations of valence $p\sigma$ and s orbitals of involved ligands. It is convenient to note that A is proportional to α_M^2 which is *higher* than the charge related to Tl(6s) because of the antibonding nature of this orbital. Therefore, the reduction experienced by A when passing from free Tl^{2+} ($A_0 = 175$ GHz) to KBr:Tl^{2+} is close to 50% which is higher than the charge reported in table 3.

Although a more detailed study of the hyperfine coupling is currently under way, polarized MS–Xα calculations already stress that for Tl^{2+} impurities the contribution to A coming from the polarization of core s levels by the unpaired electron is only ~0.3% of that due to the unpaired a_{1g}^* electron alone. Therefore, at variance with what happens in the case of 3d cations (Abragam and Bleaney 1970), in the present cases the core polarization can be discarded in the analysis of the experimental hyperfine constant.

Going further into the analysis of experimental data it becomes necessary to discuss in some detail the origin of *all* bands associated with the $t_{1u}(\pi) \rightarrow a_{1g}^*$ and $t_{1u}(\sigma) \rightarrow a_{1g}^*$ transitions, as well as their MCDA sign. To this end it is crucial to consider the effect of the spin–orbit coupling. As for a p level of the central ion, one t_{1u} level leads to two levels when the spin–orbit coupling is taken into account. These levels belong to the γ_{6-} and γ_{8-} representations of the cubic double group, and in the case of the t_{1u}^* level they are often denoted as $P_{1/2}$ and $P_{3/2}$, respectively. In contrast to what happens for t_{1u}^* the splitting Δ between γ_{6-} and γ_{8-} for $t_{1u}(\pi)$ and $t_{1u}(\sigma)$ strongly depends upon the ligand spin–orbit coefficient, ξ_L.

For calculating Δ let us first formularize the z component of a $|t_{1u}\rangle$ wavefunction as

$$|t_{1u}, z\rangle = \alpha|Tl(6p_z)\rangle + \beta_\pi|\chi_{p\pi}, z\rangle + \beta_\sigma|\chi_{p\sigma}, z\rangle \tag{2}$$

where $|\chi_{p\pi}, z\rangle$ and $|\chi_{p\sigma}, z\rangle$ are linear combinations of p-ligand orbitals described in figure 2. Similar to what has been obtained for Cu^{2+} in chlorides (Barriuso *et al* 1997) the $t_{1u}(\pi)$ and $t_{1u}(\sigma)$ levels in the present cases are found to be mainly built from these ligand orbitals, while the amount of Tl(6p) admixture is small, but not negligible. As the $|\chi_{p\pi}, z\rangle$ and $|\chi_{p\sigma}, z\rangle$ LCAOs are, in principle, degenerate, both wavefunctions are strongly mixed in the two $t_{1u}(\pi)$ and $t_{1u}(\sigma)$ levels. The highest $t_{1u}(\pi)$ level is an antibonding level with respect to the *ligand–ligand* interaction and so in this level β_π and β_σ have the same sign leading to a diminution of the electronic density in the middle region between two closest ligands. The opposite happens in the case of the $t_{1u}(\sigma)$ level, which exhibits a bonding character with respect to the ligand–ligand interaction and thus $\beta_\sigma\beta_\pi$ is negative. As previously discussed

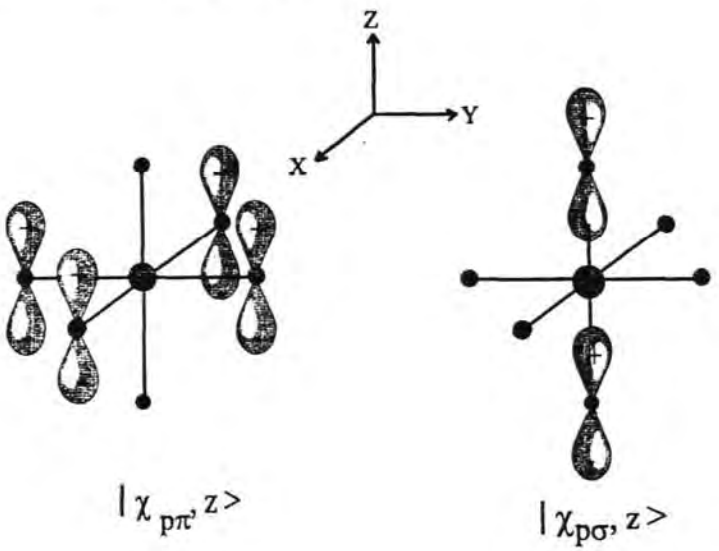

Figure 2. Pictorial description of the two linear combination of ligand p orbitals belonging to t_{1u} and transforming like z. $|\chi_{p\sigma}\rangle$ and $|\chi_{p\pi}\rangle$ involve a σ and π character, respectively, with respect to the metal–ligand interaction.

(Barriuso *et al* 1997), when the Tl(6p) admixture is switched on, it enhances the σ character of $t_{1u}(\sigma)$ and thus decreases the σ character of $t_{1u}(\pi)$. As regards the numerical values, the present calculations lead to $\alpha^2 \cong 5\%$ $\beta_\sigma\beta_\pi \cong -0.37$ for the $t_{1u}(\sigma)$ level, while $\alpha^2 \cong 1\%$, $\beta_\sigma\beta_\pi \cong 0.46$ for the $t_{1u}(\pi)$ level.

Provided that, in a first approximation, the spin–orbit operator is diagonalized within the $t_{1u}(j) \times \gamma_6$ manifold ($j = \pi, \sigma$), the value of Δ can simply be expressed as

$$\Delta = \tfrac{3}{2}i\langle t_{1u}, x|T_z|t_{1u}, y\rangle \tag{3}$$

where the spin–orbit operator for an electron, h_{SO}, is given by

$$h_{SO} = \boldsymbol{T} \cdot \boldsymbol{s} \tag{4}$$

and $\boldsymbol{T}$ is an operator transforming like the orbital angular momentum, $\boldsymbol{l}$, which can be expressed (Misetich and Buch 1964, Misetich and Watson 1966) as

$$\boldsymbol{T} = \sum_k \xi(\boldsymbol{r} - \boldsymbol{R}_k)\boldsymbol{l}_k. \tag{5}$$

In (5) $\boldsymbol{l}_k$ represents the orbital angular momentum referred to the nucleus at $\boldsymbol{R}_k$ as origin and the $\xi(\boldsymbol{r} - \boldsymbol{R}_k)$ function is especially important in the vicinity of such a nucleus (Misetich and Watson 1966, Al-Mobarak and Warren 1973). Due to this fact $\xi(\boldsymbol{r} - \boldsymbol{R}_k)$ only connects two atomic orbitals, both belonging to the atom placed at $\boldsymbol{R}_k$. Taking hence into account (2)–(5) and figure 2 the expression of Δ is found to be

$$\Delta = \tfrac{3}{2}\{\alpha^2\xi_M + \xi_L(\sqrt{2}\beta_\sigma\beta_\pi + \beta_\pi^2/2)\} \tag{6}$$

where $\Delta = 3/2\xi_M$ for the case of a *free* central ion as it should be.

To estimate Δ by means of (6), $\xi_M = 1010$ meV is used for Tl, while the atomic values $\xi_L(\mathrm{Cl}) = 72$ meV, $\xi_L(\mathrm{Br}) = 300$ meV and $\xi_L(\mathrm{I}) = 628$ meV are employed for ligands (Moore 1971). The calculated values (table 4) of the splitting Δ for the two $t_{1u}(\pi)$ and

Table 4. Values of the splitting, Δ (in meV), produced by the spin–orbit coupling in the $t_{1u}(\pi)$ and $t_{1u}(\sigma)$ charge transfer levels, obtained through the present MS–Xα calculations and (6) for the indicated complexes. The value (in Å) of the metal–ligand distance R at which calculations have been carried out is also given.

	R	$t_{1u}(\pi)$	$t_{1u}(\sigma)$
$TlCl_6^{4-}$	2.80	110	30
$TlBr_6^{4-}$	3.00	450	−130
TlI_6^{4-}	3.25	920	−340

$t_{1u}(\sigma)$ levels in $TlCl_6^{4-}$ and $TlBr_6^{4-}$ reproduce the main trends displayed by the experimental splittings (part I, figure 2). It is worth stressing that for the $t_{1u}(\pi)$ level, Δ is always positive, while it can be negative for the $t_{1u}(\sigma)$ one, as a result of the σ–π hybridization. The present results indicate that Δ can, in fact, be negative for the $t_{1u}(\sigma)$ level of $TlBr_6^{4-}$ and TlI_6^{4-}. This means, for instance, that the 2.55 eV and 3.05 eV peaks in KBr:Tl^{2+} should be ascribed, respectively, to the γ_{8-} and γ_{6-} components of $t_{1u}(\pi)$ while the 3.57 eV and 4.0 eV peaks should be associated with the γ_{6-} and γ_{8-} components of $t_{1u}(\sigma)$, respectively.

Regarding the sign of Δ, the MCDA technique is a good tool for its *direct* measurement (Spaeth *et al* 1992). For an atomic-like s → p transition if $\Delta > 0$, the MCDA sign of the γ_{6-} component is negative, while that of the γ_{8-} component is positive (Paus 1980). In fact, the MCDA at $T = 0$ K in the γ_{6-} component is determined by the matrix element $\langle a_{1g}^*, M_J = -1/2|J_-|t_{1u}^*\gamma_{6-};\ M_J = 1/2\rangle$ thus giving rise to a left circular light absorption. The MCDA pattern of a normal s → p transition can be represented as (−; +). Here, the first (second) part refers to the lowest (highest) energy side and a positive value in the bracket implies a positive value of the MCDA in figure 2 of part I.

In the case of CT transitions the situation is somewhat different. In fact, in a $t_{1u}(j) \rightarrow a_{1g}^*$ ($j = \pi, \sigma$) transition the electron reaches the *empty* $|a_{1g}^*, M_J = 1/2\rangle$ level and thus the γ_{6-} component is determined by the matrix element $\langle t_{1u}(j);\ \gamma_{6-};\ M_J = -1/2|J_-|a_{1g}^*;\ M_J = 1/2\rangle$. As the $t_{1u}(j)$ levels are lying *below* a_{1g}^*, the γ_{6-} component now still appears in the *high* energy side provided $\Delta > 0$. Therefore, a $t_{1u}(j) \rightarrow a_{1g}^*$ CT transition should give rise to a (+; −) MCDA pattern if $\Delta > 0$. This is *opposite* to what is found for an atomic-like s → p transition. As Δ is found to be positive for $t_{1u}(\pi)$, the two bands arising from the $t_{1u}(\pi) \rightarrow a_{1g}^*$ transition should follow that pattern.

This conclusion is consequently in agreement with what is observed for chlorides and bromides (part I, figure 2). Table 4 furthermore indicates that in the case of the chlorides the Δ value related to the $t_{1u}(\sigma)$ level is much smaller than that corresponding to $t_{1u}(\pi)$. Therefore the near absence of an MCDA signal for KCl:Tl^{2+} and RbCl:Tl^{2+} associated with the $t_{1u}(\sigma) \rightarrow a_{1g}^*$ transition can be reasonably be explained now. In fact, when the spin–orbit coupling is not directly seen in the absorption spectrum, the MCDA signal is just proportional to Δ (Paus 1980). The experimental results displayed in figure 2 of part I for MBr:Tl^{2+} (M = K, Rb) indicate that MCDA signs in the $t_{1u}(\sigma) \rightarrow a_{1g}^*$ region follow the pattern (−; +), thus confirming the negative value of Δ estimated for $TlBr_6^{4-}$ in table 4.

Let us finally discuss the MCDA spectra due to Tl^{2+} in iodides, where five and not four CT maxima are clearly seen, as was discussed in part I. When observing the experimental results on chlorides and bromides, it is reasonable to relate four of the observed maxima to transitions emerging from $t_{1u}(\pi) \rightarrow a_{1g}^*$ and $t_{1u}(\sigma) \rightarrow a_{1g}^*$. Taking into account the estimated Δ values in table 4 only one assignment is found to be reasonable. For KI:Tl^{2+} that

assignment is as follows: the peaks at 1.6 eV and 2.45 eV are the γ_{8-} and γ_{6-} components related to $t_{1u}(\pi)$, while peaks at 2.8 eV and 3.43 eV are the γ_{6-} and γ_{8-} components, respectively, associated with $t_{1u}(\sigma)$. As is clearly observed in the experimental spectrum, the first couple exhibits a (+; −) MCDA pattern, while the second one exhibits an inverse pattern in agreement with the negative Δ value given in table 4.

After this analysis it becomes clear that the peak observed at 2.07 eV in KI:Tl^{2+} and 2.03 eV in RbI:Tl^{2+} is the *new* peak, which cannot be understood on the basis of $t_{1u}(j) \rightarrow a_{1g}^{*}$ ($j = \pi, \sigma$) transitions split off by the action of the spin–orbit coupling. As the tagged MCDA spectra stress that the seven peaks seen for MI:Tl^{2+} (M = K, Rb) are *all* related to a Tl^{2+} impurity in a local cubic symmetry, it is reasonable to firstly search for an explanation for the new peak on the basis of unperturbed TlI_6^{4-} units. Bearing in mind that in the full series the new peak is clearly observed only in the iodides, it could reasonably be associated with *another* manifestation of the ligand spin–orbit coupling.

When looking at the molecular orbitals built from the valence p levels of six ligands (Ballhausen and Gray 1965), only one *odd* linear combination is found besides the $|\chi_{p\pi}\rangle$ and $|\chi_{p\sigma}\rangle$ combination described in figure 2. Such an orbital is purely non-bonding with respect to the metal–ligand interaction and transforms like t_{2u} instead of t_{1u}. Although the parity-allowed $t_{2u} \rightarrow a_{1g}^{*}$ transition is strictly forbidden in the absence of a spin–orbit coupling, it is no longer true when switching on such an interaction (figure 1). Actually, a t_{2u} level gives rise to γ_{7-} and γ_{8-} levels when the spin–orbit coupling is taken into account. Therefore, *only one* of these components would give rise to an electric-dipole-allowed transition and so the number of permitted charge transfer transitions would in fact be five and not four.

For supporting this attractive possibility it now becomes necessary to observe where the t_{2u} level is located with respect to $t_{1u}(\pi)$ and $t_{1u}(\sigma)$. The present calculations indicate (figure 1) that t_{2u} is always located *just below* $t_{1u}(\pi)$, the separation between them being smaller than ~0.15 eV. This separation remains when calculating the corresponding transitions to the a_{1g}^{*} level. The $t_{2u}(\gamma_{8-}) \rightarrow a_{1g}^{*}$ transition is hence suggested to be located a little above the $t_{1u}(\pi; \gamma_{8-}) \rightarrow a_{1g}^{*}$ one from which it borrows oscillator strength if ξ_L increases.

On the other hand, as the calculated separation between $t_{1u}(\pi)$ and t_{2u} is never much higher than the involved ligand spin–orbit coefficient, ξ_L, the allowed $t_{2u}(\gamma_{8-}) \rightarrow a_{1g}^{*}$ transition would *also* appear to be present in the case of bromides and chlorides. This idea can now explain the puzzling asymmetry displayed by the MCDA signal in the $t_{1u}(\pi) \rightarrow a_{1g}^{*}$ region (part I, figure 2), where the intensity of the $t_{1u}(\pi, \gamma_{6-})$ peak is clearly smaller than that due to $t_{1u}(\pi, \gamma_{8-})$. This effect could result from the *simultaneous* presence of the $t_{2u}(\gamma_{8-}) \rightarrow a_{1g}^{*}$ positive MCDA signal in the high energy side of the $t_{1u}(\pi) \rightarrow a_{1g}^{*}$ MCDA band. Although this explanation seems reasonable, a deeper analysis of the influence of spin–orbit coupling on charge transfer levels is currently being carried out.

Apart from this relevant aspect and a more detailed study of the hyperfine constant and g factor, other points deserving further investigation are: (i) the nature of the t_{1u}^{*} level, where a hybridization with lowest levels of the conduction band of the host lattice appears to play an important role; (ii) the correct value of the equilibrium distance between the Tl^{2+} impurity and nearest anions.

To clarify these points, calculations on 81 atom clusters using density functional theory as implemented in the ADF program system (Baerends and Ellis 1973, te Velde and Baerends 1992) have been initiated. In the first calculation a value $R_e = 2.75$ Å for the equilibrium distance in KCl:Tl^{2+} has been obtained. Thus the existence of an important inwards lattice relaxation indirectly obtained through the present work appears to be more strongly supported. Further work along this line is now under way.

Acknowledgments

This work has been partially supported by the CICYT under project No PB95-0581. I Cabria is indebted to the Spanish Ministerio de Educacion y Ciencia for a postgraduate grant.

References

Abragam A and Bleaney B 1970 *Electron Paramagnetic Resonance of Transition Ions* (Oxford: Oxford University Press) p 702
Al-Mobarak R and Warren K D 1973 *Chem. Phys. Lett.* **21** 513
Aramburu J A, Barriuso M T and Moreno M 1996 *J. Phys.: Condens. Matter* **8** 6901
Aramburu J A and Moreno M 1997 *Phys. Rev.* B **56** 604
Aramburu J A, Moreno M and Barriuso M T 1992 *J. Phys.: Condens. Matter* **4** 9089
Baerends E J and Ellis D E 1973 *Chem. Phys.* **2** 42
Ballhausen C J and Gray H B 1965 *Molecular Orbital Theory* (New York: Benjamin) p 103
Barriuso M T, Aramburu J A, Daul C and Moreno M 1997 *Int. J. Quant. Chem.* **61** 563
Barriuso M T and Moreno M 1984 *Phys. Rev.* B **29** 3623
Bramanti D, Mancini M and Ranfagni A 1971 *Phys. Rev.* B **3** 3670
Cabria I, Barriuso M T, Aramburu J A and Moreno M 1997 *Int. J. Quant. Chem.* **61** 627
Delbecq C J, Ghosh A K and Yuster P H 1966 *Phys. Rev.* **151** 599
Jørgensen C K 1970 *Prog. Inorg. Chem.* **12** 101
Misetich A A and Buch T 1964 *J. Chem. Phys.* **41** 2524
Misetich A A and Watson R E 1966 *Phys. Rev.* **143** 335
Moore C E 1971 *Atomic Energy Levels* National Bureau of Standards
Moreno M 1979 *J. Phys. C: Solid State Phys.* **12** L921
——1980 *Chem. Phys. Lett.* **76** 597
Nistor S V, Goovaerts E and Schoemaker D 1995 *Solid State Commun.* **96** 491
Nistor S V, Schoemaker D and Ursu I 1994 *Phys. Status Solidi* b **185** 9
Norman J G 1976 *Mol. Phys.* **31** 1191
Paus H J 1980 *Habilitationsschrift* Universität Stuttgart
Rogulis U, Dietze C, Pawlik Th, Hangleiter Th and Spaeth J-M 1996 *J. Appl. Phys.* **80** 2430
Rogulis U, Spaeth J-M, Cabria I, Moreno M, Aramburu J A and Barriuso M T 1998 *J. Phys.: Condens. Matter* **10** 6473
Sakurai J J 1967 *Advanced Quantum Mechanics* (Reading, MA: Addison-Wesley)
Schwarz K 1972 *Phys. Rev.* B **5** 2466
Slater J C 1974 *Quantum Theory of Molecules and Solids* vol 4 (New York: McGraw-Hill)
Spaeth J-M, Niklas J R and Bartram R H 1992 *Structural Analysis of Point Defects in Solids, (Springer Series of Solid State Sciences 43)* (Berlin: Springer)
te Velde G and Baerends E J 1992 *J. Comput. Phys.* **99** 84
Wood J H and Boring A M 1978 *Phys. Rev.* B **18** 2701

OPTICAL PROPERTIES OF Tl^{2+} HOLE CENTRES IN ALKALI HALIDES INVESTIGATED WITH OPTICAL DETECTION OF PARAMAGNETIC RESONANCE

J.-M. SPAETH* and U. ROGULIS**

*University of Paderborn, Fachbereich Physik, D-33098 Paderborn, Germany

**Institute of Solid State Physics, University of Latvia, LV-1063, Riga, Latvia

ABSTRACT

The optical absorption band of Tl^{2+} hole centres have been investigated by measuring the magnetic circular dichroism of the absorption bands (MCDA) as well as MCDA-detected electron paramagnetic resonance (MCDA-EPR). Several new absorption bands were found using the excitation spectra of the MCDA-EPR lines of Tl^{2+}. In the iodides there is a total of 7 MCDA bands, more than predicted by the molecular orbital picture discussed so far in the literature.

Keywords: Magnetic circular dichroism of the absorption (MCDA), MCDA-EPR, Tl^{2+} hole centres, alkali halides

1 INTRODUCTION

Upon x-irradiation at room temperature of alkali halides doped with Tl^{+}, Tl^{2+} hole centres are generated. They have been studied previously by electron paramagnetic resonance (EPR) in several alkali halides [1,2] and also by optical absorption spectroscopy which identified several absorption bands (see e.g. [3] for KCl). RbI:Tl^{+} is an x-ray storage phosphor, where Tl^{2+} acts both as a hole trap centre and activator. Upon photostimulation of F centres and recombination of the F electron with the Tl^{2+} centre, the Tl^{+} centre luminesces, which is used for the image formation [4]. It was therefore of great interest to identify all absorption bands of Tl^{2+}, since excitation in the Tl^{2+} absorption bands also leads to a Tl^{+} emission with simultaneous creation of V_K centres at low temperature [4].

2 EXPERIMENTAL RESULTS

Figure 1 shows as an example the MCDA-detected EPR spectrum of Tl^{2+} in RbI. In all measured alkali halides one broad structureless line appears due to the $|1,-1> \rightarrow |1,0>$ transition of the Tl^{2+} with the quantum numbers $F = 1$, $m_F = 0, \pm 1$ due to the large hyperfine (hf) interaction A with the two magnetic isotopes ^{203}Tl (29.5% abundance) and ^{205}Tl (70.5% abundance), $I = 1/2$ for both [1]. For RbI $A = 48 \pm 3$ GHz; g was assumed to be 2.01 (for further details and data of the other alkali halides see [5]). Figure 2 shows the MCDA bands obtained by measuring the MCDA excitation spectra of the Tl^{2+} resonance line. The peak positions of the measured MCDA bands are collected in table 1 along with those previously published and with the absorption band peaks. There are numerous bands yet unknown, which are clearly due to Tl^{2+}, since the EPR of Tl^{2+} can be measured in all bands.

3 DISCUSSION

The electronic configuration of Tl^{2+} is $6s^1$ in an octahedral crystal field: $Tl^{2+}\text{-}X_6^{6-}$ (X^- = halogen$^-$).The a_{1g} ground state is paramagnetic. The optical transition from $^2S_{1/2}$ to the spin-orbit split $^2P_{3/2}$ and $^2P_{1/2}$ excited states gives rise to the two UV transitions, of which, except for RbI, only the one with lower energy ($^2P_{1/2}$) is shown in figure 2. The reversal of sign is typical for a spin-orbit-split excited state and has been reported before [6]. Further transitions are possible according to Moreno [11, 12] into the σ and π linear combinations of halogen p-orbitals with t_{1u} symmetry resulting in two further transitions, which should have a reversal of signs in MCDA as observed, accounting for 4 further MCDA bands at lower energy. The energy splittings between the positive and negative bands decrease on going from the iodides to bromides and chlorides according to the decrease of the spin-orbit coupling. However, the additional low energy transition in the iodides is not explained. An explanation is offered by Cabria *et al.* [13] using an MS-Xα calculation and including the ligand spin-orbit effects.

REFERENCES

1. W. Dreybrodt and D. Silber, *Phys. Stat. Sol.* **20**, 337 (1967)
2. W. Frey, R. Huss, H. Seidel and E. Werkmann, *phys. stat. sol.(b)* **68**, 217 (1975)
3. C. J. Delbecq, A. K. Gosh and P. H. Yuster, *Phys. Rev.* **151**, 599 (1966)
4. U. Rogulis, C. Dietze, Th. Pawlik, Th. Hangleiter and J.-M. Spaeth, *J. Appl. Phys.* **80**, 2430 (1996)
5. U. Rogulis, J.-M. Spaeth, I. Cabria, M. Moreno, J. A. Aramburo and M. T. Barriuso, *J. Phys.: Condens. Matter* **10**, 6473 (1998)
6. J. H. Beaumont, W. Hayes and R. T. S. Laiho, *J. Phys. C: Solid State Phys.* **6**, 6479 (1973)
7. M. Roth and A. Halperin, *J. Phys. Chem. Sol.* **43**, 609 (1982)
8. W. B. Hadley, S. Polick, R. G. Kaufman and H. N. Hersh, *J. Chem. Phys.* **45**, 2040 (1966)
9. H. N. Hersh, *J. Chem. Phys.* **31**, 909 (1959)
10. R. A. Kink, *Doctoral Thesis*, Tartu (1968)
11. M. Moreno, *J. Phys. C.: Solid State Phys.* **12**, L921 (1979)
12. M. Moreno, *Solid State Comm.* **29**, 653 (1979)
13. I. Cabria, M. Moreno, J. A. Aramburo, M. T. Barriuso, U. Rogulis and J.-M. Spaeth, *J. Phys.: Condens. Matter* **10**, 6481 (1998) and this conference

FIGURE AND TABLE CAPTIONS

Figure 1 MCDA detected EPR spectra of Tl^{2+} in RbI measured at 1.5 K and 23.7 GHz

Figure 2 The spectra of the 'tagged MCDA' of the Tl^{2+} centres of 6 alkali halide crystals measured at 1.5 K in the EPR lines of Tl^{2+}. For RbCl, KBr and RbI crystals the low energy part of the spectra was scaled up.

Table 1 Band positions of the MCDA bands and of the absorption bands of Tl^{2+} centres in 6 alkali halide crystals (values in eV).

KCl ABS	3.40; 4.22 [3]	4.73; 5.63 [3]
KCl MCDA	3.35; 3.6; 4.05 (v. weak)	4.73; 5.67[6]
RbCl MCDA	3.15; 3.50	4.75
KBr ABS	2.58 [7]	4.46 [7]
KBr MCDA	2.55; 3.05; 3.57; 4.0	4.48
RbBr MCDA	2.48; 2.95; approx. 3.45; 3.9	4.40
KI ABS	1.58; 2.25; 2.79; 3.42 [8-10]	4.06; 4.82 [8-10]
KI MCDA	1.60; 2.07; 2.45; 2.8; 3.43	4.05; 4.82 [6]
RbI MCDA	1.57; 2.03; approx. 2.35; 2.7; 3.25	4.07; 4.82

Table 1

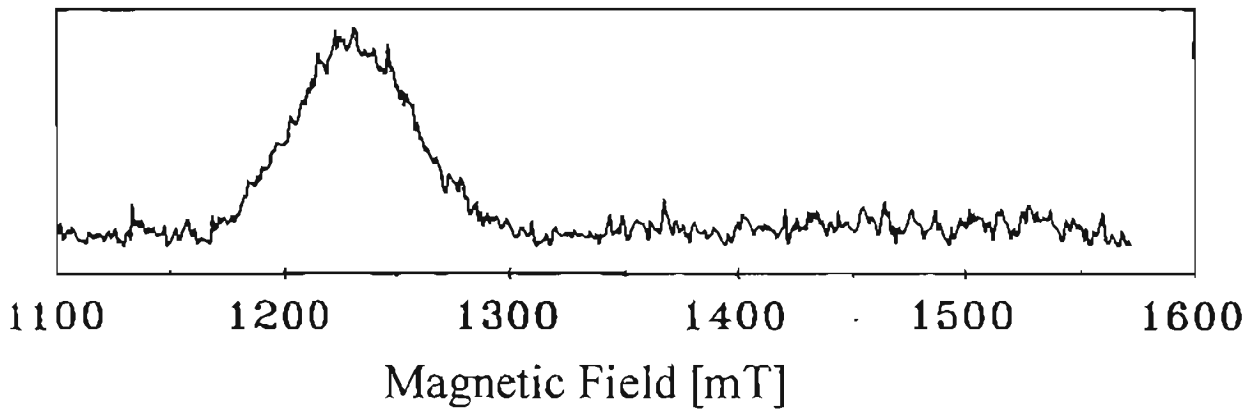
1100
1200
1300
1400
1500
1600
Magnetic Field [mT]

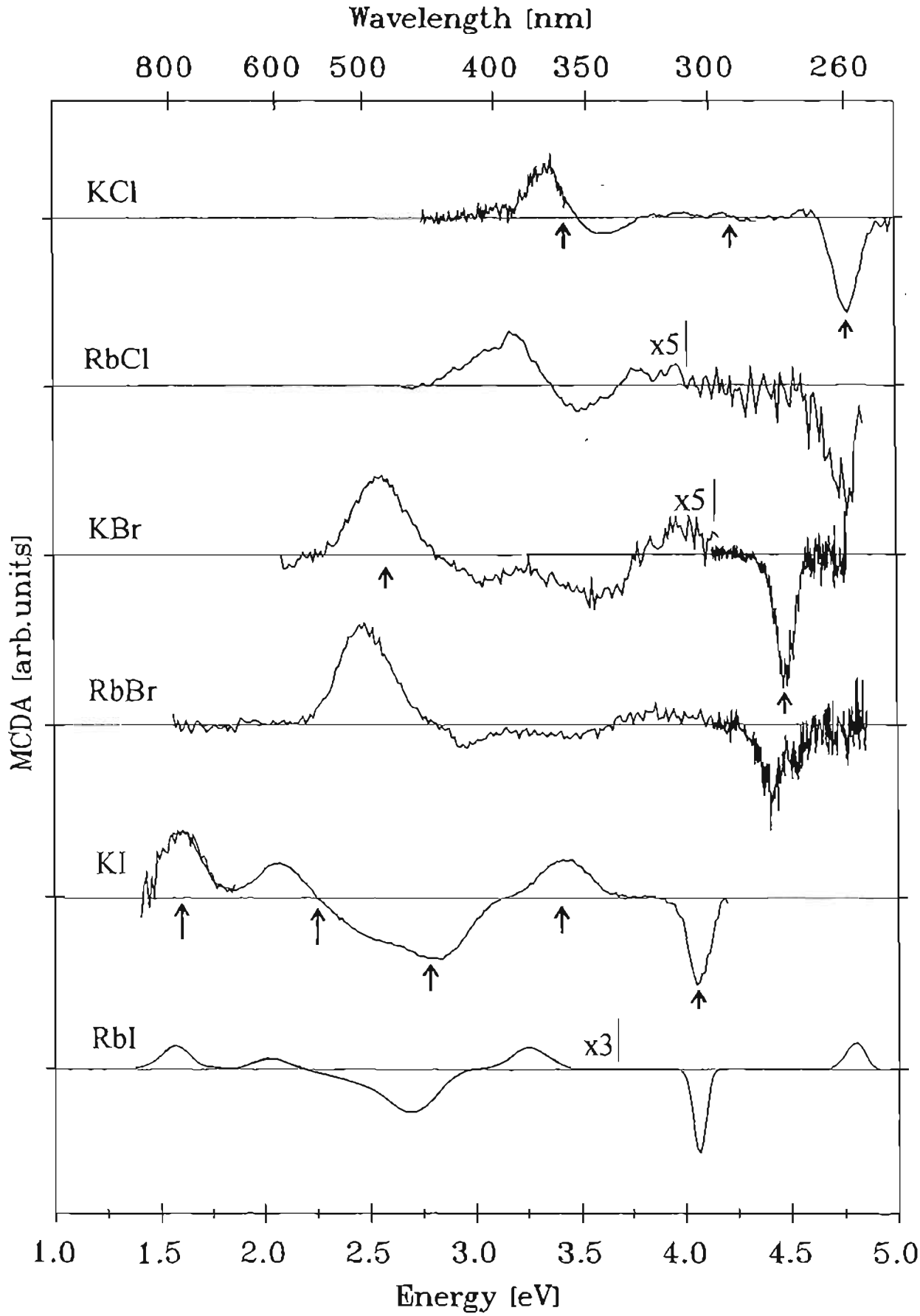
Wavelength [nm]
800
600
500
400
350
300
260
KCl
RbCl
x5
KBr
x5
RbBr
KI
RbI
x3
MCDA [arb.units]
1.0
1.5
2.0
2.5
3.0
3.5
4.0
4.5
5.0
Energy [eV]

Radiation Effects and Defects in Solids, 1995, Vol. 135, pp. 361–365
Reprints available directly from the publisher
Photocopying permitted by license only

ODMR OF CD IMPURITY CENTERS IN GG IRRADIATED BaF_2 CRYSTALS

U. ROGULIS, J. TROKŠS, Ā. VEISPĀLS, I. TĀLE, P. KŪLIS and M. SPRIŅĢIS

Inst. of Solid State Physics, University of Latvia, 8 Ķengaraga Str., LV-1063, Rīga, Latvia

The magnetic circular dichroism of the optical absorption (MCD), optically detected magnetic resonance (ODMR) as well as ESR and luminescence in Cd- doped BaF_2 crystals γ-irradiated at RT were investigated. MCD signals centered at 295 nm, 290 nm and 365 nm are observed, together with corresponding radiation induced optical absorption bands in the same wavelength regions. The ODMR detected in all these bands is caused by hyperfine (hf) interaction of unpaired spin with Cd- nucleus. Three types of different Cd- related defects have been separated: 1) Cd^+_c represented by the MCD of derivative type centered at 295 nm and hf constant $A_{Cd} = 480$ mT, 2) Cd^+_c-center having lowered symmetry of the nearest neighbours and represented by derivative- type MCD centered at 290 nm and $A_{Cd} = 370$ mT. The nature of perturbation is not clear yet. The ESR spectrum of perturbed Cd^+_c-center significantly differs from that of the regular Cd^+_c-center. 3) Center represented by the MCD around 365 nm and the hf constant $A_{Cd} = 380$ mT which is attributed to $Cd^+(1)$-type center.

Key words: BaF_2-Cd; Impurity defects; MCD; ODMR; Optical absorption; Luminescence

BaF_2 single crystals find widespread use as fast scintillators, however, only the lead and oxygen—impurity bands have been identified in UV spectral region so far. The optical properties of Cd- related defects are not known. Substitutional Cd^+_c-defects in alkaline-earth fluorides were recently studied by the ESR technique.[1] ODMR due to Cd- centers detected by tunnelling—recombination luminescence have been observed in CaF_2.[2] ODMR spectra of Cd^+_c and A_F(Cd) defects have been detected in KCl and NaCl crystals.[3]

We studied Cd- defects in BaF_2-Cd crystals using the MCD, ODMR, ESR, optical absorption and luminescence techniques. Cd- doped BaF_2 crystals were grown in vacuum and contained approximately 0.02 at.% Cd. Part of the crystals (denoted as type I) contained at least an order of magnitude less impurities. The impurity content of the other crystals (type II) was comparable to or exceeding (up to 10^{-1} at.% for alkali metal ions) the Cd concentration. The impurity content was controlled by atomic absorption and mass-spectrometry.

Samples were γ-irradiated at room temperature (doses 10^5–10^8 rad). MCD measurements were performed in helium-immersion cryostat (T = 2–4.2 K) in the spectral range 205–530 nm, the applied magnetic field being up to 3.4 T. Frequency range 38-53 GHz (microwave power on the sample in nonresonance system $\sim$ 5 mW) were used for ODMR measurements.

Characteristic γ -induced absorption band of the type I crystal (Figure 1a), located at $\sim$ 295 nm has a derivative type line shape MCD spectrum (Figure 1b). The spectrum of the MCD of the type II crystal (Figure 1c) is shifted to shorter wavelengths $\sim$ 290 nm in respect to that of the type I. The distortion of the line-shape is due to excessive optical density in the type II samples. Additionally, another MCD band located at $\sim$ 365 nm with a shoulder at long wavelength side occurs.

The observed ODMR signals are qualitatively the same for all MCD bands (located at 290, 295 and 365 nm) in both types of samples (Figure 2a, Figure 2b). In the frequency range from 38 GHz to 53 GHz the ODMR spectrum has a central line at $g \sim 2$, the splitting of the side lines is frequency- independent and evidently is the hf splitting (hfs). Analysis indicate that the observed hf splitting is due to Cd-isotopes Cd^{111} (12.8% nat. abundance) and of Cd^{113} (12.2%) both having spin I=1/2. The average values of hfs for

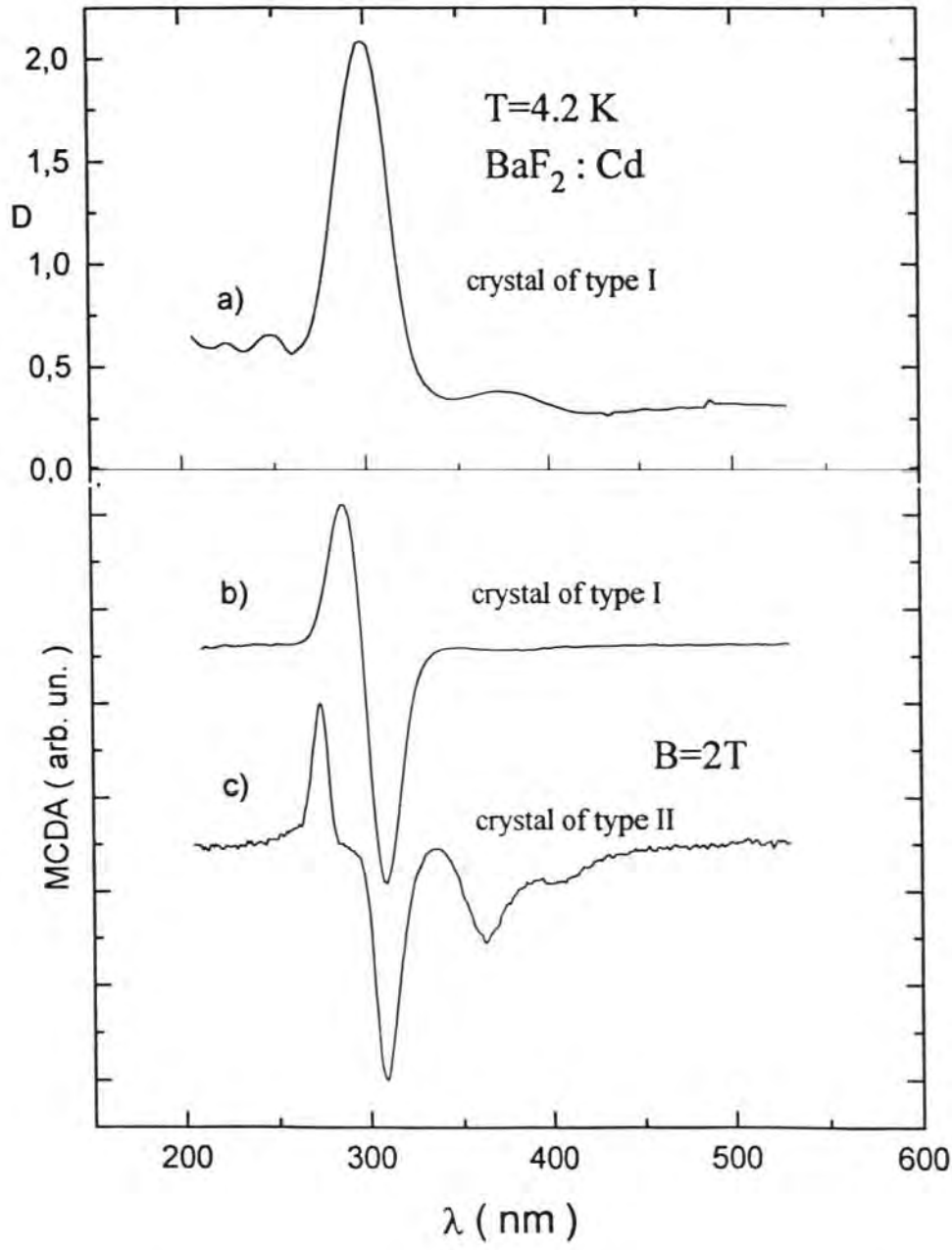

FIGURE 1 The spectrum of the γ-ray induced absorption of the BaF_2-Cd (0.02 at.%) crystal of type I (curve a) and the spectrum of the magnetic circular dichroism of the crystal of type I (curve b) and of type II (curve c).

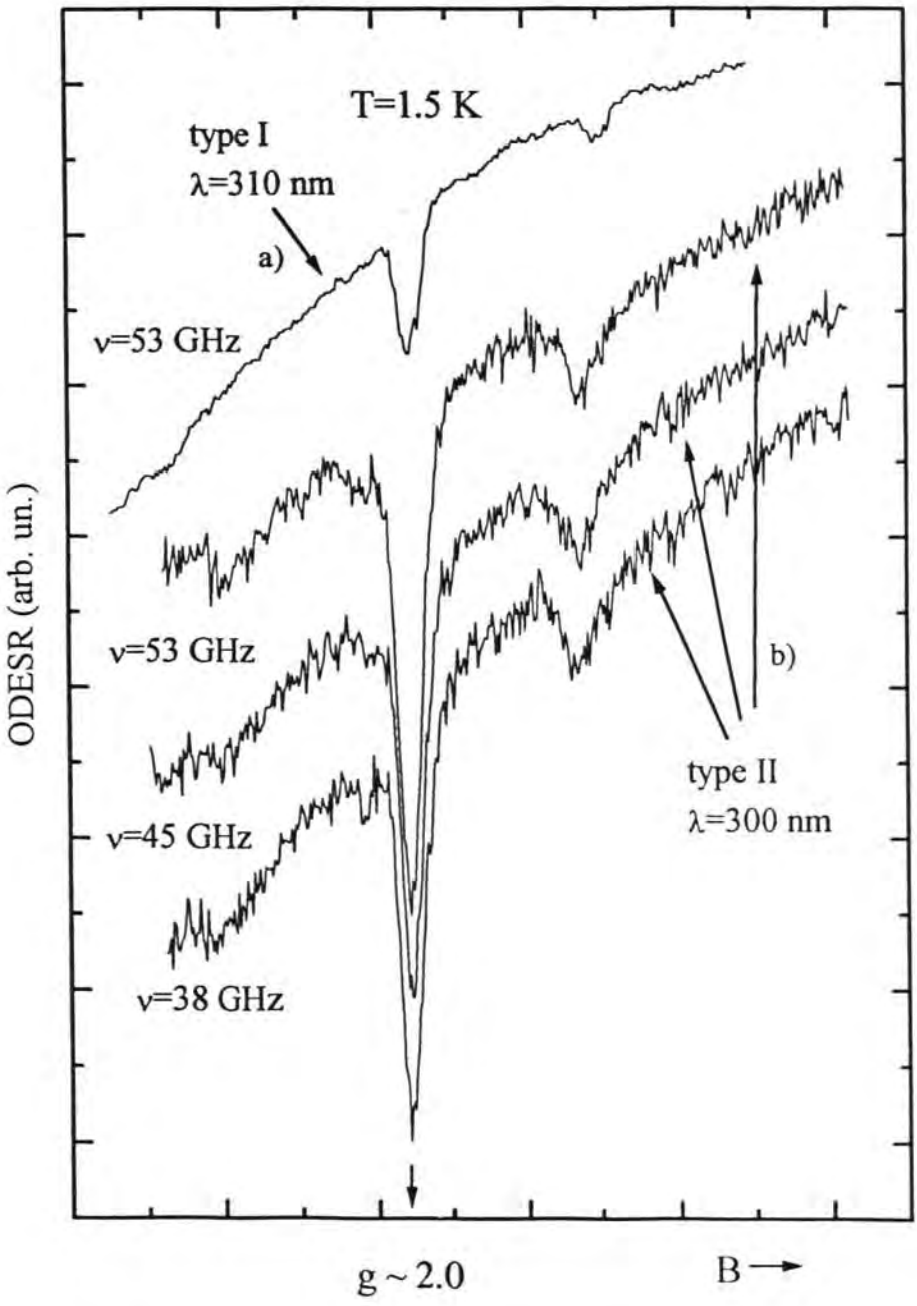

FIGURE 2 The spectrum of the ODESR of the BaF_2-Cd crystal of type I, detected at 310 nm MCD band (curve a), of the crystal of type II, detected at 300 nm MCD band (curves b).

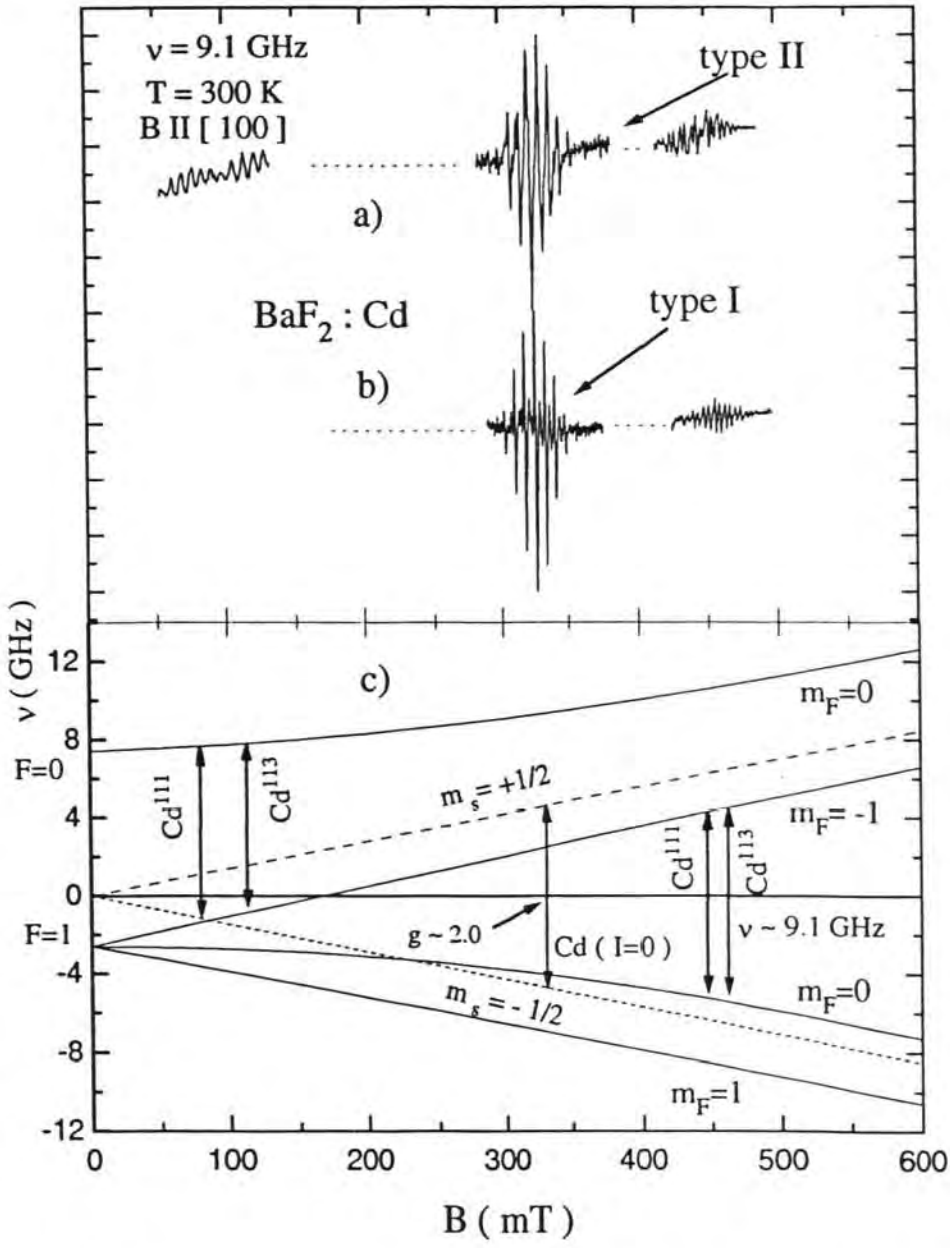

FIGURE 3 The spectrum of the conventional ESR of the BaF_2-Cd crystal of the type II (curve a) and, for comparison, the ESR spectrum of the crystal of the type I (curve b), which has the same parameters as the ESR of the Cd^+_c center known from the literature.[1]
Curve c–Breit-Rabi diagram for the ESR spectrum of the sample of type II.

different MCD bands differ, the expected slight difference between the hfs due to Cd^{111} and Cd^{113} is not resolved because of the large width of the ODMR lines. Although the hf splitting for 290 nm (A = 370 mT) and for 365 nm (A = 380 mT) MCD bands of type II crystals has close values, the difference in thermal annealing kinetics of the corresponding optical absorption bands indicate their different nature.

The spectrum of the conventional ESR of the BaF_2 -Cd crystal of the type I (Figure 3b) is consistent with the parameters observed earlier for Cd^+_c-centers:[1] hf interaction is isotropic with $A(^{111}Cd) = 12.51$ GHz and $(^{113}Cd) = 13.06$ GHz, the isotropic g-factor is $g = 1.9846$ at 300 K. Two significant differences are observed in the ESR spectrum of the crystals of the type II (Figure 3a): (i) The central group no more has correctly 'binomial' shf interaction with 8 equivalent fluorine nuclei, nature of the perturbation causing this deviation is not clear at now. (ii) A low- field ESR group from Cd- hf interaction occurs. The hf parameter values obtained from the ESR spectrum are $A(^{111}Cd) = 10.04 \pm 0.03$ GHz and $(^{113}Cd) = 10.51 \pm 0.03$ GHz at 300 K.

The values of hf splitting parameter A, estimated by ODMR both for the 290 nm band and for the 365 nm band, within the measurement accuracy coincides with those obtained by ESR (taking into account characteristic changes of the hf constant A with the temperature).[1] Because in the samples of type II the 290 nm MCD band strongly dominates and no other ESR signal can be separated, we attribute the obtained ESR signal to the 290 nm MCD band.

So, there are at least three types of Cd- defects, which occur in BaF_2- Cd crystals after irradiation: a) Cd_c^+-defect, b) perturbed Cd_c^+-defect, nature of perturbation is not clear at now, c) following the peculiarities of the activator-vacancy associate centers observed in alkali- halides[3] we attribute the center with the 365 nm MCD band to Cd^+ (1) type center which involves adjacent anion vacancy, where the unpaired spin is mostly localised at Cd^+ ion.

Excitation in the region of the discussed absorption bands at 290 nm and 295 nm results as well in photoluminescence bands at $E \sim 730$ nm and 750 nm respectively, both with approximately the same half-width ~ 0.35 eV. The intensity of this luminescence increases insignificantly upon cooling from 300 K down up to 77 K.

REFERENCES

1. V. F. Krutikov, N. I. Silkin and V. G. Stepanov. *Sov. Phys. Sol. State*, **18**, 2958 (1976).
2. P. G. Baranov, V. A. Vetrov, N. G. Romanov, *Sov. Phys. Sol. State*, **25**, 1364 (1983).
3. N. G. Romanov, V. V. Dyakonov, V. A. Vetrov and P. G. Baranov. *Phys. Stat. Sol.*, **B147**, K171 (1988).

OPTICAL AND SPECTRAL PROPERTIES OF THE Cd- CONTAINING BaF_2

M. Spriņģis, Ā. Veispāls, P. Kūlis, U. Rogulis, I. Tāle, J. Trokšs
Institute of Solid State Physics, University of Latvia, Ķengaraga Str., Riga, Latvia

Abstract. The Cd is presented as an alternative to Pb for extraction of the oxygen from BaF_2. In Cd- containing crystals γ- irradiation induces new absorption bands at 295, 290 and 360 nm, caused by three different Cd- related defects: Cd^+_c, $Cd^+(x)$ and $Cd^+(I)$ respectively. These bands does not affect the crossluminescence (the fast component of UV emission) but diminishes the self- trapped exciton luminescence (slow componente of UV emission).

The application of the BaF_2 scintillators for photon calorimetry in high energy particle colliders requires use of large crystals transparent in the spectral region from 190 to 230 nm, where UV emission band (crossluminescence) with two maxima at 195 and 220 nm and extremely fast decay time (600- 800 ps) is located [1]. In addition to the fast luminescence band, the BaF_2 crystal has a slow emission component at 310 nm with a decay time of 600ns, caused by the self trapped excitons (STE) and being undesirable for high count rate applications [1].

Unfortunately, BaF_2 crystals, usually grown using the Bridgman method, have absorption bands around 200nm, caused by oxygen. To avoid a contamination of the crystal with the oxygen, so called "scavenger" is added to the starting material. This is another fluoride, that easily reacts with oxygen and subsequently evaporates from the melt.

The PbF_2 is mostly used as "scavenger" in the case of BaF_2. It was shown, that the Pb has also the absorption band at 205 nm and an extra scintillation emission band at 257nm, the main part of which consists of slow scintillation components (t~0.1ms) [1]. Thus, the absorption bands either of oxygen or Pb may be present in the case of deficit or in excess of Pb with respect to the amount of oxygen.

The addition of the CdF_2 in the melt is alternative to Pb technology to diminish the oxygen content in the BaF_2. The present report discuss the use of Cd for extraction of the oxygen and optical and magnetooptical characteristics of the Cd- related defects in BaF_2 -Cd crystals.

Three types of Cd-doped BaF_2 crystals, grown (in vacuum) by Bridgman method, have been examined. Part of the crystals (denoted as type I) contained approximately 10^{-2} at.% Cd. and at least an order of magnitude less another impurities. The impurity content of the other crystals (type II) was comparable to or exceeded (up to 10^{-1} at.% for alkali metal ions) the Cd (10^{-2} at.%) concentration. The crystals of the type III contained no detectable concentration of Cd (less than 10^{-4} at.%) and of order of 10^{-3} at.% for another impurities. The impurity content was controlled by atomic absorption and mass-spectrometry.

Unirradiated (as grown) samples of all the three types are transparent in the visible and UV spectral regions (Fig. 1a) and exhibit no significant absorption bands in the investigated crystals.

γ- irradiation (doses 10^3- 10^6 Gy) of the BaF_2 crystals of the types I and II results in creation of new absorption band centred at 290- 300nm (Fig.1b and Fig.1c correspondingly). An additional absorption band at the long wavelength side at 365 nm occurs for the crystal of the type II. The crystals of the type III show practically no induced absorption bands after the γ- irradiation.

Proc. Int. Conf. on Inorganic Scintillators and Their Applications, SCINT95,
1996, Delft University Press, The Netherlands

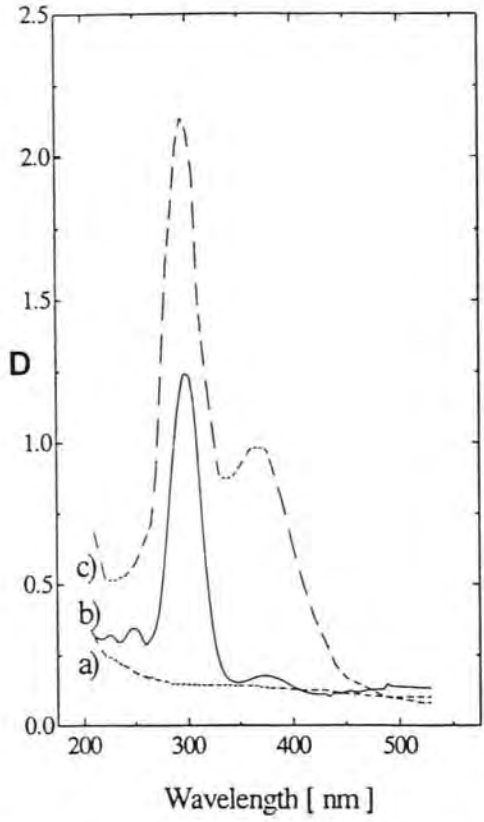

Fig.1. The spectra of optical absorption of the BaF_2 - Cd: a) unirradiated samples, b) typeI, γ- irradiated at 300 K,measured at 4.2 K
c) type II, γ- irradiated at 300 K, measured at 300 K

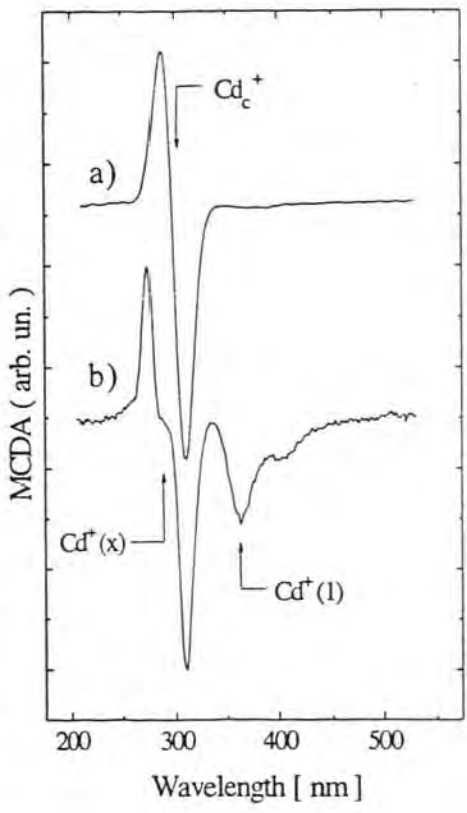

Fig. 2. The spectra of the MCD (at T=2K and B= 2T) of the BaF_2 - Cd crystals after γ- irradiation at 300 K :
a) of the type I,
b) of the type II.

We have investigated the defects created in the samples of BaF_2-Cd by use of the magnetooptical technique: the magnetic circular dichroism (MCD) and the MCD-optically detected EPR (OD EPR).

The samples of all the three types showed no MCD before the γ- irradiation. After the γ- irradiation, only two types of samples (I and II) have the MCD spectra, which we have identified as Cd- related defects by use of the method of the OD EPR. No signals of the magnetic circular dichroism have been observed, which we would attribute to Cd- defects in the crystals of the type III. We propose that in this case the impurity oxygen and Cd (added in the melt) concentrations were in such relation, that after the growth the crystal contains no Cd. In this case, the another impurities in concentration below 10^{-3} at.% create no significant changes in the absorption spectra after the γ- irradiation.

In the Fig.2 the spectra of the MCD are shown for the γ- irradiated BaF_2-Cd crystals of the type I (a) and of the type II (b). Qualitatively the same pattern of the OD EPR spectrum have been detected in whole the MCD bands. These spectra of the OD EPR are collected in the Fig. 3. and our analysis allows to identify them as caused by the different Cd- related defects, this analysis have been reported earlier in [2].

The corresponding MCD bands of Cd- related defects are scown in the Fig.2 by arrows. The whole MCD band of the derivative type is attributed to the Cd^{+}_{c} center (Cd^{2+} substituting Ba^{2+} and captured an electron) in the sample of the type I (Fig. 2a). We have

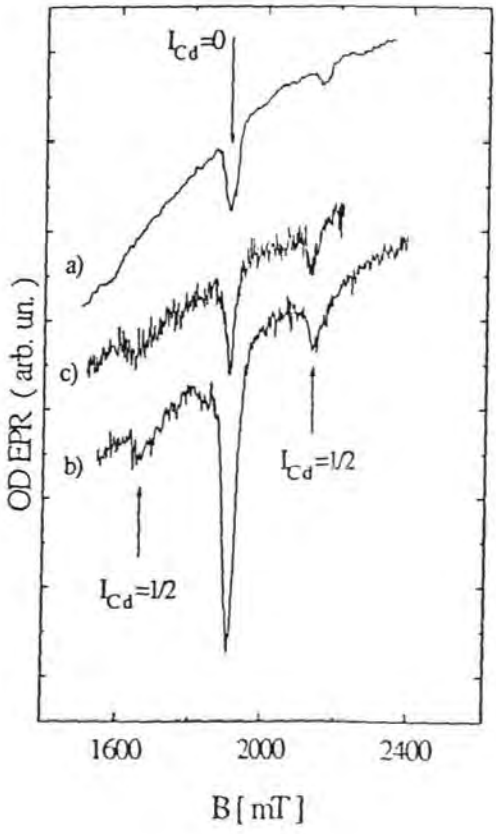

Fig. 3. The spectra of the OD EPR (at T=2K and ν = 53 GHz) :
a) type I, at 310 nm MCD band,
b) type II, at 300 nm MCD band,
c) type II, at 365 nm MCD band.

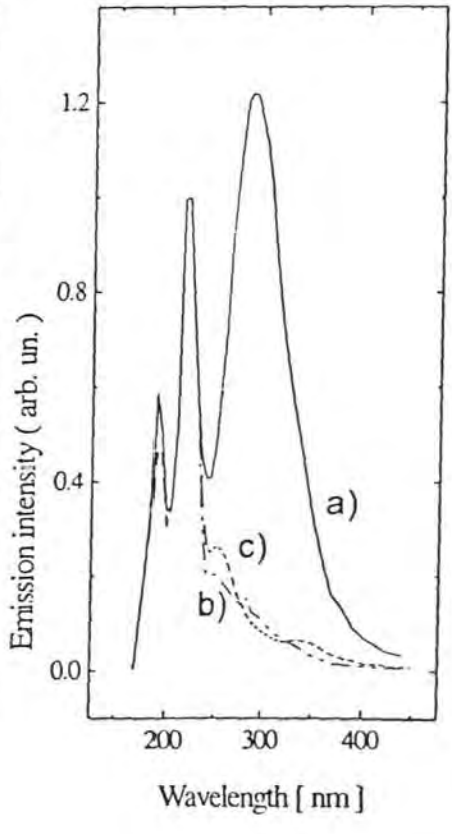

Fig. 4. The X- ray induced emission spectra of the BaF_2 - Cd crystals :
a) undoped, unirradiated sample,
b) Cd- doped, unirradiated sample of the type I,
c) Cd- doped, γ- irradiated sample of the type I.

interpreted the two MCD bands at about 275 nm and 310 nm to the perturbed Cd^{+}_{c} center (the nature of the perturbation stays unknown up to now) in the spectrum of the MCD of the sample of the type II. We have attributed the MCD band at 365 nm (as well as the little shoulder at the long- wavelength side, where the same spectrum of the OD EPR occurs) to the Cd^{+} (1) centers- an electron captured mostly on Cd^{2+} with the adjacent F- vacancy.

Excitation in the region of the discussed absorption bands at 290 nm and 295 nm results as well in photoluminescence bands at E~730 nm and 750 nm respectively, both with approximately the same half-width ~0.35 eV. The intensity of this luminescence increases insignificantly upon cooling from 300 K down up to 77 K. In the spectra of the X-ray induced luminescence these bands are about a factor of 100 weaker that the UV luminescence bands of the BaF_2 crystals.

Moreower, the presence of Cd does not affect significantly the crossluminescence in unirradiated and γ- irradiated crystals, but diminishes the intensity of the STE luminescence (Fig.4). As a result, the intensity of the STE luminescence in unirradiated samples is lower than that of crossluminescence, but comparable with the intensity of the crossluminescence in the γ- irradiated samples. No qulitative difference have been observed between the UV luminescence properties of the Cd- doped samples of the types I and II.

Thus, the Cd as an alternative to Pb allowed to diminish the oxygen content in BaF_2 and is perspective for production of high quality scintillators.

REFERENCES

[1] P. Schotanns et. al. IEEE Transact. on Nucl. sci., v.36, p.132-136 (1989).
[2] U.Rogulis et. al. Proceedings and Abstracts (p.291) of the EURODIM'94.

Pergamon

Radiation Measurements Vol. 29, No. 3–4, pp. 287–289, 1998

Printed in Great Britain

PII: S1350-4487(98)00027-4

1350-4487/98 $19.00 + 0.00

EPR OF MOLYBDENUM-RELATED DEFECT IN $CdWO_4$ CRYSTAL

U. ROGULIS

Institute of Solid State Physics, University of Latvia, 8 Kengaraga Street, LV-1063 Riga, Latvia

Abstract—EPR spectra of a molybdenum-related structure defect have been observed at a temperature of 20 K in $CdWO_4$ scintillator crystal, being as-grown "blue-coloured". Mo^{95} and Mo^{97} isotope superhyperfine (*shf*) splittings have been resolved. Further splittings in EPR spectra have been interpreted as arising from *shf* interactions with W nuclea. In the present model of the defect, the unpaired spin is localised in the Cd-site position and molybdenum replaces one of the neighbouring W atoms. © 1998 Elsevier Science Ltd. All rights reserved

1. INTRODUCTION

The luminescence properties of the well known scintillator crystal $CdWO_4$ could be influenced by structure defects appearing during crystal growth as well as by uncontrolled impurities. $CdWO_4$ has a tungstenite-type monoclinic structure (Wyckoff, 1965) and cleaves in the [010] plane. Electron paramagnetic resonance (EPR) spectra have been reported on several transition metal ions such as Cr^{3+}, Mn^{2+}, Fe^{3+}, Cu^{2+}, Co^{2+}, and Gd^{3+} in $CdWO_4$. New EPR spectra of molybdenum-related structural defects in $CdWO_4$ scintillator crystal were observed at temperatures of about 20 K. Although the EPR spectra were only observed in as-grown blue-coloured samples, there is as yet no direct evidence concerning the relation of the EPR spectrum to the defect responsible for the blue colour of the crystal. In as-grown uncoloured crystals this EPR signal is not present.

2. EXPERIMENTAL DETAILS

The investigated $CdWO_4$ crystals were grown by the Czochralski technique reported in Ovechkin *et al.* (1989), such crystals contained Mo as a common impurity at concentrations of about $5 \cdot 10^{-5}$ mol.%. No impurities were specially added to the melt, but the presence of the molybdenum impurity was unambiguously detected by the EPR measurements through the resolved Mo^{95} and Mo^{97} superhyperfine (*shf*) structure.

EPR spectra were measured on a conventional X-band (9 GHz) EPR spectrometer, equipped with a helium gas flow cryostat.

3. RESULTS

Figure 1, spectrum (a), shows the EPR spectrum for an orientation of the magnetic field parallel to the [010] direction of the $CdWO_4$ crystal, measured at 20 K applying a microwave frequency of 9.08 GHz. This EPR signal can also be observed at temperatures lower than 20 K. The spectrum shows splittings, which are positioned symmetrically to the intense central line. These splittings are found to be nearly isotropic.

The EPR spectrum can be described by the conventional spin-Hamiltonian:

$$\hat{H} = \mu_B \cdot \hat{S} \cdot \hat{g} \cdot \mathbf{B} + \sum_{i=1}^{n} \hat{S} \cdot \hat{A}_i \cdot \hat{I}_i. \qquad (1)$$

Hereby, the first term relates to the electron Zeeman interaction whereas the second term describes the *shf* interactions of the unpaired electron spin with several sets of equivalent neighbour nuclei.

The splittings in the EPR spectrum labelled with Mo^{95} and Mo^{97}, respectively, can be explained by a *shf* interaction of an unpaired spin $S = 1/2$ with molybdenum isotopes. The lines labelled with Mo^{95} are due to a *shf* interaction with Mo^{95} ($I = 5/2$ with a natural abundance of 15.9%), the lines labelled with Mo^{97} are due to a *shf* interaction with Mo^{97} ($I = 5/2$ with a natural abundance of 9.6%). The splittings in the EPR spectrum labelled with W_1 and W_2, respectively, can be explained by a *shf* interaction of the unpaired spin $S = 1/2$ with two different *shf* interactions with the tungsten nuclei W^{183} ($I = 1/2$ with a natural abundance of 14.3%). The ratio between the line intensity of the central line and the *shf* line indicates that the W_1 *shf* interaction is due to three and the W_2 *shf* interaction due to four equivalent tungsten nuclei. The isotropic *shf* parameters used for the calculations are listed in Table 1. Figure 1, spectrum (b), shows a simulated spectrum. All details of the experimental spectrum [Fig. 1, spectrum (a)] are well reproduced, even the relative intensities of the main *shf* lines.

One should note that it was possible to take an alternative set of *shf* parameters. This other set

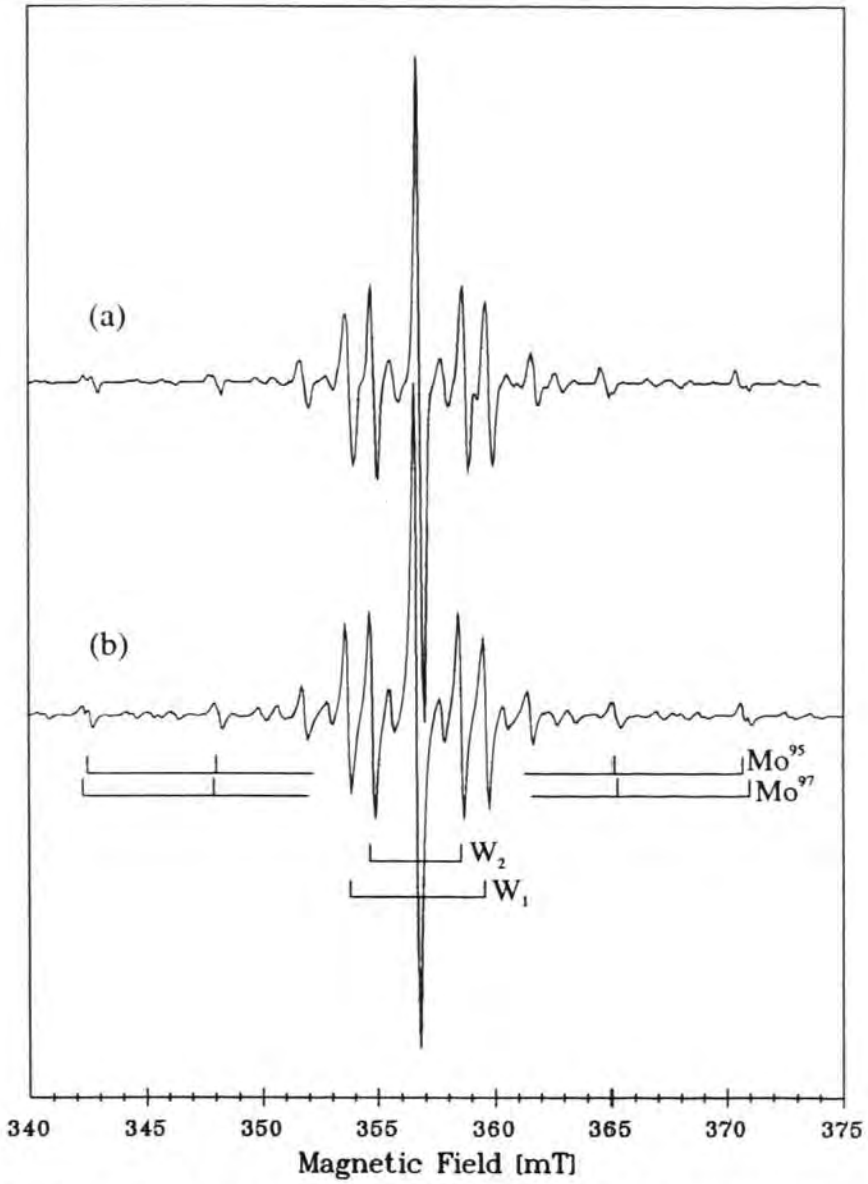

Fig. 1. (a) EPR spectrum of a $CdWO_4$ crystal, measured at 20 K for B|| [010] applying a microwave frequency of 9.08 GHz. (b) Simulated EPR spectrum with spin-Hamiltonian parameters listed in Table 1. The bars show the lines attributed to the *shf* interactions with two Mo-isotopes and two sets of equivalent W-nuclei.

included, besides the Mo *shf* interaction, two different *shf* interactions with two pairs of equivalent Cd neighbours (Cd^{111} has $I = 1/2$ with a natural abundance of 12.8% and Cd^{113} has $I = 1/2$ with a natural abundance of 12.2%). Additionally, further *shf* interactions with two different W^{183} nuclei were necessary to reproduce the measured *shf* lines. Also in this case the relative intensities of the main *shf* lines could not be reproduced exactly enough, therefore we preferred the set of parameters shown in Table 1.

Only one EPR spectrum for an arbitrary orientation of the crystal could be observed, no site split-

Table 1. Isotropic *shf* interaction parameters A_{iso} used for the simulation of the experimental spectrum in Fig. 1(a) with $g_{[010]} = 1.82$, a microwave frequency of 9.08 GHz, and an EPR linewidth of 5 MHz

Nucleus	Nuclear spin I	Abundance (%)	A_{iso} (MHz)	Equivalent neighbours
Mo^{97}	5/2	15.9	143	1
W^{183} (W_1)	1/2	14.3	153	3
W^{183} (W_2)	1/2	14.3	97	4

tings due to equivalent centre orientations were present. The EPR spectrum for different magnetic field orientations was positioned at g-values of $g < 2$. The g-value for a magnetic field along the [010] direction is $g = 1.82$. The g-tensor has not yet been determined exactly but it seems to have an axial symmetry, with the main axis along one of the crystallographic axes. The $g = 1.82$ value along the [010] axis is neither the minimal nor the maximal one for a rotation of the magnetic field from parallel [010] to perpendicular [010]. Therefore, we conclude that the main axis of the g-tensor must be either along the [100] axis or the [001] axis of the $CdWO_4$ crystal.

4. DISCUSSION AND SUMMARY

Let us discuss the possible structural model of the molybdenum-related defect according to the results of the analysis of the *shf* interactions of the EPR spectrum. We found the *shf* interactions of the unpaired electron with one Mo-neighbour as well as with two sets of equivalent W^{183}- nuclei, altogether with eight neighbour nuclei. In the present model of the molybdenum-related defect, the unpaired spin is localised in the position of the Cd-site in the structure of $CdWO_4$ crystal. Hereby, molybdenum replaces one of the neighbouring W atoms, since the *shf* interaction constant with the Mo-nucleus is about the same order of magnitude as that for W-nuclei. This situation is shown in Fig. 2, for a schematic presentation of the $CdWO_4$ structure similar to that shown by Watterich *et al.* (1991). No hyperfine splitting from Cd- or other nuclei at this Cd-site position has been observed. This means, either the unpaired electron is localised on a Cd-vacancy, or it is localised on an unknown ion, which has no nuclear spin. The unpaired spin at the Cd-site probably may have a charge compensation, so far as the EPR is present in as-grown $CdWO_4$ crystal. This hypothetical charge compensator may cause an axial shift of the unpaired electron from the Cd-site, probably in a direction along the [100] axis. The axial shift reduces the distance of the unpaired electron to the W_1- neighbours and it enlarges the distance to the W_2- neighbours. This allows us to explain the observed two groups of equivalent W-nuclei, with the significantly different (about a factor of 1.5) *shf* interaction constants.

In conclusion, a molybdenum-related structure defect has been investigated in the $CdWO_4$ scintillator crystal, being as-grown "blue-coloured". From the EPR data, the unpaired spin is localised in the Cd-site position and molybdenum replaces one of the neighbouring W atoms.

Acknowledgements—This work was partially supported by the Scientific Council of Latvia, Grant Nr. 960746. The author wishes to express his gratitude to Dr J. Trokss for experimental assistance, Dr V. Nagornaya for supplying the samples and Professor I. Tale for stimulating discussions.

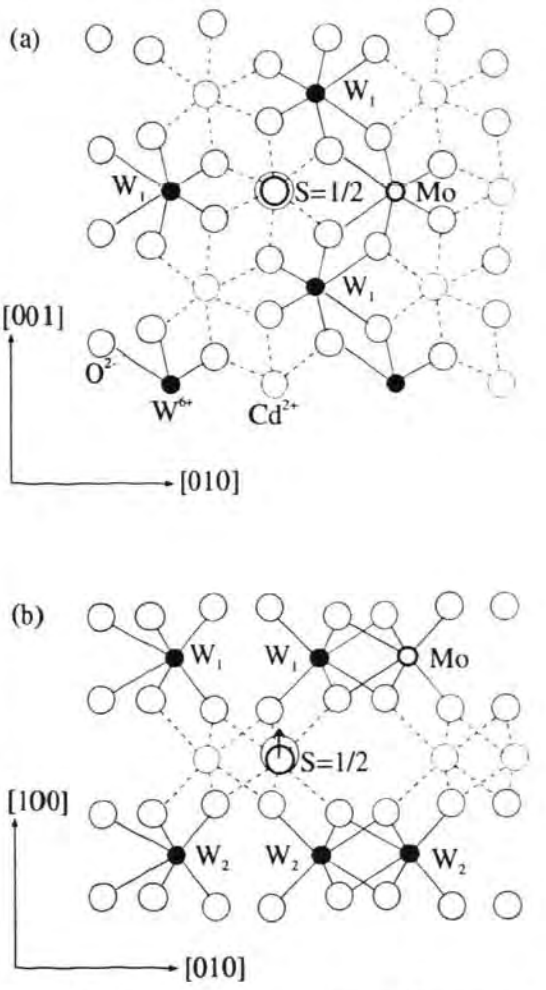

Fig. 2. Possible structural position of the unpaired spin $S = 1/2$ of the Mo-containing defect shown in two planes of the $CdWO_4$ crystal: (a) (100); (b) (001). Tungsten neighbours are labelled as W_1 and W_2 and Mo-ion replaces one of the W_1- neighbours. An hypothetical axial shift of the unpaired electron in [100] direction is shown by the arrow.

REFERENCES

Ovechkin, A. E., Nagornaya, L. L., Tupitsina, I. A. and Vostretsov, YaYa (1989) Colour centres in $CdWO_4$ crystals. *Journal Prikladnoi Spektroskopii* **51**, 146–148(in Russian).

Watterich, A., Edwards, G. J., Gilliams, O. R., Kappers, L. A., Madacsi, D. P., Raksanyi, K. and Voszka, R. (1991) ESR of platinum impurity ions in $ZnWO_4$ single crystals. *Journal of Physical Chemistry of Solids* **52**, 449–455.

Wyckoff, R. W. G. (1965) *Crystal Structures*, 2nd edn, Vol. 3, pp. 42–43. Interscience, New York.

Solid State Communications, Vol. 81, No. 9, pp. 745-748, 1992.
Printed in Great Britain.

0038-1098/92$5.00+.00
Pergamon Press plc

MAGNETIC CIRCULAR DICHROISM OF THE OPTICAL ABSORPTION AND OPTICALLY DETECTED ESR OF X-IRRADIATED Tb^{3+} DOPED AND UNDOPED $CaO{\cdot}P_2O_5$ GLASSES

D.Bricis*, J.Ozols*, U.Rogulis**, J.Trokss**

Faculty of Physics and Mathematics*, Institute of Solid state Physics**, University of Latvia, 19 Raina bulvaris, 226098, Riga, Latvia

W.Meise, J.-M.Spaeth

Fachbereich Physik, University of Paderborn, Warburgerstr. 100, D4790 Paderborn, F.R.G.

(Received 13 Dec. 91 by M. Cardona)

The magnetic circular dichroism of the optical absorption (MCDA) and optically detected ESR of $CaO{\cdot}P_2O_5$ and $CaO{\cdot}P_2O_5$-Tb_2O_3 glasses X-irradiated at RT are investigated. For the first time a direct correlation is obtained between the ESR spectra and magneto-optical absorption bands of radiation-induced defects in phosphate glasses. It is found that both PO_4^{2-} and PO_3^{2-} centers have several strongly overlapping absorption bands in the visible and infrared spectral regions. In Tb^{3+}- doped $CaO{\cdot}P_2O_5$ glass an intense derivative-like MCDA signal around 3.25 eV is assigned to the hole center Tb^{4+}.

1. Introduction

One of the main problems when studying radiation defects in glasses is the correlation between the optical absorption bands and the electron spin resonance (ESR) spectra of radiation-induced paramagnetic defects. For silicate glasses activated by Tb^{3+} it was established earlier[1] with the method of the magnetic circular dichroism of the optical absorption (MCDA) that the ionizing irradiation induced an absorption band around 3.75 eV which is caused by paramagnetic tetravalent Tb^{4+} centers. It was also noted that the hole centers responsible for the absorption bands of undoped silicate glasses observed in the visible and UV regions do not show MCDA effects. It was concluded that they may be diamagnetic.[1]

As is known from recent investigations the ESR spectra of irradiated phosphate glasses contain doublet lines due to a ^{31}P hyperfine interaction from the ion-radical PO_4^{2-} with a hyperfine-splitting of A=4 mT; the ESR lines with A > 80 mT were attributed to PO_3^{2-} radical defects.[2-5]

For irradiated phosphate glasses the problem of the correlation between the main absorption bands at 2.4 eV and ≈ 3.0 eV and the ESR lines of radiation-induced paramagnetic defects was examined recently using indirect methods. The 2.4 eV absorption band was connected with the ESR signal of the PO_4^{2-} radicals[3,4]. In phosphorus-doped SiO_2 glasses, the PO_3^{2-} defect was found to absorb at 0.8 eV in the spectral region of interest for fiber-optic communications.[5] However, no direct proof could be given for the assignments, nor was it clear whether all absorptions of these defects were found.

In the present report, the MCDA and optically detected ESR (ODESR) via the MCDA as well as "MCDA tagged by ESR"[6,7] were used to investigate irradiated undoped and Tb^{3+} activated calcium phosphate glasses. These magneto-optical methods are suitable for the establishment of the paramagnetism of a defect having an absorption band and for the correlation between this absorption band and the ESR spectrum of the paramagnetic defect.[6,7]

With these methods we were able to establish the correlation between the optical absorption and the ESR spectra of the radiation-induced defects in the phosphate glasses and we have discovered new absorption bands for the PO_4^{2-} and PO_3^{2-} defects.

2. Experimental

The undoped and Tb^{3+}- doped (0.1 mol. %) $CaO{\cdot}P_2O_5$ glasses were obtained from the S.I. Vavilov State Optical Institute, St. Petersburg, Russia. Polished X-irradiated samples (1-2 mm thick) were used for the MCDA investigations in the spectral range from 250 nm to 1700 nm at temperatures between 1.5 and 4.2 K and in the magnetic field region between B = 0 T and 2 T. The MCDA measures the differential absorption of right and left circular polarized light in a longitudinal static magnetic field B. The MCDA of a paramagnetic defect contains a small diamagnetic part which is temperature independent and can usually be neglected and a paramagnetic part which is temperature dependent. At very low temperatures the paramagnetic part varies approximately proportional to B/T.[6,7] When inducing microwave transitions between the ground state levels the MCDA is changed, which is utilized to detect the ESR transitions.

MCDA, ODESR and excitation spectra of the ODESR ("MCDA tagged by ESR"[6,7]) were measured with a custom built computer controlled K- band (24 GHz) spectrometer at the University of Paderborn and part of the MCDA measurements in the spectral range from 250 up to 750 nm were performed also in the University of Latvia, Riga.

The spin-lattice relaxation times were obtained by measuring the time needed for the MCDA signal to return to its thermal equilibrium value after switching off the microwave power inducing ESR transitions.

The radiation-induced changes of the absorption coefficient k were determined after X- irradiation at RT (50 kV, 10 mA, 30 min).

3. Results and Discussion

Figure 1 shows the spectra of the radiation-induced change of the absorption coefficient k (curve a) and the MCDA (curve b) of an undoped calcium-phosphate glass. The main MCDA signal changes sign at 2.5 eV (in the region of the radiation-induced absorption band at 2.4 eV) and the two less intense MCDA maxima are located at 0.85 eV and 1.2 eV. All these MCDA bands are dependent on temperature and magnetic field, indicating that one measures paramagnetic centers. The main MCDA signal in the region of the radiation

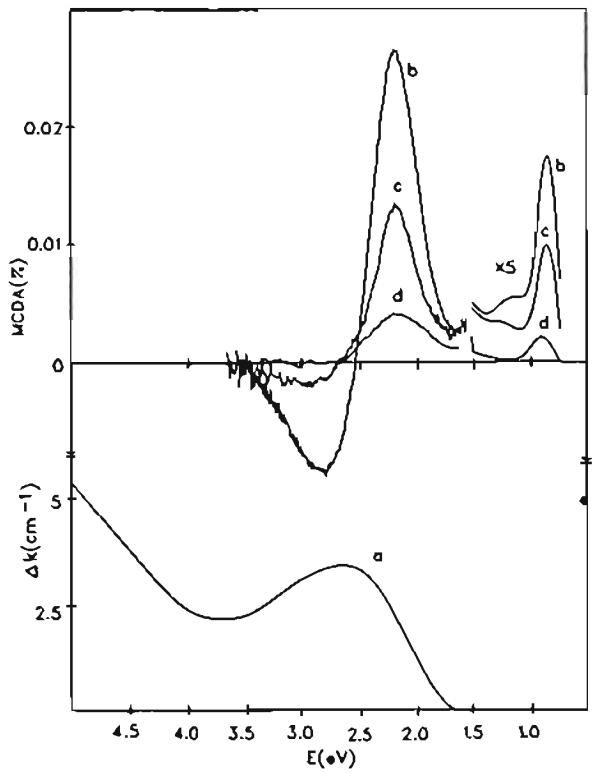

[Fig. 1.] Radiation-induced change of the optical absorption (curve a) and MCDA spectrum (curve b) of an undoped $CaO{\cdot}P_2O_5$ glass after X- irradiation at RT. "MCDA tagged by ESR" spectra for the ODESR of the PO_4^{2-} center (curve c) measured at B=875 mT and for the PO_3^{2-} center (curve d) measured at B=835 mT are also shown. Microwave frequency was 24.1 GHz, T=1.5 K.

induced absorption band at 2.4 eV decreases after thermal destruction of the PO_4^{2-} centers, which was controlled by parallel ESR measurements using a conventional ESR spectrometer.

Figure 2 (curve a) shows the ODESR spectrum of the X-irradiated undoped $CaO{\cdot}P_2O_5$ glass measured at 1.5 K and at 2.2 eV. One observes a strong central ODESR line in the region of g= 2 with a small, hardly resolved hyperfine splitting of $A=4\pm0.5$ mT and a weaker doublet with $A=90\pm3$ mT. These doublets belong to the PO_4^{2-} centers and PO_3^{2-} centers, respectively. The measured spin-lattice relaxation times have the following values: for PO_4^{2-} centers: $T_1=(6.5\pm0.5)$ sec. at 1.5 K and $T_1=(2.0\pm0.5)$ sec. at 4.2 K, for PO_3^{2-} centers: $T_1=5\pm0.5$ sec. at 1.5 K (at 4.2 K the signal was too weak for a T_1 measurement).

In the case of such a long spin-lattice relaxation time it is difficult to obtain a good resolution of the hyperfine doublet structure in the ODESR spectrum at 1.5 K due to saturation broadening. As one can see in Fig. 2, curve b, at a temperature of about 4.2 K it is possible to achieve a somewhat better resolution of the $^{31}PO_4^{2-}$ hyperfine structure.

It is possible to obtain the MCDA bands and thus to estimate also the corresponding absorption transitions for the paramagnetic PO_4^{2-} and PO_3^{2-} radicals by measuring the ODESR excitation spectra with the method of "MCDA tagged by ESR". Such spectra are shown in Fig.1. When setting the magnetic field to the PO_4^{2-} ESR line (875 mT), curve c is

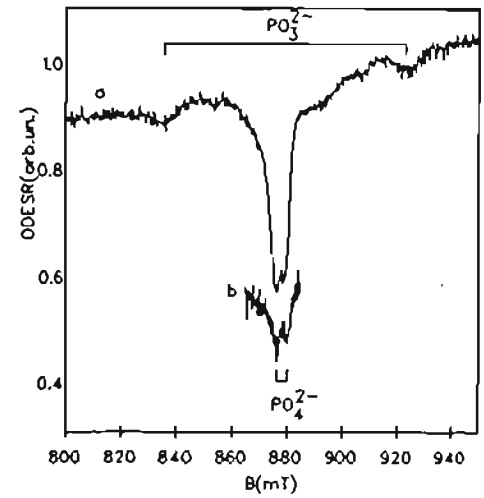

[Fig. 2.] The ODESR spectra of undoped $CaO{\cdot}P_2O_5$ glasses measured at 2.2 eV for T=1.5 K (curve a) and T= 4.2 K (curve b).

obtained, while curve d is obtained for the 835 mT line of PO_3^{2-} centers. The ODESR lines of the PO_4^{2-} centers are observable in all measured MCDA bands (compare curve b), but a small part of the MCDA belongs also to the PO_3^{2-} centers (curve d). It is evident, that the PO_4^{2-} centers have besides the main absorption band at 2.4 eV also absorption bands in the infrared region at 0.85 eV and at 1.2 eV which were not known so far. The radiation-induced optical absorption is too weak to be measured directly in this spectral region. Only with the MCDA technique these optical transitions are detectable. The PO_3^{2-} center has also an

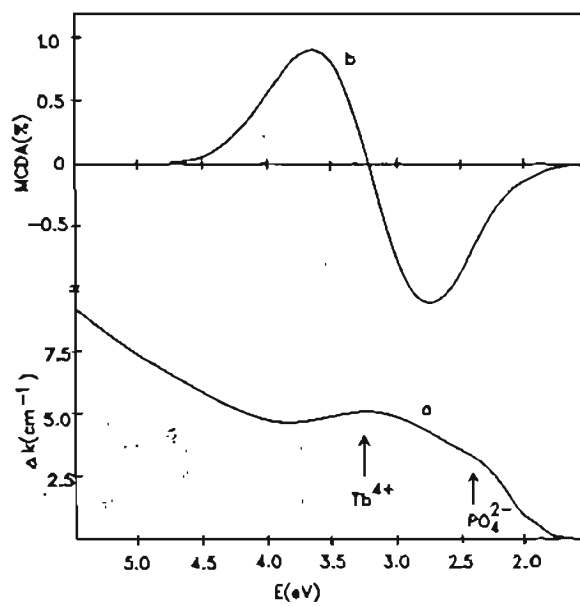

[Fig. 3.] Radiation-induced change of the optical absorption (curve a) and MCDA (curve b) spectra of a $CaO{\cdot}P_2O_5$-Tb^{3+} glass after X- irradiation at RT. The MCDA signal of the Tb^{3+}- doped glass is approximately two orders of magnitude more intense than the MCDA signal of the undoped glass.

already identified transition near 0.8 eV. However, while the absorption of PO_4^{2-} extends beyond 2.7 eV to higher energies that of PO_3^{2-} seems to vanish above 2.7 eV. It seems that PO_4^{2-} centers have two bands in the visible spectral region while PO_3^{2-} centers have only one.

The X-irradiation produces obviously also other defects with absorption bands above approximately 3 eV which seem to be diamagnetic since no clear MCDA effect could be observed (Fig. 1).

As far as we know, this is the first direct correlation between the ESR spectra of the paramagnetic PO_4^{2-} and PO_3^{-} radicals and the absorption bands in this undoped glass.

Figure 3 shows the spectra of the radiation-induced change of the absorption (curve a) and the MCDA (curve b) of Tb^{3+}- doped $CaO-P_2O_5$ glasses. In addition to the well known absorption of the PO_4^{2-} center at 2.4 eV one additional radiation-induced absorption maximum at 3.25 eV is seen.

The MCDA signal of the irradiated Tb^{3+}- doped glass is about two orders of magnitude more intense than that of the irradiated undoped glasses. It has a derivative like structure with a sign change near 3.25 eV. The MCDA of the Tb^{3+} doped glass is dependent on temperature and magnetic field. However, the temperature dependence of the MCDA signal is not as strong as that of the PO_4^{2-} centers. It has, for example, at B = 500 mT between T = 1.5 K and 4.2 K only a decrease of 30% while for these temperatures PO_4^{2-} has a decrease of approximately 60%. This observation is an indication that one deals with a system which has S > 1/2. Otherwise it should follow the temperature dependence of the Langevin function as does PO_4^{2-} with S = 1/2. Unfortunately all attempts to observe an ODESR signal in the MCDA of the Tb^{3+}- doped calcium phosphate glasses were unsuccessful.

A radiation-induced absorption band, peaking at 3.25 eV of Tb^{3+}- activated barium- phosphate glass was connected with electronic color centers.[3] Our experimental data enable us to associate the MCDA signal and the radiation-induced absorption band at 3.25 eV of Tb^{3+}- doped glass with Tb^{4+} centers using the following arguments:

1. The MCD signal of the Tb^{3+}- doped glass is more intense by a factor of about 100 than that for undoped glasses and its spectral shape is different.

2. In silicate glasses the MCDA signal of the Tb^{4+} center was found approximately in the same spectral region of 3.75 eV.[1]

The MCDA signal of the Tb^{3+}- doped glasses has a derivative structure and resembles the observations made for F centers in alkali halides.[8]

We propose that the MCDA signal is due to Tb^{4+} similarly to that observed in the silicate glasses. We must explain, at least qualitatively, that for Tb^{4+} a left and right circular polarized absorption occurs (Fig. 4). The ground state of the Tb^{4+} ion is $^8S_{7/2}$ ($4f^7$); in a magnetic field in many cases[9-11] the lowest Zeeman sublevel is that with $m_J = -9/2$. The nearest excited state will have the $4f^65d$ electronic configuration. In order to obtain an optical transition with $\Delta m_J = -1$ we need to assume the existence of J = 9/2 and 5/2 in the excited state. We propose that in the manifold of states in the $4f^65d$ configuration there are ^8P states which are able to explain our results. The optical transitions go to the spin-orbit split $^8P_{9/2}$ and $^8P_{5/2}$ "ionic" states. In the glass there may be an additional crystal field splitting. The left circular polarized transition goes from $^8S_{7/2}$ to $^8P_{9/2}$, the right circular polarized one to $^8P_{5/2}$ in analogy to the atomic model used to explain the F center results[12] in alkali-halides were transitions go from $^2S_{1/2}$ to $^2P_{1/2}$ and $^2P_{3/2}$. Similarly as has done for the F centers, that is assuming that the optical matrix elements are the same for the transitions with the $^8P_{m_J}$ levels and considering the relative matrix elements for the different circular polarized transitions one expects an intensity ratio of the left and right circular polarized transitions of about 4:3 and a derivative like structure for the MCDA, since the phonon width exceeds the splitting of the excited states. This ratio is indeed observed confirming the theoretical value. The minimal splitting of the $^8P_{9/2}$ and $^8P_{5/2}$ states, needed to explain the observed MCDA spectrum, is approximately 10 meV assuming a line width of about 1 eV for the absorption band. Such a width is usually observed in glasses. The existence of an excited ^8P state was also assumed previously to explain optical absorption data of the isoelectronic Eu^{2+} in a crystal field.[13]

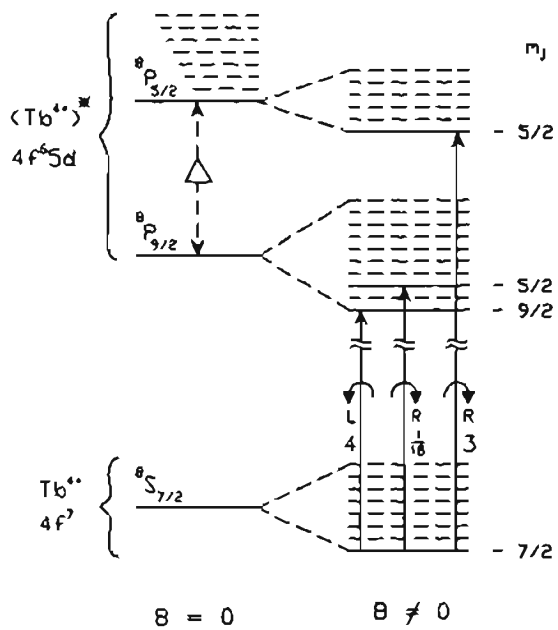

[Fig. 4.] Allowed MCDA transitions in the Tb^{4+} ion in the magnetic field B > 0. The ground state term $^8S_{7/2}$ of the $4f^7$ configuration of the Tb^{4+} ion splits into Zeeman sublevels with the lowest one with $m_J = -7/2$. In order to obtain two circular polarized components in the absorption, we propose $^8P_{9/2}$ and $^8P_{5/2}$ levels split due to spin- orbit interaction in the excited state of the Tb^{4+} ion.

It is not obvious how to explain the large difference between the MCDA signals of Tb^{4+} centres and PO_4^{2-} radicals of two orders of magnitude taking into account that both defects have approximately equal concentrations (approximately 10^{18} cm^{-3}). The concentration of PO_4^{2-} was determined by conventional ESR. Tb^{3+} was doped into the glass at a level of 0.1 mol. %. After irradiation Tb^{3+} was not changed detectably. Thus, Tb^{4+} can be present at most at a level of 10^{18} cm^{-3}. The absorption coefficients of PO_4^{2-} at 2.4 eV and that of Tb^{4+} at 3.25 eV are probably of the same order both being allowed transitions.

The reason for the very weak MCDA of the paramagnetic PO_4^{2-} centers may be the specific nature of the electronic states of the PO_4^{2-} molecule in a crystal field[14]. A qualitative analysis of the possible MCDA transitions in these molecules suggests that only in certain favourable PO_4^{2-} center orientations, i.e., orientations of the symmetry axes relative to the external magnetic field direction, circularly polarized transitions are allowed. Then an averaging procedure for all the randomly oriented centers in the glassy matrix can lead to a very weak MCDA signal.

4. Conclusions

1. Using magneto-optical techniques we have shown that the absorption bands attributed previously to PO_4^{2-} and PO_3^{2-} centers in oxide glasses do indeed belong to these

centers. We have identified also absorptions in particular in the infrared (between 0.7 and 1.3 eV) which may be of importance for the use of oxide glasses in fiber communication technology.

2. A strong MCDA spectrum was found to Tb^{4+}, which is qualitatively interpreted as arising from transitions of the $^8S_{7/2}$ to $^8P_{9/2}$ and $^8P_{5/2}$ excited states.

Acknowledgements - The authors would like to thank V. Masalskis for cooperation during the course of this research. We are also very grateful to Prof. J. Kliava for helpful discussions. The work was supported by a stipend. granted to one of us (U.R.) by the DAAD.

References

1. V.I. Arbuzov, J.J. Ozols, M.N. Tolstoi & M.A. Elerts. Sov.-Phys. Chem. of Glasses, 12, 608 (1986).
2. G.O. Karapetyan, A.K. Sherstyuk & D.M. Yudin. Opt. Spektrosk., 22, 443 (1967).
3. T.V. Bocharova, G.O. Karapetyan & O.A. Yaschurschinskaya. Sov.-Phys. Chem. of Glasses, 11, 677 (1985).
4. N.N. Vilchinskaya, A.V. Dmitryuk, E.G. Ignatyev, G.O. Karapetyan & G.T. Petrovskii. Sov. Phys.- Dokl., 274, 158 (1984).
5. D.L. Griscom, E.J. Friebele, K.J. Long & J.W. Fleming. J. Appl. Phys, 54, 3743 (1983).
6. J.-M. Spaeth & F. Lohse. J. Phys. Chem. Solids, 51, 861 (1990).
7. F.J. Ahlers, F. Lohse, J.-M. Spaeth & L.F. Mollenauer. Phys. Rev.B, 28, 1249 (1983).
8. R. Romestain & J. Margerie. J. Compt. Rend., 258, 2525 (1964).
9. D.J. Newmann & W. Urban. Adv. in Phys., 24, 793 (1975).
10. R. Bramley & S.J. Strach. Chem. Rev., 83, 49 (1983).
11. W. Low & R.S. Rubins. Phys. Rev., 131, 2527 (1963).
12. F. Lüty & J. Mort. Phys. Rev. Lett., 12, 45 (1964).
13. M.V. Yeremin. Sov.-Opt. Spectr., 26, 578 (1969).
14. P.W. Atkins & M.C.R. Symons. The Structure of Inorganic Radicals, Elsevier Publ. Comp., 1967.

DIRECT EXPERIMENTAL EVIDENCE FOR THE SPATIAL CORRELATION OF F AND H CENTERS IN KBr AFTER THEIR GENERATION AT LOW TEMPERATURE

W. Meise, U. Rogulis*, F. K. Koschnick, J.-M. Spaeth
Universität-GH Paderborn, FB Physik, Postfach 1621, D-4790 Paderborn
**Institute of Solid State Physics, University of Latvia, 19 Raina bulvaris, 226098, Riga, Latvia*

The dominant mechanism for intrinsic defect creation by ionizing irradiation in alkali halides is the decay of the self trapped excitons which leads to the formation of pairs of F and H (Br_2^--centers in KBr) centers (Itoh, 1982). Until now there are theoretical arguments and some experimental indications that these F and H center pairs are spatially correlated when created at low temperature, but no direct evidence.

We have investigated F and H centres in KBr, which was X irradiated at 4.2K, using optically detected ESR via the magnetic circular dichroism of the absorption (MCDA). Measuring ODEPR in the MCDA band of the F centre, we have found an ODEPR signal arising from H centers. As this measurement was performed in the low energy part of the F center MCDA, where no overlap of the optical absorption of F and H centers takes place, this observation is due to a cross-relaxation process between F and H centres. Figure 1) shows the ODEPR of H centers perpendicular to the magnetic field. (curve a) and the cross-relaxation effect (curve b) at different field positions of the H center ODEPR, measured in the low energy part of the F center MCDA. The MCDA of the F centers can increase as well as decrease, depending on the magnetic field position within the ODEPR spectrum of the H centres.

After heating the crystal for a few minutes to a temperature of 28K, where H centres become mobile, and recooling to the measuring temperature of 1.5K,

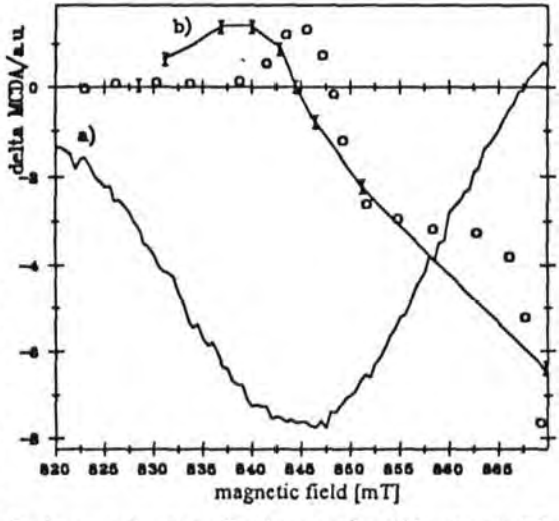

Fig.1: cross relaxation effect between F and H centers in KBr. a) ODEPR spectrum of H centers in KBr, b) measured cross-relaxation effect in the MCDA of the F centers, calculated cross-relaxation effect.

the ODEPR experiments indicate a small decrease of about 5% in the H centre concentration, however the cross-relaxation effect had completely vanished. The reason for this is a thermal dissociation of the correlated F-H pairs at the temperature around 28K.

We monitored the spin-lattice relaxation processes of the F center MCDA as a function of time and microwave power, as well as those of the H.

The cross-relaxation process can be qualitatively understood as a spin flip flop coupling between the electron spins of the F and the H centres involving cross-relaxation transitions between the hyperfine split energy levels of the H center. The probability for a spin flip-flop process due to point dipole-dipole- interaction is proportional to $1/R^6$, where R is the distance between the two spins. This way one gets information about the spatial correlation of two defects. The measured cross-relaxation

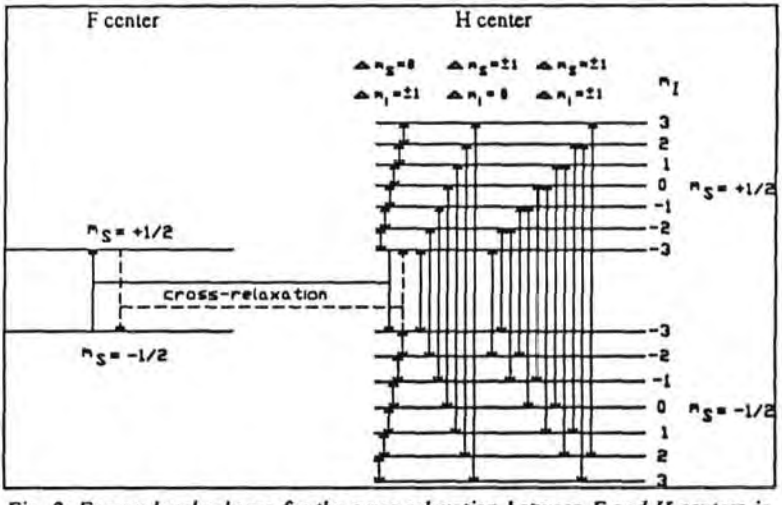

Fig. 2: Energy level scheme for the cross-relaxation between F and H centers in KBr. The vertical arrows indicate the transitions we involved in our calculation for the simulation of the cross-relaxation model.

effect is explained with a rate equation system including allowed and forbidden spin lattice relaxations in the H center and F center and a cross-relaxation parameter, CR, which contains the probability for a spin flip flop process [for details see Spaeth et al, 1992]. The circles in figure 1 show a fit of the rate equation system to the experiment. In figure 2 our model for the calculation of the F-H cross-relaxation is shown. The assumptions for our calculation are as follows:

1) Only rate equations are used where the nuclear Spin I does not change.
2) Only H centers with the total nuclear moment I = 3 couple to F centers.
3) We involve weak relaxations with $\Delta m_S = 0$ and $\Delta m_I = \pm 1$ and strong relaxations with $\Delta m_S = \pm 1$ and $\Delta m_I = \pm 1,0$.

4) The parameter CR (to be determined) is the cross-relaxation rate, $CR \sim 1/R^6$

For our calculations of the cross-relaxation effect, we used two models:

1) All H centers are correlated with F centers

In this case the rate equations fitted to the cross-relaxation effect yield a separation $R_{F,H}$ between the F and H centers of about $R_{F,H} \sim 20A$ from the fitted value of CR, which explains the cross-relaxation effect of about 5% of the F center ODEPR.

2) Only a fraction of H centers are correlated with F centers

Here the separation between correlated F and H centers becomes smaller than 20A. If for example the separation of F and H centers would be 14.1A, according to 3 halogen separations, 20% of the F and H centers must be correlated and about 80% should have a spacing of 5 or more halogen places in the [110] direction.

The observation can only be explained by spatially correlated F-H centre pairs with a separation of about 20A or smaller. 4 separations are possible for the F-H configuration (see figure 3). The nearest distance in KBr would bee 4.6A. In this case one would expect a large fine-structure splitting in the EPR spectrum. We calculated the point dipole-dipole-Interaction for all 4 configurations. For the 3 first next nearest configurations the fine structure splitting is bigger or equal to the line width (10G) of the H center hyperfine lines measured by Känzig et al. (1958). Only for the last separation of about 18.6A in KBr (see figure 3) there is a fine structure splitting smaller than the width of the H center hyperfine line. From this calculation the probable separation between the F and H centers is 4 halogen places in the [110] direction.

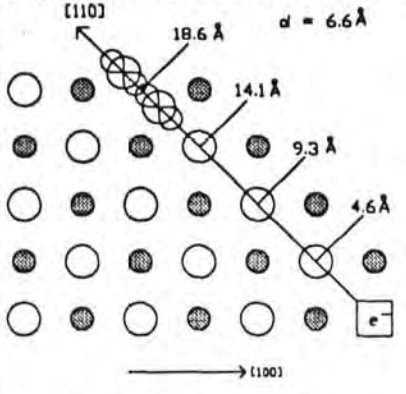

Fig. 3): Model for the spatial separation of F and H center pairs in KBr.

The observed cross-relaxation processes are the first direct experimental evidence of the spatial correlation of F and H centres after their creation at low temperatures.

References:
N. Itoh, Advances in Physics, 31, (1981), 491
W. Känzig, T. O. Woodruff, J. Phys. Chem. Solids, 9, (1958), 70
J.-M. Spaeth, W. Meise, U. Rogulis, to be published, (1992)

We would like to thank W. G. Mc Dugle (Eastman Kodak Co.) for providing the pure KBr crystal, necessary for our experiments.

Laser Materials

SPATIAL CORRELATION OF RADIATION-INDUCED DEFECTS IN BAFBR AND KBR STUDIED BY CROSS-RELAXATION ODMR SPECTROSCOPY

F. K. KOSCHNICK*, W. MEISE, U. ROGULIS**, J.-M. SPAETH AND R. S. EACHUS***

Fachbereich Physik, University of Paderborn,
Warburger Str. 100, 4790 Paderborn, Germany
*present address: Sherman Fairchild Center for Solid State Studies 161,
Lehigh University, Bethlehem, PA 18015-3185, USA
**University of Latvia, Riga, Latvia
***Eastman Kodak Laboratories, Rochester, NY, USA

ABSTRACT

Two examples are presented in which spatial correlations of defects play a decisive role. The first example is the correlation between the activator ion Eu^{2+} and electron and hole traps generated by X irradiation which is thought to be important for the mechanism of photostimulated emission of the X-ray storage phosphor $BaFBr:Eu^{2+}$. The second example is the F-H formation process in KBr where F and H centres are created by X irradiation at 4.2K. Both systems, the X-ray storage phosphor $BaFBr:Eu^{2+}$ and the alkali halide KBr, were investigated by cross-relaxation spectroscopy measured by optically detected electron paramagnetic resonance taking advantage of cross-relaxations between spin systems of different kinds of paramagnetic defects. We report the first direct experimental evidence for correlations among the radiation defects and the activator ion Eu^{2+} in the storage phosphor $BaFBr:Eu^{2+}$. We also could show that F centres and H centres in KBr created after the decay of the self trapped exciton at 4.2K are correlated and separated by about 4 lattice spacings along a [110] direction.

1. Introduction

Barium fluorobromide doped with Eu^{2+} is an important storage phosphor in which X-ray produced images are stable for long periods in the dark at room temperature[1-3]. Its dynamic range for image formation of over 5 orders of magnitude makes it superior to conventional X-ray films for many applications in medicine, crystallography and biochemistry. For readout, the phosphor is optically stimulated, frequently with a He-Ne laser (633nm), leading to an Eu^{2+} activator emission at 390 nm. Until now, the mechanisms of the storage and readout processes have not been understood, preventing improvements in the efficiency of the phosphor material and

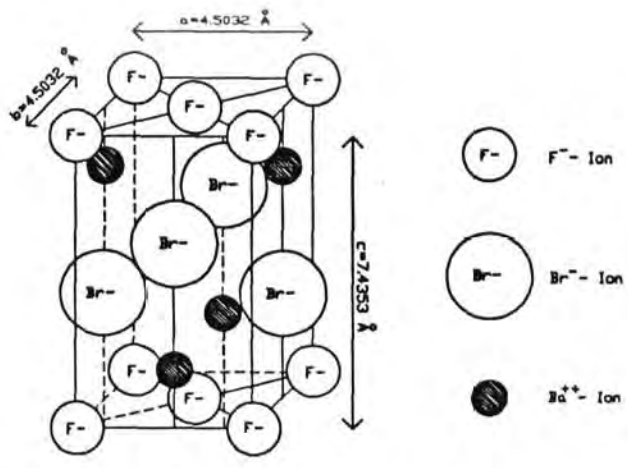

Figure 1: Structure of BaFBr. Two different types of F centres are possible. One is an electron bound to a bromine vacancy ($F(Br^-)$), the other is located at fluorine site ($F(F^-)$). Eu^{2+} occupies the substitutional Ba^{2+} lattice site.

providing a challenging fundamental problem of defect interactions. There is general agreement that electron and hole traps are involved in the process, the former being F centres on either the Br^- or F^- sublattices (BaFBr crystallizes with the PbFCl structure[4,5]). There are controversial views about the nature of the hole centres and the F centre production mechanism. Takahashi et al.[6,7] proposed that, upon X irradiation, Eu^{2+} is ionized to Eu^{3+} and the free electron is subsequently captured by an existing Br^- vacancy to form an $F(Br^-)$ centre. Von Seggern et al.[8,9,10] argued that high energy radiation creates free excitons which decay near Eu^{2+} to form an F-H pair. They assumed that the vacancies needed to form F centres are created by the irradiation process, in contrast to the views of Takahashi et al.[6,7]. The F-H centre production (the H centre is a Br_2^- ion occupying a Br^- site[8]) is thought to be analogous to the process known in the alkali halides. From a study of the temporal dependence of the photostimulated luminescence (PSL), von Seggern et al.[9] claimed that the hole trap, the electron trap and the Eu^{2+} activator must be in close proximity, a conclusion arrived at independently by Hangleiter et al.[11] from the temperature dependence of the PSL effect. There has been no experimental proof, however, for these spatial correlations.

A similiar question of defect correlations arises from the F-H mechanism in alkali halides. The F-H process, proposed by Itoh[8], is a formation process of radiation defects in which a self trapped exciton (STE) created by ionizing radiation decays into an F centre and an H centre. This process is thought to be the fundamental

radiation damage process in alkali halides. Until now there is no direct experimental evidence for a spatial correlation between the F centre and the H centre after the decay of an STE, i.e. whether these centres are created in a certain stable separation from each other or whether they are separated statistically.

In this paper we present the first direct experimental evidence that in BaFBr: Eu^{2+} the irradiation created electron centres, hole centres and the Eu^{2+} activators are correlated and not statistically distributed by detecting cross-relaxations among them using optically detected electron paramagnetic resonance (ODEPR). We also show that in KBr F centres and H centres are correlated after the decay of the STE at low temperature.

2. Experimental

Experimental evidence for the correlation of the various defects is obtained from the magnetic circular dichroism of the absorption (MCDA) and MCDA-detected ODEPR. The MCDA is the differential absorption for left and right polarized light propagating along a static magnetic field. It is proportional to the spin polarization of the ground state of a paramagnetic Kramers defect. Upon inducing EPR transitions in the ground state the spin polarization can be diminished. This is monitored as a decrease of the MCDA. ODEPR was measured with a custom built, computer controlled spectrometer working at K-band (24GHz) and at 1.5K[12]. A "tagged" MCDA spectrum[12], the excitation spectrum of the ODEPR effect with respect to the wavelength, could be measured by holding the magnetic field at the EPR resonance condition and detecting the difference in the MCDA with and without microwaves at various wavelengths[12]. With the tagged MCDA it is possible to separate superimposed MCDA bands of different paramagnetic defects if their ODEPR spectra are at least partly separated.

To measure spin lattice relaxation times T_1 of the paramagnetic defects time resolved ODEPR experiments were performed. During the experiments the EPR resonance condition of a special EPR transition was fulfilled and the MCDA was monitored. With a microwave switch the microwave power which was coupled to the ODEPR cavity and which induced the EPR transitions, was modulated. With an IBM compatible personal computer and a transient recording board, which was triggered by the microwave switch controller, the MCDA signal was recorded time resolved during the switching-off phase of the microwaves. The decay of the ODEPR effect, i.e. the recovery of the MCDA after switching off the EPR transition, was measured.

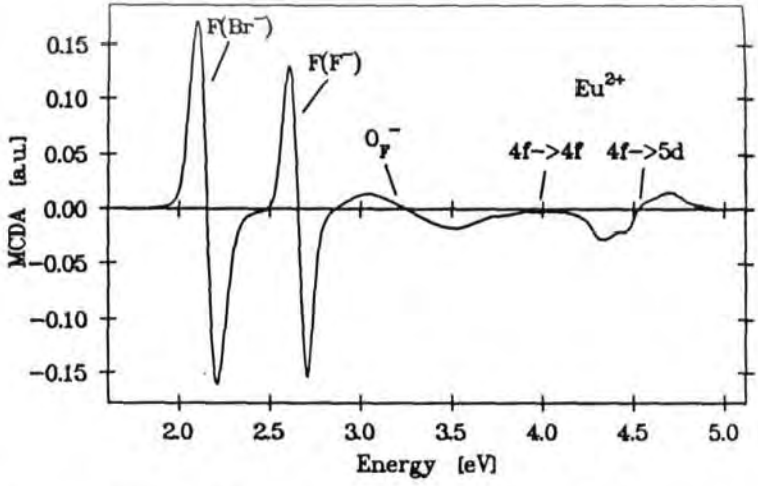

Figure 2: MCDA of BaFBr: 100ppm Eu^{2+}, X-irradiated at 300K, measured with B = 3T parallel to the c axis at 1.5K.

3. Experimental Results and Discussion

3.1 Investigations of the Storage Phosphor BaFBr:Eu^{2+}

In Fig. 2 the MCDA is shown for a BaFBr crystal containing 100ppm Eu^{2+}, as doped in the melt, following its exposure to X rays at room temperature. At low photon energy two MCDA bands are measured which are caused by $F(Br^-)$ and $F(F^-)$ centres as was shown previously by ODEPR and optically detected electron nuclear double resonance (ODENDOR)[13,14]. The MCDA spectrum associated with the 4f-5d transition of Eu^{2+} appears at 4.5eV. The spectral region between approximately 3 and 4eV is a superposition of MCDA signals from at least two defects, one of which was identified as being O^- on a F^- site (O_F^-)[15].

In Fig. 3, the upper curve shows the MCDA spectrum from a crystal doped with 100ppm Eu^{2+} measured at 4.30eV, i.e. in the Eu^{2+} transition, at 1.5K as a function of the magnetic field under continuous microwave irradiation of 24GHz. The continuous MCDA increase with field reflects the thermal equilibrium magnetization (Brillouin function[16]). The dips and peaks are caused by the EPR transitions of the paramagnetic Eu^{2+} ion ([Xe]$4f^7$; S=7/2). The expected seven fine structure lines are measured in the high field region[17,18]. The corresponding forbidden transitions with $\Delta m_S = \pm 2$ are seen at lower field. There is a remarkable change of sign in the

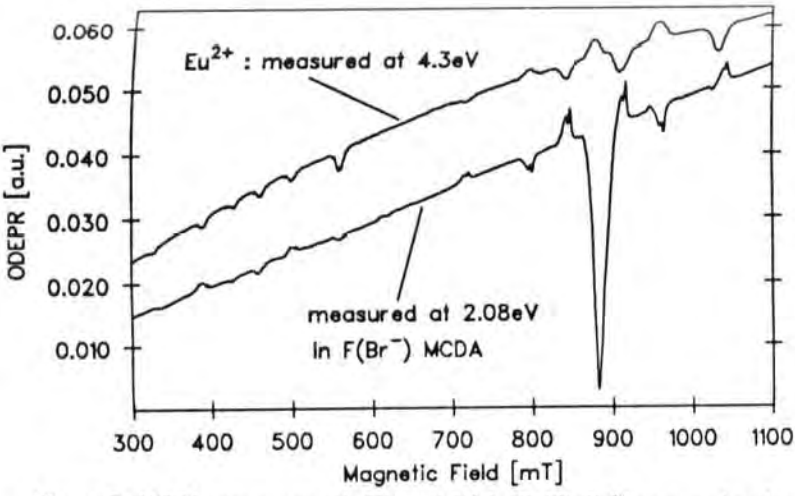

Figure 3: MCDA versus magnetic field at 1.5K for BaFBr:Eu^{2+} measured under continuous microwave irradiation of 24GHz. Curve a: at 4.30eV prior to X irradiation, 100ppm Eu^{2+}, curve b: at 2.08eV (in the $F(Br^-)$ band) after X irradiation at 296K, 10ppm Eu^{2+}.

allowed ODEPR lines compared to the forbidden signals, which all have the expected negative sign. This phenomenon is not influenced by the light intensity, i.e. it is not due to optical pumping effects[19]. It can be explained by a "forbidden" spin lattice relaxation within the Eu^{2+} Zeeman levels which connects $\Delta m_S = \pm 2$ states faster than those with $\Delta m_S = \pm 1$. This effect does not appear in the forbidden EPR transitions where only $\Delta m_S = \pm 2$ states are connected by the microwaves. Details of the Eu^{2+} spin lattice relaxation will be published elsewhere[20]. The effect of an anomalous spin lattice relaxation on the sign of the EPR lines can only show up in optical detection where the total spin polarization of the ground state is measured. In conventional EPR one measures only the absorption of the microwave quanta which induce an EPR transition[20].

In Fig. 3, the lower curve shows a similar result to that in Fig. 3, upper curve, but after the crystal was X-irradiated at 296K. The optical wavelength is set to 590nm (2.08eV), i.e. into the $F(Br^-)$ band. The crystal was doped with 10ppm Eu^{2+}. As well as the EPR line of $F(Br^-)$ centres, which occurs at about 880mT, the Eu^{2+} fine structure transitions are seen due to a cross-relaxation (CR) effect. CR is possible if the EPR spectra of two defects overlap and if there is a sufficiently

Table 1: decay times of the ODEPR effect measured via the F(Br^-) MCDA band at 1.5K with various Eu^{2+} doping levels. The decay times of the different satellite lines (Eu^{2+} fine structure cross-relaxation lines) are the same. If more than one decay time is listed, a multi-exponential decay was observed.

Eu^{2+} doping level	decay times of F(Br^-) resonance at 880mT	decay times of Eu^{2+} CR lines
0	10	-
10ppm	6s, 1s	1s
36ppm	3s, 0.5s, 0.09s	0.5s, 0.09s
100ppm	0.3s, 0.08s	0.3s, 0.08s

strong spin-spin interaction to induce spin flip-flop processes between the two spin systems[21]. The Eu^{2+} +1/2 to -1/2 transition and the F centre transition overlap to a large extent. The spin-spin interaction causing CR is, however, weak so that neither the F centre spectrum nor the Eu^{2+} fine structure splitting are affected. In order to further elucidate the mechanism of CR, time resolved ODEPR measurements were performed. The T_1 times of the ODEPR lines detected via the F(Br^-) MCDA band were measured at various Eu^{2+} concentrations. In all investigated Eu^{2+} doped samples a multi-exponential decay of the ODEPR effect was observed. Table 1 shows the decay times which were extracted from the time resolved experiments for the F(Br^-) resonance at 880mT as well as for the satellite lines due to CR. In general, the decay times decrease with increasing Eu^{2+} concentration. However, the relaxation of the F(Br^-) spin system does not become faster than that of the Eu^{2+} spin system. The Eu^{2+} spin system relaxes with mainly two different relaxation times. The longer relaxation time is about 0.3s and is due to the allowed $\Delta m_S = \pm 1$ relaxation. The other one is about 0.06s and is caused by the fast forbidden $\Delta m_S = \pm 2$ relaxation[20].

3.2 Analysis of cross-relaxation effects

The probability of a spin flip-flop process between different paramagnetic defects is given[21]:

$$R_{ij} = \frac{1}{16\hbar^2}(S_\alpha - m_{s,\alpha})(S_\alpha + m_{s,\alpha} + 1)(S_\beta + m_{s,\beta})(S_\beta - m_{s,\beta} + 1)g_i^2 g_j^2 \beta^4 \times (1 - 3\cos^2\theta_{ij})^2 \frac{1}{r_{ij}^6} g_{\alpha\beta} \quad (1)$$

with

$$g_{\alpha\beta} = \int g_\alpha(\nu) g_\beta(\nu) d\nu \quad (2)$$

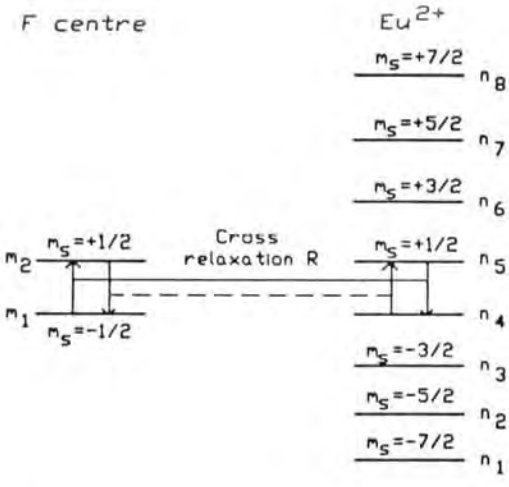

Figure 4: Mechanism of cross-relaxation between F centres and Eu^{2+} ions.

α, β denote the different types of paramagnetic species; i,j denote the individual spins between which the CR takes place. $g_{\alpha\beta}$ is the overlap integral of the EPR shape functions g_α and g_β of defects α and β. In the case of CR between F centres and Eu^{2+}-ions, only the EPR transition $m_S = -\frac{1}{2} \rightarrow m_S = +\frac{1}{2}$ of the Eu^{2+} contributes to the overlap between Eu^{2+} and F centres. Fig. 4 shows the mechanism of CR between Eu^{2+}-ions and F centres. The CR effect can be calculated with the solution of the coupled rate equation systems of the F centre and the Eu^{2+} which are given explicitely in Ref. 20. The non-linear coupling of the rate equations is caused by the CR rates:

$$m_1 \cdot R \cdot n_5 \text{ and } m_2 \cdot R \cdot n_4 \tag{3}$$

where m_1 and m_2 are the populations of the F centre Zeeman levels and n_4 and n_5 are the corresponding populations of the $m_S = \pm\frac{1}{2}$ levels of the Eu^{2+}, respectively (see Fig. 4). R is the CR probability of eq. 1. The shape of the CR lines in the ODEPR spectrum of Fig. 3, lower curve, is determined by the differentiation of the overlap integral $g_{\alpha\beta}$ with respect to the magnetic field:

$$\text{shape}_{CR} \propto \frac{d}{dB} g_{\alpha\beta} \propto g_\alpha(B) \cdot g_\beta(B) \tag{4}$$

In first order the differentiation of $g_{\alpha\beta}$ is proportional to the product of g_α(B) and g_β(B). Fig. 5a shows the calculated overall CR spectrum of the $F(Br^-)$ centre assuming a simplified rectangular line shape and Fig. 5b shows the calculated and measured shapes of a single CR line.

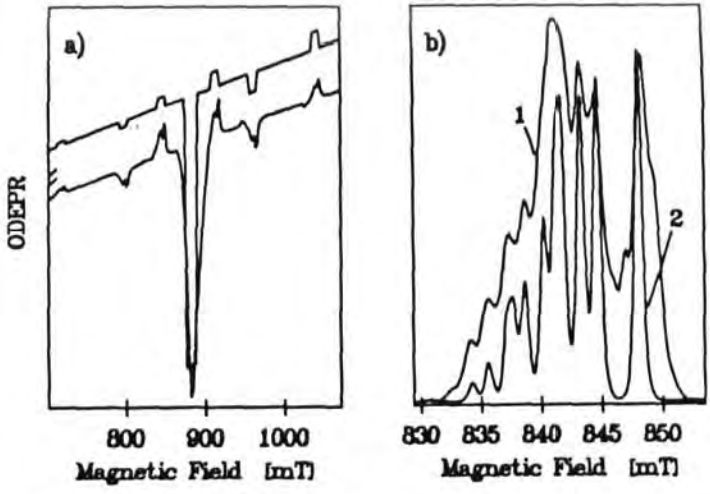

Figure 5: a) Calculated and measured CR spectrum of $F(Br^-)$, microwave frequency 24GHz. For simplicity a square shape of each line was assumed for the calculated spectrum, b) curve 1: shape of an Eu^{2+} CR line measured in the MCDA of the $F(Br^-)$ centre, curve 2: calculated line shape of the same signal.

A CR effect is seen if the CR rate, R_{CR}, is an appreciable fraction of the spin lattice relaxation rate, R_{rel}. For $F(Br^-)$ centres at 1.5K, R_{rel} is $0.1s^{-1}$ [20]. An R_{CR} value exceeding $0.05s^{-1}$ should give a measurable effect. In order to estimate whether a CR effect could be observed for a statistical distribution of $F(Br^-)$ centres (concentration about $10^{16}cm^{-3}$) and the Eu^{2+} activators, we have assumed that a dipole-dipole interaction causes the spin flip-flop processes[21]. For 10ppm Eu^{2+}, less than 5% of the F centres will, on average, have a Eu^{2+} ion closer than 60Å. For this distance, R_{CR} is only $0.005s^{-1}$. We have clearly observed the CR effect between F centres and Eu^{2+} for a dopant concentration as low as 5ppm ($6.5 \cdot 10^{16}cm^{-3}$). Therefore, F centres and Eu^{2+} activators must be present in a correlated fashion after X irradiation. A CR effect caused by a statistical distribution would only be seen if the Eu^{2+} concentration exceeded 100ppm. However, the Eu^{2+} and F centres cannot be nearest neighbors since the dipole-dipole interaction in this case would have caused measurable effects on the shapes of the respective EPR spectra. The details of the CR effects seen in Fig. 3, lower curve, are fully understood on the basis of the appropriate rate equations, and will be published elsewhere[20]. A CR effect of the F centres was not observed in the Eu^{2+} MCDA, which is explained by the fact that the spin-lattice relaxation time of Eu^{2+} at 1.5 K is 30 times shorter than that

of the F centre and that a population change between the $m_S = \pm 1/2$ states in Eu^{2+} has a smaller influence on its total spin polarization, to which eight levels contribute (S=7/2). It is the total spin polarization that is measured by the MCDA technique. The spin polarization of the F centre, which has only two Zeeman levels, is much more sensitive to changes in their occupancy. Furthermore, the concentration of Eu^{2+} is much higher than that of the F centres so that their influence on the total Eu^{2+} must be relatively small.

In order to explain the relaxation behaviour (see table 1), we assume that the relaxation and cross-relaxation rates can at least qualitatively be described with the simple model of a shunt. The relaxation of the $F(Br^-)$ spin system becomes faster, if a second relaxation path is established via CR. In this model, the total relaxation rate T_1^{-1} is:

$$T_1^{-1} = T_{1,F}^{-1} + \frac{1}{R^{-1} + T_{1,Eu}} \tag{5}$$

T_1 is the effective relaxation time of the $F(Br^-)$ spin system. $T_{1,F}$ and $T_{1,Eu}$ are the spin lattice relaxation times of the $F(Br^-)$ and the Eu^{2+} centres, respectively. With $T_{1,F} >> T_{1,Eu}$, it can be easily seen, that T_1 approaches $T_{1,Eu}$ with increasing CR rate R. This was measured at a doping level of about 100ppm and more. Then, the $F(Br^-)$ centres have the same relaxation time as the Eu^{2+} defects. The relaxation time of 0.3s (see table 1) corresponds to the allowed Eu^{2+} spin lattice relaxation and that of 0.08s is nearly the same as for the forbidden $\Delta m_S = \pm 2$ relaxations mentioned before. The complex relaxation behavior of the Eu^{2+} spin system can be observed indirectly via the $F(Br^-)$ MCDA due to CR at sufficient doping levels. Then, the Eu^{2+}concentration is high enough for strong CR to the $F(Br^-)$ centres even at a statistical defect distribution. For lower doping levels, the situation is more complicated. We do not want to exaggerate the simple shunt model. However, the long relaxation time of 6s for the doping level of 10ppm Eu^{2+}, which is shorter than the spin-lattice relaxation time of the $F(Br^-)$ centres, may be caused by weak CR between statistically distributed Eu^{2+} and $F(Br^-)$ defects. The faster relaxation of about 1s may be caused by stronger CR due to correlated defects. This assumption is supported by the fact that the long relaxation time could not be measured at the satellite CR lines which are mainly produced by strong CR due to correlated defects.

Similar effects as described above were observed for the $F(F^-)$ centre and for the O_F^- defect (see Fig. 2). Also CR between $F(Br^-)$ centres and Br_2^--V_k centres which can be produced in oxygen containing crystals by X irradiation below 120K and which consist of a hole shared by two adjacent bromine ions to form a Br_2^- molecule were measured[14]. By an analysis of the MCDA spectra and the CR effects it can be concluded that $F(Br^-)$, Br_2^--V_k and O_F^- defects were produced in a spatially correlated way[14].

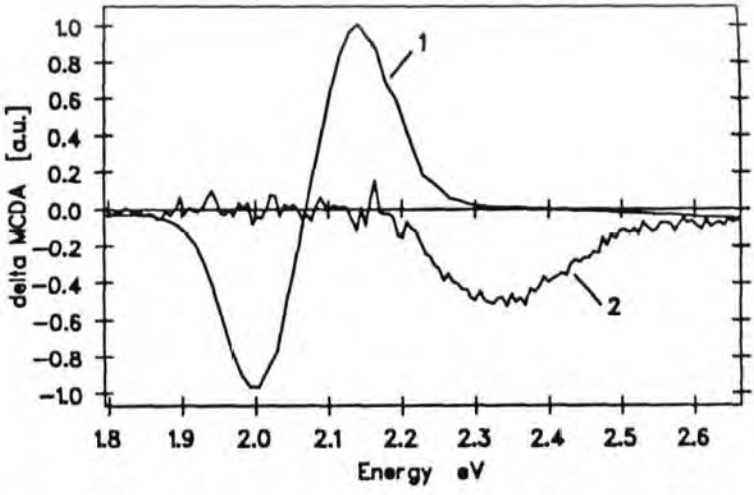

Figure 6: Tagged MCDA spectra of F centres (1) and H centres (2) in KBr X irradiated at 4.2K, the magnetic field was parallel to the [100] direction.

3.3 Investigations of the F-H Process in KBr

A KBr single crystal was X-irradiated at 4.2K for several hours (Voltage 60kV, current 15mA, distance crystal anode 10cm). After this procedure, ODMR spectroscopy at 1.5K was performed without warming up the crystal. In Fig. 6 the MCDA bands of the F centres and H centres in KBr are shown. The spectrum was taken with the magnetic field parallel to the [100] direction of the crystal. The ODMR showed that only H centres which were oriented perpendicular to the magnetic field could be measured. The two bands could be separated by the procedure of tagged MCDA described before. The MCDA band of the H centres was investigated in detail by Meise et al.[22]. It can be seen clearly that there is no superposition of the F centre MCDA and the H centre MCDA in the photon energy range between 1.9eV and 2.1eV. In Fig 7a the ODEPR spectra measured at 2.4eV (curve 1) and at 2.0eV (curve 2) are shown. In the ODEPR spectrum of curve 2 measured at 2.0eV only the F centre resonance should be detectable because there is no other MCDA band except that of the F centre. But, as it can be seen in Fig. 7a, curve 2, beside the F centre ODEPR line, in the magnetic field range of the H centre resonance, we could observe an ODEPR signal which is definitely not due to the F centres. In Fig. 7b this effect is shown with higher resolution with respect to the H centre ODEPR. This effect is caused by CR between H and F centres. We performed annealing experiments to show this. Remarkable is the change in sign of the CR signal observed via

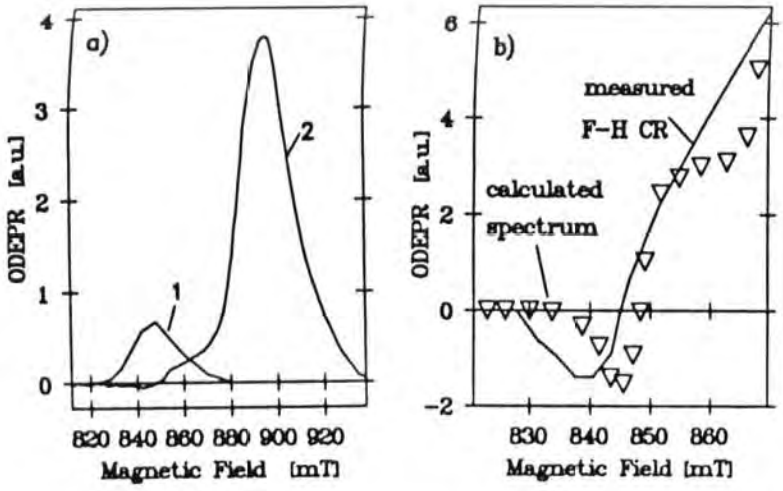

Figure 7: a) ODEPR spectra of H centres (curve 1, photon energy 2.4eV) and F centres (curve 2, photon energy 2.0eV) at 24GHz with the magnetic field parallel to [100]. b) CR effect of spectrum a), curve 2 in the magnetic field range between 820mT and 860mT with higher resolution, the triangles represent the calculated CR effect. For details, see text.

the F MCDA band going from the high magnetic field flank to the low field flank of the H centre resonance (see Fig. 7b). Calculations which are explained below showed that only H centres which are oriented perpendicular to the magnetic field contribute to the measured CR effect. After warming up the crystal to about 70K where all H centres are surely destroyed, the cross-relaxation effect vanished. Moreover, we performed the following experiment. We warmed a KBr crystal after X irradiation at 4.2K to about 30K for one minute. At 30K, there is the maximum of the thermoluminescence glow peak due to F-H recombination[23]. After recooling the crystal to 1.5K, we found that the concentration of the H centres had decreased by about 10%, however, the CR effect had decreased by about 50%. From this experiment, we can conclude that F and H centres which showed CR were influenced by the annealing procedure. In other words, spatially correlated F and H centres which showed CR at low temperature partly recombined with each other or were separated from each other due to H centre diffusion which is known to occur in this temperature range.

We tried to calculate the CR effect with some simple assumptions: H centres in KBr have two central nuclei, each with spin 3/2. The total spin can be 0, 1, 2 or 3. Only H centres with a total spin of 3 can couple via CR to the F centres because only

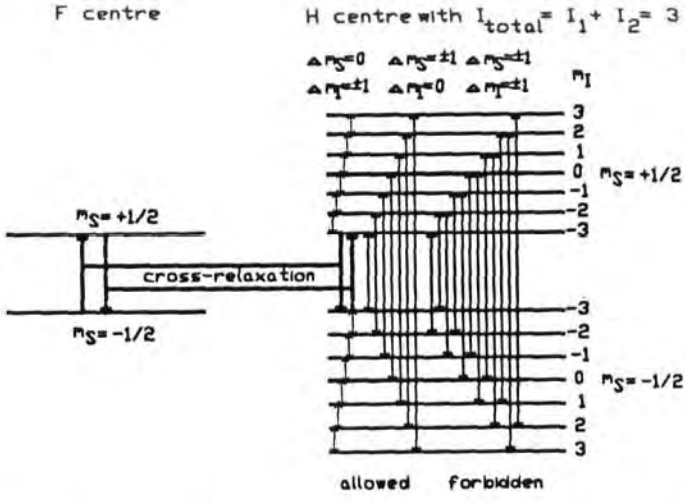

Figure 8: Simple model of CR between F and H centres. The F centre Zeeman levels are coupled to the both $m_I = -3$ levels of the H centre spin system. Allowed and "forbidden" relaxations are represented by the arrows. For details, see text.

the EPR signal of these centres overlaps with the EPR of the F centres. Therefore, we assumed that only H centres with a total spin of 3 contribute to the CR effect and that the total spin does not change within the time scale of the CR. Also we only took into account H centres which were oriented perpendicular to the magnetic field. Cross-relaxations between H centres with 45^0 orientation with respect to the magnetic field which was parallel to a [100] axis of the crystal could not be observed. To simplify the situation further, we neglected isotope effects (bromine has two isotopes, each with nuclear spin of 3/2). Furthermore, we assumed that only allowed ODEPR transitions with $\Delta m_S = \pm 1$ and $\Delta m_I = 0$ would occur within the Zeeman levels of the H centre (m_I is the magnetic quantum number of the total nuclear spin). For the relaxations which occur within the Zeeman levels of the H centre, we assumed slow nuclear spin relaxations ($\Delta m_I = \pm 1, \Delta m_S = 0$) and relatively fast electron spin relaxations ($\Delta m_S = \pm 1, \Delta m_I = 0$) in comparison to the nuclear spin relaxations. In order to explain the change in sign of the CR line we had to introduce efficient forbidden relaxations, where the magnetic quantum number of the total nuclear spin as well as that of the electron spin relaxes simultaneously ($\Delta m_S = \pm 1, \Delta m_I = \pm 1$). Our CR model is shown in Fig. 8 as a level scheme of the two Zeeman levels of an F centre which are coupled to the H centre spin system, where the two $m_S = \pm 1/2$ levels are further split by the hyperfine interaction with the total nuclear spin of 3.

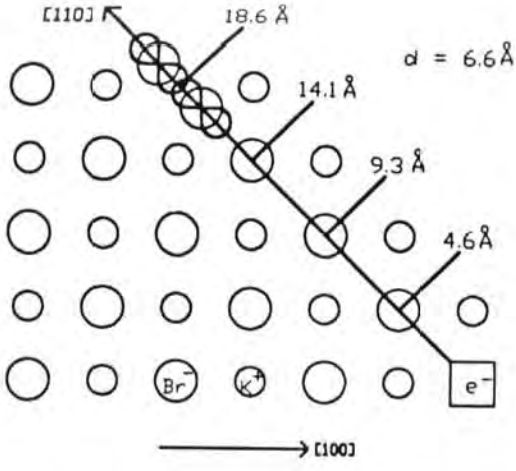

Figure 9: Model of the F-H centre correlation in KBr obtained by CR calculations and an estimate of the H centre EPR line width. For details, see text.

All relaxations taken into account are indicated. With these assumptions the rate equations which describe the CR were solved. The details of the CR rate equations will be published elsewhere[24]. The result is seen in Fig. 7b (triangles). For this calculation we assumed that all F and H centres are correlated within a distance of 4 lattice spacings along [110] (about 19Å). Qualitatively, the calculations explain the measured CR effect. However, it is not possible to estimate whether all F and H centres are correlated or only a fraction. If it is only a fraction, then, it must be greater than 10%. Because of a missing splitting of the EPR spectra of F and H centres due to spin-spin interaction (see also the conventional EPR spectra of Kaenzig et al.[25]), the minimum separation must be about four lattice spacings assuming a point-dipole dipole interaction. However, the maximum distance of correlated defects was roughly estimated by our CR calculations to be about 19Å (about four lattice spacings). The connection line between the two defects must be the [110] direction because of the decay mechanism of the STE[8]. In Fig. 9, a schematic sketch of the possible constellation between correlated F-H pairs in KBr is shown which is compatible with the point-dipole dipole estimate of the EPR line shape of the H centre and with the CR calculations. In our model based upon a simple CR analysis, F and H centres in KBr which were created at 4.2K and kept below 30K are separated by about 4 lattice distances in [110] direction.

4. Conclusions

In conclusion, the CR spectroscopy shows that irradiation-produced F centres, hole centres and the Eu^{2+} activator ions are spatially correlated with each other although their local environments, as far as can be determined by ODMR spectroscopy, are regular. We think that this spatial correlation is not a strict and rigid one, but it has certain statistical features. Probably there are enough "triple configurations" among F, hole and Eu^{2+} centres to make the PSL process possible without thermal activation, as was observed by von Seggern[9]. The PSL replenishment effect observed after exhaustion at low temperatures and subsequent warming[11], shows that this correlation is not fortuitous. At this stage we can only speculate on the reason for the correlation. It could be the result of a combination of local lattice distortions around the smaller substitutional Eu^{2+} ion and the unusual double-layered structure of the BaFBr system or a result of a decay of an exciton trapped in the neighbourhood of an Eu^{2+} ion which substitutes the bigger Ba^{2+}.

The analysis of the CR between F and H centres in KBr also showed that these defects are spatially correlated after their creation by a decay of an STE. With a simple CR model, we estimated the separation of the F and H centres after their creation at 4.2K to be about 4 lattice constants in [110] direction.

References:

1. G. W. Luckey, U.S. Patent 3,859,527 (1975), Revised 31847 (1983).
2. N. Kotera, S. Eguchi, J. Miyahara, S. Matsumoto, H. Kato, U.S. Patent 4,239,968 (1980).
3. Y. Amemiya, J. Miyahara, *Nature (London)* **336** (1988) 89.
4. B. W. Liebich, D. Nicollin, *Acta. Cryst.* **B 33** (1977) 2790.
5. H. P. Beck, *Z. Anorg. Allg. Chem.* **451** (1979) 73.
6. K. Takahashi, K. Kohda, J. Miyahara, Y. Kanemitsu, K. Amitani, S. Shionoya, *J. Lumin.* **31 & 32** (1984) 266.
7. K. Takahashi, J. Miyahara,Y. Shibahara, *J. Electrochem. Soc.* **132** (1985) 1492.
8. N. Itoh, *Adv. Phys.* **31** (1982) 491.
9. H. von Seggern, T. Voigt, W. Knupfer, G. Lange, *J. Appl. Phys.* **64** (1988) 1405.
10. H. H. Ruter, H. von Seggern, R. Reininger, V. Saile, *Phys. Rev. Lett.* **65** (1990) 2438.
11. Th. Hangleiter, F. K. Koschnick, J.-M. Spaeth, R. H. D. Nuttall, R. S. Eachus, *J. Phys.: Condens. Matter* **2** (1990) 6837.
12. F. J. Ahlers, F. Lohse, J.-M. Spaeth, L. F. Mollenauer, *Phys. Rev.* **B 28** (1983) 1249.

13. F. K. Koschnick, Th. Hangleiter, J.-M. Spaeth, R. S. Eachus, *6th Europhysical Topical Conference: Lattice defects in Ionic Materials* (Groningen, The Netherlands, Sept. 1990) in *J. Radiation Effects and Defects in Solids* **119-121** (1991) 837.

14. F. K. Koschnick, Th. Hangleiter, J.-M. Spaeth, R. S. Eachus, *J. Phys.: Condens. Matter* **4** (1992) 3001, 3015.

15. R. S. Eachus, W. G. McDugle, R. H. D. Nuttall, M. T. Olm, F. K. Koschnick, Th. Hangleiter, J.-M. Spaeth, *J. Phys.: Condens. Matter* **3** (1991) 9327.

16. C. Kittel *Introduction to Solid State Physics* (5th Edition, John Wiley & Sons, New York, 1976).

17. D. Nicollin, H. Bill, *J. Phys. C: Solid State Phys.* **11** (1978) 4803.

18. A. Abragam, B. Bleaney, *Electron Paramagnetic Resonance of Transition Ions* (Clarendon Press, Oxford, 1970) p. 148.

19. S. Geschwind, *Electron Paramagnetic Resonance*, ed. by S. Geschwind, (Plenum Press, New York, 1972) p. 353.

20. F. K. Koschnick, M. Rac, R. S. Eachus, J.-M. Spaeth, submitted to J. Phys. Condens. Matter (1992).

21. N. Bloembergen, S. Shapiro, P.S. Pershan, J. O. Artman, in *Cross-Relaxation in Spin-Systems and Spin-Lattice Relaxation in Ionic Solids*, ed. by A. A. Manenkov and R. Orbach (Harper and Row, New York, 1966).

22. W. Meise, U. Rogulis, J.-M. Spaeth, *proceedings of the International Conference on Defects in Insulating Materials* (Nordkirchen, Aug. 1992).

23. Yu. V. Kolk, A. Ch. Luschik, *Sov. Phys.: Solid State* **28** (1986) 805.

24. W. Meise, U. Rogulis, F. K. Koschnick, J.-M. Spaeth, to be published.

25. W. Kaenzig, T. O. Woodruff, *Phys. Chem. Solids* **9** (1959) 70.

THE ROLES OF OXYGEN IMPURITIES AND DEFECT AGGREGATION IN THE PERFORMANCE OF THE STORAGE PHOSPHOR BaFBr:Eu^{2+}

R. S. EACHUS*, F. K. KOSCHNICK**, J.-M. SPAETH**,
R. H. D. NUTTALL*, M.T. OLM* AND W. G. MCDUGLE*.

*Corporate Research Laboratories, Eastman Kodak Company, Rochester, NY 14650-2021, USA.

** University of Paderborn, FB Physik, Postfach 1621, D-4790 Paderborn, Germany.

1. Introduction

Eu^{2+}-doped BaFBr is an important storage phosphor in which images produced by X- irradiation are stable for long periods in the dark at room temperature.[1] For readout, the irradiated phosphor is optically stimulated between 450 and 800 nm leading to a photostimulated luminescence (PSL) at 390 nm from the Eu^{2+} activator. The mechanisms of the storage and readout processes have been sources of conjecture for several years. It is generally agreed that the image is comprised of trapped electron and hole centres.[2,3] BaFBr crystallises with the layered PbFCl (matlockite) structure [4,5] so that the trapped electron species could be F centres formed on either the F^- or Br^- sublattices. The nature of the hole centre(s) is less well established. Eu^{3+} ions[2] and Eu^{2+}-associated H centres[3] have been suggested, but experimental evidence has been circumstantial. The effects of impurities have generally been ignored. Studies of the temporal[6] and temperature[7] dependences of the PSL have suggested that the trapped electron centre(s) and the trapped hole centre(s) are spatially correlated. This paper summarises the results of EPR, ENDOR and magneto-optic studies of imaging in BaFBr and Eu^{2+}-doped BaFBr materials that provide the first direct experimental evidence for spatial correlations between the radiation-produced defects and for the involvement of oxide impurities in the imaging mechanisms.

2. Experimental

Single crystals of BaFBr were grown by the rf-Bridgman method.[8,9] EPR data indicated that these crystals were contaminated with at least 10^{18} oxygen-containing impurities cm^{-3}, in spite of taking the usual precautions first developed to remove oxygen from the alkali halides. Eu^{2+} was introduced by the addition of EuF_3 and growth of the crystals in a reducing atmosphere. Anhydrous BaO enriched to 40% in the ^{17}O (I=5/2) isotope was used for doping some crystals with $^{17}O^{2-}$. The spectrometers and irradiation systems used in this study have been described previously.[9]

3. Results and Discussion

Oxide is an ubiquitous impurity in the matlockite class of fluorohalides and as much as 6% O^{2-} has been successfully incorporated by us into single crystals of BaFBr. Optical absorption, EPR, ENDOR and ODMR experiments show that the oxide substitutes for halide to give O^{2-}_F and O^{2-}_{Br}, with charge compensation being provided by the formation of additional Br^- vacancies.[8-10] BaFBr has a direct bandgap of approximately 8.5 eV. The addition of oxide produces a new optical absorption peaking at 4.96 eV (250 nm).

Reprinted from

NIM B

Beam Interactions with Materials & Atoms

Nuclear Instruments and Methods in Physics Research B 91 (1994) 175–182
North-Holland

Cross relaxation in magnetic resonance as a tool to study spatial correlations between defects in insulators

J.-M. Spaeth [a,*], F.K. Koschnick [a], W. Meise [a] and U. Rogulis [b]

[a] *University Paderborn, Department of Physics, D-33095 Paderborn, Germany*
[b] *University of Riga, Latvia*

ELSEVIER

Nuclear Instruments and Methods in Physics Research B 91 (1994) 175–182
North-Holland

NIM B
Beam Interactions with Materials & Atoms

Cross relaxation in magnetic resonance as a tool to study spatial correlations between defects in insulators

J.-M. Spaeth [a,*], F.K. Koschnick [a], W. Meise [a] and U. Rogulis [b]

[a] University Paderborn, Department of Physics, D-33095 Paderborn, Germany
[b] University of Riga, Latvia

Direct experimental evidence for the spatial correlation between paramagnetic defects can be obtained by measuring the dipole–dipole interaction-induced cross relaxation effects between the defects using optical detection of the electron paramagnetic resonance via the magnetic circular dichroism of the absorption. This novel experimental method is explained. It is applied to the formation of F and H centres during relaxation of the self-trapped exciton in KBr at 1.5 K. Direct experimental evidence is presented that F and H centres are separated by four lattice spacings along ⟨110⟩ directions. This correlation is lost after warming to 30 K when H centres can diffuse away.

1. Introduction

In insulating crystals often trapped electron and hole centres are formed by ionising radiation. Both types of centres are paramagnetic and thus observable with electron paramagnetic resonance. One common origin of these trapped electron and hole centres is the creation of electrons and holes in the conduction and valence bands, respectively, by radiation with energy above the band gap energy. At low temperature both electrons and holes may therefore be trapped at sites which are near to each other and thus a spatial correlation between the trapped electron and hole centres could result. At higher temperatures the correlation may be destroyed because of diffusion of the centres. Such a spatial correlation is expected to exist between F centres (electrons trapped at anion vacancies) and H centres (X_2^- molecular ions at anion sites) at very low temperatures in alkali halides, when they are formed during relaxation of the self-trapped exciton of the lowest energy as a result of the adiabatic instability against axial relaxations of the system [1,2]. The question is, how far apart are F and H centres after generation before the H centres can diffuse?

Another example of spatially correlated paramagnetic centres is expected in the so-called X-ray storage phosphors. The basic mechanism for their functioning is believed to be the following: Upon X-irradiation trapped electron and hole centres are formed which "store" the X-ray information. During the readout process by optical stimulation of e.g. the trapped electron centres, the recombination energy of the electron–hole centre recombination is transferred to an additionally doped activator, which then emits light. For a practical system to work satisfactorily one must claim that a spatial correlation between the radiation damage centres and the activators exists, since otherwise for the achievable activator doping levels and the low X-ray doses necessary for medical applications such a mechanism seems very improbable if operating purely statistically.

It is obvious from the two examples mentioned, that one would like to have an experimental tool to measure the spatial correlation between paramagnetic defects directly. In the EPR spectrum of the paramagnetic defect the near presence of another paramagnetic defect is only seen as a splitting effect on the EPR lines, when the two defects are rather near to each other. For example, if they are nearest neighbours then the two unpaired spins may couple via exchange interaction, an effect which is easily detectable. The magnetic dipole–dipole interaction will cause line splittings of the order of 2 mT if the separation is about 10 Å, i.e. 2 to 3 typical lattice spacings. Such an effect would only be seen for narrow EPR lines. Mostly in ionic solids the lines are broader and such a dipole–dipole interaction would hardly be detected. However, the dipole–dipole interaction is also responsible for a different effect: it induces spin flip-flop processes between two neighbouring paramagnetic defects. For example, induced by EPR transitions the spins of one type of defects are flipped between the Zeeman levels and the spin polarisation of these defects is changed. This change in spin polarisation can be transferred under certain circumstances via spin flip-flop processes

* Corresponding author.

SSDI 0168-583X(93)E1015-E

to neighbouring paramagnetic defects of another type. The polarisation transfer is called cross-relaxation (CR). With conventional EPR spectroscopy such CR effects are normally not noticed. The reason is that the effective relaxation times of the spins are difficult to interpret. One would need to measure the difference of the effective spin–lattice relaxation times for correlated and non-correlated defect pairs if one wanted to use this effect to extract the information on the spatial correlation. However, when using optical detection, then CR effects can be detected. This method was first used to study spatial correlations between radiation damage centres and the activator Eu^{2+} in the X-ray storage phosphor $BaFBr:Eu^{2+}$ [3].

In this paper the application of this technique is described for the relaxation of the self-trapped exciton into F and H centres in KBr at 1.5 K. It will be shown that it could be used to provide the first experimental evidence that approximately all F and H centres are separated by four lattice spacings along the ⟨110⟩ directions when created at 1.5 K and that they lose this correlation after warming the crystal to 30 K.

The method is briefly described in the next section. After presentation of the experimental results the quantitative analysis of the CR effects for F–H centre pairs are presented in detail.

2. Experimental methods

Consider two paramagnetic defects A and B, both with $S = \frac{1}{2}$, which are at a certain separation r_0 from each other. If one drives an EPR transition in defect B by inducing a spin flip from $m_s = -\frac{1}{2}$ to $m_s = +\frac{1}{2}$, then (provided the spin–lattice relaxation time is very long) one thus changes the spin polarisation $(n_- - n_+)/(n_+ + n_-)$ of this defect (it is decreased). If there is a spin flip-flop process to defect A, then upon flipping the spin of defect B from $m_s = +\frac{1}{2}$ to $m_s = -\frac{1}{2}$, the spin of defect A is flipped from $m_s = -\frac{1}{2}$ to $m_s = +\frac{1}{2}$, thus decreasing the spin polarisation of defect A (see Fig. 1). The probability R for the spin flip-flop process, i.e. the CR process, is in the dipole approximation given by $R \sim r_0^{-6}$ (see section 4 for details). Therefore, in order to detect the occurrence of the separation-dependent cross relaxation effect, one needs to measure the change of spin polarisation in one defect (e.g. A) upon inducing EPR transitions in the other defect (e.g. B). This can be achieved by measuring the magnetic circular dichroism of the optical absorption (MCDA) of defect A, since this quantity is proportional to the spin polarisation for defects in low crystal fields (see e.g. refs. [3,4]). For defects with a spin of $S = \frac{1}{2}$, like F and H centres, the MCDA is always proportional to the spin polarisation $(n_- - n_+)/(n_+ + n_-)$. The MCDA is the differential absorption of left and right circularly polarised light propagating along the magnetic field direction. Thus, an EPR transition induced in defect B will change the MCDA in defect A provided the CR rate R is of the order of or faster than the spin–lattice relaxation time T_1 of defect A. Of course, for the spin flip-flop processes to occur, also the energy conservation must be fulfilled, i.e. the EPR shape functions of both defects must overlap. The CR rate is proportional to the overlap integral between the two EPR shape functions (see section 4).

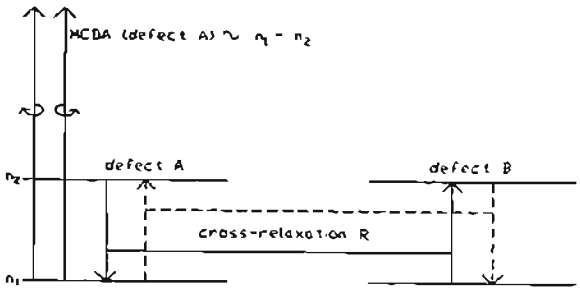

Fig. 1. Schematic representation of the CR effects between defect A and B.

For a quantitative assessment of the CR effects on the MCDA of centre A it is necessary to know, apart from the EPR transition probability in centre B (proportional to the microwave power), the spin–lattice relaxation times T_1 of both defects. Possibly also "forbidden" spin–lattice relaxations ($\Delta m_s = \pm 1$, $\Delta m_I = \pm 1$) and nuclear relaxation times have to be considered in case of inhomogeneous EPR lines due to hyperfine interactions, since the net effect is a combination of various dynamical contributions. If all defects A and B have the same separation, then R can be determined from the experimental observation, provided the relaxation times had been measured, which can be easily performed with the MCDA-detected EPR (see e.g. ref. [4]). From R the separation can be deduced. For the example of F–H centre pairs the quantitative analysis is presented in section 4. The situation is more complicated if there is a distribution of separations between centres A and B. Then for each fraction of defects having a certain separation the CR effect must be calculated and all contributions must then be added up. Nevertheless, also in this case one can obtain valuable information about spatial correlations. For the X-ray storage phosphor $BaFBr:Eu^{2+}$ it could be shown that the observed CR effect could not be explained with a statistical centre distribution [3].

The crystal used in this study was an extremely pure KBr crystal provided by G. McDugle (Eastman Kodak, Co.). It was irradiated with X-rays in the microwave cavity at 4.2 K for about 15 h in order to produce enough H centres. Simultaneously also V_k centres were

generated. The experiments were performed with a custom built computer-controlled K-band MCDA/ODEPR spectrometer (24 GHz), which operated between 250 nm and 1700 nm at temperatures between 1.5 K and 300 K.

3. Experimental results

X-irradiations of the pure KBr crystal at 4.2 K produced H centres, F centres and V_k centres. Fig. 2a shows the optical absorption bands of these centres according to the literature and Fig. 2b shows the MCDA spectrum. It was shown recently that H centres have an MCDA superimposed on the high energy flank of the F centre absorption, which is caused by those H

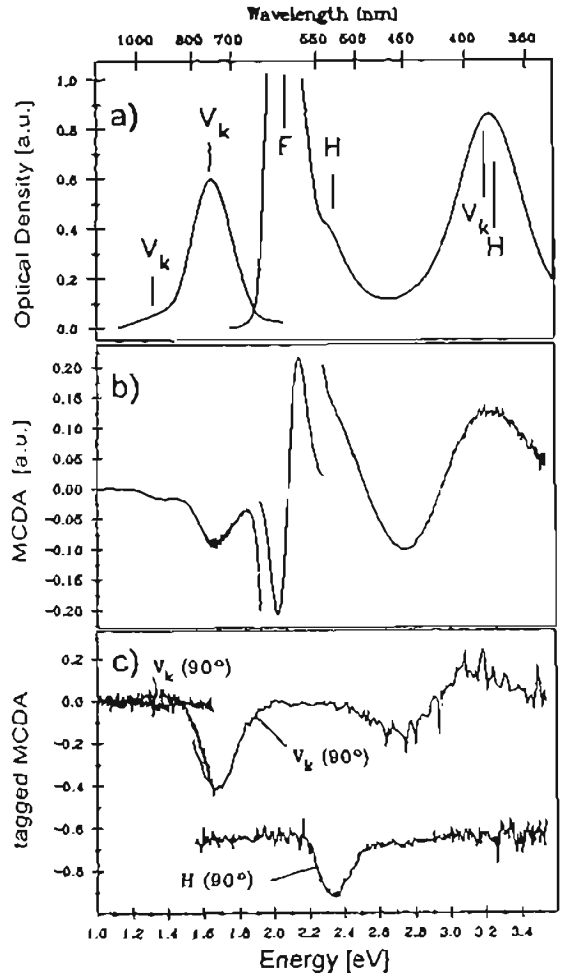

Fig. 2. (a) Absorption of V_k, H, and F centres in KBr X-irradiated below 20 K. (b) MCDA spectrum of KBr X-irradiated at 4.2 K in situ, measured at 1.5 K, magnetic field 2 T. (c) Tagged MCDA spectra of V_k and H centres in KBr, $B_0 \| [100]$.

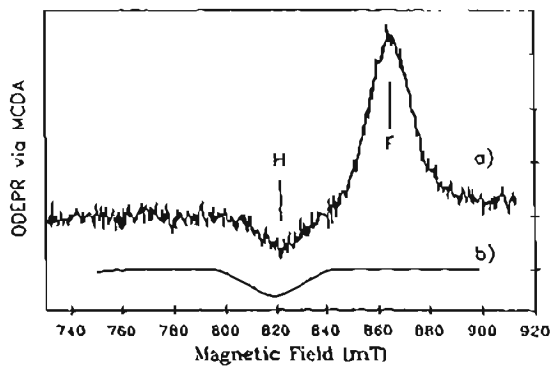

Fig. 3. (a) ODEPR spectrum of KBr X-irradiated at 4.2 K in situ, measured at 1.5 K, microwave frequency 23.8 GHz, photon energy 2.4 eV, $B_0 \| [100]$. (b) EPR simulation of H centres in KBr with their axes perpendicular to B_0, $A_\perp = 5$ mT, $g_\perp = 2.074$, half width of hyperfine lines 5 mT.

centres with their molecular axes perpendicular to the static magnetic field. Parallel H centres have no MCDA in the spectral region between 1.0 and 3.4 eV [5,6]. Fig. 3, trace a, shows the ODEPR spectrum of the perpendicular H centres measured at 2.4 eV together with an EPR spectrum calculated with the known $g_\perp$ value and assuming a hyperfine interaction constant $A_\perp$ of 5 mT (for details see ref. [5]). At 2.4 eV one also measures F centres (see Fig. 2b), which therefore appear also in Fig. 3, trace a. The V_k centres, simultaneously present, have different MCDA bands from those of the H centres. This is seen in the MCDA tagged by EPR [7], a kind of excitation spectrum of the ODEPR lines (Fig. 2c). Thus, e.g. at 2.38 eV (520 nm) one can measure the H centre EPR without inducing simultaneously the V_k centre EPR. It is also seen that the H centre MCDA band does not overlap with the low energy flank of the F centre MCDA. Therefore, when measuring the ODEPR at 2.0 eV (620 nm) at the low energy flank of the F centres one should not detect any H centre EPR: In Fig. 4 the results of the ODEPR measurements at 2.0 eV (low energy flank of F centre) and at 2.38 eV (H centre MCDA) are shown. At 2.38 eV both the F centre and the H centre EPR lines appear (trace a) due to the overlap of the two MCDA bands. However, at 2.0 eV no H centre EPR should appear. The fact that it does, shows the presence of a CR effect. A change in the H centre spin polarisation is transferred to the F centre spin-polarisation [8].

The effects of polarisation transfer are also seen in time resolved measurements. Figs. 5b and 5c show the temporal behaviour of the MCDA of F and H centre MCDA bands after switching off the microwaves which had induced the F centre and H centre EPR transitions, respectively. The MCDA bands reach the thermal equilibrium with the characteristic spin–lattice re-

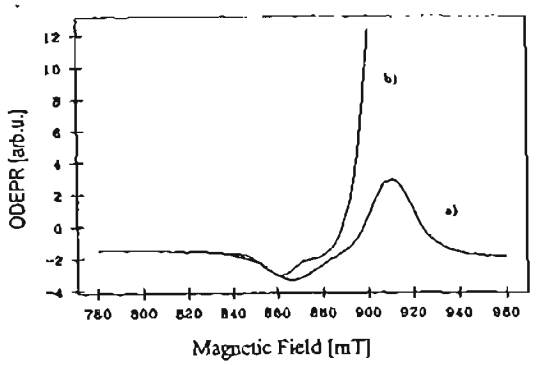

Fig. 4. ODEPR spectra of pure KBr X-irradiated at 4.2 K in situ for about 15 h, measured at 1.6 K, microwave frequency 24.5 GHz. (a) ODEPR via the H centre MCDA at 2.38 eV (520 nm). (b) ODEPR via the F centre MCDA at 2.0 eV (620 nm).

laxation times T_1 for the F and H centres ($T_{1F} = 20$ s, $T_{1H} = 2$ s at 1.5 K). When inducing the H centre EPR and monitoring it in the F centre MCDA, the temporal behaviour is approximately the same as inducing the F centre ODEPR directly. The cross relaxation effect changes also its sign at 845 mT when changing the field position within the H centre EPR line. This effect is demonstrated in Fig. 6(2), where the CR effect is measured for the H centre field position at 837 mT (Fig. 6(2), trace a) and at 846 mT (Fig. 6(2), trace b). The vertical bars indicate the measured effects. Due to the light-induced F–H centre recombination, the measurements were performed with very weak light with the consequence of a rather low signal-to-noise ratio.

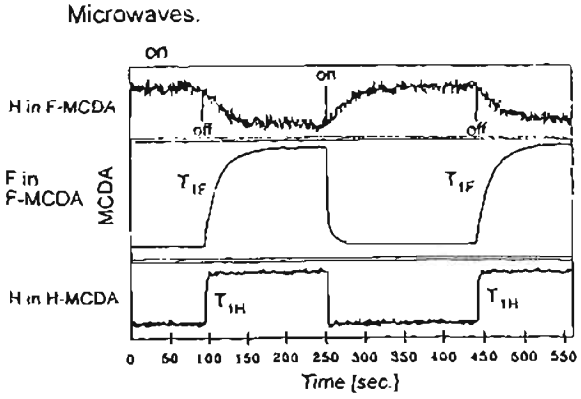

Fig. 5. Time resolved measurement of the ODEPR effect after switching on and off the microwaves. (a) Behaviour of the MCDA of the F centres when inducing the H centre EPR (cross relaxation). (b) Behaviour of the MCDA of the F centres inducing the F centre EPR (T_{1F}). (c) Behaviour of the MCDA of the H centres inducing the H centre EPR (T_{1H})

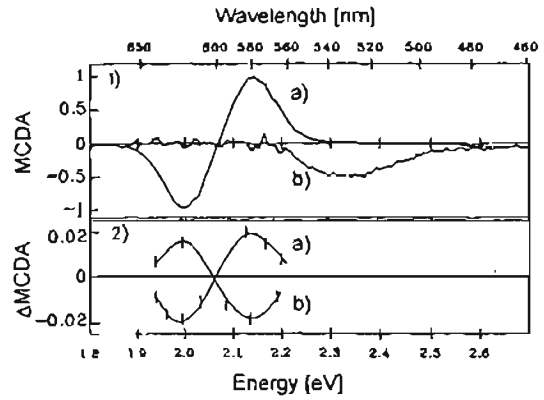

Fig. 6. (1) Trace a): MCDA spectra of the F centres; trace b): MCDA spectrum of the H centres. (2) Trace a): cross relaxation effect exciting the H centre resonance at $B_0 = 837$ mT measured as a function of the photon energy; trace b): the same as above, only exciting the H centre resonance at $B_0 = 846$ mT.

The CR signals follow the shape of the F centre MCDA (Fig. 6(1), trace a), but at 845 mT at the peak of the H centre EPR line, it changes sign. For $B > 845$ mT the F centre MCDA decreases, for $B < 845$ mT it increases.

Upon warming the crystal to 30 K for about 5 min, a thermally stimulated luminescence is observed because of a partial recombination of F and H centres. However, the CR effects were completely lost. This means that the spatial correlation between F and H centres is lost because of the fact that H centres could move away in a thermally stimulated diffusion.

A close proximity of F and H centres after their low temperature generation could also show up in the conventional EPR spectra, since a spin–spin interaction could be seen either as an additional line splitting or as a line broadening effect. We therefore measured the EPR spectrum of parallel centres at 5 K after X-ray generation of H centres at 10 K, a temperature where the CR effect is not yet destroyed. Fig. 7 shows a section of the EPR spectrum: the lowest field superhyperfine line for $I_1 = I_2 = \frac{3}{2}$. There are three lines due to the combination of the two Br isotopes ^{79}Br and ^{81}Br as indicated in Fig. 6 (^{79}Br has 50.69% abundance, $g_I = 1.40427$ and ^{81}Br has 49.31% abundance and $g_I = 1.5137$). All single lines have a peak to peak width of 0.30 mT. Upon warming the crystal for 5 min to 30 K and cooling again to 5 K for the measurement, the line width did not change measurably, only a portion of the signal was lost because of F–H centre recombination.

4. Discussion of the cross-relaxation effects

4.1. Cross-relaxation mechanism between F and H centres

In order for cross-relaxation between two paramagnetic defects to occur, the overlap integral of the shape function of the EPR lines of the two defects must not disappear. The probability of a cross-relaxation process between two $S = \frac{1}{2}$ systems assuming a dipole–dipole interaction is [9]:

$$R_{ij} = \hbar^{-2} \| H_{ij} \|^2 g_{\alpha\beta},$$

with

$$\| H_{ij} \|^2 = \frac{1}{16} g_i^2 g_j^2 \beta^4 \frac{\left(1 - 3\cos^2\theta_{ij}\right)^2}{r_{ij}^6},$$

$$g_{\alpha\beta} = \int g_\alpha(\nu') g_\beta(\nu')\, d\nu'. \qquad (1)$$

$g_{\alpha\beta}$ is the overlap integral of the shape functions of the EPR lines of both defect types α and β. The indices i and j characterise the individual defects of each type taking part in the cross-relaxation and having a distance r_{ij} and angle θ_{ij} between the connection line and the magnetic field. β is the gyromagnetic ratio in the CGS system and g_i, g_j are the g factors.

In the following we will derive the rate equations which describe the cross-relaxation effect between the F and H centres. We will do this in a similar way as it was performed by Koschnick et al. in the case of the cross-relaxation between F centres and the activator Eu^{2+} in the X-ray storage phosphor BaFBr:Eu [3]. If we consider the cross-relaxation between H and F centres in KBr, only the hyperfine transition with $m_I = -3$ within the H centre spin system has a contribution to the overlap integral with the $S = \frac{1}{2}$ system of the F centre. I is the total spin of the two central nuclei of the H centre. Therefore, only H centres with a total nuclear spin of $I = 3$ can interact via cross-relaxation with F centres. All other combinations of a total spin ($I = 0, 1, 2$) can be neglected in order to calculate the cross-relaxation effect. Fig. 8 shows the coupling of the two different defects schematically. The two middle levels of the H centre spin system with a total nuclear spin of three ($m_s = -\frac{1}{2}$, $m_I = -3 \rightarrow m_s = +\frac{1}{2}$, $m_I = -3$) are coupled to the F centre. Thus only the spin occupancies of these two levels are important for the cross-relaxation. If an ODEPR transition is excited in the H centre spin system, then these two levels are influenced either indirectly by spin–lattice relaxation or directly by an ODEPR transition directly between these levels. The change in the occupancies of the two levels which are coupled to the F centre are transferred to the Zeeman levels of the F centre by cross-relaxation. Since the occupancy ratio of the two middle H centre Zeeman levels is thus responsible for the sign of the H centre cross-relaxation lines in the F centre ODEPR spectrum, there is a different sign in the spectrum of fig. 9, curve a) than when the H centre ODEPR is measured directly via the H centre MCDA, in which the sign of the H centre ODEPR depends on the behaviour of the overall ground-state polarisation.

For the sake of simplicity we limit ourselves to cross-relaxing defects consisting of one F centre and one H centre which interact with each other with a certain cross-relaxation probability. This means according to Eq. (1) that there is a population consisting of F centres and H centres with a special distance between each other. Further, we only take into account H centres with a total nuclear spin of three as mentioned before. We neglect isotope effects to prevent further

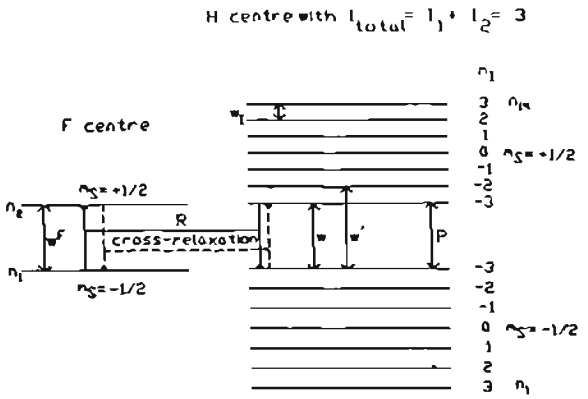

Fig. 8. Energy level scheme for the cross relaxation between F and H centres in KBr. The arrows indicate possible relaxations. The cross relaxation process is a spin flip-flop process which is caused by a coupling of the Zeeman levels of the F centre to the $m_I = 3$ levels of the H centre.

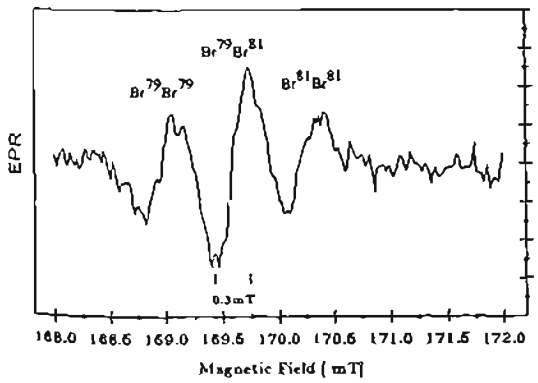

Fig. 7. Conventional EPR spectrum of KBr X-irradiated at 10 K in situ for about 5 hs, measured at 5 K, microwave frequency 9.4 GHz. Shown is the hyperfine transition $\Delta m_s = 1$, $m_I = 3$.

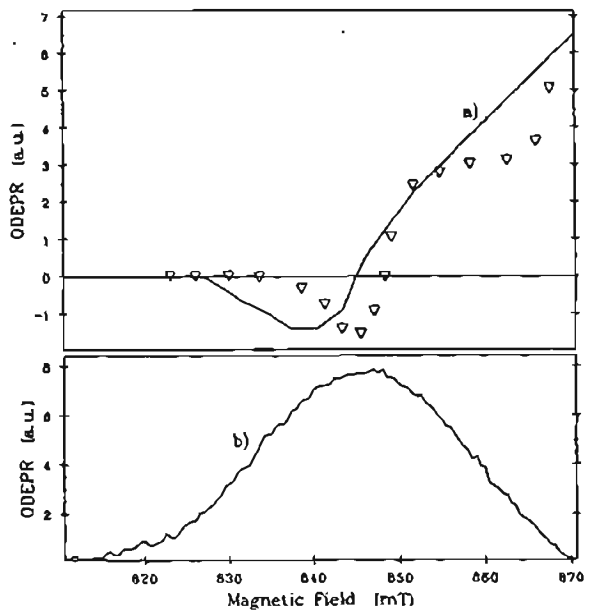

Fig. 9. (Trace a) experimental cross relaxation effect measured in the low energy flank of the F centre MCDA. Trace b): ODEPR spectrum of H centres in KBr. Open triangles: cross relaxation effect calculated with the rate equations described in the text.

complications. Bromine has two isotopes ^{79}Br and ^{81}Br each with a nuclear spin of $\frac{3}{2}$ but with slightly different nuclear g factors (as mentioned before). A very important assumption is the ansatz that the total nuclear spin of three of the cross-relaxing H centres does not change within the cross-relaxation time $\tau_R \propto R^{-1}$. This assumption is justified with the well-known fact that nuclear spin–lattice relaxation is slow in comparison with electron spin lattice relaxation. With this assumption it is possible to describe the cross-relaxation effect with rate equations for a hyperfine split spin system with an electron spin of $S = \frac{1}{2}$ and a fixed central nuclear spin of $I = 3$. This system is then coupled to the F centre as mentioned before (see fig. 8). The cross-relaxation probabilities for a spin flip at the F centre or the H centre ($R_{\mathrm{F},-\frac{1}{2}\to+\frac{1}{2}/+\frac{1}{2}\to-\frac{1}{2}}$ or $R_{\mathrm{H},-\frac{1}{2},-3\to+\frac{1}{2},-3/+\frac{1}{2},-3\to-\frac{1}{2},-3}$) can be written as follows:

$$
\begin{aligned}
R_{\mathrm{F},+\frac{1}{2}\to-\frac{1}{2}} &= n_7 R,\\
R_{\mathrm{F},-\frac{1}{2}\to+\frac{1}{2}} &= n_8 R,\\
R_{\mathrm{H},+\frac{1}{2},-3\to-\frac{1}{2},-3} &= m_1 R,\\
R_{\mathrm{H},-\frac{1}{2},-3\to+\frac{1}{2},-3} &= m_2 R, \qquad (2)
\end{aligned}
$$

where R is the cross-relaxation probability and n_7, n_8, m_1, m_2 are the occupancy numbers of the H and F centre states, respectively (see Fig. 8). R is equal for the two processes, namely spin-up for the F centre and spin-down for the H centre and vice versa. If the rate equation for an F centre is formulated taking into account cross-relaxation and the standardisation condition of the F centre occupancies ($m_1 + m_2 = 1$), one obtains:

$$
\begin{aligned}
\frac{\mathrm{d}m_1}{\mathrm{d}t} &= -\left[R(n_7+n_8) + 2P^{\mathrm{F}} + w^{\mathrm{F}}_{1,2} + w^{\mathrm{F}}_{2,1}\right] m_1\\
&\quad + P^{\mathrm{F}} + w^{\mathrm{F}}_{2,1} + R n_7, \qquad (3)
\end{aligned}
$$

where P^{F} is the ODEPR transition probability and $w^{\mathrm{F}}_{1,2}$ and $w^{\mathrm{F}}_{2,1}$ are the F centre relaxation rates between the levels m_1 and m_2. Within the H centre hyperfine split spin system we took into consideration EPR transitions $P_{i,j}$ between the levels i and j and the following spin–lattice relaxations:

– $w_{i,i+1}$ with $1 \le i \le 13$ and $i \ne 7$ for the total nuclear spin ($\Delta m_s = 0$ and $\Delta m_I = \pm 1$). We made the assumption that the nuclear spin–lattice relaxations $w_{i,i+1}$ are very slow in comparison with the electron spin–lattice relaxations.

– $w_{i,15-i}$ with $1 \le i \le 7$ as allowed electron spin–lattice relaxations ($\Delta m_s = \pm 1$ and $\Delta m_I = 0$).

– $w_{i,14-i}$ and $w_{i+1,15-i}$ as forbidden spin–lattice relaxation ($\Delta m_I = \pm 1$ and $\Delta m_s = \pm 1$) with $1 \le i \le 6$. The forbidden relaxation had to be introduced to explain the change in sign of the cross-relaxation effect. For all relaxations and EPR transitions the following relations are valid:

$$
\begin{aligned}
w_{i,j} &= w_{j,i}\exp\left(-\Delta E_{i,j}/kT\right),\\
P_{i,j} &= P_{j,i}. \qquad (4)
\end{aligned}
$$

The rate equations for the H centre spin system including the hyperfine splitting can now be written in the following way:

$$
\begin{aligned}
\frac{\mathrm{d}n_1}{\mathrm{d}t} &= -(w_{1,2} + w_{1,14} + P_{1,14} + w_{1,13})n_1 + w_{2,1}n_2\\
&\quad + w_{13,1}n_{13} + (w_{14,1} + P_{14,1})n_{14},\\
\frac{\mathrm{d}n_2}{\mathrm{d}t} &= w_{1,2}n_1 - (w_{2,1} + w_{2,3} + w_{2,12} + w_{2,13}\\
&\quad + w_{2,14} + P_{2,13})n_2 + w_{3,2}n_3 + w_{12,2}n_{12}\\
&\quad + (w_{13,2} + P_{13,2})n_{13} + w_{14,2}n_{14},\\
\frac{\mathrm{d}n_3}{\mathrm{d}t} &= w_{2,3}n_2 - (w_{3,2} + w_{3,4} + w_{3,11} + w_{3,12}\\
&\quad + w_{3,13} + P_{3,12})n_3 + w_{4,3}n_4 + w_{11,3}n_{11}\\
&\quad + (w_{12,3} + P_{12,3})n_{12} + w_{13,3}n_{13},\\
\frac{\mathrm{d}n_4}{\mathrm{d}t} &= w_{3,4}n_3 - (w_{4,3} + w_{4,5} + w_{4,10} + w_{4,11}\\
&\quad + w_{4,12} + P_{4,11})n_4 + w_{5,4}n_5 + w_{10,4}n_{10}\\
&\quad + (w_{11,4} + P_{11,4})n_{11} + w_{12,4}n_{12},
\end{aligned}
$$

$$\frac{dn_5}{dt} = w_{4,5}n_4 - (w_{5,4} + w_{5,6} + w_{5,9} + w_{5,10} + w_{5,11} + P_{5,10})n_5 + w_{6,5}n_6 + w_{9,5}n_9 + (w_{10,5} + P_{10,5})n_{10} + w_{11,5}n_{11},$$

$$\frac{dn_6}{dt} = w_{5,6}n_5 - (w_{6,5} + w_{6,7} + w_{6,8} + w_{6,9} + w_{6,10} + P_{6,9})n_6 + w_{7,6}n_7 + w_{8,6}n_8 + (w_{9,6} + P_{9,6})n_9 + w_{10,6}n_{10},$$

$$\frac{dn_7}{dt} = w_{6,7}n_6 - (w_{7,6} + w_{7,8} + w_{7,9} + P_{7,8} + (1 - m_1)R)n_7 + (w_{8,7} + P_{8,7} + Rm_1)n_8 + w_{9,7}n_9,$$

$$\frac{dn_8}{dt} = w_{6,8}n_6 + (w_{7,8} + P_{7,8} + (1 - m_1)R)n_7 - (w_{8,9} + w_{8,7} + w_{8,6} + P_{8,7} + Rm_1)n_8 + w_{9,8}n_9,$$

$$\frac{dn_9}{dt} = w_{8,9}n_8 - (w_{9,5} + w_{9,6} + w_{9,7} + w_{9,8} + w_{9,10} + P_{9,6})n_9 + w_{10,9}n_{10},$$

$$\frac{dn_{10}}{dt} = w_{4,10}n_4 + (w_{5,10} + P_{5,10})n_5 + w_{6,10}n_6 + w_{9,10}n_9 - (w_{10,4} + w_{10,5} + w_{10,6} + w_{10,9} + w_{10,11} + P_{10,5})n_{10} + w_{11,10}n_{11},$$

$$\frac{dn_{11}}{dt} = w_{3,11}n_3 + (w_{4,11} + P_{4,11})n_4 + w_{5,11}n_5 + w_{10,11}n_{10} - (w_{11,3} + w_{11,4} + w_{11,5} + w_{11,10} + w_{11,12} + P_{11,4})n_{11} + w_{12,11}n_{12},$$

$$\frac{dn_{12}}{dt} = w_{2,12}n_2 + (w_{3,12} + P_{3,12})n_3 + w_{4,12}n_4 + w_{11,12}n_{11} - (w_{12,2} + w_{12,3} + w_{12,4} + w_{12,11} + w_{12,13} + P_{12,3})n_{12} + w_{13,12}n_{13},$$

$$\frac{dn_{13}}{dt} = w_{1,13}n_1 + (w_{2,13} + P_{2,13})n_2 + w_{3,13}n_3 + w_{12,13}n_{12} - (w_{13,1} + w_{13,2} + w_{13,3} + w_{13,12} + w_{13,14} + P_{13,2})n_{13} + w_{14,13}n_{14},$$

$$\frac{dn_{14}}{dt} = (w_{1,14} + P_{1,14})n_1 + w_{2,14}n_2 + w_{13,14}n_{13} - (w_{14,1} + w_{14,2} + w_{14,13} + P_{14,1})n_{14} \quad (5)$$

To simplify the problem and to reduce the number of parameters we made the assumption that all nuclear spin–lattice relaxations $w_{i,i+1}$ have the same value w_l. The same assumption was made for the allowed and forbidden electron spin–lattice relaxations (w, w', respectively). From T_{1F}, the F centre spin lattice relaxation time which was measured to be 20 s at 1.5 K, the relaxation probabilities w_{ij}^F of the F centre were estimated. The sum of the allowed and forbidden electron spin–lattice relaxation probabilities could be estimated from the H centre spin–lattice relaxation time T_{1H}, which is 2 s at 1.5 K. With a simple two-level approximation where the hyperfine splitting of the total nuclear spin is neglected, one can show that the following relation for T_{1H} measured via the MCDA is valid:

$$T_{1H}^{-1} = (w + w')(1 + \exp(\overline{\Delta E}/kT)). \quad (6)$$

$\overline{\Delta E}$ is the average of the energy differences of all hyperfine EPR transitions of the H centre. For a temperature of $T = 1.5$ K, it follows that: $w + w' = 0.16$ s^{-1}. Only the ratio of the allowed and forbidden electron spin–lattice relaxation probabilities w/w' and the cross-relaxation probability R are free parameters which were fitted to the cross-relaxation spectrum. w_l turned out not to enter critically in the calculations if it is much slower than $w + w'$. The EPR transition probabilities are the same for all allowed H centre transitions. For the F and H centres both transition probabilities were estimated by fitting the calculated relative ODEPR effect to the measured one. (The calculation of the ODEPR effect was also performed with the above system of rate equations.) The line shapes of the EPR transitions were assumed to be rectangular to simplify the calculations. To consider the statistical weight for the case of a total nuclear spin of three, the cross-relaxation effect calculated with the above rate equation system and the above explained assumption had to be multiplied with a factor of $\frac{7}{16}$. (There are 7 orientations of a total spin of 3 and there are 16 possibilities to combine two spins of $\frac{1}{2}$.)

The differential equation system is a non-linear system which contains products of the occupancies of the F centre and the H centre – for example $m_1(t)Rn_8(t)$. Only the steady-state solution of the differential equation system was evaluated. If the time derivatives of the spin occupations are set to zero in order to calculate the steady-state solution, a non-linear equation system is obtained. This equation system can be solved by an iterative method. With an initial value for m_1 (F centre spin occupation number), the H centre occupancy (n_i) is determined first. Then the occupation number m_1 for the F centre is calculated with the values n_7 and n_8. The m_1 value is then inserted into the H centre equation system again. This method converges so rapidly that three iterations are sufficient to obtain a simulation of the cross-relaxation ODEPR spectrum which remains stable. The result of the calculations for cross-relaxation between F and H centres is shown in Fig. 9. The open triangles are the calculated effect trace a) the experimental result, while trace b) shows the ODEPR line of the H centres for

comparison. The best fit was obtained with a ratio $w/w' \approx 1$ and a cross-relaxation probability of $R = 0.1$ s^{-1}. Therefore, it follows that $w = w' = 0.08$ s^{-1}. The EPR transition probability was determined to be 10 s^{-1} for both defects.

The magnitude of the cross-relaxation effect can be explained with our model. The change in sign of the cross-relaxation can be reproduced by introducing the forbidden spin–lattice relaxation w' where the electron and total nuclear spin flip simultaneously. The discrepancies between the measured and calculated spectrum are probably caused by the simplifications of our model: the rectangular lineshape of the EPR transitions, the neglect of isotope effects and the assumption about the total nuclear spin.

4.2. *Estimate of the spatial correlation between F and H centres after their creation from exiton decay*

The obtained value of R can be interpreted with Eq. (1) assuming a certain spatial correlation between F and H centres.

– After low temperature generation all F and H centres are correlated with one separation between them. In this case the observed cross-relaxation effect of about 5% of the ODEPR of the F centres can be explained by assuming a separation of about $r_{FH} \approx 20$ Å (Fig. 10).

– Only a fraction of the F and H centres are correlated. Then the separation between the correlated pairs must be smaller than 20 Å to explain the experimental observations. If, for example, the separation were 14.1 Å (3 halogen separations along [110]), 20% of the pairs must be correlated, 80% must have a separation of 5 or more halogen sites in the [110] direction.

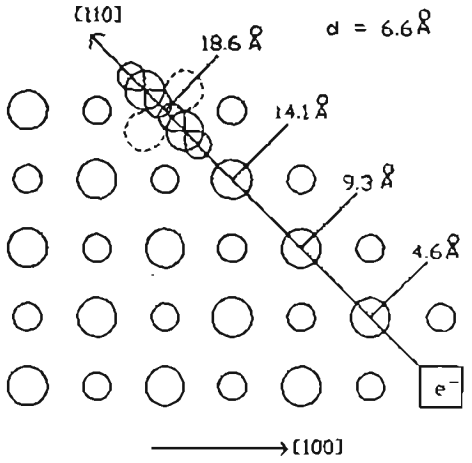

Fig. 10. Model for the spatial correlation of F and H centre pairs as estimated from the cross relaxation.

However, the dipole–dipole interaction between the unpaired F centre electron and the hole of the H centre would be about 0.7 mT for the 20% correlated pairs with 14 Å separation: this would have been seen in the EPR spectrum as a line splitting effect, which was not observed. For a separation of 4 lattice spacings along [110] this interaction is only 0.3 mT and thus smaller than the half width of the EPR lines.

Therefore, we conclude that approximately all F–H pairs have the same separation of 4 halogen spacings along [110], which seems to be the stable F–H pair configuration (fig. 10).

5. Conclusion

As could be demonstrated for the F–H pairs in KBr as well as for F and O^- centres in BaFBr being correlated with the activator Eu^{2+}, CR effects are measurable through the MCDA and the quantitative analysis of the CR effects allows one to deduce either the separation between defects or at least detailed information about spatial correlations within certain limits. The interesting point is that rather "distant" separations of the order of 20 Å or more can be measured in this way. This CR spectroscopy represents a novel tool for the study of point defects which may be particularly fruitful for the investigation for radiation damage centres, since there – depending on a mobility of the created defects – spatial correlation should occur, perhaps more so than realised up to now.

References

[1] K.S. Song and R.T. Williams, Self Trapped Excitons 1993, Springer Series of Solid State Sciences, Vol. 105.
[2] K.S. Song and R.C. Baetzold, Proc. Int. Conf. on Insulating Materials 1992, Nordkirchen, eds. O. Kanert and J.-M. Spaeth (Springer, Berlin, Heidelberg) p. 69
[3] F.K. Koschnick, J.-M. Spaeth and R.S. Eachus, J. Phys.: Cond. Matter 4 (1992) 8919.
[4] J.-M. Spaeth, J.R. Niklas and R.H. Bartram, Structural Analysis of Point Defects in Solids, Springer Series of Solid State Sciences, Vol. 43 (Springer, 1992).
[5] J.-M. Spaeth, W. Meise and K.S. Song, J. Phys.: Cond. Matter, to be published.
[6] W. Meise, Doctoral Thesis, Paderborn, Germany (1993).
[7] F.J. Ahlers, F. Lohse, J.-M. Spaeth and L.F. Mollenhauer, Phys. Rev. B 28 (1983) 1249.
[8] W. Meise, U. Rogulis, F.K. Koschnick and J.-M. Spaeth, Proc. Int. Conf. on Defects in Insulating Materials, Nordkirchen, 1992, eds. O. Kanert and J.-M. Spaeth (Springer, Berlin, Heidelberg) p. 252.
[9] N. Bloembergen, S. Shapiro, P.S. Pershau and J.O. Artmann, Phys. Rev. 114 (1959) 445.

J. Phys.: Condens. Matter 6 (1994) 1815–1824. Printed in the UK

Experimental evidence for spatial correlation between F and H centres formed by exciton decay at low temperatures in KBr

W Meise†, U Rogulis‡, F K Koschnick†, K S Song§† and J M Spaeth†

† Fachbereich Physik, Universität-GH Paderborn, Warburger Strasse 100A, 33098 Paderborn, Germany

‡ Physical Technical Institute, University of Latvia, Riga, Latvia

§ Department of Physics, University of Ottawa, Ottawa, Ontario, Canada K1N 6N5

Received 9 November 1993

Abstract. Optical detection of electron paramagnetic resonance of F–H-centre pairs created by low-temperature x-ray irradiation of KBr was performed via the magnetic circular dichroism of the optical absorption (MCDA) whereby cross-relaxation (CR) effects between the H and F centres were detected in the MCDA of the F centres. A quantitative analysis of the CR effects yielded direct experimental evidence that all F and H centres are spatially correlated after their low-temperature formation with a separation of four lattice sites along the ⟨110⟩ directions. A theoretical analysis of the CR result yields an estimate of the F-centre formation time of 2 ps, in agreement with other experimental evidence, and also shows that the F–H separation obtained is the first stable F–H-centre pair configuration.

1. Introduction

The formation and the decay of excitons have been the subject of intensive studies in the alkali halides (for a recent comprehensive review see Song and Williams 1993a). Exciton decay causes a luminescence on the one hand, and on the other hand the formation of the fundamental trapped electron and trapped hole centres: F centres (electron trapped at an anion vacancy) and H centres, halogen$_2^-$ molecular ions on substitutional halogen sites. F–H pairs were formed during relaxation of the self-trapped exciton (STE) of the lowest energy as a result of the adiabatic instability against axial relaxation of the system (Song and Williams 1993a, Song and Baetzold 1993). Their formation happens in a time faster than the lifetime of the π and σ luminescence (Bradford *et al* 1975, Suzuki *et al* 1979). As was shown by Toyozawa (1974), there is no barrier against the hole relaxation, which is very fast (10^{-13}–10^{-12} s). Electrons move very fast in the conduction band before they are captured by a relaxed or an unrelaxed hole (Williams *et al* 1978). Thus, the total lifetime of the exciton decay is the sum of the lifetime of the electron, the relaxation time of the unrelaxed excited state to the relaxed excited state and the formation time of F- and H-centre pairs. When irradiating an alkali halide crystal with ionizing radiation, the formation of F–H pairs is the dominating process (Faraday and Compton 1965). The majority of the F centres formed decays in a very short time due to the recombination of close F–H centre pairs (Kondo *et al* 1969). At temperatures below 25 K the decay time is temperature independent, while above this temperature there is a thermally activated process with an activation energy of 20 meV (Kondo *et al* 1969). The simplest explanation for the decay of F–H-centre pairs

0953-8984/94/091815+10$19.50

in the first few microseconds is the assumption that F–H pairs are direct neighbours along a ⟨110⟩ direction and that those pairs that are stable at 4.2 K have a separation of at least two lattice spacings along a ⟨110⟩ direction, where they are localized separately. However, there is no direct experimental proof for such a spatial correlation between F–H-centre pairs created at 4.2 K, nor is it clear how far apart the pairs need to be in order to remain stable.

In this paper we report on experiments that for the first time give direct experimental evidence for a spatial correlation of F–H-centre pairs formed at 4.2 K in KBr. In the experiment optical detection of the electron paramagnetic resonance (EPR) of the correlated F and H centres is measured via the magnetic circular dichroism of the absorption (MCDA) whereby cross-relaxation (CR) effects between the correlated defects are used to deduce the spatial correlation (Koschnick *et al* 1992).

2. Experiment

The crystal used in this study was a particularly pure KBr crystal provided by G McDugle (Eastman Kodak Co.). It was irradiated with x-rays in the microwave cavity at 4.2 K for about 15 h in order to produce enough H centres. V_K centres were also generated simultaneously.

The experimental method used to detect a spatial correlation between F and H centres was that of optically detected electron paramagnetic resonance (ODEPR) via the MCDA with detection of CR effects (Koschnick *et al* 1992). This is briefly explained as follows.

The MCDA, which is the differential absorption of right and left circularly polarized light, propagating along an external magnetic field, is proportional to the spin polarization of the ground state of a paramagnetic Kramers defect within the approximation of a free atom or ion. For a system with a spin of $\frac{1}{2}$ the MCDA is proportional to the population difference of the two Zeeman levels. The change in spin polarization by EPR transitions can be monitored as a change of the MCDA of the defect (Ahlers *et al* 1983). If there is a sufficiently strong spin–spin interaction between the two paramagnetic defects to induce spin flip-flop processes between the two spin systems, then an EPR-induced change of the spin polarization of one defect can cause a change in the spin polarization of the other, which can be monitored as a change in its MCDA. Thus, if there is such a CR effect, then the EPR of one defect can be monitored in the MCDA of the other defect linked to it by CR. Such a link is expected if the two defects are sufficiently near to each other (see below). Another condition to observe the CR effects in the MCDA is that the EPR spectra of the two defects have a partial overlap to ensure energy conservation (for further details see Koschnick *et al* 1992).

The experiments were performed with a custom-built computer-controlled K-band MCDA/ODEPR spectrometer (25 GHz), which operated between 250 nm and 1700 nm at temperatures between 1.5 K and 300 K.

3. Experimental results

X-irradiations of the pure KBr crystal at 4.2 K produced H centres, F centres and V_K centres. Figure 1(*a*) shows the optical absorption bands of these centres according to the literature, and figure 1(*b*) the MCDA spectrum. It was shown recently that H centres have an MCDA superimposed on the high-energy flank of the F-centre absorption, which is caused by those H centres with their molecular axes perpendicular to the static magnetic field. Parallel H

centres have no MCDA in the spectral region between 1.0 and 3.4 eV (Spaeth *et al* 1993, Meise 1993). Figure 2, trace a shows the ODEPR spectrum of the perpendicular H centres measured at 2.4 eV together with an EPR spectrum calculated with the known $g_\perp$-value and assuming a hyperfine interaction constant $A_\perp$ of 5 mT (figure 2, trace b; for details see Spaeth *et al* 1993). At 2.4 eV one also measures F centres (see figure 1(*b*)), which therefore also appear in figure 2, trace a. The V_K centres, simultaneously present, have MCDA bands different from those of the H centres. This is seen in the 'MCDA tagged by EPR', a kind of excitation spectrum of the ODEPR lines (Ahlers *et al* 1983) (figure 1(*c*)). Thus, e.g. at 2.38 eV (520 nm) one can measure the H-centre EPR without inducing simultaneously the V_K-centre EPR. It is also seen that the H-centre MCDA band does not overlap with the low-energy flank of the F-centre MCDA. Therefore, when measuring the ODEPR at 2.0 eV (620 nm) at the low-energy flank of the F centres one should not detect any H-centre EPR.

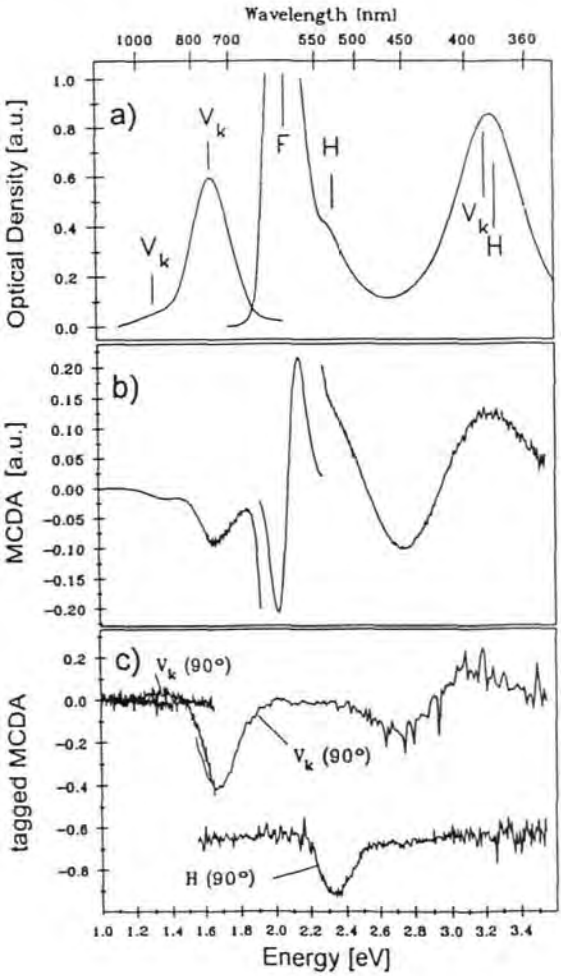

Figure 1. (*a*) Absorption of V_K, H and F centres in KBr x-irradiated below 20 K. (*b*) MCDA spectrum of KBr x-irradiated at 4.2 K *in situ*, measured at 1.5 K; magnetic field, 2 T. (*c*) Tagged MCDA spectra of V_K and H centres in KBr; $B_0 \parallel [100]$.

In figure 3 the results of the ODEPR measurements at 2.0 eV (low-energy flank of the F centre) and at 2.38 eV (H-centre MCDA) are shown. At 2.38 eV both the F-centre and the H-centre EPR lines appear (trace a) due to the overlap of the two MCDA bands. However,

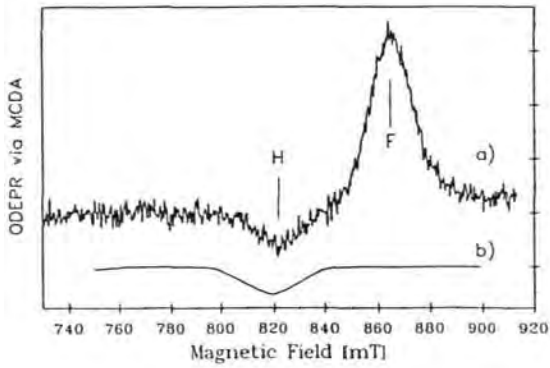

Figure 2. Trace a, ODEPR spectrum of KBr x-irradiated at 4.2 K *in situ*, measured at 1.5 K; microwave frequency, 23.8 GHz; phonon energy, 2.4 eV; $B_0 \parallel [100]$. Trace b, EPR simulation of H centres in KBr with their axes perpendicular to B_0; $A_\perp = 5$ mT; $g_\perp = 2.074$; half width of HF lines, 5 mT.

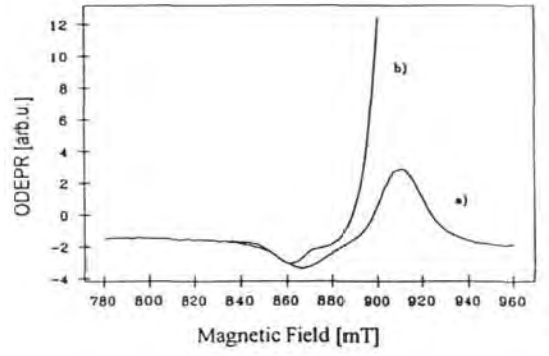

Figure 3. ODEPR spectra of pure KBr x-irradiated at 4.2 K *in situ* for about 15 h, measured at 1.6 K; microwave frequency, 24.5 kHz. Trace a, ODEPR via the H-centre MCDA at 2.38 eV (520 nm); trace b, ODEPR via the F-centre MCDA at 2.0 eV (620 nm).

at 2.0 eV no H-centre EPR should appear. The fact that it does shows the presence of a CR effect. A change in the H-centre spin polarization is transferred to the F-centre spin polarization (Meise *et al* 1993).

The effects of polarization transfer are also seen in time-resolved measurements. Figure 4(*b*) and (*c*) shows the temporal behaviour of the MCDA of F- and H-centre MCDA bands after switching off the microwaves that had induced the F-centre and H-centre EPR transitions, respectively. The MCDA bands reach thermal equilibrium with the characteristic spin-lattice relaxation times T_1 for the F and H centres ($T_{1F} = 20$ s, $T_{1H} = 2$ s at 1.5 K). When inducing the H-centre EPR and monitoring it in the F-centre MCDA, the temporal behaviour is approximately the same as inducing the F-centre ODEPR directly. The CR effect also changes its sign at 845 mT when changing the field position within the H-centre EPR line. This effect is demonstrated in figure 5(2), where the CR effect is measured for the H-centre field position at 837 mT (figure 5(2), trace a) and at 846 mT (figure 5(2), trace b). The vertical bars indicate the measured effects. Due to the light-induced F–H-centre recombination, the measurements were performed with very weak light with the consequence of a rather low signal-to-noise ratio. The CR signals follow the shape of the F-centre MCDA (figure 5(1), trace a), but at 845 mT, at the peak of the H-centre EPR line, it changes sign. For $B > 845$ mT the F-centre MCDA decreases; for $B < 845$ mT it increases.

Upon warming the crystal to 28 K for about 5 min, a thermally stimulated luminescence is observed because of a partial recombination of F and H centres. However, the CR effects were completely lost. This means that the spatial correlation between F and H centres is lost because of the fact that H centres could move away in a thermally stimulated diffusion.

A close proximity of F and H centres after their low-temperature generation could also

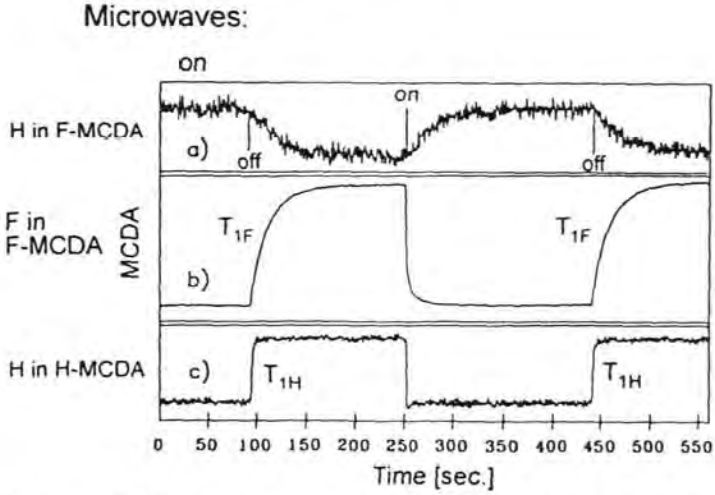

Figure 4. Time-resolved measurement of the ODEPR effect after switching on and off the microwaves: (*a*) behaviour of the MCDA of the F centers when inducing the H-centre EPR (CR); (*b*) behaviour of the MCDA of the F centres when inducing the F-centre EPR (T_{1F}); (*c*) behaviour of the MCDA of the H centres inducing the H-centre EPR (T_{1H}).

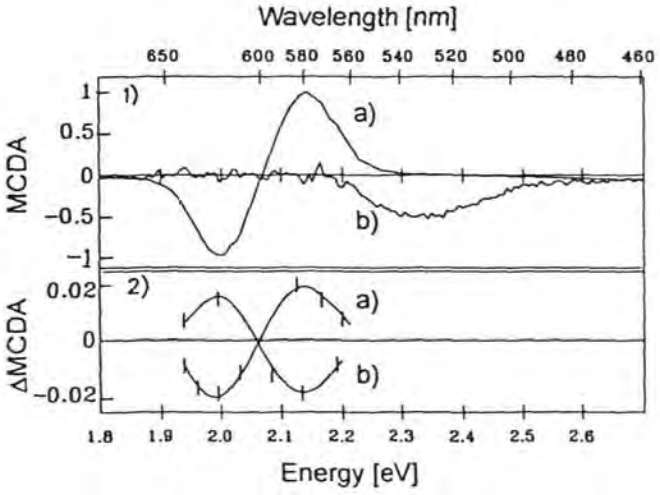

Figure 5. (1) Trace a, MCDA spectrum of the F centres; trace b, MCDA spectrum of the H centres. (2) Trace a, CR effect exciting the H-centre resonance at $B_0 = 837$ mT, measured as a function of the photon energy; trace b, as above, but exciting the H-centre resonance at $B_0 = 846$ mT.

show up in the conventional EPR spectra, since a spin–spin interaction could be seen either as an additional line splitting or as a line-broadening effect. We therefore measured the EPR spectrum of parallel centres at 5 K after x-ray generation of H centres at 10 K, a temperature where the CR effect is not yet destroyed. Figure 6 shows a section of the EPR spectrum: the lowest-field superhyperfine line for $I_1 = I_2 = \frac{3}{2}$. There are three lines due to the combination of the two Br isotopes ^{79}Br and ^{81}Br as indicated in figure 6 (^{79}Br has 50.69%

abundance, $g_I = 1.404\,27$ and ^{81}Br has 49.31% abundance, $g_I = 1.5137$). All single lines have a peak-to-peak width of 0.30 mT. Upon warming the crystal for 5 min to 30 K and cooling again to 5 K for the measurement, the line width did not change measurably, but a portion of the signal was lost because of F–H-centre recombination.

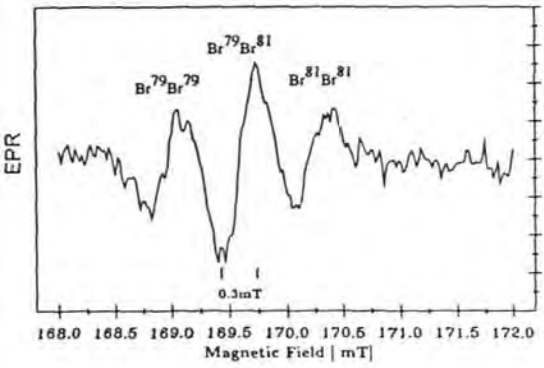

Figure 6. Conventional EPR spectrum of KBr x-irradiated at 10 K *in situ* for about 5 h, measured at 5 K; microwave frequency 9.4 GHz. The HF transition $\Delta m_s = 1$, $m_I = 3$ is shown.

4. Discussion

4.1. Cross-relaxation effects

For an estimate of the spatial correlation between F and H centres one can perform a quantitative calculation of the CR effects and compare with the experiment. The CR probability between two spin systems assuming a dipole–dipole interaction is given by (Bloembergen *et al* 1959)

$$R_{ij} = \hbar^{-2}|H_{ij}|^2 g_{\alpha\beta}$$
$$|H_{ij}|^2 = g_i^2 g_j^2 \beta^4 (3 - \cos^2 \Theta_{ij})^2 / r_{ij}^6 \qquad (1)$$
$$g_{\alpha\beta} = \int g_\alpha(\nu') g_\beta(\nu')\, \mathrm{d}\nu'.$$

$g_{\alpha\beta}$ is the overlap integral of the shape function of the EPR lines of both defect types, α and β, which can be determined experimentally from the EPR spectra. The indices i and j characterize the individual defect of each type taking part in the CR and having a distance r_{ij} and an angle Θ_{ij} between the connection line and the magnetic field. β is the gyromagnetic ratio in the CGS system and g_i, g_j are the electronic g factors. The dynamical behaviour of the spin polarization of a paramagnetic defect can be calculated by a set of rate equations describing the occupation of the Zeeman levels. The occupations are influenced by EPR transitions and spin-lattice relaxations. If two different spin systems are coupled by CR, additional terms due to CR enter the rate equations, which become non-linear. For the CR effects between F centres and Eu^{2+} activators in the x-ray storage phosphor system BaFBr:Eu the rate equations have been described in detail (Koschnick *et al* 1992). We have performed an analogous calculation here. In figure 7 the energy-level scheme is shown for the CR between F and H centres. All transitions and relaxations that were used to calculate

the CR effect quantitatively are indicated. Because of energy conservation during a spin-flip-flop process only those H centres whose total nuclear spin I is equal to three couple via CR to F centres. In principle the two central Br nuclei of an H centre can couple to a total spin of 0, 1, 2 and 3. In all calculations effects due to the two different isotopes of ^{79}Br and ^{81}Br are neglected. We further assumed that the total spin of three does not change within the CR time τ_{CR}. τ_{CR} is approximately R_{ij}^{-1}. To explain the change in sign of the CR effect (see figure 5(1)) we had to introduce 'forbidden' spin-lattice relaxations with $\Delta m_s = \pm 1$ and $\Delta m_I = \pm 1$ besides allowed spin-lattice relaxations $\Delta m_s = \pm 1$, $\Delta m_I = 0$ and weak nuclear spin relaxations $\Delta m_s = 0$ and $\Delta m_I = \pm 1$.

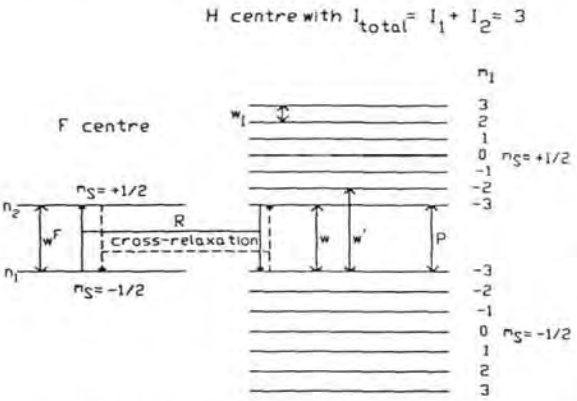

Figure 7. Energy-level scheme for the CR between F and H centres in KBr. The arrows indicate possible relaxations. The CR process is a spin-flip-flop process, which is caused by a coupling of the Zeeman levels of the F centre to the $m_I = -3$ levels of the H centre.

The following experimental parameters were used: $T = 1.5$ K, $T_{1F} = 20$ s, $T_{1H} = 2$ s. For details of the rate equations and calculations of the CR effects see the article by Spaeth *et al* (1993).

With the CR probability R_{ij} as a fit parameter the CR effect on the MCDA of the F centres was calculated and compared with experiment. In figure 8 the open triangles are the calculated effect and trace a the experimental result, while trace b shows the ODEPR line of the H centres for comparison (see section 3). The obtained value of R_{ij} can be interpreted with (1) assuming a certain spatial correlation between the F and H centres, as follows.

(i) After low-temperature generation all F and H centres are correlated with one separation between them. In this case the observed CR effect of about 5% of the ODEPR of the F centres can be explained by assuming a separation of $r_{F,H} \simeq 20$ Å.

(ii) Only a fraction of the F and H centres is correlated. Then the separation between the correlated pairs must be smaller than 20 Å to explain the experimental observations. If, for example, the separation was 14.1 Å (three halogen separations along [110]), 20% of the pairs must be correlated, and 80% must have a separation of five or more halogen sites in the [110] direction.

However, the dipole–dipole interaction between the unpaired F-centre electron and the hole of the H centre would be about 0.7 mT for the 20% correlated pairs with 14 Å separation: this would have been seen in the EPR spectrum as a line-splitting effect, which was not observed. For a separation of 18.6 Å this interaction is only 0.3 mT and thus smaller than the half widths of the EPR lines.

Therefore we conclude that approximately all F–H pairs have the same separation of four halogen spacings along (110), which seems to be the stable F–H pair configuration (figure 9). We have no information about the orientation of the molecular axis of the H centres relative to the F–H connection line.

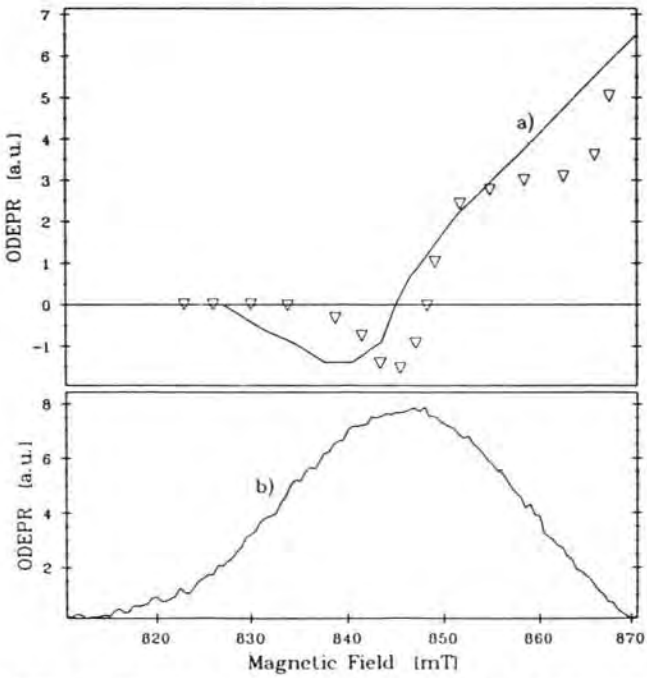

Figure 8. Trace a, experimental CR effect measured in the low-energy flank of the F-centre MCDA; open triangles, CR effect calculated with the rate equations described in the text; trace b, ODEPR spectrum of H centres in KBr for comparison.

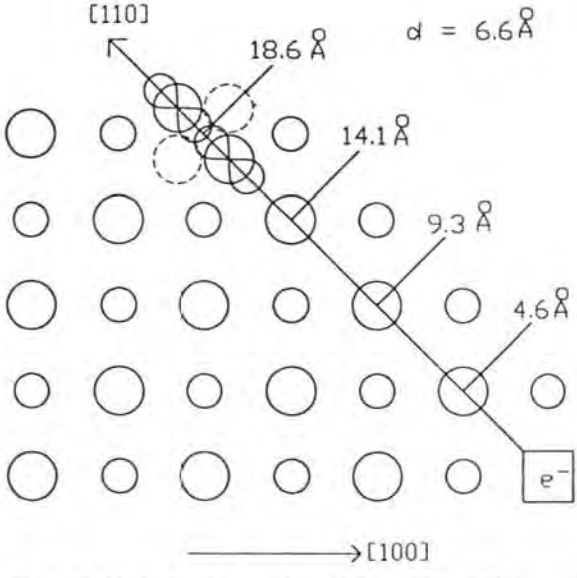

Figure 9. Model for the spatial correlation of F- and H-centre pairs as estimated from the CR. The orientation of the H centre cannot be inferred from the experiments.

4.2. Estimate of the F–H separation from exciton decay

Recent works strongly indicate that the relaxed STE is axially off-centre such that the electron and hole do not occupy a common centre. As such it should be viewed as equivalent to a primitive F–H pair. Well separated and therefore stable F–H pairs are further down on the common actiabatic potential energy surface (APES). A geometrically ideal first-neighbour F–H pair is unlikely to exist when the interaction between the electron and hole is considered. Such species are indeed one of the possible configurations of the STE and they usually recombine radiatively or non-radiatively. From theoretical calculations of both approximate and *ab initio* Hartree–Fock methods, as well as from a careful analysis of the parameters of the spin Hamiltonian (Song *et al* 1990), it appears that in KBr the relaxed STE is at a separation of about 5 Å between the hole and electron, which is between one and two lattice spacings along ⟨110⟩. Associated with this axial relaxation is an energy gain (lowering) of about 1 eV (Song *et al* 1989, Song and Baetzold 1992) relative to the on-centre configuration, which provides enough kinetic energy to be utilized in propelling the hole (localized on the H centre) further from the electron (localized on the F centre). This mechanism is believed to be at the origin on the F–H pair formation at very low temperature (Song *et al* 1989). Also, energetic halogen atom desorptions with kinetic energies as large as about 1 eV are observed in the alkali halides in which the efficient low-temperature F-centre formation is observed (Szymonski 1990).

Here we present a qualitative description of the observed correlated pairs in KBr with a separation of about 20 Å (fourth NN). We assume that the covalent bond-switching event that propels the H centre along a ⟨110⟩ axis (the same as the replacement sequence) can be approximated as a projectile motion of a halogen atom that is initially given a kinetic energy of about 1 eV. A damping mechanism linear to the velocity is assumed, and contributes to slowing down the process. When the residual kinetic energy has reached about 0.1 eV, it is assumed that the process comes to an end and results in the correlated F–H pairs. This limit of 0.1 eV is about the potential barrier height of H-centre thermal diffusion (see e.g. Song and Williams 1993b). With this model an elementary calculation shows that in the case of KBr, the process takes about 1.8 ps to reach a separation of about 20 Å (the fourth NN along ⟨110⟩). The energy loss at successive F–H separations is 0.18, 0.32, 0.24 and 0.16 eV, respectively.

This description is obviously crude and qualitative. We know, for example, that some fraction will lose all its energy earlier and decay radiatively as a relaxed STE at a shorter separation. Assuming that the energy loss is accounted for in terms of emitted LO phonons, each step would represent about 10 LO phonons. Taking the initial kinetic energy of 1 eV as an upper limit, the time required to reach the fourth NN found here, 1.8 ps, would be a lower limit. This range of time seems not unreasonable when compared with the F-centre formation time in KBr of 2 ps after the electron–hole pair creation (Williams *et al* 1990). Tokizaki *et al* (1991) have observed in their sub-picosecond studies in NaCl that after the relaxed STE is excited to higher excited states, F centres appeared in about 3 ps.

If the separation were five lattice spacings along ⟨110⟩, the total separation time would be 2.3 ps, and for three spacings 1.3 ps. Within this estimate of the displacement time of H centres for the third, fourth and fifth lattice spacings we cannot safely discriminate between them when comparing to the formation time of F centres.

From the relaxation between the electron–hole separation and the radiative lifetime of the triplet STE in KBr (Song and Chen 1989) we have estimated the lifetimes for different F–H separations.

For the separation of four lattice spacings along ⟨110⟩ the lifetime is found to be in the range of 10^4–10^6 s depending on the value taken for the recombination energy, assumed to

be 2 eV and 0.5 eV, respectively. Thus this F–H pair separation corresponds to a stable pair configuration. However, assuming as the electron–hole separation three lattice spacings along ⟨110⟩, the lifetime varies between 10 s and 10^3 s for the same range of recombination energies. This result shows that three lattice spacings do not correspond to a stable F–H pair configuration. Thus our experimental results do agree very well with the theoretical predictions of the exciton decay mechanism explaining the F–H pair creation.

5. Conclusions

The present work establishes for the first time the stable F–H pair separation in KBr at low temperature to be four lattice spacings along ⟨110⟩ before thermally activated diffusion of the H centres destroys this correlation. Using results of previous theoretical work on the STE in KBr the estimate of the F-centre formation time as well as the lifetime of the correlated F–H pair yields results consistent with the experimental results obtained from very different kinds of approach: CR spectroscopy, EPR spectroscopy and time-resolved optical spectroscopy. Thus a consistent picture emerges for the F–H pair formation through the STE decay.

References

Ahlers F J, Lohse F, Spaeth J-M and Mollenhauer L F 1983 *Phys. Rev.* B **28** 1249

Bloembergen N, Shapiro S, Pershau P S and Artman J O 1959 *Phys. Rev.* **114** 445

Bradford J M, Williams R T and Faust W L 1975 *Phys. Rev. Lett.* **50** 79

Faraday B J and Compton W D 1965 *Phys. Rev.* A **138** 893

Kondo Y, Hirai M, Yoshinari T and Ueta M 1969 *J. Phys. Soc. Japan* **26** 1553

Koschnick F K, Spaeth J M and Eachus R S 1992 *J. Phys.: Condens. Matter* **4** 8919

Meise W 1993 *Doctoral Thesis* University of Paderborn

Meise W, Rogulis U, Koschnick F K and Spaeth J-M 1993 *Proc. Int. Conf. on Defects in Insulating Materials (Nordkirchen 1992)* ed O Kanert and J M Spaeth (Singapore: World Scientific) p 1078

Song K S and Baetzold R C 1992 *Phys. Rev.* B **46** 1960

Song K S and Baetzold R C 1993 *Proc. Int. Conf. on Defects in Insulating Materials (Nordkirchen 1992)* ed O Kanert and J M Spaeth (Singapore: World Scientific) p 69

Song K S and Chen L F 1989 *J. Phys. Soc. Japan* **58** 3022

Song K S, Leung C H and Spaeth J M 1990 *J. Phys.: Condens. Matter* **2** 6373

Song K S, Leung C H and Williams R T 1989 *J. Phys.: Condens. Matter* **1** 683

Song K S and Williams R T 1993a *Self Trapped Excitons (Springer Series in Solid State Sciences 105)* (Berlin: Springer)

—— 1993b *Self Trapped Excitons (Springer Series in Solid State Sciences 105)* (Berlin: Springer) ch 6

Spaeth J M, Koschnick F K, Meise W and Rogulis U 1993 *Proc. 7th Int. Conf. on Radiation Effects in Insulators (Nagoya); Nucl. Instrum. Methods* B at press

Suzuki Y, Okunura M and Hirai M 1979 *J. Phys. Soc. Japan* **47** 184

Szymonski M 1990 *Desorption Induced by Electronic Transitions DIET IV (Springer Series in Surface Sciences 19)* ed G Betz and P Varga (Berlin: Springer) p 270

Tokizaki T, Makimura T, Akiyama H, Nakamura A, Tanimura K and Itoh N 1991 *Phys. Rev. Lett.* **67** 2701

Toyozawa Y 1974 *Vacuum Ultraviolet Radiation Physics* ed E E Koch, R Haensel and C Kunz (Oxford: Pergamon)

Williams R T, Bradford J M and Faust W L 1978 *Phys. Rev.* B **18** 7038

Williams R T, Liu H and Williams G P Jr 1990 *Rev. Solid State. Sci.* **4** 445

Hole-trapping sites and the mechanism of the photostimulated luminescence of the x-ray storage phosphor RbI:Tl^+

U. Rogulis
Institute of Solid State Physics, University of Latvia, 8 Kengaraga Street, LV-1063 Riga, Latvia

C. Dietze, Th. Pawlik, Th. Hangleiter, and J.-M. Spaeth[a)]
Fachbereich Physik, University of Paderborn, D-33095 Paderborn, Germany

(Received 2 January 1996; accepted for publication 29 April 1996)

Radiation damage centers generated by x irradiation at 80 and 300 K in the storage phosphor RbI:Tl^+ were investigated with optically detected magnetic resonance and optical measurements. It is shown that the intensity of the photostimulated luminescence depends on the concentration of Tl^{2+} centers. Bleaching into any of the seven identified Tl^{2+} absorption bands destroys the Tl^{2+} centers and leads to a Tl^+ emission as well as to V_K centers. Proportionally to photodestruction of Tl^{2+} centers, the photostimulated luminescence is decreased. The traps for information storage in RbI:Tl^+ are F centers and Tl^{2+} centers. © *1996 American Institute of Physics.*
[S0021-8979(96)08315-6]

I. INTRODUCTION

X-ray storage phosphors such as BaFBr doped with Eu^{2+} were intensely investigated. The x-irradiation-induced defects were studied in particular in order to understand the mechanism of the information storage and photostimulation process. The x-ray information is usually stored in electron trap centers such as F centers (electrons trapped at anion vacancies) and in hole centers.

For the commercially used material BaFBr:Eu^{2+}, in spite of many efforts to understand the mechanism of the information storage and read-out process, no complete understanding has yet been achieved.[1,2] In particular, the nature of room-temperature-stable hole centers is not clear, nor the mechanism of the energy transfer to the activator after photostimulated F center electrons have recombined with the hole centers (Refs. 1 and 2 and further references therein).

It was proposed that in BaFBr:Eu^{2+} aggregates of F centers, hole centers, and the activator Eu^{2+} are formed that are the photostimulable "defects." Upon photostimulation of an F center, the F center electron recombines with the hole center. The recombination energy of this process is transferred to the activator, which is excited and subsequently emits at 390 nm.[3–5]

It was shown recently that in BaFBr:Eu^{2+} an apparently unavoidable oxygen contamination greatly influences the formation of electron trap centers and provides hole trapping defects.[3,4] An alternative to the aggregate model to explain the photostimulated luminescence (PSL) process is the hypothesis of an F center–Eu^{3+} center pair model,[6] in which the hole center is Eu^{3+}. However, for the pair model, there is yet no direct experimental evidence. Moreover, it cannot explain the so-called replenishment effect of the PSL,[7,8] which is the observation that after exhaustive read-out of the stored information at low temperature by photostimulating F centers there is a recovery of the photostimulability after warming the phosphor to temperatures above 200 K. The replenishment effect occurs because of the thermally activated formation of new photostimulable aggregates. The explanation of this effect, thus, requires the presence of the more complex aggregate center model.[7,8] In the case of KBr:In^+ it was assumed that after x-irradiation, F centers and In^{2+} centers are formed,[9] which can be excited and read-out by stimulation in the F center absorption band. Also, for the KBr:In^+ phosphor, the simple pair model cannot explain all experimental facts, such as the recently observed replenishment effect.[10] For all phosphors yet discussed in some detail, the nature of the hole centers is not clear.

Recently, it was postulated, however, that in RbI doped with Tl^+ the so-called V_{KA} centers fulfill the role of the hole centers involved in the PSL mechanism. V_K centers, which are trapped hole centers where the hole is shared between two adjacent halogen ions along the ⟨110⟩ direction, were claimed to be stabilized near substitutional Tl^+ defects (so-called V_{KA} centers) at room temperature, at least for a short time.[11] The purpose of the present work was to study the hole centers and their role in the PSL process in RbI:Tl^+ by use of magneto-optical, optically detected magnetic resonance as well as luminescence spectroscopy. It was found that no V_{KA} centers can be detected. Tl^{2+} hole centers were identified and it is shown that they are directly correlated with the PSL intensity. RbI:Tl^+ seems to be the only system so far where a simple pair model (F center–Tl^{2+} center pairs) explains the PSL mechanism. Accordingly, no replenishment effect of the PSL was observed in RbI:Tl^+ crystals.

II. EXPERIMENTAL DETAILS

A. Samples

The RbI samples were doped with 1 mol % Tl in the melt and grown by the Czochralski method under inert gas. Comparative measurements with a sample doped with a 0.1 mol % yielded essentially the same results.

B. Optical measurements

Emission spectra, excitation spectra of the photostimulated luminescence and absorption spectra were measured

a)Electronic mail: sp_sp@physik.uni-paderborn.de

 0021-8979/96/80(4)/2430/6/$10.00

with a single beam spectrometer, in which two 0.25 m double monochromators (Spex) were used. The samples were excited with either a halogen lamp for the visible spectral range or a deuterium lamp for the ultraviolet range. A high intensity xenon lamp, sometimes in combination with filters, was used for the bleaching experiments. The emission and excitation spectra were detected using a photomultiplier and single photon counting. All spectra were corrected for the spectral response of the monochromator, the lamp intensity, and the detector sensitivity. The samples could be x irradiated in the cryostat in the temperature range from 10 to 310 K. For low temperature x irradiation, commonly 80 K was used.

C. Magneto-optical and electron paramagnetic resonance measurements

The spectra of the magnetic circular dichroism of the optical absorption (MCDA), which is the differential absorption of left and right circularly polarized light, and the MCDA-detected electron paramagnetic resonance (MCDA-EPR) were measured with a custom-built, computer-controlled spectrometer working in the K band (24 GHz). For details see, for example, Ref. 12. Some EPR measurements were also performed in a conventional x-band spectrometer at $T=10$ K.

Samples ($2\times3\times4$ mm^3) were x-irradiated "*in situ*" at $T=80$ K and measured at 4.2 K (MCDA) or 1.5 K (MCDA-EPR). Intermediate temperatures between 1.5 K and room temperature could be stabilized (error of absolute temperature ±5 K). As a light source for the optical bleaching of the MCDA a xenon lamp in connection with a double grating monochromator and, in some cases, additional optical glass filters were used.

III. EXPERIMENTAL RESULTS

A. Thermal treatments

The thermoluminescence glow curve of RbI:Tl$^+$ was shown previously to have two characteristic peaks at 125 and 175 K. Accordingly and similarly to Thoms *et al.*,[11] we chose a three-step temperature sequence for our measurements: (a) x irradiation at 80 K, (b) subsequent thermal annealing to 150 K, and (c) subsequent thermal annealing to 220 K. The corresponding PSL excitation and MCDA spectra are shown in Figs. 1 and 2. In the PSL excitation spectrum drastic changes occur as a consequence of these temperature steps: after step (a), a single peak appears at 1.72 eV coinciding with the F center absorption band (Fig. 1, curve a), which increases by a factor of 20 after step (b) (Fig. 1, curve b). Besides this, a second band appears at 2.27 eV. This band at 2.27 eV and two bands at 0.87 and 1.32 eV were assigned by Thoms *et al.*[11] to the Tl^0 center in analogy to results obtained in x irradiated KCl:Tl$^+$.[13] Upon step (c), the Tl^0 bands disappear, and the PSL peak at 1.72 eV is reduced by a factor of 6 (Fig. 1, curve c). The F center absorption remains the same during all temperature steps.

The temperature behavior was further studied with MCDA and MCDA-EPR. In the initial step (a), the MCDA (Fig. 2) shows the well-known F center band centered at

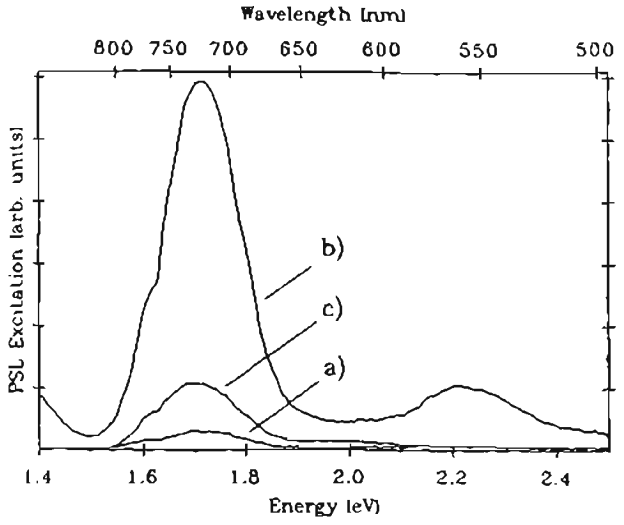

FIG. 1. Excitation spectra of the PSL of RbI:Tl: (a) after x irradiation at $T=80$ K, (b) after annealing to $T=150$ K, and (c) after annealing to T 220 K. The emission was detected at 2.86 eV in the Tl$^+$ emission band at $T=80$ K.

1.72 eV with its typical derivative structure. The optical absorption of V_K centers in RbI contains 2 bands: one in the UV peaking at 3.06 eV and one in the near infrared peaking at 1.56 eV. These bands are explained as optical transitions between the Σ_u ground state in a molecular (halogen)$_2$ model (i.e., the Σ_u linear combination of the two adjacent halogen p

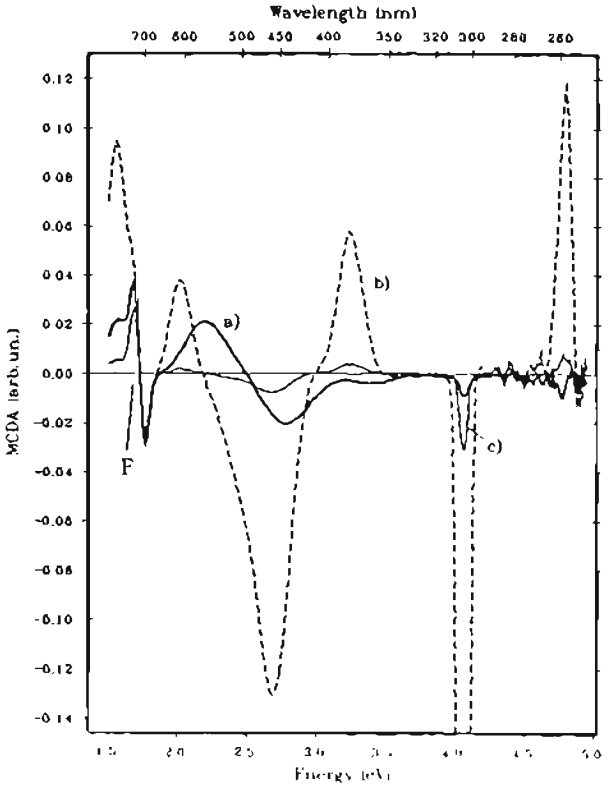

FIG. 2. MCDA spectra of RbI:Tl$^+$, measured at $T=4.2$ K and $B=2$T. (a) immediately after x irradiation at $T=80$ K, (b) after subsequent heating up to $T=150$ K, and (c) after subsequent heating to $T=220$ K.

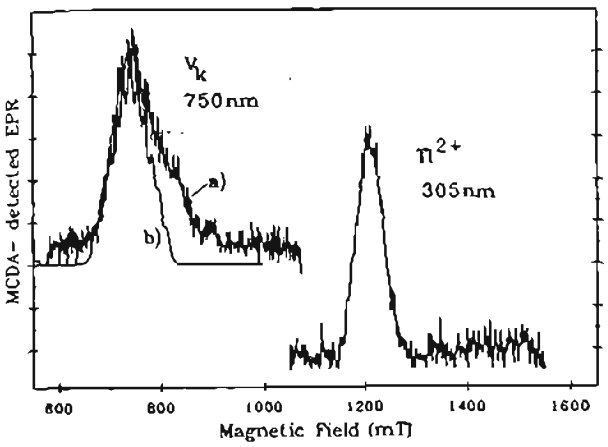

FIG. 3. MCDA-EPR spectra of V_K centers (measured at 1.56 eV) and Tl^{2+} centers (measured at 4.07 eV) in RbI:Tl^+ (T=1.5 K, microwave frequency 23.7 GHz). The simulation of the MCDA-EPR spectrum (left part, curve b) of the "perpendicular" V_K centers used parameters taken from Ref. 16. As a half-width of the individual hyperfine EPR lines 10 mT was assumed.

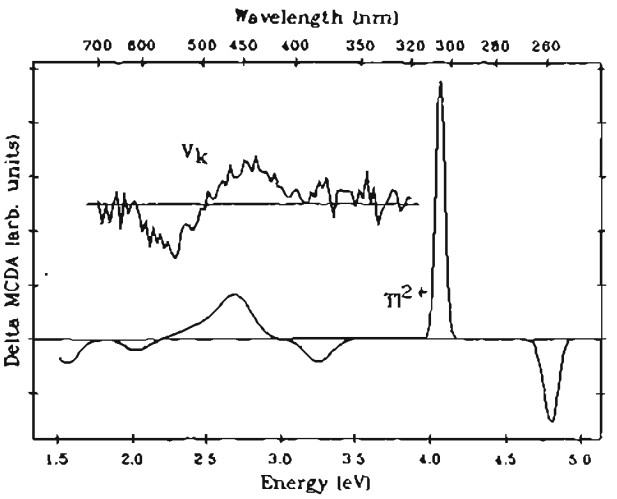

FIG. 4. "Tagged" MCDA spectra of the V_K and Tl^{2+} centers in RbI:Tl^+ (T=1.5 K, microwave frequency 23.7 GHz). The low energy V_K transition at 1.56 eV was not measured.

orbitals) and the corresponding Σ_g (UV transition) and Π_g states.[14] In the MCDA we find two bands of V_K centers: one with derivative structure, centered at 2.50 eV and a second one at 1.56 eV, which coincides with the peak position of the $\Sigma_u \rightarrow \Pi_g$ transition of V_K centers. The band at 2.5 eV is redshifted compared to the UV transition $\Sigma_u \rightarrow \Sigma_g$. It is attributed to the parity forbidden $\Sigma_u \rightarrow \Pi_u$ transition. For a justification of this attribution of the 2.5 eV band see Ref. 15. The assignments of the two bands to V_K centers are confirmed by the MCDA-EPR spectrum of the V_K centers detected in both bands. The EPR spectrum of V_K centers is also explained in the (halogen)$_2$-molecular model: The hole interacts with two equivalent halogen nuclei yielding a hyperfine (hf) split EPR spectrum. In case of RbI, there are 11 hf lines per center orientation. For the magnetic field parallel to the molecular ⟨110⟩ axis, the hf splitting is largest, for the field perpendicular to the axis it is smallest. If the field is parallel to [100], one measures V_K centers with their axes parallel, perpendicular, and under 45° with respect to the field orientation. In conventional EPR, all center orientations are measured.[16] However, in MCDA-EPR only those V_K centers having their axes perpendicular and under 45° with respect to the field orientation are detectable, as was explained in detail in Ref. 17. In Fig. 3, the MCDA-EPR spectrum measured at 1.56 eV and for the field parallel to [100] is shown of those V_K centers that have their axes perpendicular to the magnetic field (90° centers). The calculated spectrum using the EPR parameters of Ref. 16 agrees very well with the low field part of the experimental spectrum. In the high field flank of the line, centers having their axes at 45° to the magnetic field appear superimposed. The excitation spectrum of the MCDA-EPR ("tagged MCDA," see Ref. 12) confirms that the band at 2.50 eV indeed belongs to the V_K centers (see Fig. 4).

A comparatively weak MCDA band is observed at 4.07 eV. The MCDA-EPR spectrum measured in it shows a peak at a relatively high magnetic field, which is significantly higher than expected for the g factor g=2. The MCDA-EPR spectrum is isotropic. It can be identified as a resonance from the Tl^{2+} center, transition (F=1, m_F=−1)↔(F=1, m_F=0) in analogy to what is known from KCl, RbCl, and KBr.[18,19] For the assignment we proceeded as follows: from the alkali chlorides it is known from conventional EPR that the g factor is g=2.01 (Refs. 18 and 19) and the Tl hf interaction A~110 GHz. In KBr g=2.07 (Ref. 19) and A=95 GHz. Following this trend, we have assumed for RbI g=2.1 and obtained with this g value A=50 GHz. This hf interaction may be uncertain to ±≈8 GHz depending on the choice of the correct g value. The slight difference between the hf splitting of two magnetic isotopes ^{203}Tl and ^{205}Tl as well as superhyperfine interactions with the neighbor iodine nuclei cannot be resolved in the MCDA-EPR spectra. Unfortunately, we were not able to measure the second resonance from the (F=1, m_F=0)↔(F=1, m_F=1) transition in the K band because it lies at magnetic fields above the range of our spectrometer (≤3.5 T). Therefore, we had to proceed as described above for the identification.

After annealing to 150 K (step b), the MCDA spectrum changes in intensity and new bands appear as shown in Fig. 2, curve b. The negative part of the MCDA of the F centers remains unchanged as expected from the absorption spectrum. However, a complicated series of additional strong MCDA bands appears in the whole spectral region. The MCDA-EPR spectra obtained in all new bands are identical to the Tl^{2+} MCDA-EPR spectrum shown in Fig. 3. We have to conclude that all the new or increased bands belong to the Tl^{2+} center. This becomes even more obvious in the "tagged MCDA" of the Tl^{2+} centers (Fig. 4).

However, when "tagging" the resonance of the V_K center, there is no MCDA response showing that the V_K centers have disappeared. Similarly, it was observed that the V_K centers, which could easily be measured with conventional EPR after step a, could not be detected any more after annealing to 150 K. No other MCDA bands could be measured. In particular, no MCDA due to Tl^0 centers could be identified.

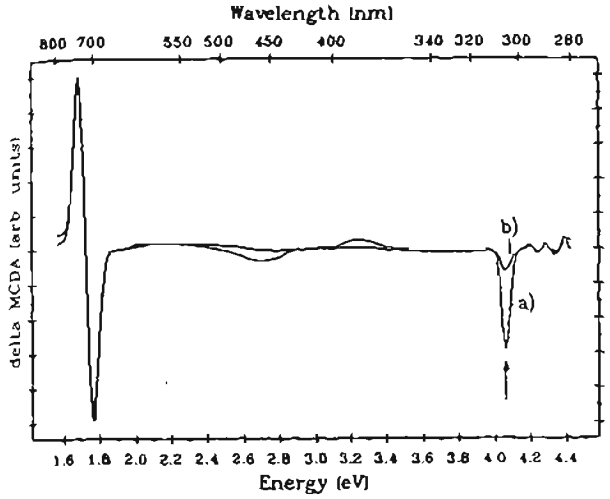

FIG. 5. MCDA spectra of RbI:Tl$^+$ (measurement temperature 1.8 K) (a) after x irradiation at 80 K and annealing to 220 K and (b) after bleaching at 4.07 eV.

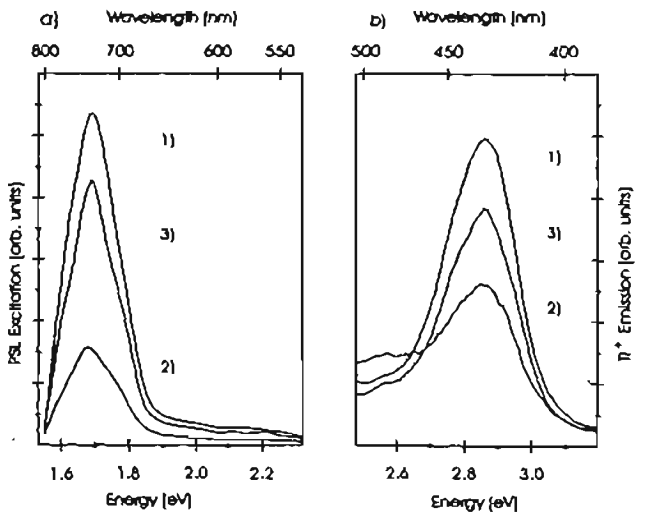

FIG. 6. Tl$^+$ emission (b) excited at 4.07 eV and the PSL excitation spectrum (a) measured at 80 K. Curves (1) after x irradiation and annealing to $T=220$ K, (2) after optical bleaching at 4.07 eV, and (3) after annealing to $T=150$ K.

In Fig. 2(c), the MCDA spectrum after the last heating step c to 220 K is shown. While the MCDA of the F centers does not change, the MCDA bands of the Tl^{2+} centers are reduced by a factor of 15. Again, no other centers contributing to the MCDA could be found.

8. Optical bleaching

1. *F band bleaching*

X-ray storage phosphors are normally used at room temperature. However, in RbI:Tl$^+$ at 300 K the PSL is stable only for a short time of the order of a few minutes. We simulated a room temperature irradiation by performing the x-ray irradiation at $T=80$ K and, subsequently, annealed the sample to 220 K, which destroyed the Tl^0 centers.

By bleaching in the F band at 4.2 K, one observes a relatively weak reduction of the F center MCDA and significant changes in all MCDA bands of the Tl^{2+} centers. By further bleaching of the F band, the Tl^{2+} centers can be completely destroyed. Concurrently, it is observed that upon F band bleaching the PSL intensity decreases with time, also at low temperature. After complete destruction of the Tl^{2+} centers, no PSL is observable any more.

2. *Tl^{2+} bleaching*

When exciting any of the Tl^{2+} bands, we found no emission of Tl^{2+} centers. Surprisingly, we found only a single emission band identical within experimental error with the Tl$^+$ emission peaking at 2.86 eV [Fig. 6(b), curve 1]. This emission fades as a function of excitation time as shown in Fig. 7. This observation suggests that the Tl^{2+} centers are unstable under irradiation into their absorption bands.

In Fig. 5, the effect of the optical bleaching in the 4.07 eV MCDA band of the Tl^{2+} centers is shown. All Tl^{2+} related bands are reduced, whereas the MCDA of the F centers stays constant. The same effect occurs for all Tl^{2+} center bands. We have compared the relative bleaching efficiencies of different Tl^{2+} bands both with respect to the effect on their MCDA bands and on their emission. The relative bleaching efficiencies are the same. The MCDA band at 2.35 eV shows the highest bleaching efficiency. Only in the 4.82 eV band (not shown in Fig. 5), we observe a bleaching effect with a relative efficiency significantly lower than in the other MCDA bands.

Parallel to the reduction of the Tl^{2+} center concentration, the PSL intensity is reduced [compare the PSL intensity marked by a in Fig. 7 with that obtained after bleaching Tl^{2+} centers marked by c].

The observation of a Tl$^+$ center emission upon exciting Tl^{2+} centers suggests that the excitation results in a charge transfer process, in which a hole must have been released to the lattice. The nature of that hole turned out to be a self-trapped hole, i.e., a V_K center. This is shown in the reappear-

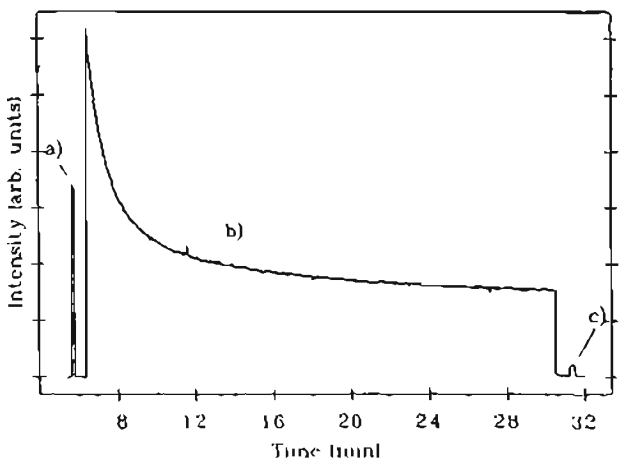

FIG. 7. Tl$^+$ emission at 2.8 eV. (a) The starting level of the PSL (excited in the F band at 1.7 eV, detected at 2.86 eV), (b) the kinetics of the Tl$^+$ emission excited in Tl^{2+} at 4.07 eV and detected at 2.86 eV during the continuous bleaching, and (c) the final level of the PSL, excited after the bleaching process of the Tl^{2+} centers.

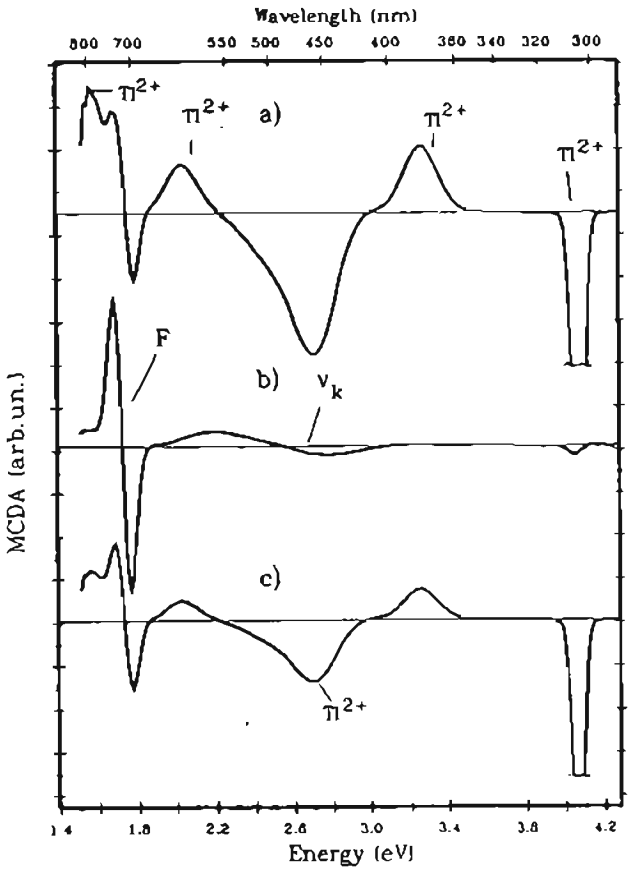

FIG. 8. MCDA spectra of the RbI:Tl^+ crystal, measured at $T=4.2$ K and $B=2$ T after x irradiation at $T=80$ K, (a) after heating to $T=150$ K, (b) after optical (4.07 eV) bleaching at $T=4.2$ K (enlarged by a factor of 2 compared to (a) and (c), and (c) after repeated heating to $T=150$ K.

ance of the MCDA of the V_K centers (Fig. 8) and in the conventional EPR measurement, not shown here.

In Fig. 8, curve a, the MCDA after x irradiation at 80 K and heating to 150 K is shown. Apart from F centers, there are prominent Tl^{2+} bands. Then, the MCDA of Tl^{2+} at 4.07 eV was bleached almost completely. This MCDA band of the Tl^{2+} centers has no overlap with the absorption bands of the Tl^0 centers. After this treatment, shown in Fig. 8(b), we observed the appearance of the MCDA of V_K centers.

After a similar treatment, also the conventional EPR spectrum of V_K centers could be observed. V_K centers cannot be produced by 4.07 eV bleaching in a sample that has not been x irradiated before. Obviously, the formation of V_K is connected with the bleaching of Tl^{2+} centers. Subsequent annealing to 150 K (Fig. 8, curve c) destroys the V_K centers again and a large portion of the Tl^{2+} centers is recovered.

The same treatment steps show that a reduction of the PSL and of the Tl^+ emission, due to the bleaching of Tl^{2+} bands, can both be recovered by thermal annealing above the thermal decay temperature of the V_K centers (Fig. 6). Moreover, we can observe during thermal annealing the thermoluminescence that is typical for a recombination of V_K centers.

A more detailed analysis of the Tl^{2+} bleaching in various bands and its recovery observed in the MCDA bands and the Tl^+ emission and a comparison with the PSL signal shows a clear correlation between the Tl^{2+} concentration and PSL intensity.

When bleaching Tl^{2+} in the 4.07 eV band, 95% of the Tl^{2+} centers could be recovered by annealing above the V_K stability temperature. Thus, the conclusion is that the V_K centers, generated in this way, are spatially correlated to the Tl^{2+} centers. When performing an analogous experiment by bleaching the 2.2 eV band, only 65% of the Tl^{2+} centers can then be recovered. This may be explained by a simultaneous F center ionization in higher F center transitions (K band) at that energy, which would cause an irreversible Tl^{2+} recombination.

3. Replenishment effect

When x irradiating the RbI:Tl^+ samples at room temperature and bleaching in the F band to create the PSL effect immediately afterwards at low temperature (10 K), one can exhaust the PSL effect completely by bleaching long enough into the F band. After subsequent warming, one cannot recover any PSL effect any more. In contrast to other phosphors, such as BaFBr:Eu^{2+}, there is no replenishment effect in RbI:Tl^+. The same result is obtained when x irradiating at somewhat lower temperature, e.g., 220 K.

IV. DISCUSSION

As a mechanism for the information storage in RbI:Tl^+, it was proposed by Thoms *et al.* that upon x irradiation V_{KA} (Tl^+) centers are formed as electron and hole trap centers.[11] It was speculated that the V_{KA} centers were V_K centers stabilized near or at Tl^+ activators. However, no direct spectroscopic evidence could be given by Thoms *et al.* for the existence of V_{KA} (Tl^+) centers.[11] We have not found the existence of any V_{KA} centers. Since we observed V_K centers, both with MCDA-EPR and conventional EPR, we should have seen V_{KA} centers, had they been present. From our measurements it follows that Tl^{2+} centers are formed and that these centers act as those hole trap centers that control the PSL. From the MCDA observation we know that upon F center bleaching the PSL intensity increases or decreases with the Tl^{2+} center concentration, independently of the way in which the Tl^{2+} concentration was varied. We, therefore, propose that in RbI:Tl^+ a simple pair mechanism operates, in which the pair F center–Tl^{2+} center is the electron-hole pair storing the information and that recombines upon photoexcitation of the F center electron to produce the photostimulated luminescence directly as a luminescence from the excited Tl^+ state into its ground state. In accordance with the proposed model, we failed to observe a replenishment effect. Probably, there is a certain spatial correlation between F centers and Tl^{2+} centers about which we do not know any details yet. Our results confirm in a sense the model suggested previously by von Seggern *et al.*,[5] Eachus *et al.*,[4] and Koschnick *et al.*[3] for BaFBr:Eu^{2+} that there exists no single pair mechanism. It was thought that an aggregate of electron and hole trap centers and the activator are responsible for the PSL and information storage. From the observed replenish-

ment effect,[7] it was concluded that the formation of new such aggregates can occur with thermal activation after exhaustion of the PSL at low temperature.

With our MCDA measurements and tagged MCDA-EPR experiments we have identified seven absorption bands of Tl^{2+} centers. Since the bleaching in all bands produces V_K centers, i.e., hole centers, we conclude that all bands measured have charge transfer character. As summarized by Nistor *et al.*,[20] according to Moreno,[21] there should be two high-energy transitions from the Tl^{2+} 6s (a_{1g}) electron to the $^2P_{1/2}$ and $^2P_{3/2}$ spin-orbit split excited states and, in addition, two charge transfer transitions from the Tl^{2+} 6s (a_{1g}) state to $t_{1u}(\pi)$ and $t_{1u}(\sigma)$ linear combination of halogen orbitals of the I ligands. Our observations, however, are not explained with this scheme. The two high-energy transitions at 4.0 and at 4.85 eV have also charge transfer character, since they can be bleached with the creation of V_K centers. Furthermore, we have observed more than just two charge transfer transitions: altogether five. It is at present an open question how to explain these optical transitions of the Tl^{2+} centers. For the low-energy charge transfer transitions, possibly a suggestion made by Osminin *et al.*,[22] assuming also charge transfer transitions to second and higher shell halogen neighbors, may be true. Further theoretical work is needed. The charge transfer process apparently leads to a localized hole in the halogen neighborhood with a spatial correlation to Tl^+ centers. Otherwise, the high proportion of recovery of Tl^{2+} upon thermal mobilization of V_K centers would not be understood.

In conclusion, we have shown that in RbI:Tl^+, a simple pair mechanism of F center–Tl^{2+} center explains the information storage and read-out process. It seems that this is the only x-ray storage phosphor at present for which the mechanism is understood and for which, in particular, the hole center has been identified. Tl^{2+} absorption bands all seem to have charge transfer character and further work is needed to understand the observed spectra.

[1] G. Blasse, J. Alloys Compd. **192**, 17 (1993).
[2] J.-M. Spaeth, Th. Hangleiter, F.-K. Koschnick, and Th. Pawlik, Radiat. Eff. Defects Solids **135**, 499 (1995).
[3] F.-K. Koschnick, J.-M. Spaeth, R. S. Eachus, W. G. McDugle, and R. H. D. Nuttal, Phys. Rev. Lett. **67**, 357 (1991).
[4] R. S. Eachus, W. G. McDugle, R. H. D. Nuttal, M. T. Olm, F. K. Koschnick, and J.-M. Spaeth, J. Phys. Condens. Matter **3**, 9327, 9339 (1991).
[5] H. von Seggern, T. Voigt, W. Knüpfer, and G. Langer, J. Appl. Phys. **64**, 1405 (1988).
[6] Iwabuchi, N. Mori, K. Takahashi, T. Matsuda, and S. Shionoya, Jpn. J. Appl. Phys. **33**, 178 (1994).
[7] Th. Hangleiter, F.-K. Koschnick, J.-M. Spaeth, R. H. D. Nuttal, and R. S. Eachus, J. Phys. Condens. Matter **2**, 6837 (1990).
[8] Th. Hangleiter, F.-K. Koschnick, J.-M. Spaeth, and R. S. Eachus, J. Radiat. Eff. Defects Solids **11**, 615 (1991).
[9] P. F. Braslavets, A. Kalnins, I. Plavina, A. I. Popov, B. I. Rapoport, and A. Tale, Phys. Status Solidi B **170**, 395 (1992).
[10] U. Rogulis, I. Tale, Th. Hangleiter, and J.-M. Spaeth, J. Phys. Condens. Matter **7**, 3129 (1995).
[11] Thoms, H. von Seggern, and A. Winnacker, J. Appl. Phys. **76**, 1800 (1994).
[12] J.-M. Spaeth, J. R. Niklas, and B. H. Bartram, *Structural Analysis of Point Defects in Solids*, Springer Series in Solid State Sciences 43 (Springer, Berlin, 1992).
[13] C. J. Delbecq, A. K. Ghosh, and P. H. Yuster, Phys. Rev. **151**, 599 (1966).
[14] R. B. Murray and F. J. Keller, Phys. Rev. **153**, 993 (1967).
[15] U. Rogulis, K. S. Song, and J.-M. Spaeth, J. Phys. Condens. Matter **7**, 7699 (1995).
[16] D. Schoemaker, Phys. Rev. B **7**, 786 (1973).
[17] J.-M. Spaeth, W. Meise, and K. S. Song, J. Phys. Condens. Matter **6**, 1801 (1994).
[18] W. Dreybrodt and D. Silber, Phys. Status Solidi **20**, 337 (1967).
[19] W. Frey, R. Huss, H. Seidel, and E. Werkmann, Phys. Status Solidi **68**, 257 (1975).
[20] S. V. Nistor, D. Schoemaker, and I. Ursu, Phys. Status Solidi B **185**, 9 (1994).
[21] M. Moreno, J. Phys. C **12**, L921 (1979).
[22] V. S. Osminin, G. S. Zavt, S. G. Zazubovich, and A. I. Niilisk, Izv. Akad. Nauk SSSR, Ser. Fiz. **38**, 1235 (1974).

Radiation Effects and Defects in Solids, 1995, Vol. 134, pp. 471–475
Reprints available directly from the publisher
Photocopying permitted by license only

ODEPR OF INDIUM COLOUR CENTRES IN THE X- IRRADIATED STORAGE PHOSPHOR KBr:In

U. ROGULIS, J.-M. SPAETH,* I. TALE, E. RUZA

Inst. of Solid State Physics, University of Latvia, 8 Kengaraga str., LV1063, Riga, Latvia;
** Universität-GH Paderborn, FB Physik, Postfach 1621, D–33095, Paderborn, Germany*

The results of measurements of the magnetic circular dichroism of the optical absorption (MCDA) and optically detected electron paramagnetic resonance (ODEPR) of X-irradiated KBr:In crystals are presented. The MCDA bands and ODEPR parameters of In°(1) centers and In^{2+} centres have been measured. The mechanism of the energy storage in KBr:In crystals is found not to be simply the formation of correlated F centre-In^{2+} centre pairs as was assumed previously. Considerable similarities to the storage phosphor BaFBr:Eu^{2+} were found for the photostimulated emission and read-out properties.

Key words: X-ray storage phosphor, In centres, paramagnetic resonance.

1 INTRODUCTION

Materials to produce X-ray storage phosphors have attracted much interest recently because of their higher sensitivity compared to X-ray films and because of the possibility to create digitized X-ray images. There is a search for new materials besides the well-known system BaFBr:Eu^{2+}. Recently it has been shown that KBr:In has an X-ray storage efficiency comparable to that of BaFBr:Eu^{2+} [1].

On the basis of recent extensive studies of optical absorption in the visible and near UV region and of optically and thermally stimulated recombination luminescence it was proposed that X-ray energy storage in KBr:In crystals is mainly due to the formation of close F center-In^{2+} centre pairs [2]. The question is, however, whether upon X-irradiation of KBr:In indeed spatially correlated F centre-In^{2+} centre pairs are formed and if so, whether only correlated pairs are generated.

According to recent investigations with optically detected electron paramagnetic resonance (ODEPR) the X-ray energy storage in BaFBr:Eu^{2+} is indeed based on aggregates involving F centres as electron trap centres, spatially correlated both to O_F^-- and Eu^{2+} centres [3,4].

Therefore an investigation of the radiation damage centres in KBr:In was undertaken using magneto-optical and optically detected electron paramagnetic resonance techniques. We show that indeed In^{2+} centres are formed, but that the mechanism for energy storage and read-out is more complicated than assumed by Plavina *et al.* [2] with the simple idea of correlated In^{2+}-F centre pairs.

2 EXPERIMENTAL RESULTS AND DISCUSSION

KBr:In ($1 - 5 \times 10^{17}$ cm^{-3}) crystals were X- irradiated at RT with a dose of 10^3 Gy. The magnetic circular dichroism of the absorption (MCDA) at 1.5 K (Figure 1) exhibits several bands in the UV and IR in addition to the strong MCDA of F-centres (derivative structure, transition through zero at 2.06 eV).

An ODEPR spectrum similar to that found for In°(1) centres in KCl:In crystals is obtained [5]. The ODEPR spectrum of the In°(1) centres in KBr:In is shown in Figure 2.

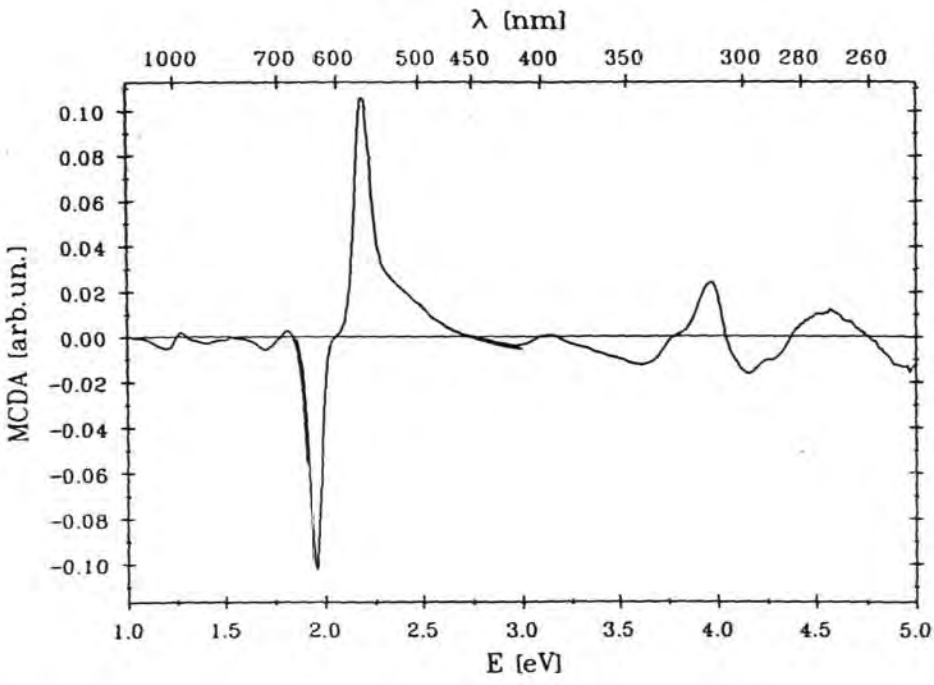

FIGURE 1 MCDA spectrum of a KBr:In crystal X-irradiated at room temperature, measured at T = 1.5 K, B = 2 T.

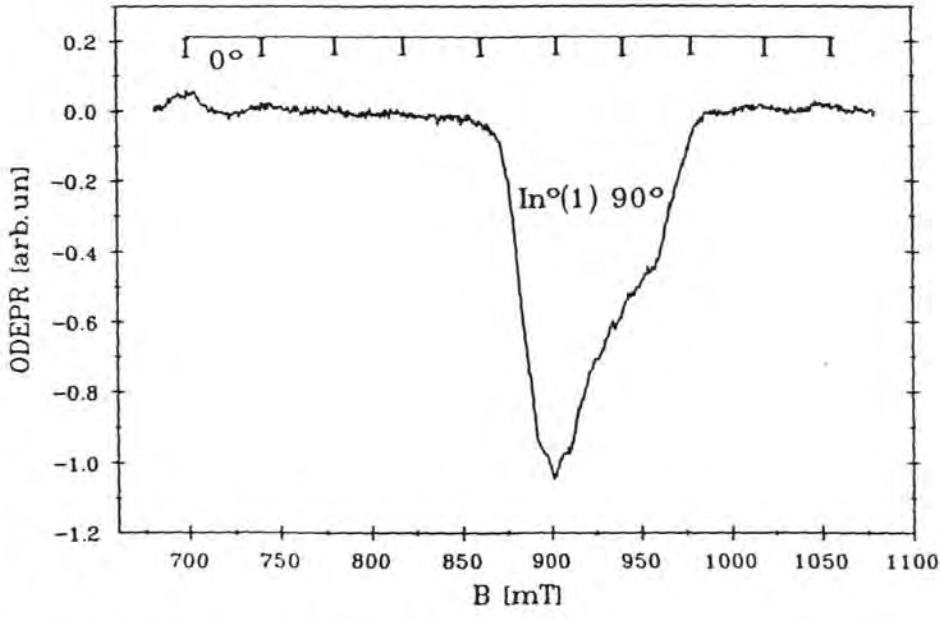

FIGURE 2 ODEPR spectrum of In°(1) centres in KBr measured as microwave-induced change of the MCDA spectrum of Figure I at λ = 1015 nm.
For $B_0 \parallel [100]$ (microwave frequency 24.21 GHz, T = 1.5 K) In°(1) centres were produced by X-irradiation at room temperature. The bars indicate the HF structure for parallel centres ($I_{In} = 9/2$), the strong line is due to perpendicular centres.

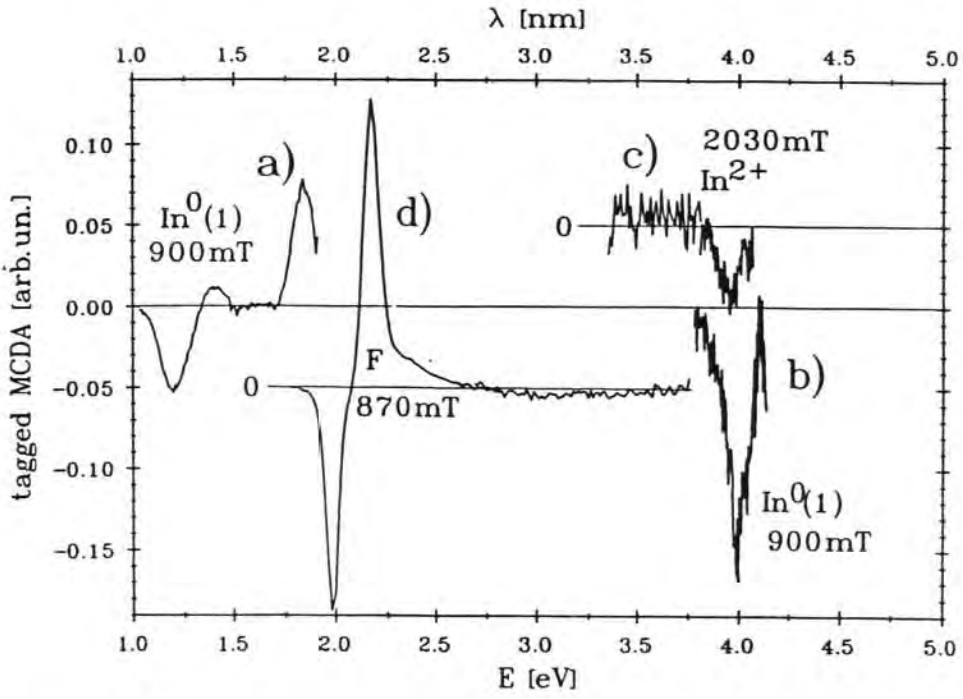

FIGURE 3 Tagged MCDA spectra of In°(1) centres (curves a and b, measured at 900 mT), F centres (curve d, measured at 870 mT) and In^{2+} centres (curve c), measured at 2030 mT) in KBr after X-irradiation at room temperature.

The values of the EPR parameters are as follows: $g_{\parallel} = 1.97 \pm 0.02$; In-hyperfine (HF) splitting constant $A_{\parallel} = (40 \pm 2)$ mT; $g_{\perp} = 1.88 \pm 0.02$; $A_{\perp} = (8 \pm 1)$ mT; $P = (-0.2 \pm 0.05)$ mT. The MCDA bands of In°(1) centres are located at 3.99 eV and 1.85 eV, 1.4 eV and 1.2 eV. They were determined by measuring the 'tagged' MCDA (see e.g. [6]). The 'tagged' MCDA spectrum (i.e. the excitation spectrum of the In°(1) ODEPR lines) is shown in Figure 3, curves a and b.

In the UV region several MCDA bands appear. The ODEPR line (Figure 4, curves a and b), detected in the 3.95 eV MCDA band, is located at 2040 mT. From the Breit-Rabi calculation (Figure 4, upper part c) this line is attributed to In^{2+} hole centres with an In-HF splitting constant of A = 13.2 ± 0.1 (GHz), g ~ 2. Only one EPR transition could be recorded with our microwave frequency of about 24 GHz. A hole is trapped on an In^{+}-ion on the cation site. A superhyperfine splitting from bromine nuclei could not be resolved in the weak EPR line. The 'tagged' MCDA spectrum in the UV region contains a MCDA band located at 3.95 eV which overlaps the MCDA band for In°(1) centres at 3.99 eV (halfwidth for both MCDA bands is above 0.1 eV) (see Figure 3, curves b and c).

Because of the strong overlap of the MCDA bands of both the In^{2+} and the In°(1) centres, both ODEPR signals are present simultaneously. However, up to now we have not observed any cross relaxation effects in the ODEPR spectra caused by an interaction between In^{2+} and In°(1) nor between In^{2+} and F centres.

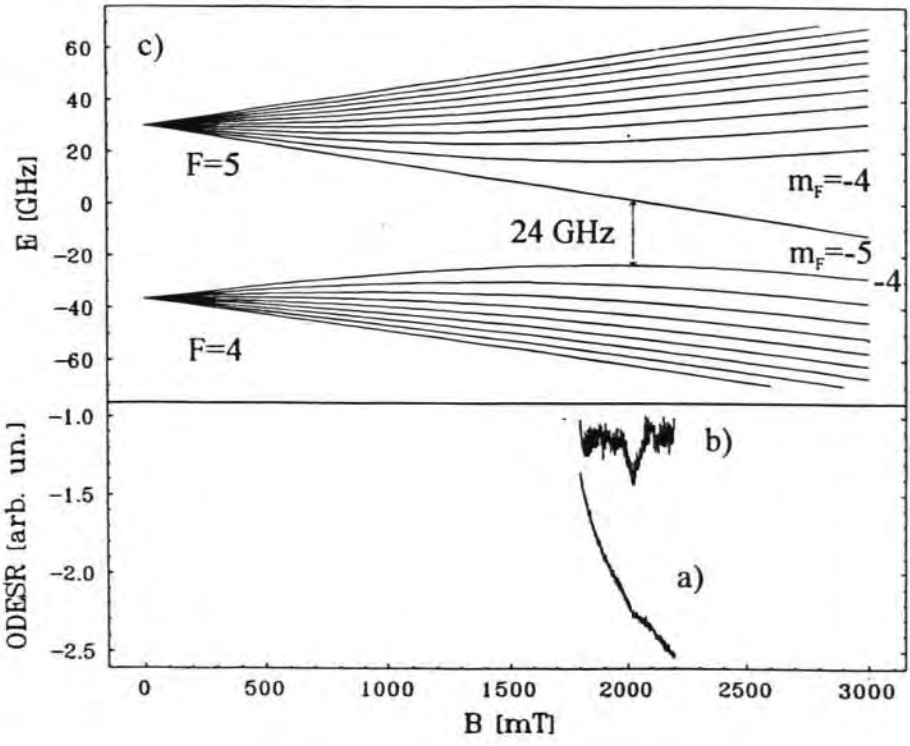

FIGURE 4 ODEPR spectrum of In^{2+} centres in KBr:In X-irradiated at room temperature (curve a: as measured, curve b: without MCDA background) The upper part c) represents the calculated Breit-Rabi diagram for the In^{2+} centres.

Such cross relaxation effects had been observed in the ODEPR spectra of F centres and Eu^{2+} centres in $BaFBr:Eu^{2+}$ and gave direct experimental evidence for a spatial correlation between the radiation-induced F centres and the activator Eu^{2+} [4].

We have carried out preliminary experiments on the bleaching of F centres using the light of a He-Ne laser at RT as well as at low temperatures. These experiments show that the mechanism of the energy storage in KBr:In crystals is considerably more complicated than described by the assumption that only the F centre-In^{2+} centre pairs are formed and recombine during the read-out process. After exhaustion of the photostimulated emission at low temperature, only a fraction of the F centres is bleached, and very few In^{2+} centres have disappeared. Also the In°(1) centres remain.

Similarily to the observations in $BaFBr:Eu^{2+}$ crystals [7], also in the KBr:In crystals the photostimulated luminescence can be exhausted by low temperature (4 K) read-out with the light of the He-Ne laser, and then be restored again partially by warming up to RT in the dark (so-called replenishment effect [7]).

Thus it may be speculated that similarily as in the case of $BaFBr:Eu^{2+}$ there are aggregates of F centres, In+ centres and an unknown hole centre which leads to the photostimulated luminescence, if F centres are excited and recombine with the hole centres, upon which process the In^{+} is excited and emits the observed In^{+}-related luminescence

[1,2]. According to our results it seems unlikely that the dominating process is that of an F centres-In^{2+} center recombination, as was assumed by Plavina *et al.* [2].

According to a recent report [8], the spectrum of the excitation of the photostimulated luminescence significantly differs from the absorption band of the F centres and includes additionally a long wavelength region, where the absorption band of the In°(1) centres occurs.

The role of In°(1) centres is at present not clear. Since they are also electron trap centres, they may be excited similarily as F centres for a read-out process.

REFERENCES

1. A. Kalnins, I. Plavina, L. Trinklere, M. Trinklere, *Proc. of the LUMDETR'91*, Rìga, **E18** (1991).
2. I. Plavina, I. Tale, A. Tale, *Proc. of the LUMDETR'91*, Rìga, **D4** (1991).
3. R. S. Eachus, F. K. Koschnick, J.-M. Spaeth, R. H. D. Nuttall, M. T. Olm, W. G. McDugle. *Proc. of the ICDIM'92*, World Scientific, **1**, 267 (1993).
4. F. K. Koschnick, J. M. Spaeth, R. S. Eachus, W. G. Mc Dugle and R. H. D. Nuttall, *Phys. Rev. Letters* **67**, 3571 (1991).
5. F. J. Ahlers, F. Lohse, Th. Hangleiter, J. M. Spaeth and R. H. Bartram, *J. Phys.: Solid State Physics*, **17**, 4877 (1984).
6. J. M. Spaeth, J. R. Niklas, R. H. Bartram, *Structural Analysis of Point Defects in Solids* (Springer Series of Solid State Sciences 43) (1992).
7. T. Hangleiter, F. K. Koschnick, J.-M. Spaeth, R. H. D. Nuttall and R. S. Eachus, *J. Phys. C: Cond. Matter*, **2**, 6837 (1990).
8. I. Tale, V. Tale, P. Kulis, M. Springis and A. Veispals *Proc. of the ICDIM'92*, World Scientific, **2**, 1262 (1993).

J. Phys.: Condens. Matter 7 (1995) 3129–3137. Printed in the UK

The photostimulation process in the x-ray storage phosphor KBr:In

U Rogulis†, I Tale†, Th Hangleiter‡ and J-M Spaeth‡

† Institute of Solid State Physics, University of Latvia, 8 Kengaragh Street, LV-1063 Riga, Latvia

‡ Fachbereich Physik, Universität-GH Paderborn, D-33095 Paderborn, Germany

Received 5 December 1994, in final form 1 February 1995

Abstract. The nature of the radiation damage centres generated by x-irradiation at 300 K, 100 K and 10 K and the photostimulation process are investigated in KBr:In. Measurements of the optical absorption, the magnetic circular dichroism of the optical absorption (MCDA) and the MCDA-detected electron paramagnetic resonance, as well as of the photostimulated In^+ emission, are utilized. At room temperature, F centres, In^{2+} centres and $In^0(1)$ centres are generated. In^{2+} centres are not produced at low temperature and therefore are not primary hole defects. It is shown that the photostimulation process does not occur within F–In^{2+} centre pairs, as previously proposed. It involves an aggregate between F centres, In^+ centres and an unknown, room-temperature-stable hole centre. The photostimulation process, including replenishment effects, seems very similar to the one found earlier for the well known x-ray storage phosphor BaFBr:Eu^{2+}.

1. Introduction

X-ray storage phosphors are materials capable of storing images produced by the absorption of x-radiation. During image formation, radiation-induced defects are formed. It is generally believed that room-temperature-stable electron and hole trap centres are involved in the image formation. For the read-out process, usually the electron trap centres are photoexcited, and the luminescence of a doped activator is recorded. The x-ray storage phosphors can offer a number of advantages compared to conventional x-ray films: high sensitivity and a higher dynamical range (10^4–10^5) as well as the possibility of directly obtaining digitized x-ray images. Therefore, there is much interest in finding suitable systems. Several systems have been proposed (for a concise recent review, see Blasse 1993). The best known x-ray storage phosphor is BaFBr:Eu^{2+}, which is already used commercially (Sonoda *et al* 1983). In spite of many efforts to understand the mechanism of the information storage and read-out process, no complete understanding has yet been achieved (see, e.g., Blasse 1993, Spaeth *et al* 1994a). In particular, the nature of the room-temperature-stable hole centres is not clear, nor the mechanism of energy transfer to the activator after photostimulated F centre electrons have recombined with the hole centres (Spaeth *et al* 1994a and references therein). It was shown recently that in BaFBr:Eu^{2+} an apparently unavoidable oxygen contamination greatly influences the formation of electron trap centres and provides hole trapping defects (Koschnick *et al* 1991, Eachus *et al* 1991).

It has been shown recently that KBr doped with In also has x-ray storage phosphor properties, whereby the efficiency of this material is of the same order of magnitude as that of BaFBr:Eu^{2+} (Kalnins *et al* 1991). It was postulated on the basis of optical investigations

0953-8984/95/163129+09$19.50

that the x-ray energy storage is mainly due to the formation of F centre-In^{2+} centre pairs (Plavina *et al* 1991). If this were true, one would possibly have with KBr:In a simple model system to study the mechanism of the storage and read-out processes in detail.

It was the purpose of this investigation to use magneto-optical and optically detected electron paramagnetic resonance techniques to identify the nature of the radiation-induced defects in KBr:In and to study their role in the storage and read-out processes. The electron paramagnetic resonance (EPR) of the defects was measured via magnetic circular dichroism of the optical absorption (MCDA) (see e.g. Spaeth *et al* 1992) because with this method the high sensitivity necessary to detect the radiation damage centres was achieved as well as a correlation to their optical absorption bands. The development of the MCDA bands upon x-irradiation at various temperatures and their changes caused by the photostimulation process was studied.

It turned out that the postulation of In^{2+}–Fe centre pairs as electron hole trap centres for the energy storage in KBr:In was not correct and that the storage and read-out mechanism seems to be very similar to the one thought to be present in $BaFBr:Eu^{2+}$.

A preliminary but incomplete account of this work was presented elsewhere (Rogulis *et al* 1994).

2. Experimental details

The KBr:In single crystals were grown with the Bridgman–Stockbarger method. The KBr was treated prior to the crystal growth with NH_4 Br to minimize the oxygen contamination. The In doping level was $(1–2)\times10^{17}$ cm^{-3}. This was determined using the optical absorption with the In^+ oscillator strength (Smith and Dexter 1972).

X-irradiation was performed with a fine-structure tube with either 50 kV, 30 mA or 60 kV, 15 mA. The irradiation times were 0.5–2 h. The samples could be x-irradiated *in situ* in the spectrometer to measure the MCDA and MCDA-detected paramagnetic resonance at 4.2 K. In this irradiation the x-ray tube was further away from the sample compared to the room-temperature irradiation.

The photostimulation was performed with an He–Ne laser (5 mW) in the ODEPR apparatus, while in the optical spectrometer a combination of halogen lamp (150 W) and a double monochromator were used. The photostimulation time varied between 1 min (RT) and 15 min (low temperature). The optical absorption and emission spectra could be measured between 10 K and 300 K with a computer-controlled custom-built optical spectrometer, using a 0.25 Spex double monochromator and a phototube for the visible spectral range.

The MCDA, which is the differential absorption for right and left circularly polarized light, is proportional to the population difference of the Zeeman levels of the ground state of a paramagnetic defect. Upon saturating microwave transitions between the Zeeman levels it decreases, which can be used to detect the EPR of the ground state of the paramagnetic centre (see e.g. Spaeth *et al* 1992). This MCDA-detected EPR was used to identify the various paramagnetic radiation-induced defects. The MCDA, its excitation spectra ('tagged' MCDA) and MCDA-detected EPR were measured in a computer-controlled custom-built K band (24 GHz) MCDA–EPR spectrometer, usually at 1.5 K. For the infrared spectral range, a Ge detector (Northcoast) was used.

3. Experimental results

3.1. X-irradiation at room temperature

KBr:In crystals were irradiated with x-rays at room temperature for approximately 2 h, then

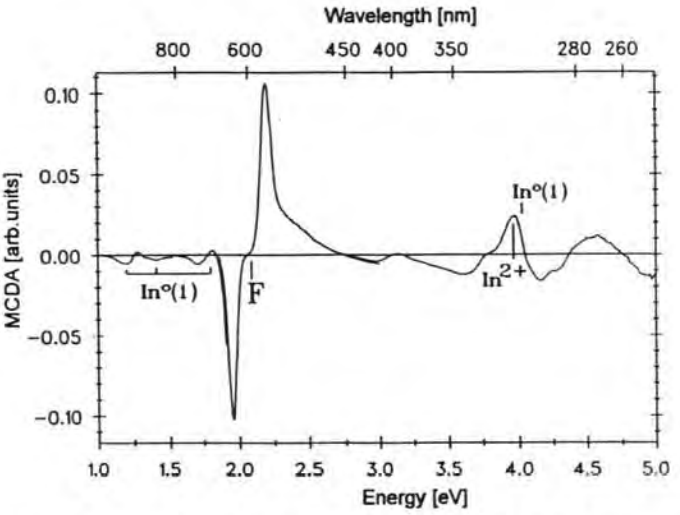

Figure 1. The MCDA spectrum of a KBr:In crystal x-irradiated at room temperature, measured at $T = 1.5$ K, $B = 2$ T. The MCDA bands of those paramagnetic defects identified by MCDA-detected EPR measurements are marked.

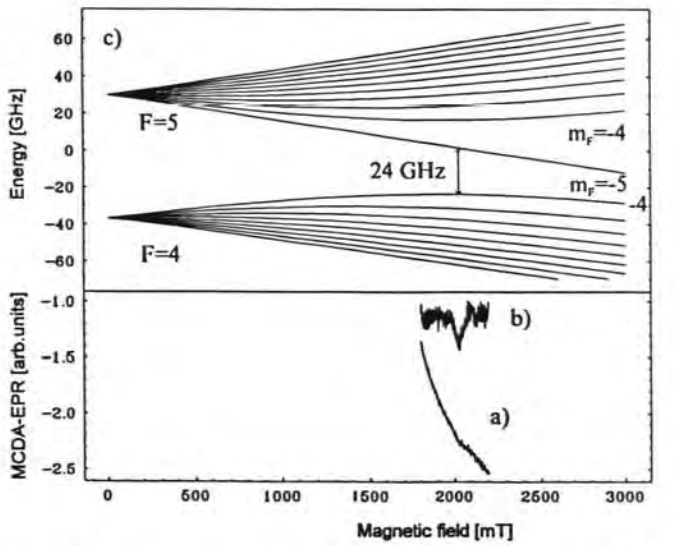

Figure 2. Lower part, EPR spectrum of In^{2+} centres in KBr:In measured as a microwave-induced change of the MCDA spectrum of figure 1 at 3.95 eV. $B_0 \parallel [100]$, $\nu_{ESR} = 24.21$ GHz, $T = 1.5$ K. Curve a, as measured; curve b, after subtraction of the MCDA background signal. Upper part, c, calculated Breit–Rabi diagram for the In^{2+} centre.

cooled to 1.5 K for magneto-optical measurements. Figure 1 shows the MCDA measured between 1.0 and 5.0 eV. The strongest MCDA band with a derivative-like structure centred at 2.06 eV is from F centres. The three bands at the low-energy side are due to $In^0(1)$ centres, i.e. In^0 atoms on cation sites next to a halogen vacancy (Ahlers *et al* 1984). The MCDA

bands at about 4.0 eV are due to a superposition of bands from $In^0(1)$ and In^{2+} centres as well as some unknown defects. Figure 2 (lower part) shows the MCDA-detected spectrum of In^{2+} centres measured at 3.95 eV. A weak EPR line is seen at 2040 mT. The spectrum is isotropic. In figure 2 (upper part) the Breit–Rabi diagram shows that only one EPR transition could be recorded with the microwave frequency of 24 GHz. The analysis yields that the In^{2+} hyperfine constant is $A = (13.2 \pm 1)$ GHz and $g = 2$. A hole is trapped at the In^+ ion and forms the paramagnetic In^{2+} ion, which has a $5s^1$ electron configuration (Rogulis *et al* 1994). In figure 3, the 'tagged' MCDA spectrum, which is an excitation spectrum of the MCDA-detected EPR line (see e.g. Spaeth *et al* 1992), shows that the In^{2+} MCDA band strongly overlaps one MCDA band of the $In^0(1)$ centres at 3.99 eV (figure 3, curves b and c). Thus, upon room-temperature x-irradiation, the electron traps $In^0(1)$ and F centres as well as the hole traps In^{2+} are produced. Apart from those MCDA bands identified by their MCDA-detected EPR spectra, there are other bands that are temperature dependent and therefore are caused by paramagnetic defects. The MCDA in the spectral range between 4.3 and 5.0 eV coincides with an absorption band associated with the V_2 centres, which are thought to be due to halogen di-interstitials (Ishii 1966). However, we could not observe any MCDA-detected EPR spectra. In the spectral range between 2.5 and 3.5 eV, the weak MCDA bands are also from paramagnetic centres. Their appearance depends on the crystal purity. In some crystals, a perturbed In^0 centre was identified ($In^0(X)$) with MCDA bands at 2.3 and 3.0 eV (to be published). In particular, we did not find the MCDA-detected EPR of O^- centres in spite of a careful search.

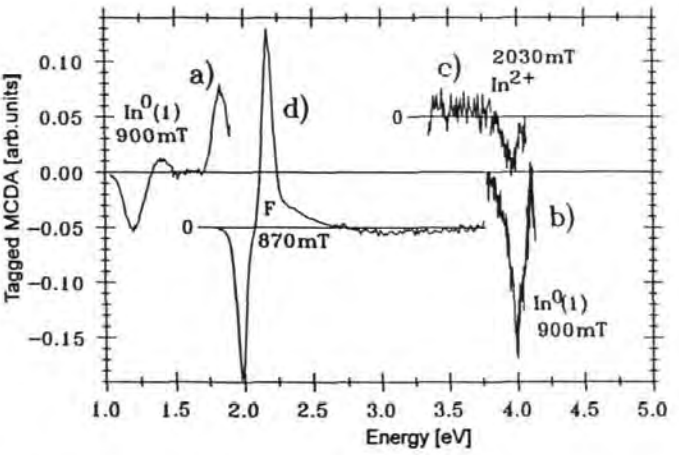

Figure 3. The tagged MCDA spectra of $In^0(1)$ centres (curves a and b, measured at 900 mT), F centres (curve d, measured at 870 mT) and In^{2+} centres (curve c, measured at 2030 mT) in KBr after x-irradiation at room temperature.

Upon photostimulation into the F band at room temperature, two luminescence bands of In^+ centres are observed around 2.9 eV and 2.4 eV (Kalnins *et al* 1991, Plavina *et al* 1991, Trinklere *et al* 1993, Fukuda 1970) (figure 4). The intensity of the photostimulated luminescence (PSL) bands cannot be compared with those measured at low temperature because of the fast decay of the PSL as shown in figure 5 (see below). After exhaustion of the PSL, the crystal was cooled to 1.5 K, and the MCDA was again measured. After a strong bleaching at room temperature all F centres have disappeared, as well as all In^{2+}

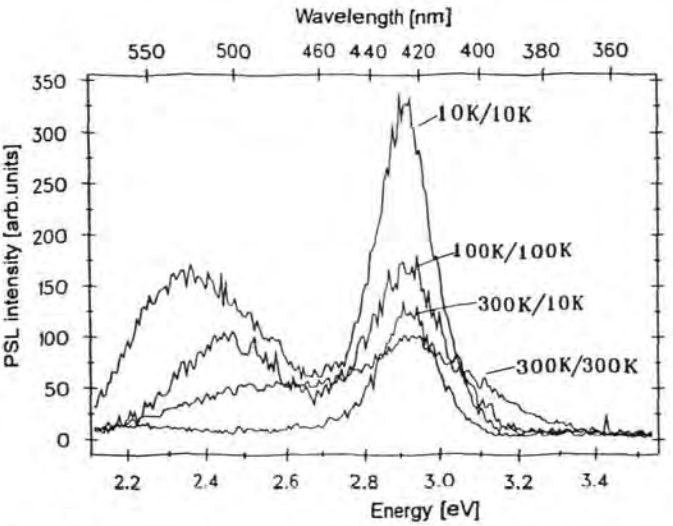

Figure 4. Photostimulation spectra of KBr:In after x-irradiation at 300 K, 100 K and 10 K (first temperature at curves) and measurement at 300 K, 100 K and 10 K (second temperature at curves). The photostimulation was performed at 604 nm with very weak light, such that only a very low loss of luminescence, i.e. of photostimulable centres, occurs during the measurement. For the low-temperature photoexcitation, the different luminescence intensities can be compared, because the conditions (exciting light intensity and decay times) are the same. For the room-temperature luminescence, the intensity is not comparable to the other ones because of the much faster decay that occurred during the measurement.

centres, whereas the $In^0(1)$ centres remained unchanged. If the bleaching is finished when over 95% of the PSL has occurred, then about one-third of the initial F centre band remains. The disappearance of the In^{2+} centres could lead to the conclusion that F centres and In^{2+} centres are the correlated electron–hole pairs responsible for the energy storage and photostimulation. However, as is seen from the following experiments, this is too simple a picture.

When x-irradiating a crystal at room temperature and subsequently cooling it down to 10 K, a photostimulation in the F band at 10 K also generates the In^+ luminescence band at 2.9 eV. At low temperature, only the band at 2.9 eV is observed (Fukuda 1970). The luminescence intensity is shown in figure 4 in comparison to that measured after low-temperature x-irradiation (see below). Its intensity is smaller than that found for low-temperature irradiation. Figure 5 shows the PSL intensity as a function of time for continuous bleaching. It is seen that, when exciting at room temperature, the PSL decays much faster than when exciting at 10 K. In contrast to the photostimulation at room temperature, only a small fraction of the F centres has disappeared. The MCDA of In^{2+} centres has not changed measurably, nor that of $In^0(1)$ centres. The MCDA between 4.3 and 5.0 eV does not change either. Thus, this MCDA is not from hole centres involved in the PSL process, and F centres and In^{2+} centres are not spatially correlated such that they can easily recombine at low temperature. However, the following experiments show that at higher temperatures dynamical effects are involved in the PSL mechanism. We have observed a replenishment effect similar to the effect observed previously in the storage phosphor BaFBr:Eu^{2+} by Hangleiter *et al* (1990, 1991).

After exhausting the PSL at 10 K, warming the crystal to room temperature and again cooling to 10 K, the crystal regained photostimulability. Again, the In^+ PSL can be generated

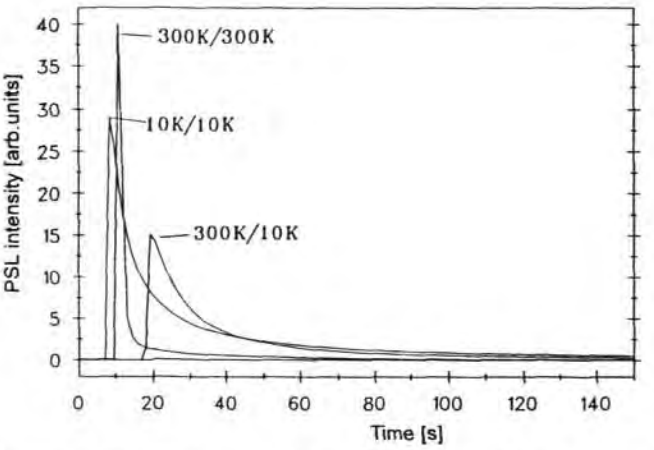

Figure 5. PSL measured at 2.9 eV as a function of time during continuous photoexcitation at 2.05 eV. Given by the curves are the x-irradiation temperature (the first temperature) and that of the PSL measurement (the second temperature). The three starting times of the measurements are shifted with respect to each other to enable a clearer presentation of the results.

by bleaching into the F band, although weaker compared to the first time. About one-third to one-half of the first PSL intensity could be observed again. Thus, a thermally activated process occurs, which, after exhaustion of the photostimulation centres, apparently produces new ones. We have performed a series of similar experiments, i.e. x-irradiation at room temperature, a first and second photostimulation at 10 K with intermediate annealing and variation of the annealing temperature. Annealing up to about 280 K did not cause a replenishment effect. To observe it, we had to anneal above 280 K. This result differs from what was found for BaFBr:Eu^{2+} previously (Hangleiter *et al* 1991). There, a small replenishment was observed even for 200 K.

It was further observed that after exhausting the PSL at 300 K and waiting for a long time (for about 1 d), again a PSL effect could be observed. It is, however, only very small, below 1% of the PSL intensity observed during the first reading. Such an effect was also observed in BaFBr:Eu^{2+} (unpublished). For an explanation, we propose that after photostimulation at 300 K there are still F centres and hole centres that can aggregate by thermal activation at 300 K to form photostimulable centres, a feature we have denoted as the 'replenishment' effect above. We cannot, however, exclude that further unknown defects may play a role. For example, during the photostimulation electrons may be captured by other thermally unstable traps and then be thermally released and form photostimulable centres. However, we have not found experimental evidence for such traps.

After x-irradiation at 300 K, about 20–30% of the generated F centres decay within about 20–30 min.

3.2. X-irradiation at helium temperatures

The MCDA measured in a crystal x-irradiated at 4.2 K contained the MCDA bands of F centres, V_K and H centres, the latter two having been identified recently by Spaeth *et al* (1994b). No $In^0(1)$ centres, nor any In^{2+} centres could be found.

The number of F centres produced by the same x-ray irradiation dose is about half that found for room-temperature x-irradiation. Photostimulation into the F band produces also an In^+ luminescence band at 2.9 eV and another one at 2.3 eV, which is from the self-trapped

excitons formed by recombination processes between the F centres and the intrinsic hole centres (Song and Williams 1993). Figure 5 shows the decay time of the PSL at 2.9 eV after x-irradiation under continuous excitation at 10 K. It is approximately the same as that after room-temperature x-irradiation when stimulating 10 K. The F centres bleach by about 50%. H centres and V_K centres vanish together with the F centres, both by about 50%. Upon annealing to 60–70 K, the H centres thermally decay; the number of F centres decreases to about one-third of the initial value. Upon further annealing to 200 K, the V_K centres also thermally decay, and there remains about 10% of the initial number of F centres.

At 4.2 K, clearly no In^{2+} centres are created by x-rays that would recombine with F centres to give the PSL emission at 2.9 eV. Only a very weak replenishment effect was observed after warming to 300 K. This effect is only $\sim 1/100$ that observed when x-irradiating at room temperature.

3.3. X-irradiation at 100 K

Upon x-irradiation for the same time as usual (2 h) at 100 K, F centres are generated, approximately as many as after x-irradiation at 4.2 K. The MCDA shows a strong band from F centres, a very weak one from V_K centres and around 3.5–4.0 eV two weak bands, which are paramagnetic, but no MCDA–EPR could be detected in those bands.

Upon photostimulation into the F band, two In^+ PSL bands appear: one at 2.9 eV and one at 2.4 eV (Fukuda 1970) (figure 4). The integral In^+ luminescence is about the same as that of the 2.9 eV luminescence measured at 10 K, thus the In^+ luminescence is the same for x-irradiation at 10 and 100 K (the precision of the luminescence intensity measurements is about ±20%). The F centres did not bleach measurably during the photostimulation. After annealing to 300 K, the number of F centres decreased by approximately 20%.

4. Discussion

The failure to detect In^{2+} centres after x-irradiation at low temperature in spite of generating F centres demonstrates that In^{2+}–F centre pairs are not produced as primary radiation defects. The doped In^+ impurities do not act as primary hole traps. The observation of In^{2+} centres at room temperature, however, shows that the formation of In^{2+} centres is a thermally activated process. From a mobile hole centre of unknown nature, the In^+ must have captured the hole to form In^{2+}. The MCDA-detected EPR measurements of In^{2+} showed an isotropic spectrum (isotropic In hyperfine interaction and an isotropic g factor), suggesting that no other defect such as a nearest-neighbour vacancy is associated with the In^{2+} centre. Possibly, a V_k centre annihilates at the In^+ to form In^{2+}.

The observation that, after room-temperature x-irradiation and subsequent photostimulation at 10 K, the MCDA of the In^{2+} centres was not affected by the photostimulation shows that In^{2+} is not primarily involved in the photostimulated luminescence process. The In^+ luminescence is not a radiative decay of an F–electron–In^{2+} recombination process. Thus, we must conclude that the electron–hole recombination involves another hole centre. It is thought that, upon recombination of that hole centre with the photostimulated electron from the F centre, the recombination energy is transferred to a nearby In^+ centre, which is then excited and subsequently emits the characteristic In^+ luminescence. This would be very similar to what is thought to happen also in BaFBr:Eu^{2+}. There, upon x-irradiation, no Eu^{3+} is formed, and the PSL is thought to involve a triple aggregate between a hole centre, the Eu^{2+} activator and an F centre (Hangleiter *et al* 1990, 1991). The recombination between the excited F electron and the hole centre takes place via tunnelling within that

aggregate (de Leeuw *et al* 1987, v. Seggern *et al* 1988, Spaeth *et al* 1994a). It seems that also in KBr:In such a triple aggregate is formed. In BaFBr:Eu^{2+} the nature of the hole centre is not yet clear. It was speculated that the oxygen contamination (O_F^- centres) plays an important role. Here, there is no evidence for any oxygen contamination and, because of the careful growth process, there should not have been much oxygen incorporated. We have no information on the nature of the room-temperature-stable hole centre.

Support for the assumption of the formation of an aggregate as the responsible defect arrangement is the observation of the 'replenishment' effect. A very similar phenomenon was observed in BaFBr:Eu^{2+} (Hangleiter *et al* 1991). The fact that, after exhaustion of photostimulable aggregates at low temperature, new photostimulable aggregates are formed after warming above 280 K suggests that F centres and possibly also the unknown room-temperature-stable hole centres become mobile near that temperature and that the formation of the aggregate is energetically favoured over the statistical distribution.

That radiation defects are mobile at room temperature is not only seen from the replenishment effect but also from the observation that, after x-irradiation at room temperature, about 20–30% of the initially generated F centres decay within a few minutes.

It seems that there is a thermodynamical equilibrium distribution of triple aggregates between F and hole centres and In^+, which is restored after its perturbation by a PSL process, provided the temperature is sufficiently high for the mobility of aggregate partners. At room temperature, the PSL process must occur until all photostimulable centres have aggregated and recombined.

The question arises of why there is almost no replenishment effect when x-irradiating at 4.2 K, and why it is very similar when irradiating at 100 K and 300 K. For an explanation it may be speculated that the hole centre is mobile at 100 K and above and forms already a pair aggregate with In^+ during the x-irradiation. After warming to 280 K, the F centres become mobile and join the pair aggregate to form the triple aggregate. For irradiations at 4.2 K, none of the centres is mobile, so that only those triple aggregates that are directly formed contribute.

It was argued previously from the kinetics of the PSL that F–In^{2+} pairs are the responsible defects for the PSL effect, since the decay curves were almost the same whether the pairs were created by UV or x-irradiation (Braslavets *et al* 1992). Of course, the same decay time is also observed if the recombination involves tunnelling within the triple aggregate.

The low-temperature PSL experiments show that only a fraction of the F centres are involved in the PSL process. This is best seen for x-irradiation at 100 K, where there is not the complication with a recombination between F centres and other hole centres as at helium temperatures. This conclusion is supported by an interesting observation made recently by Tale *et al* (1993), comparing the optical absorption and photostimulation spectra at room temperature and 80 K. It was found that the photostimulation band does not coincide with the F centre absorption band. Its peak is shifted to lower photon energy. The shifted photostimulation spectrum was observed also for very low x-ray doses (a factor of 50 lower than usually used here). The photostimulation spectrum changes during the course of the read-out process. The low-energy part is measured first, then the photostimulation spectrum resembles more that of the F centres (Springis 1994).

For an explanation it may be speculated that the major PSL effect is due to F centres perturbed by the nearby presence of the In^+ and unknown hole centre, which shows up in the peak energy of the photostimulation band. The observation does give further support for our speculation that the PSL effect is primarily due to triple-centre aggregates.

This observation of the spectral shift of the photostimulation band may provide a key for a better identification of the photostimulable centres. Possibly with optically detected

electron nuclear double resonance (ODENDOR), one can investigate the microscopic structure of the perturbed F centres that appear after x-irradiation. In addition, the yet unidentified MCDA bands between 2.5 and 3.5 eV need to be investigated further. They are probably due to hole centres. The prospect of identifying the centres involved in the PSL mechanism is probably better in this system (KBr:In) compared to BaFBr:Eu, because it is easier to remove oxygen completely and because of the cubic structure of KBr, which makes an MCDA-detected EPR and ENDOR investigation feasible. In BaFBr such measurements are only possible for the magnetic field orientation along the *c* axis, which does not allow the measurement of the angular dependencies of the EPR/ENDOR spectra. These are necessary for an analysis that may lead to the determination of the microscopic structures.

It may be noted that in preliminary experiments with the x-ray storage phosphor RbBr:Tl, the replenishment effect was also observed similarly as here (to be published).

In conclusion, we have shown that the x-ray energy storage and the read-out process do not involve primarily In^{2+}–F centre pairs. The In^{+} luminescence is due to a recombination between an unknown hole centre and F centres, whereby the recombination energy is transferred to the In^{+} centres. It is thought that triple aggregates between In^{+}, F and hole centres are the responsible configuration within which the PSL process happens.

References

Ahlers F J, Lohse F, Hangleiter Th, Spaeth J-M and Bartram R H 1984 *J. Phys. C: Solid State Phys.* **17** 4877

Blasse G 1993 *J. Alloys Compounds* **192** 17

Braslavets P F, Kalnins A, Plavia I, Popov A I, Rapoport B I and Tale A 1992 *Phys. Status Solidi* b **170** 395

de Leeuw D M, Kovats T and Herko S P 1987 *J. Electrochem. Soc.* **134** 491

Eachus R S, McDugle W G, Nuttal R H D, Olm M T, Koschnick F K, Hangleiter Th and Spaeth J M 1991 *J. Phys.: Condens. Matter* **3** 9327, 9339

Fukuda A 1970 *Phys. Rev.* B **1** 4161

Hangleiter Th, Koschnick F-K, Spaeth J-M and Eachus R S 1991 *J. Radiat. Eff. Defects Solids* **11** 615

Hangleiter Th, Koschnick F-K, Spaeth J-M, Nuttal R H D and Eachus R S 1990 *J. Phys. C: Solid State Phys.* **2** 6837

Ishii T 1966 *J. Phys. Soc. Japan* **21** 2202

Kalnins A, Plavina I, Popov A I and Tale A 1993 *Phys. Status Solidi* b **180** K31

Kalnins A, Plavina I, Trinklere L and Trinklere M 1991 *Proc. Lumdetr 91 (Riga)* (Riga: University of Latvia) p E18

Koschnick F K, Spaeth J M, Eachus R S, McDugle W G and Nuttal R H D 1991 *Phys. Rev. Lett.* **67** 357

Plavina I, Tale I and Tale A 1991 *Proc. Lumdetr 91 (Riga)* (Riga: University of Latvia) p D4

Rogulis U, Spaeth J-M, Tale I and Ruza E 1994 *Proc. EURODIM 94 (Lyon)*

Smith D Y and Dexter D L 1972 *Prog. Opt.* **10** 165

Song K S and Williams R T 1993 *Self Trapped Excitons (Springer Series in Solid State Sciences 105)* (Berlin: Springer)

Sonoda M,Takano M, Miyahara J and Kato H 1983 *Radiology* **148** 833

Spaeth J-M, Hangleiter Th, Koschnick F-K and Pawlik Th 1994a *Proc. EURODIM 94 (Lyon)*

Spaeth J-M, Meise W and Song K S 1994b *J. Phys.: Condens. Matter* **6** 1801

Spaeth J-M, Niklas J R and Bartram B H 1992 *Structural Analysis of Point Defects in Solids (Springer Series in Solid State Sciences 43)* (Springer)

Springis 1994 Private communication

Tale I, Tale V, Kulis P, Springis M and Veispals A 1993 *Proc. 12th Int. Conf. on Defects in Insulating Materials (Nordkirchen, 1992)* p 1262

Trinklere L E, Trinklere M F and Popov A I 1993 *Phys. Status Solidi* b **180** K31

von Seggern H, Voigt T, Knüpper W and Lange G 1988 *J. Appl. Phys.* **66** 1405

THE X-RAY STORAGE PHOSPHORS RbI:Tl^+ AND KBr:In^+ AND OTHER In^+ AND Ga^+ DOPED ALKALI HALIDES

Th. Hangleiter*, U. Rogulis†, C. Dietze*, J.-M. Spaeth*
P. Willems‡, L. Struye‡, P.J.R. Leblans‡

*Fachbereich Physik, University of Paderborn, D-33095 Paderborn, Germany
†Institute of Solid State Physics, University of Latvia, Riga, Latvia
‡Agfa-Gevaert N.V., Septestraat 27, B-2640 Mortsel, Belgium

ABSTRACT: The X-ray storage phosphors KBr:In^+ and RbI:Tl^+ show similar properties as the well-known phosphor BaFBr:Eu^{2+}. The radiation damage defects as well as the photostimulated In^+ or Tl^+ emissions were investigated with optical measurements and optically detected magnetic resonance methods between 1.5 K and 300 K. The photostimulation luminescence was also measured in In^+ and Ga^+ doped RbBr, RbI, CsBr and CsI crystals.

INTRODUCTION

X-ray storage phosphors such as BaFBr doped with Eu^{2+} were intensively investigated in the last years. With special interest the radiation-induced defects were studied to understand the mechanism of the photostimulation process. The X-ray information is stored in electron traps usually as F centres and in hole centres. In the case of KBr:In^+ it was assumed that after X-irradiation F- and In^{2+}-pairs are formed [1,2], which can be excited and read-out by stimulation of the F-absorption band. In Tl^+ doped RbI V_K centres stabilised nearby the activator Tl^+ were postulated to be the relevant hole centres [3].

EXPERIMENTAL RESULTS

Single crystals with an activator dopant concentration of 100 to 1000 ppm in the melt were grown with the Bridgman method under inert gas. The radiation defects were produced by X-irradiation with 60 kV, 15 mA for approximately 10 to 60 min at low temperatures or at room temperature. We measured the radiation defects with optical absorption, luminescence, optically detected magnetic resonance (ODMR) and electron paramagnetic resonance (EPR).

a) RbI:Tl^+

RbI:Tl^+ crystals were X-irradiated at 80 K. Fig.1 shows the spectrum of the magnetic circular dichroism (MCD) at 1.5 K. After X-irradiation F centres, V_K centres and Tl^{2+} centres are produced. Additionally Tl^0 centres can be detected by their optical absorption at 2.27 eV (546.3 nm) [3]. The V_K centres were identified with optically detected electron paramagnetic resonance (ODEPR) using the MCD or conventional EPR. The V_K centres disappear after annealing at 150 K and the Tl^{2+} bands (see fig.1) increase as a consequence of the annealing out of V_K centres. The disappearance of V_K can also be shown with thermoluminescence and EPR. However, no disturbed V_K centres like V_{K_A}(Tl) could be detected. The highest intensity of the photostimulated luminesence can be achieved after X-irradiation at low temperatures and annealing to 150 K. At 180 K the Tl^0 centres recombine with Tl^{2+} centres and the MCD signal of Tl^{2+} becomes smaller.

Proc. Int. Conf. on Inorganic Scintillators and Their Applications, SCINT95,
1996, Delft University Press, The Netherlands

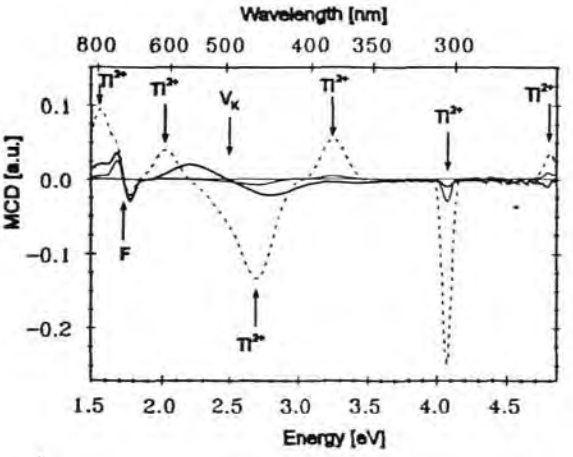

Fig. 1. Spectrum of the magnetic circular dichroism of RbI:Tl^+ at 1.5 K (a) after X-irradiation at 80 K, (solid thick line), (b) after annealing at 150 K (broken line), (c) after annealing at 220 K (thin line)

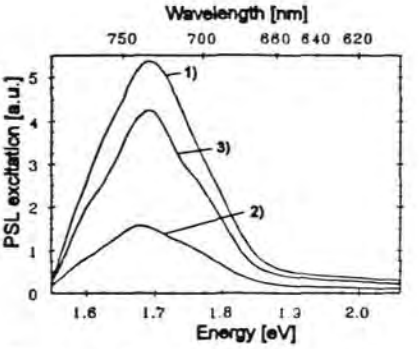

Fig. 2. PSL excitation spectrum of RbI:Tl^+ at 80 K detected at 433 nm. The crystal was X-irradiated, annealed at 220 K (1), bleached at 305 nm (2) and annealed again at 150 K (3).

If Tl^{2+} is bleached with 305 nm (4.07 eV) light, the MCD of the Tl^{2+} centres vanishes. At the same time the photostimulated luminescence (PSL) excited in the F band decreases. EPR measurements show that V_K centres are created by this process at low temperatures (below 150 K). After this procedure warming the crystal to 150 K destroys the V_K centres again, which can be seen in the thermoluminescence spectrum, then the PSL signal is restored to about 80% of its original value (recovery effect, shown in fig.2). The MCD of Tl^{2+} comes back. This indicates that Tl^{2+} is the primary hole centre.

At temperatures above 150 K the Tl^{2+} centre recombines with the F centre as a consequence of photo-exciting in the F band giving rise to the Tl^+ luminescence, i.e. the PSL effect. On the basis of the bleaching experiments at 80 K we assume the following processes to occur in RbI:Tl^+:

Exciting of Tl^{2+} at 80 K:

$$Tl^{2+} + h\nu\,(305\,nm) \longrightarrow \left(Tl^{+}\right)^{*} + V_K$$

$$\longrightarrow Tl^{+} + h\nu(433\,nm) + V_K$$

$$Tl^{+} + V_K \xrightarrow{150\,K} Tl^{2+} \qquad \text{"recovery-effect"}$$

Photostimulated luminescence (PSL):

$$F + h\nu\,(735\,nm) + Tl^{2+} \longrightarrow \left(Tl^{+}\right)^{*}$$

$$\longrightarrow Tl^{+} + h\nu(433\,nm)$$

In RbI:Tl^+ there is no replenishment effect [5].

b) KBr:In^+

X-irradiation of KBr:In^+ at low temperatures (< 120 K) produces F centres, In^0 and V_K centres, which can be detected with MCD and ODEPR [4]. In KBr crystals with a higher In^+ concentration also In^{2+} centres were found. The V_K centres decay at temperatures above 150 K [6] and only the In^{2+} centres remain as hole centres. By bleaching the In^{2+} (315 nm) at 80 K the In^{2+} centres decrease and new V_K centres are generated. In contrast to RbI:Tl^+ no In^{2+} centres are restored upon annealing to higher temperatures. The PSL spectra after different annealing steps (fig.3) show that the PSL signal is much higher before the V_K centres are destroyed. This means that the V_K centre is the dominant hole centre at low temperatures.

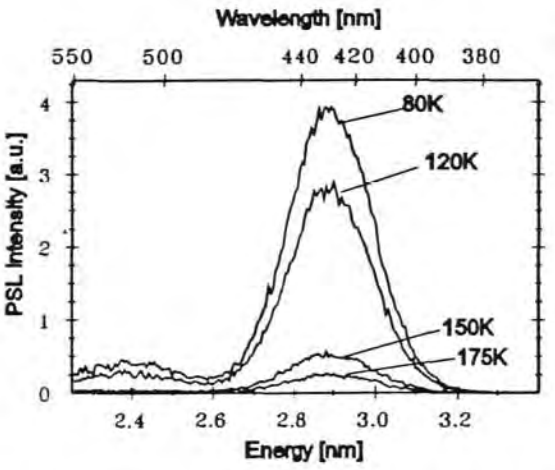

Fig. 3. PSL spectrum of KBr:In^+ at 80 K excited at 605 nm. The crystal was X-irradiated at 80 K (1), gradually annealed to 120 K (2), 150 K (3) and 175 K (4).

After X-irradiation at room temperature only In^{2+}, In^0 and F centres are found. Further hole centres could not be detected until now.

The replenishment effect in KBr:In^+ depends on the In^+ concentration. Apart from this the effects in KBr:In^+ are similar as in RbI:Tl^+.

c) RbBr, RbI, CsBr and CsI crystals doped with In^+ and Ga^+

RbBr, RbI, CsBr and CsI crystals were doped with 200 to 1000 ppm Indium or Gallium in the melt. The maximum of the PSL excitation is at longer wavelength than that in BaFBr:Eu^{2+} (see table 1). CsI:Ga^+ shows no storage effect. The values for the ratio of the conversion efficiency and the stimulation energy of Ga^+ doped RbBr and CsBr are in the same order of magnitude as commercial X-ray storage screens (for details of the figures of merit CE/SE see [7]).

	stimulation wavelength [nm]	max. of the PSL [nm]	max. of the PSL stimulation [nm]	conversion efficiency (CE) [pJ/mm^2/mR]	stimulation energy (SE) [μJ/mm^2]	CE/SE * 10^3
BaFBr:Eu^{2+} screen	633[1)]	390	550	20.4	15.7	1300
BaFBr:Eu^{2+} screen	680[2)]	390	550	14.4	28	510
RbBr:In^+	680[2)]	490	700	1.9	25.0	77
RbBr:Ga^+	680[2)]	550	705	5.6	3.9	1470
RbI:Ga^+	680[2)]	620	770	3)	3)	3)
	856[2)]	620	770	0.0024	131	0.0183
CsBr:In^+	680[2)]	504	700	3.0	23.0	140
CsBr:Ga^+	680[2)]	515	685	5.4	4.3	1370
CsI:Ga^+	680[2)]	-	-	-	-	-

Tab. 1. Data of some In^+ and Ga^+ doped X-ray storage phosphors in comparison with a standard BaFBr:Eu^{2+} X-ray storage phosphor screen. [1)] *HeNe-laser,* [2)] *laser diode* [3)] *not measurable with the 680 nm laser diode.*

CONCLUSION

RbI:Tl^+ shows no PSL via Tl^+-emission after low temperature X-irradiation. It could be shown that Tl^{2+} is the responsible hole centre for the PSL process in RbI:Tl^+. The situation differs in KBr:In^+ where V_K centres are the relevant hole centres at temperatures below 140 K. The In^{2+} centre could be identified as the hole centre at room temperature. It is also shown that RbBr and CsBr crystals doped with Ga^+ are very efficient X-ray storage phosphors.

REFERENCES

[1] I. Plavina, I. Tale and A. Tale, Proc. of the LUMDETR'91, Riga, **D4** (1991)

[2] P.F. Braslavets, A. Kalnins, I. Plavina, A.I. Popov, B.I. Rapoport and A. Tale, phys. stat. sol.(b) **170**, 395 (1992)

[3] M. Thoms, H. von Seggern and A. Winnacker, J. Appl. Phys. **76**, 1800 (1994)

[4] U. Rogulis, I. Tale, Th. Hangleiter and J.-M. Spaeth, J. Phys.: Condens. Matter **7**, 3129 (1995)

[5] Th. Hangleiter, F.-K. Koschnick, J.-M. Spaeth, R.H.D. Nuttall and R.S. Eachus, J. Phys.: Condens. Matter **2**, 6837 (1990)

[6] D. Schoemaker, Phys. Rev. B **7**, 786 (1973)

[7] A. Meijerink, submitted to Mat. Chem. Phys.

JOURNAL OF APPLIED PHYSICS VOLUME 84, NUMBER 8 15 OCTOBER 1998

Ga^{2+} hole centers and photostimulated luminescence in the x-ray storage phosphor RbBr:Ga^{+}

U. Rogulis,[a] S. Schweizer,[b] S. Assmann, and J.-M. Spaeth
Universität-Gesamthochschule Paderborn, Fachbereich Physik, Warburger Str. 100, D-33098 Paderborn, Germany

(Received 15 June 1998; accepted for publication 17 July 1998)

It was previously shown that RbBr doped with Ga^{+} is an efficient x-ray storage phosphor with a figure of merit comparable to that of the commercially used BaFBr:Eu^{2+}. The paramagnetic hole centers generated upon x irradiation involved in the storage and read-out process were investigated by measuring the magnetic circular dichroism of the optical absorption (MCDA), the MCDA-detected electron paramagnetic resonance (MCDA-EPR) and the photostimulated luminescence (PSL). Two different Ga^{2+} hole centers with a hyperfine interaction with ^{69}Ga of $^{69}A = 8.2$ GHz and $^{69}A = 6.0$ GHz, respectively, were found. No superhyperfine interaction was resolved. Therefore, the structural difference between the two Ga^{2+} centers could not be established from EPR. The PSL effect is correlated only to one of the two Ga^{2+} centers, namely that with $A = 8.2$ GHz. The generation mechanism of the two hole centers is investigated. It is proposed that the PSL-active Ga^{2+} center is an isolated Ga^{2+} on a Rb^{+} site, whereas the other center is a Ga^{2+}-cation vacancy complex. © *1998 American Institute of Physics.* [S0021-8979(98)08220-6]

I. INTRODUCTION

X-ray storage phosphors are used to generate digital x-ray images. They have enhanced sensitivity for x rays compared to conventional x-ray films and a higher dynamical range. The best material so far is BaFBr doped with Eu^{2+} as activator, which is actually used commercially. Although digital radiography with BaFBr:Eu^{2+} has many attractive features, it has one disadvantage compared to conventional x-ray films: the spatial resolution is still inferior. The reason for this is partially due to the matlockite structure of BaFBr. The crystal is birefringent and, therefore, there is too much light scattering from the statistical distribution of the crystallites in the film when the x-ray information is read out by a scanning laser beam. Consequently, one is interested in optically isotropic x-ray storage phosphor materials.

One such system would be RbI doped with Tl^{+} as activator. The radiation damage centers storing the information are F centers as electron trap centers (electrons captured in an I^{-} vacancy) and Tl^{++} centers as hole trap centers. During photostimulation into the F centers, the electron recombines with the Tl^{++} resulting in a Tl^{+} luminescence used to read out the information.[1] In contrast to BaFBr:Eu^{2+}, where the hole trap center has not yet been identified, the storage and read-out processes are well understood in RbI:Tl^{+}. Unfortunately, however, the stored information fades quickly away at room temperature. Therefore, the system cannot be used in practice.

It has been shown in a preliminary study that RbBr doped with Ga^{+} is a very promising x-ray storage phosphor[2] with a figure of merit as to sensitivity, x-ray conversion and read-out energy comparable to that of BaFBr:Eu^{2+}. Since this phosphor is optically isotropic, it is a promising candidate for higher spatial resolution.

In this article we present an investigation of the information storage process and the photostimulated luminescence (PSL) mechanism in RbBr:Ga^{+}. We investigated the radiation-induced paramagnetic electron and hole trap centers using the magnetic circular dichroism of the optical absorption (MCDA) and the MCDA-detected electron paramagnetic resonance (MCDA-EPR). It turns out that the electron trap centers are F centers and the hole trap centers are Ga^{2+} centers. We found two Ga^{2+} centers with different microscopic structures, of which only one center takes part in the PSL process.

Previously, Baranov and Khramtsov studied Ga^{2+} centers in KCl and NaCl with EPR.[3] Also there, two different centers were found. One was proposed to be an isolated Ga^{2+} on a cation site and the other one a Ga^{2+} on cation site associated with a cation vacancy. It is proposed that the Ga^{2+} centers found here are of similar structures.

II. EXPERIMENT

A. Sample preparation

RbBr was doped with 200 ppm Ga^{+} in the melt and single crystals were grown by the Czochralski method under inert gas. By using appropriate amounts of $GaBr_3$ and elementary gallium it was attempted to avoid the incorporation of trivalent gallium. Due to the Czochralski method, the single crystal part grown first contains only a small Ga^{+} concentration. The Ga^{+} concentration in the melt increases with the crystal growth. Therefore, the crystal's end part is doped with a much larger amount of Ga^{+}. In addition, the end part of the single crystal also contains more other unavoidable impurities than the first part. A sample from the

[a]Institute of Solid State Physics, University of Latvia, 8 Kengaraga Street, LV-1063 Riga, Latvia
Electronic mail: schweizer@physik.uni-paderborn.de

first part and one from the end part have been investigated. Henceforth, the two samples are referred to as "L" (low Ga^+ concentration) and "H" (high Ga^+ concentration). From optical absorption measurements, the Ga^+ concentration ratio between the H and L samples was about 5:1. The absolute Ga^+ concentration incorporated into the crystal could not be determined. The maximum concentration is probably one order of magnitude less than the doping level of 200 ppm.

B. Measurement techniques

Emission and excitation spectra of the photostimulated luminescence were measured with a single beam spectrometer, in which two 0.25 m double monochromators (Spex) were used. The samples were excited either with a halogen lamp for the visible spectral range or with a deuterium lamp for the ultraviolet range. The emission and excitation spectra were detected using a photomultiplier and single photon counting. The samples were x irradiated (tungsten anode, 60 kV, 15 mA, 15 min) between 10 and 300 K.

The magnetic circular dichroism of the optical absorption (MCDA), which is the differential absorption of right and left circularly polarized light in an external static magnetic field, and the MCDA-detected electron paramagnetic resonance (MCDA-EPR) were measured in a custom-built, computer-controlled spectrometer working at 24 GHz (K band). The MCDA measurements were performed at 4.2 K, the MCDA-EPR measurements at 1.5 K. The samples were x-irradiated between 4.2 and 300 K (tungsten anode, 60 kV, 15 mA, 20–60 min). For the optical bleaching experiments, a He-Ne laser (633 nm) was used.

III. EXPERIMENTAL RESULTS

A. Luminescence properties

Before x irradiation the two samples L and H show identical Ga^+ luminescence and excitation spectra. Excitation of the sample L with UV light at 80 K leads to a single luminescence band peaking at 2.21 eV (560 nm, half width 0.31 eV). This emission corresponds to the A_X $[^3T_{1u}(\Gamma_4^-) \rightarrow A_{1g}(\Gamma_1^+)]$ transition of monovalent gallium.[4] No luminescence was detected by exciting the RbBr:Ga^+ samples with light in the range of 600–800 nm.

After x irradiation at 10 K for 10 s the thermoluminescence glow curve of sample L was measured (Fig. 1). There are several peaks between 10 and 340 K. Besides the sharp peaks between 10 and 40 K, which are caused by the decay of intrinsic I centers (interstitial halide) and H centers [$(\text{halogen})_2^-$ molecules occupying single halide sites],[5] a broad maximum between 190 and 270 K appears. Note, that the V_K centers (a hole shared between two adjacent Br^- ions on lattice sites) in RbBr are only stable up to about 170 K.[6] A corresponding thermoluminescence peak at this decay temperature was not observed. Probably most of the V_K centers are trapped forming other hole centers causing at least partially the broad thermoluminescence peak mentioned above (see also below the section on generation of Ga^{2+} centers).

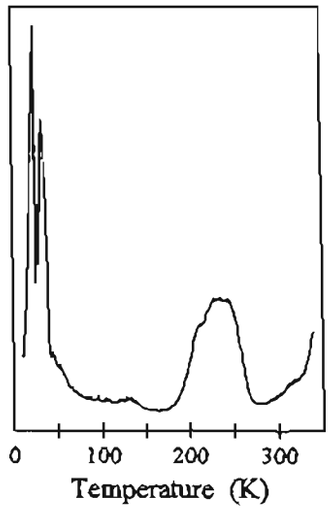

FIG. 1. Thermoluminescence glow curve of RbBr:Ga^+, sample L, after x irradiation at 10 K.

In order to obtain information about the nature of the photostimulated luminescence (PSL) of the x-irradiated RbBr:Ga crystals, PSL excitation measurements were carried out. At first, the RbBr:Ga^+ samples were x irradiated at 80 K for 15 min. Afterwards PSL excitation spectra were measured at 80 K after heating the sample first to a certain temperature and then cooling it down to 80 K again. This procedure was repeated for several temperatures. In all cases the Ga^+ luminescence at 2.21 eV (560 nm) was detected (see Fig. 2).

In Fig. 2(a) the results for the sample L are presented. While the spectra measured after annealing to 80, 130, and 150 K show no considerable changes in the weak Ga^+ luminescence, the temperature step to 180 K is followed by a slight increase of the luminescence intensity. Further heating to 200 K results in a strong increase of the luminescence

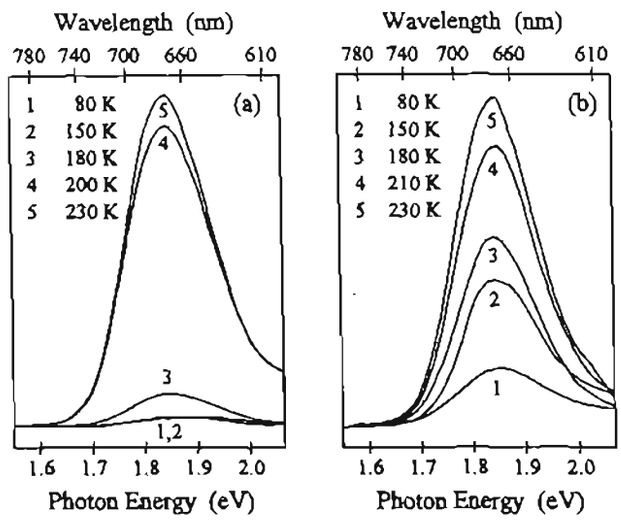

FIG. 2. Excitation spectra measured in the 560 nm emission band of (a) sample L and (b) sample H for various subsequent temperature steps after x irradiation at 80 K. All spectra were measured at 80 K.

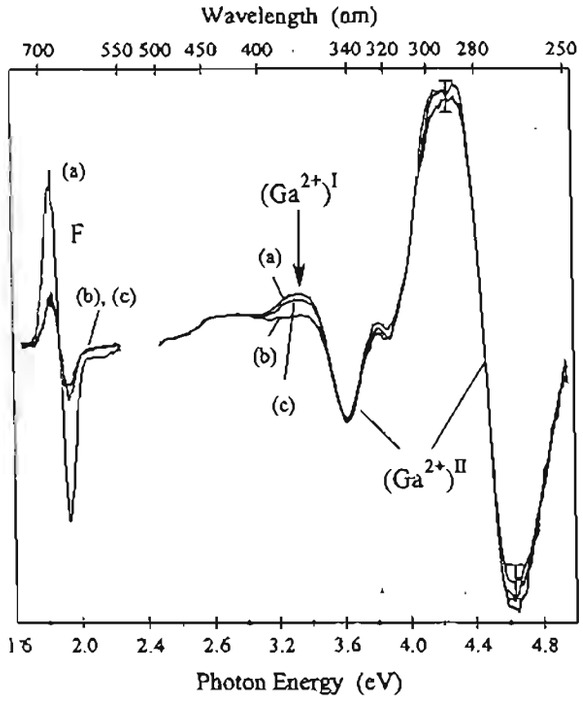

FIG. 3. MCDA spectra of sample L, curve (a) immediately after x irradiation at room temperature, curve (b) after additional bleaching in the F center absorption band at 4.2 K and curve (c) after subsequent annealing up to room temperature. All spectra were measured at 4.2 K. The slight differences in signal amplitudes of the $(Ga^{2+})^{II}$ centers as from 3.8 eV to higher photon energies are due to the worse signal-to-noise ratio in this energy range (indicated by an error bar) and not real.

intensity followed by only a small rise after the next step to 230 K.

This behavior of the temperature-dependent luminescence spectra is different for the sample H presented in Fig. 2(b). Besides the luminescence increase from 180 to 210 K, similar to that of the other sample, a rise is also observed at the annealing step from 80 to 150 K.

8. MCDA and MCDA-detected EPR

The MCDA spectrum of the sample L, after x irradiation at room temperature, is shown in Fig. 3 [curve (a)]. The band at 1.88 eV (660 nm) having a derivative-like structure belongs to the F centers. Besides the F center band, several MCDA bands were detected in the UV spectral range. After optical bleaching in the F center absorption band and thermal treatment, the intensities of several MCDA bands have changed [see Fig. 3, curves (b) and (c), to be discussed later].

The MCDA-detected EPR spectra of the x-irradiated RbBr:Ga crystal are shown in Fig. 4, measured in the MCDA band (a) at 4.29 eV (289 nm) and in the MCDA band (b) at 3.35 eV (370 nm), respectively. Several broad EPR lines appear in the magnetic field range up to 1300 mT. The line positions are isotropic within experimental error. They are due to two Ga^{2+} centers [labeled $(Ga^{2+})^I$ and $(Ga^{2+})^{II}$ in Figs. 3 and 4].

The EPR lines of each Ga^{2+} center are split by a hyperfine (hf) interaction between the unpaired electron of the Ga^{2+} ($4s^1$ state) with $S=1/2$ and the two magnetic isotopes

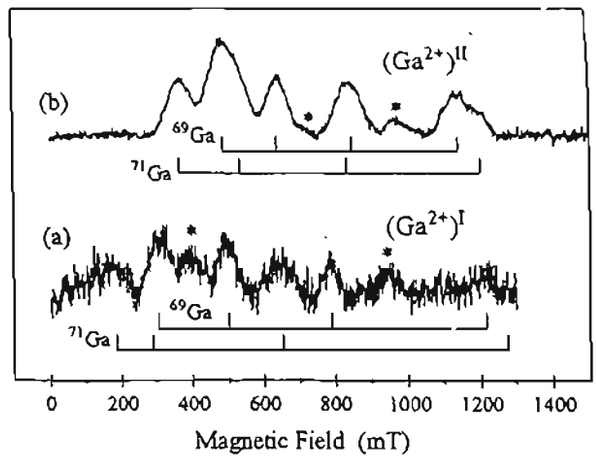

FIG. 4. MCDA-detected EPR spectra of (a) $(Ga^{2+})^I$ centers detected at 370 nm and (b) $(Ga^{2+})^{II}$ centers detected at 290 nm in x-irradiated RbBr:Ga^+, sample L, measured at 1.5 K (microwave frequency of 23.9 GHz).

^{69}Ga (60.4% natural abundance) and ^{71}Ga (39.6% natural abundance), both with a nuclear spin of $I=3/2$. The hf interaction leads to four "allowed" $\Delta m_I=0$ transitions shown in the energy level scheme of Fig. 5 and marked with bars in Fig. 4. The transitions labeled with asterisks are due to "forbidden" ($\Delta m_I=\pm1,\pm2$) transitions. The forbidden transitions are nearly as intense as the allowed ones. This can occur in the MCDA detection scheme when the allowed transitions are strongly saturated due to long spin-lattice relaxation times. The experimental conditions for this are explained in Ref. 7. The allowed quartet lines for $I=3/2$ have the same intensity. Since they are superimposed to forbidden transitions, the intensity pattern in Fig. 4 is different from the expectation for allowed transitions only.

Unfortunately, we did not observe any superhyperfine (shf) interactions with surrounding lattice neighbors. Therefore, we cannot establish the structural differences between these two Ga^{2+} centers from the EPR spectra. The isotropic g factors, the hf interaction parameters ^{69}A for ^{69}Ga, the wavelengths, at which the MCDA-detected EPR spectra were measured, as well as published data for NaCl:Ga^+ and KCl:Ga^+ are collected in Table I.

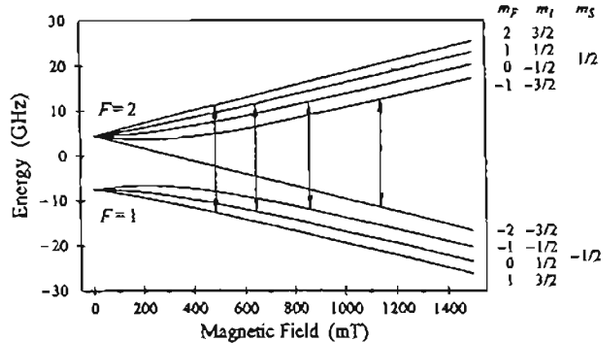

FIG. 5. Calculated Breit-Rabi diagram for the $(Ga^{2+})^I$ centers in RbBr:Ga^+ using an isotropic g factor of 2.005 and an isotropic ^{69}Ga hyperfine splitting of 6.0 GHz. The transition arrows correspond to a microwave frequency of 23.9 GHz.

TABLE I. Isotropic g factors, hf interaction parameters ^{69}A for ^{69}Ga, wavelengths, at which the MCDA-detected EPR spectra were measured, as well as published data for NaCl:Ga and KCl:Ga.

Crystal	Center	Wavelength (nm)	^{69}A (GHz)	g	Literature
RbBr	$(Ga^{2+})^{I}$	370	8.2±0.2	2.03±0.01	this work
	$(Ga^{2+})^{II}$	289	6.0±0.05	2.005±0.005	this work
NaCl	Ga_c^{2+}		9.35	2.062	Ref. 3
KCl	Ga_c^{2+}		8.86	2.012	Ref. 3
	$Ga^{2+}-V_c$		6.33	2.01	Ref. 3

The excitation spectra of the MCDA-detected EPR ("tagged MCDA," see Ref. 8) are shown in Figs. 6(a) and 6(b) for the $(Ga^{2+})^{I}$ and the $(Ga^{2+})^{II}$ center, respectively. Figure 6(a) shows that an energy of 3.35 eV (370 nm) is very suitable for measuring the MCDA-detected EPR spectrum of the $(Ga^{2+})^{I}$ centers, whereas 4.29 eV (289 nm) is suitable for the $(Ga^{2+})^{II}$ centers.

C. Production of $(Ga^{2+})^{I}$ and $(Ga^{2+})^{II}$ centers

The relative intensities of the MCDA bands of $(Ga^{2+})^{I}$ and $(Ga^{2+})^{II}$ centers created by x irradiation were found to be dependent on the Ga^{+} concentration and the irradiation temperature. In the sample L with low Ga^{+} concentration after x irradiation at room temperature a significant MCDA band of $(Ga^{2+})^{II}$ centers, but only a small band of $(Ga^{2+})^{I}$ centers were found [see Fig. 3, curve (a)]. In the sample H with high Ga^{+} concentration after x irradiation at room temperature the intensities of both MCDA bands are of the same order of magnitude with a smaller MCDA band of $(Ga^{2+})^{II}$ centers.

When x irradiating at 4.2 K, no Ga^{2+} centers appear, only F and V_K centers are observed. After annealing to about 180 K, where the V_K centers have begun to disappear, Ga^{2+} centers start to appear. In the sample L, the MCDA band of $(Ga^{2+})^{I}$ centers appears at 180 K and reaches its maximum

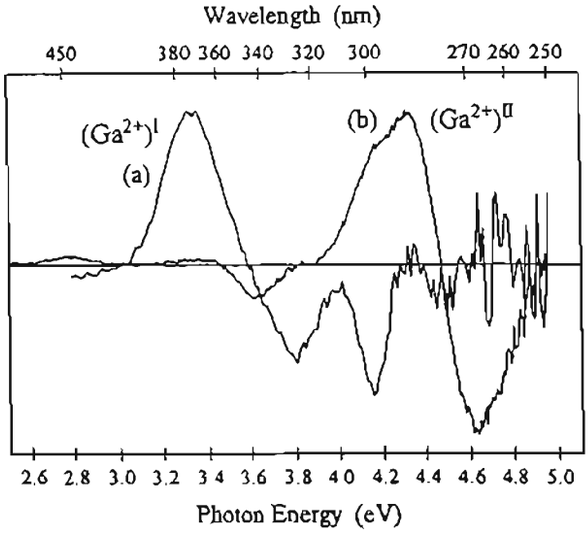

FIG. 6. "Tagged" MCDA spectra of (a) $(Ga^{2+})^{I}$ centers and (b) $(Ga^{2+})^{II}$ centers in x-irradiated RbBr:Ga^{+}. The signal-to-noise ratio of the tagged MCDA spectrum of $(Ga^{2+})^{I}$ centers as from 4.4 eV upwards is very low.

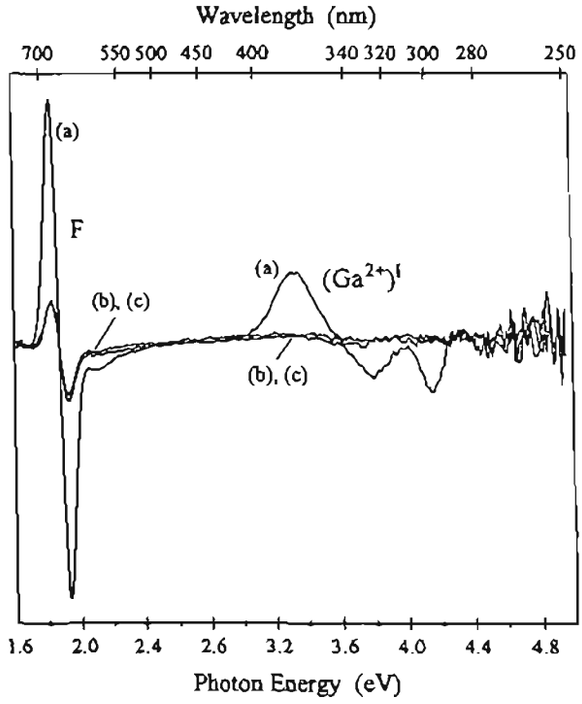

FIG. 7. MCDA spectra of sample H (a) after x irradiation at 4.2 K and subsequent annealing up to 220 K, (b) after additional bleaching in the F center absorption band at 4.2 K and (c) after subsequent annealing up to room temperature. All spectra were measured at 4.2 K.

value at 220 K. A weak MCDA band of the $(Ga^{2+})^{II}$ centers also appears at 180 K, reaches its maximum value when annealing further to 250 K and then remains unchanged to room temperature. Corresponding to the increase of the MCDA band of the $(Ga^{2+})^{II}$ centers the MCDA band of the $(Ga^{2+})^{I}$ centers decreases between 220 and 250 K. At 250 K about half of $(Ga^{2+})^{I}$ centers are destroyed. In sample H, the MCDA band of $(Ga^{2+})^{I}$ centers appears at 180 K with a further increase to its maximum value at about 220 K. No MCDA of $(Ga^{2+})^{II}$ centers is observed, even after annealing up to room temperature [see Fig. 7, curves (a) and (c)]. In general, the MCDA of $(Ga^{2+})^{I}$ centers reaches its maximum value at about 220 K, i.e., by an annealing step above the decay temperature of the V_K centers, while the MCDA of $(Ga^{2+})^{II}$ centers reaches its maximum at 250 K.

D. PSL experiments

Bleaching in the F center absorption band to stimulate the Ga^{+} luminescence could not destroy the $(Ga^{2+})^{II}$ MCDA signal, neither at room temperature nor at 4.2 K. However, the MCDA signal of the $(Ga^{2+})^{I}$ centers vanished after bleaching in the F center absorption band at 4.2 K [Fig. 7, curves (a) and (b)]. It was, however, possible to restore a part of the $(Ga^{2+})^{I}$ centers by subsequent annealing to RT in sample L (Fig. 3), but not in sample H (Fig. 7). This "replenishment" effect of the $(Ga^{2+})^{I}$ centers seems to be determined by the ratio between $(Ga^{2+})^{I}$ and $(Ga^{2+})^{II}$ before the bleaching experiment. If the $(Ga^{2+})^{II}$ center MCDA band is much bigger (sample L) than that of the $(Ga^{2+})^{I}$ center, we could observe a replenishment effect, otherwise not.

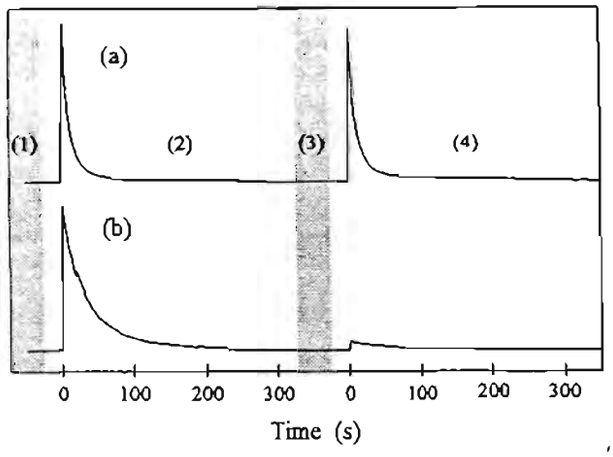

FIG. 8. PSL decay curves detected at 560 nm of (a) sample L and (b) sample H under continuous excitation with 670 nm light. The procedure for the PSL measurements of (a) was the following: (1) x irradiation at room temperature, (2) read-out process at 80 K, (3) annealing up to room temperature, (4) read-out process at 80 K. The procedure for the PSL measurements of (b) was: (1) x irradiation at 80 K and subsequent annealing up to 220 K, (2) read-out process at 80 K, (3) annealing up to room temperature, (4) read-out process at 80 K.

To investigate this replenishment behavior further, PSL experiments were carried out. x irradiation of the sample L at room temperature yields more $(Ga^{2+})^{II}$ centers than $(Ga^{2+})^{I}$ centers. Figure 8(a) shows the PSL intensity versus time of this sample during bleaching in the 1.85 eV (670 nm) band at 80 K. After having completely exhausted the PSL, the sample was annealed to room temperature and subsequently cooled to 80 K. The initial luminescence intensity of the PSL measured again amounts to 95% of the previously measured initial PSL. There is an almost complete replenishment effect. This effect is, however, x-ray dose dependent. If one applies a much lower dose (tungsten anode, 60 kV, 6 mA, 5 s), the replenishment effect is only 40%. The replenishment effect starts to appear after annealing the sample to about 200 K and reaches its maximum after annealing to RT.

After x irradiation of the sample H at 80 K with subsequent annealing to 220 K, the $(Ga^{2+})^{I}$ centers dominate. The PSL time dependency during bleaching with 1.85 eV (670 nm) light at 80 K is shown in Fig. 8(b). After annealing to 300 K and subsequent cooling to 80 K, the PSL intensity measured again amounts to only 5% of the PSL intensity measured before. Thus, the replenishment effect of the PSL is negligibly small in the sample with high Ga^{+} concentration where the $(Ga^{2+})^{I}$ centers dominate.

IV. DISCUSSION

The MCDA and MCDA-EPR measurements show that two different Ga^{2+} centers are formed by x irradiation. Since no shf is resolved, nothing can be said about the structural differences from the EPR spectra alone. However, from the generation by x irradiation at low temperature and subsequent annealing it can be concluded that $(Ga^{2+})^{I}$ centers are formed upon hole capture by Ga^{+} from a mobile V_K center, while the formation of $(Ga^{2+})^{II}$ centers needs as well the mobility of another species, thought to be vacancies. $(Ga^{2+})^{II}$ centers are proposed to be Ga^{2+}-cation vacancy complexes, similarly to what was proposed by Baranov and Khramtsov[3] to occur upon x irradiation in KCl and NaCl doped with Ga^{+}. When irradiating the sample at 4.2 K, only V_K and F centers are observed. V_K and F centers are generated either because of the presence of anion vacancies or because of the fundamental F–H process.[9] However, we have not seen an MCDA band of H centers, which, in principle, would have been seen for the magnetic fields perpendicular to their axes.[10] On the other hand, the thermoluminescence (TL) shows two low temperature peaks associated with the recombination of I and H centers.[5] Perhaps the MCDA of H centers was masked under that of the V_K centers. Important for the present study is only that V_K centers are created and that they start to decay at about 170 K.[6] Interestingly, at 170 K there is no peak in the TL. At about 180 K, $(Ga^{2+})^{I}$ centers are observed. Thus, we think that mobile V_K centers are captured by Ga^{+} centers forming $(Ga^{2+})^{I}$ centers. The V_K centers do not recombine with electrons, therefore, there is no TL peak. However, in sample L $(Ga^{2+})^{II}$ centers start to appear above 180 K, the maximum value is reached at about 250 K. The formation process of the $(Ga^{2+})^{II}$ centers is more complex than that proposed for $(Ga^{2+})^{I}$ centers. In KCl and RbCl cation vacancies become mobile at about 220 K.[11–13] A similar mobility temperature is also expected for RbBr since the migration energy of cation vacancies in RbBr (0.81 eV) is very close to that of KCl (0.84 eV) and RbCl (0.80 eV).[14] The mobile cation vacancies can be captured by a Ga^{2+}, which attracts the negative cation vacancies due to its positive charge. The resulting complex is electrically neutral and stable. Apparently, the sample L contains cation vacancies in a considerable concentration, i.e., in the same order of magnitude as the concentration of Ga^{+} in that sample. Possibly because of the doping method (see Sec. II A) Ga^{3+} centers are also incorporated causing the creation of cation vacancies. When following the formation of Ga^{2+} centers above 220 K in the sample L, the initial concentration of $(Ga^{2+})^{I}$ centers is found to decrease from 220 to 250 K at the expense of the formation of more $(Ga^{2+})^{II}$ centers. Thus, cation vacancies are attracted by the positive $(Ga^{2+})^{I}$ centers and form $(Ga^{2+})^{II}$ centers. After x irradiation at room temperature of sample L we found a significant MCDA band of $(Ga^{2+})^{II}$ centers, but only a small band of $(Ga^{2+})^{I}$ centers. This corresponds to the x irradiation at 4.2 K and subsequent annealing procedure. In sample H, we could observe $(Ga^{2+})^{II}$ centers after x irradiation at room temperature. This is contrary to the fact that after x irradiation at 4.2 K and subsequent annealing to room temperature very few $(Ga^{2+})^{II}$ centers were found. A very high mobility of the cation vacancies during the room temperature x irradiation seems to favor the creation of the $(Ga^{2+})^{II}$ centers, while after low temperature x irradiation and annealing to 220 K the V_K centers are preferentially trapped at Ga^{+} to form $(Ga^{2+})^{I}$ centers and are not converted to $(Ga^{2+})^{II}$ centers. We think that the sample H contains less cation vacancies than sample L. This together with an enhanced vacancy mobility under room temperature x irradiation may be the reason for the different ratio between

$(Ga^{2+})^{I}$ and $(Ga^{2+})^{II}$ centers when produced by low temperature x irradiation and annealing or by room temperature x irradiation.

Ga^{2+} has a $4s^1$ configuration and therefore a large isotropic hf interaction. Both Ga^{2+} centers have, within experimental error, an isotropic g factor and isotropic hf interaction. However, due to the broad EPR lines and the superposition of many forbidden lines, a small g anisotropy would not be resolved. The observation that the larger hf interaction is observed for $(Ga^{2+})^{I}$ centers and the smaller one for the Ga^{2+}-V_c complex supports the model and is in agreement with the observation by Baranov and Khramtsov in KCl and NaCl.[3]

We observed forbidden transitions where $\Delta m_I = \pm 1$. There are possibly also forbidden transitions where $\Delta m_I = \pm 2$, the line positions of which would be superimposed on the allowed ones with $\Delta m_I = 0$. We think that the forbidden transitions are caused by anisotropic shf interactions and, in the case of the $(Ga^{2+})^{II}$ centers, by a quadrupole interaction of the central nucleus. We note that without a theoretical understanding of the MCDA bands, from the relative MCDA signal intensities of the two centers one cannot conclude on their relative concentrations.

The bleaching experiment showed that only the $(Ga^{2+})^{I}$ MCDA band disappears upon photostimulation of the F centers, i.e., only the $(Ga^{2+})^{I}$ centers are participating in the read-out process. From the center models for the two Ga^{2+} centers this is understandable, since $(Ga^{2+})^{I}$ centers are positively charged attracting mobile electrons, while the neutral $(Ga^{2+})^{II}$ centers do not. The fact that the PSL effect is, indeed, correlated only with the $(Ga^{2+})^{I}$ centers is also seen in its temperature dependence [Fig. 2(a)]. In the sample L after low temperature x irradiation and annealing to 180 K the PSL starts to increase and the MCDA of $(Ga^{2+})^{I}$ centers starts to appear. At 200 K the PSL increases drastically, while at this temperature $(Ga^{2+})^{II}$ centers are not yet formed. Thus, for the use of RbBr:Ga^{+} as a storage phosphor, the generation of $(Ga^{2+})^{II}$ centers must be avoided, since they compete for primary holes but cannot be read out. The generation of $(Ga^{2+})^{II}$ centers can be avoided in the higher doped sample after x irradiation at low temperature with subsequent annealing, which is, of course, not a practical way to use a storage phosphor. Ways have to be exploited to suppress the generation of $(Ga^{2+})^{II}$ centers from a room temperature x irradiation, possibly by an improved Ga^{+} doping which avoids the formation of cation vacancies.

The observation of a replenishment effect was first reported by Hangleiter *et al.*[15,16] in BaFBr:Eu^{2+}. The phenomenon was the same as here: after exhaustion of the PSL effect at low temperature it could be recovered partly upon annealing to room temperature. In our experiments it seems that this effect is associated with the presence of $(Ga^{2+})^{II}$ centers. On the other hand, in the corresponding MCDA experiment [Fig. 3, curves (b) and (c)] it is seen that the recovery of the MCDA of $(Ga^{2+})^{I}$ centers is not accompanied by a corresponding decrease of the $(Ga^{2+})^{II}$ centers, that is they do not dissociate to form $(Ga^{2+})^{I}$ centers. This is, of course, in line with the observation that $(Ga^{2+})^{II}$ centers once formed are stable at room temperature. In the sample with the high gallium concentration the replenishment effect is not observed (or very small). For a tentative explanation of the observations, we suggest that in the sample L the total concentration of Ga^{+} does not suffice to capture all holes from the generated V_K centers. Some holes are trapped elsewhere. At room temperature they become mobile and can be trapped by Ga^{+} centers having become available for this after having been read out, i.e., after $(Ga^{2+})^{I}$ centers have recombined with a photostimulated electron. When the x-ray dose is lower, the replenishment effect decreases, since relative to the number of V_K centers there are more Ga^{+} centers available to form $(Ga^{2+})^{I}$ centers. In the sample with high concentration of Ga^{+} practically all V_K center holes are trapped at a Ga^{+}. Therefore, such a replenishment effect is very small, if at all observable. Whether or not the sample L contains additional hole traps the sample H may not have or only in a small concentration and of which nature they are, is not yet known to us.

ACKNOWLEDGMENTS

The cooperation and support by Dr. P. Willems and Dr. P. J. R. Leblans of Agfa-Gevaert company (Mortsel, Belgium) are gratefully acknowledged.

[1] U. Rogulis, C. Dietze, Th. Pawlik, Th. Hangleiter, and J.-M. Spaeth, J. Appl. Phys. 80, 2430 (1996).
[2] Th. Hangleiter, U. Rogulis, C. Dietze, J.-M. Spaeth, P. Willems, L. Struye, and P. J. R. Leblans, Proceedings of the International Conference on Inorganic Scintillators and Their Applications, SCINT95, Delft, Delft University Press, The Netherlands, 1996, p. 452.
[3] P. G. Baranov and V. A. Khramtsov, Sov. Phys. Solid State 20, 1080 (1978).
[4] A. Fukuda, Phys. Rev. B 1, 4161 (1970).
[5] Yu. V. Kolk and A. Ch. Lushchik, Sov. Phys. Solid State 28, 805 (1986).
[6] D. Schoemaker, Phys. Rev. B 7, 786 (1973).
[7] F. K. Koschnick, K. H. Wietzke, and J.-M. Spaeth, Phys. Rev. B. (in press).
[8] J.-M. Spaeth, J. R. Niklas, and B. H. Bartram, *Structural Analysis of Point Defects in Solids*, Springer Series in Solid State Sciences 43 (Springer, Berlin, 1992).
[9] K. S. Song and R. T. Williams, *Self-Trapped Excitons*, Springer Series in Solid State Sciences 105 (Springer, Berlin, 1993).
[10] W. Meise, U. Rogulis, F.-K. Koschnick, K. S. Song, and J.-M. Spaeth, J. Phys.: Condens. Matter 6, 1815 (1994).
[11] C. J. Delbecq, R. Hartford, D. Schoemaker, and P. H. Yuster, Phys. Rev. B 31, 3631 (1976).
[12] E. Goovaerts, J. Andriessen, S. V. Nistor, and D. Schoemaker, Phys. Rev. B 24, 29 (1981).
[13] F. van Steen and D. Schoemaker, Phys. Rev. B 19, 55 (1979).
[14] D. K. Rowell and M. J. L. Sangster, J. Phys. C 14, 2909–2921 (1981).
[15] Th. Hangleiter, F.-K. Koschnick, J.-M. Spaeth, R. H. D. Nuttal, and R. S. Eachus, J. Phys.: Condens. Matter 2, 6837 (1990).
[16] Th. Hangleiter, F.-K. Koschnick, J.-M. Spaeth, and R. S. Eachus, Radiat. Eff. Defects Solids 119–121, 615 (1991).

J. Phys.: Condens. Matter 7 (1995) 4939–4947. Printed in the UK

Optically detected magnetic resonance of the self-trapped exciton in NaBr

U Rogulis†§, J-M Spaeth† and K S Song‡

† Fachbereich Physik, Universität-GH Paderborn, Warburger Strasse 100, D-33098 Paderborn, Germany

‡ Department of Physics, University of Ottawa, Ottawa, Ontario, Canada K1N 6N5

Received 7 March 1995

Abstract. The optically detected electron paramagnetic resonance spectrum of the self-trapped exciton in NaBr is measured using x-ray excitation of the triplet luminescence. The zero-field splitting parameter was found to be $D = (23 \pm 2.5)$ mT, an order of magnitude smaller than that of KBr and RbBr. The self-trapped exciton in NaBr is believed to be of type I, i.e. the electron and hole occupying an on-centre geometry in contrast to the off-centre configuration of type III, found in most alkali halides. For an explanation of the small D value measured one has to assume, however, that also in NaBr the electron and hole are split as in a primitive F–H pair, with the distance between them of about 1.5–3 Å.

1. Introduction

Self-trapped excitons (STEs) in alkali halides are of fundamental importance for atomic processes induced by electronic excitations, including the photochemical formation of F centres (an electron trapped at an anion vacancy) and H centres (a halogen$_2^-$ molecular ion on an anion site, oriented along a ⟨110⟩ direction). STEs were studied extensively with a variety of spectroscopic techniques (for a recent review see e.g. Song and Williams 1993). It is now generally agreed that in alkali halides the STEs can be visualized as a primitive F–H centre pair which undergoes a radiative transition emitting π polarized light from a spin triplet state and a σ-polarized light from a singlet state. According to a series of calculations, the STEs are off centre along the ⟨110⟩ directions, i.e. the centres of the F and H centres are displaced from each other along a ⟨110⟩ direction (Song *et al* 1989, Song and Baetzold 1992, Shluger *et al* 1991). The stable F–H centre pairs are created dynamically at low temperature in those crystals in which the off-centre motion is accompanied by large relaxation energy. These crystals also have a large Stokes shift of the π band, which can be as much as 70% of the free exciton absorption energy. STEs of this kind have been classified as of type III (Kan'no *et al* 1990). They occur in the fluorides, KCl, RbCl, KBr, RbBr and RbI. In contrast, the STEs in NaBr and NaI are characterized by a small Stokes shift (~20%) and a very small F centre formation yield at low temperature. They are classified as of type I. The STEs in NaCl and KI are in between (type II).

Recent experiments have greatly contributed in confirming this general picture of the STE and its relation to the primary lattice defects created under radiation. They include the

§ Permanent address: Institute of Solid State Physics, University of Latvia, 8 Kengaraga Street, LV-1063 Riga, Latvia.

0953-8984/95/254939+09$19.50

resonant Raman scattering (RRS) of the STE in a number of crystals (Suzuki *et al* 1994), transient absorption of the STE in the group I crystals (Hirota *et al* 1991), femtosecond pulse work on the F centre creation (Tokizaki *et al* 1991) and observation of correlated F–H pairs in KBr at low temperature (Meise *et al* 1994). In particular, the RRS has shown that in type II and III crystals the hole of the STE is practically an H centre with its stretching mode frequency identical with that of the isolated H centre. On the other hand, in type I material, the frequency is the same as in a V_k centre (a hole shared between adjacent halogen ions along a ⟨110⟩ direction). This seems to indicate that whether or not the molecule-ion occupies a one-anion site or two-anion sites determines whether or not the frequency of the stretching mode is that of an H or V_k centre.

There remain, however, a few intriguing questions. One of them is whether or not the type I STE is truly on-centre with the symmetry of the D_{2h} point group. In this symmetry, the hole and the electron would share the same centre of symmetry along ⟨110⟩. None of the above experiments shed light directly on this point, except possibly the transient absorption in NaBr and NaI (Hirota *et al* 1991). In sharp contrast to other materials, the lowest absorption was found to be in the infrared region, at less than 0.2 eV. Earlier calculations assuming the D_{2h} symmetry have all shown that the lowest absorption band, corresponding to a_g–b_{3u} electron states, is in the range of 0.5 eV in sharp disagreement with the then available data in type II and III crystals which were around 2.0 eV. This was considered as a sign showing that in type I the STE is occupying a truly on-centre geometry. A recent all-electron *ab initio* Hartree–Fock calculation of the STE triplet states in NaBr for both on-centre and off-centre geometries (Baetzold and Song 1993) shows that indeed the absorption energy is better accounted for with the on-centre geometry, but the recombination luminescence is in better agreement if the off-centre geometry is assumed. Also, the adiabatic potential energy calculation indicates that the on-centre geometry is unstable in NaBr also. This problem is difficult to decide on the grounds of calculations alone due to the possibility of configuration interaction in the on-centre geometry and the limited size of the quantum cluster used in all such calculations.

A quantity which is sensitive to the relative displacement between the F centre and the H centre forming the triplet state from which the π emission occurs is the zero-field splitting parameter D. This was shown previously for the alkali fluorides (Song *et al* 1990). It was the purpose of this paper to measure the zero-field splitting for the STEs in NaBr as well as the Br hyperfine (HF) interactions of the halogen molecular ions and to investigate whether or not they can be explained with the on-centre model for the type I STEs.

2. Experimental details

The pure NaBr crystals were grown with the Czochralski method. The NaBr powder was treated before crystal growth with Br_2 to avoid oxygen contamination. The optically detected electron paramagnetic resonance (ODEPR) was measured as a microwave-induced change of the luminescence intensity in a computer-controlled custom-built K band spectrometer (24 GHz). The NaBr crystal could be x-irradiated at 1.5 K *in situ* in the cavity of the ODEPR spectrometer. The x-ray-induced fluorescence was measured with a photomultiplier. For spectral resolution several interference filters were used. The x-ray tube (60 kV, 15 mA) was placed at a distance of about 15 cm from the sample; the x-rays were passed through a Be window. It was necessary to carefully shield the static magnetic field generated by two superconducting solenoids within the tail of the helium cryostat of the ODEPR spectrometer during the spectrometer operation, since otherwise the x-ray tube did not function properly. Because of the shielding the absolute value of the magnetic field was less well known than

usual resulting in a larger error of the absolute g value ($\pm 10^{-2}$). However, field differences could be measured with the usual accuracy.

3. Experimental results

In the x-ray fluorescence band of the STEs, the ODEPR spectrum was measured for $B_0 \| [110]$ as a microwave-induced increase of the luminescence intensity. The ODEPR spectrum is shown in figure 1. It consists of a rather broad line around $g \sim 2$. The signal-to-noise ratio is rather poor. This is not altogether surprising. Apart from a rather high noise of the x-ray intensity (5–10%), the rather short radiation lifetime of 0.48 μs for the triplet STEs in NaBr prevents good EPR signals. Because of the microwave power available of only 50–100 mW in the cavity, the time for a spin-flip is only of the order of magnitude of the radiative life time of the STEs. Therefore, no efficient spin flip-induced fluorescence intensity changes can be obtained. The ODEPR line shows indications of a structure. Its line shape is 'flat' around $g \sim 2$ (at $B \approx 850$ mT), showing that this is not a single line of Gaussian shape as expected for a single inhomogeneously broadened EPR line (see below). In order to be sure to have measured the spectrum of the STE, we measured the optical excitation spectrum of the EPR spectrum by setting the magnetic field to the centre of the EPR line (850 mT). We used several interference filters with half width of about 22 nm and 25% transmission to spectrally resolve the luminescence. Figure 2 shows the optical excitation spectrum of the ODEPR line. The peak at ~270 nm agrees with the published peak of the π luminescence of the STE in NaBr at 266 nm (Song and Williams 1993, table 5.8). Also the band width is in fair agreement with that of the STE (0.46 eV) within experimental accuracy, which is not very high due to the filter width. The x-ray fluorescence intensity was not intense enough to measure the excitation spectrum through a monochromator.

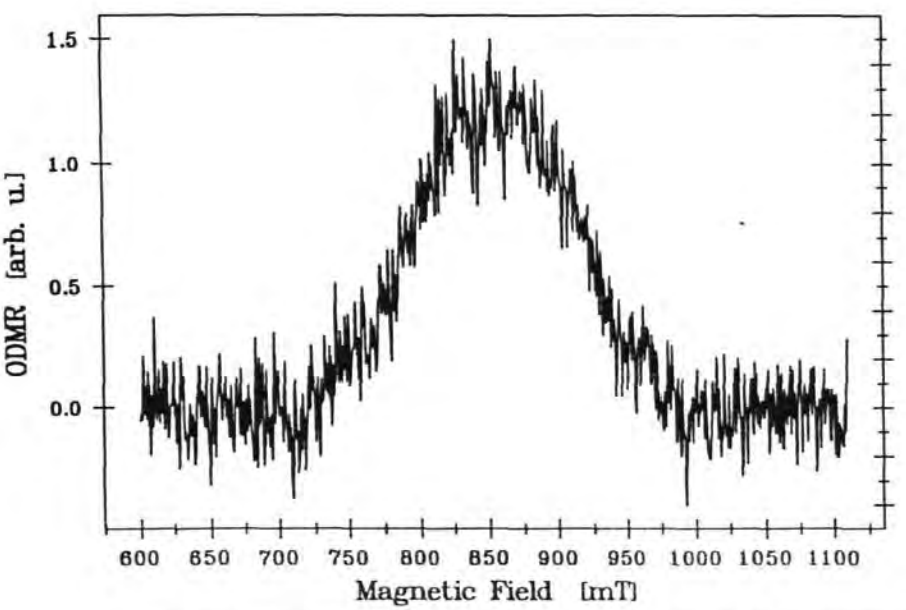

Figure 1. Optically detected EPR spectrum of the triplet STE in NaBr for $B \| [110]$, $T = 1.6$ K, ($\nu_{ESR} = 24$ GHz).

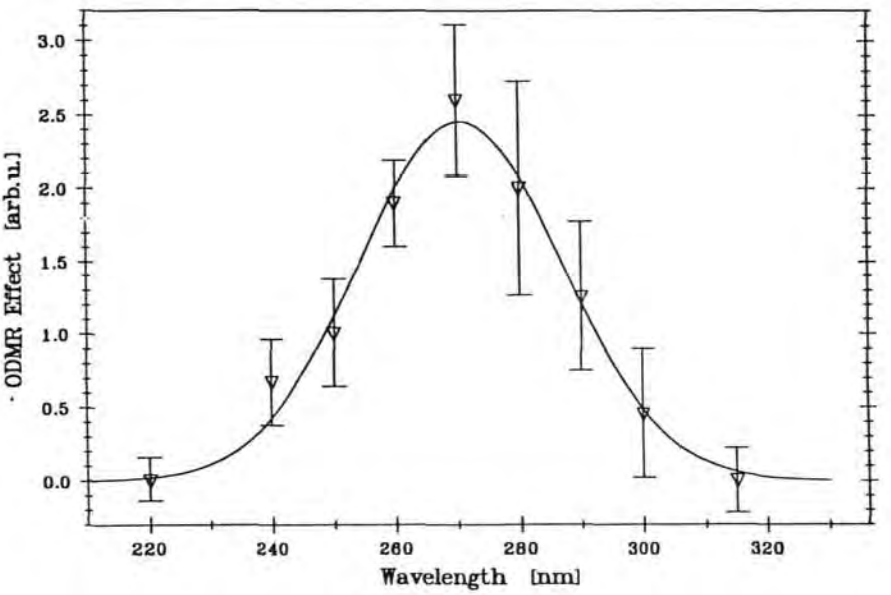

Figure 2. Excitation spectrum of the ODEPR line measured at $B = 850$ mT using a set of interference filters of 25% transmission and a half width of about 22 nm. $T = 1.5$ K, $\nu_{ESR} = 24$ GHz.

For the triplet state (electron spin $S = 1$) of an STE for the magnetic field parallel to the ⟨110⟩ orientation one expects to observe an EPR spectrum consisting of two line groups separated by the zero-field splitting, each group having a resolved structure because of the HF interaction with two equivalent halogen nuclei or being inhomogeneously broadened by this interaction. For example, such a spectrum was observed in KBr (Wasiela *et al* 1973a, Marrone *et al* 1973). Thus, the ODEPR spectrum should be described by a spin Hamiltonian of the form

$$\mathcal{H} = \mu_B B_0 \mathbf{g} S + S\mathbf{F}S + \sum_{i=1,2} I_i \mathbf{A}_i S \tag{1}$$

where the terms represent the electronic Zeeman energy, the fine-structure interaction and the hyperfine (HF) interaction with the two central halogen nuclei of the molecular ion (V_k or H centre). In NaBr, one would expect a seven-line HF structure due to the interaction with the two equivalent Br nuclei of the V_k centre (both isotopes ^{79,81}Br have $I = \frac{3}{2}$ and about equal abundances, with only a small (<10%) nuclear g factor difference). For $B \| [110]$ these two groups should be separated by the fine structure interaction. Assuming an axial fine-structure tensor $\mathbf{F}$, the splitting is expected to be given by $2D = F_{zz}$, where D represents the zero-field splitting parameter (see e.g. Song and Williams 1993, ch 5.4). The measured spectrum can be explained with a g factor of $g = (2.01 \pm 1 \times 10^{-2})$, the zero-field splitting constant of $D = (23 \pm 2.5)$ mT and a Br HF interaction $A_{zz} = (28 \pm 2)$ mT (the isotope difference was neglected).

Figure 3 compares the calculated spectrum with the experimental one. In figure 3(b) and 3(c) the two Br HF structures are shown (with an unrealistic small line width for the sake of clarity and neglecting the small isotope differences), which are displaced from each other by $2D$. Assuming an individual line width of 25 mT for the Br HF lines, one obtains the calculated spectrum in figure 3(a) (continuous line), which shows very good agreement with the experimental one. The experimental line shape would be Gaussian for $D = 0$,

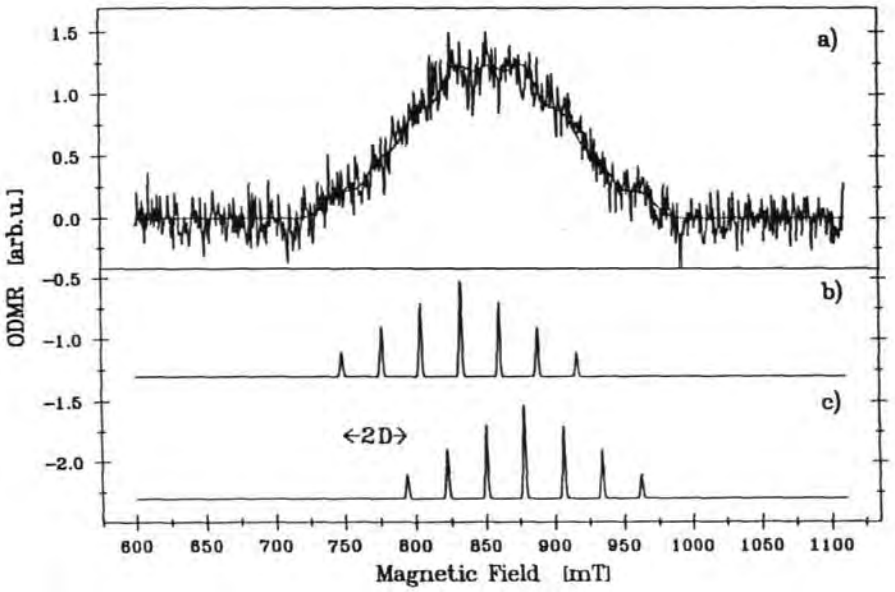

Figure 3. Comparison of the calculated and experimental ODEPR spectrum of the STE in NaBr for $B_0 \| [110]$. (b) and (c) stick spectra of the two Br hyperfine septets for two equivalent Br nuclei, split by the zero-field splitting of $2D$; (a) experimental and calculated spectrum (solid line) with $g = 2.01$, $D = 23$ mT, $A_{zz} = 28$ mT, the single Br HF lines had a width of 25 mT.

which is not observed, and would show a splitting into two separate broad lines for a larger D. Whether or not there is also a (small) deviation from axial symmetry for the zero-field splitting as found, e.g. in KBr, we cannot say. The ODEPR lines of other STE orientations are usually much weaker; they could not be detected here (see e.g. Song and Williams 1993, ch 5.4).

In figure 4 an attempt is shown to explain the spectrum assuming that the two Br nuclei of the V_k centre are not equivalent, a situation which may occur for a small displacement between the F centre and the V_k centre. A reasonable explanation of the measured spectrum could be obtained for the following set of data: $A_{zz1} = (24 \pm 2)$ mT, $A_{zz2} = (31 \pm 2)$ mT and $D = (24 \pm 2.5)$ mT. (The individual line width was again 25 mT.) With this set of data, the mathematical overall difference between the measured and calculated spectrum was the same as for the assumption of two equivalent Br nuclei as made above but the weak structure of the measured spectra may seem a little better represented by the simulation assuming equivalent nuclei. However, this is hard to decide.

The sign of the fine structure splitting D could not be measured, since attempts to measure the magnetic circular polarization of the emission were not successful.

4. Discussion

4.1. Zero-field splitting parameter

We have two parameters which could give us in principle indications as to the precise nature of the symmetry of the STE in NaBr: the zero-field parameter D and the hyperfine interaction parameter A_{zz}. In this section we first discuss the zero-field parameter D, which

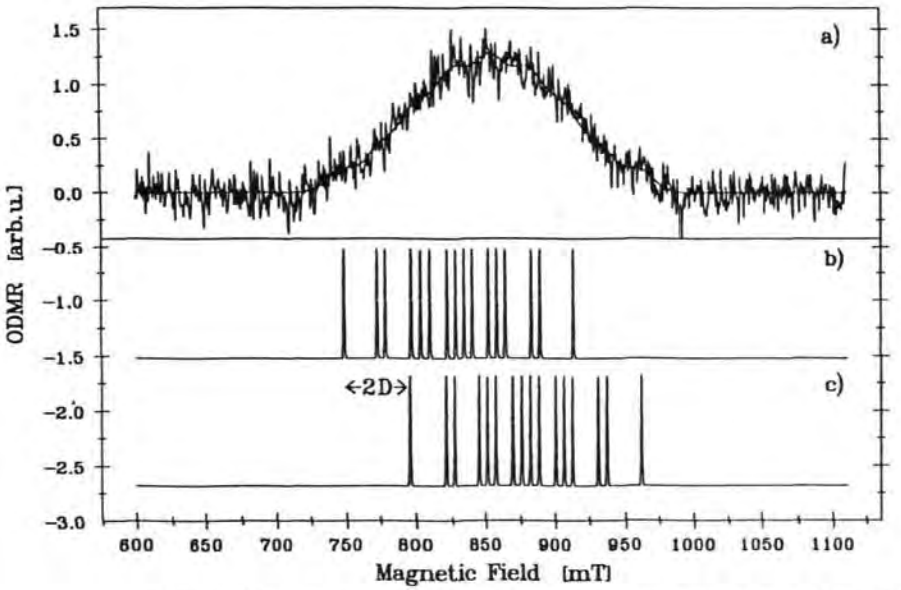

Figure 4. Comparison of the calculated and experimental ODEPR spectrum of the STE in NaBr for $B_0 \| [110]$. (b) and (c) stick spectra of two inequivalent Br nuclei split by the zero-field splitting of $2D$; (a) experimental and calculated spectrum (solid line) with $g = 2.01$, $D = 24$ mT, $A_{zz1} = 24$ mT, $A_{zz2} = 31$ mT; the single Br HF lines had a width of 25 mT.

contains two parts:

$$D = D_{so} + D_{ss}$$

where D_{so} is the spin–orbit contribution and D_{ss} the dipole–dipole term (Song and Williams 1993). The zero-field splitting parameter D is very useful in determining the geometry of the F centre relative to the H centre, and also the distance separating the two centres when the spin–orbit coupling is weak or negligible (Song *et al* 1990). In the alkali halides D_{so} is positive and D_{ss} is negative (Song and Williams 1993). Unfortunately, in the bromides the spin–orbit contribution D_{so} dominates over the dipole–dipole term D_{ss} and the analysis used in Song *et al* (1990) is not applicable until we have estimated the contribution of the spin–orbit term D_{so}. This is attempted in the following separately for the on-centre (D_{2h} point group) and off-centre (point group C_{2v}) geometries. The knowledge that the wavefunctions of the excited electron are very different in the two geometries (Song and Leung 1989, Song and Baetzold 1992, Shluger *et al* 1991) is important for the present analysis. The wavefunction is very diffuse in the on-centre case and we have used a Gaussian with $\alpha \cong 0.002$ (au) in $\exp(-\alpha r^2)$, while for the off-centre case $\alpha \cong 0.05$ (au) typically, as for an F centre. D_{so} was derived by Fowler *et al* (1973) earlier for the on-centre case:

$$D_{so} = \zeta^2 \Delta / 4E_\perp^2. \tag{2}$$

Here, Δ is the exchange energy and ζ is the spin–orbit coupling parameter. $E_\perp$ is the energy splitting between the Σ_u^+ ground state and the Π_u excited state and is taken from that of the V_k centre (= 1.95 eV) (Wasiela *et al* 1973b) and Δ is known for the free exciton (0.370 eV). Δ of the STE (off centre) is systematically smaller than in the free exciton by a factor of between $\frac{1}{3}$ and $\frac{1}{30}$ (Song and Williams 1993). For those where data are available, Δ is of the order of 10 meV. However, in the on-centre STE it is expected to be smaller than in free excitons because of the diffuse nature of the electron wavefunction. As Δ in this

case is impossible to estimate in an independent way, we simply scaled Δ from a maximum of 0.04 to a minimum of 0.004 eV to get a range of D_{so}: 2030 mT to 203 mT. Taking $D_{ss} = |D| - D_{so}$, and acknowledging that we do not have the sign of D, D_{ss} is found to be in the range of $-(2000 \pm 23)$ mT to $-(200 \pm 23)$ mT. On the other hand, we have evaluated D_{ss} using a simplified basis of Gaussians. The hole is represented by p-like Gaussians centred on the two sites of Br_2^-, with $\alpha_h = 0.3$ (au) and the excited electron centred at the mid-point of Br_2^- with $\alpha_e = 0.002$–0.01. We obtained $D_{ss} = -22$ mT to -160 mT. This shows that the value of D_{ss}, including its sign (negative), could be explained only with a diffuse excited electron and for a very small value of Δ. We will come back to this result below.

For the off-centre geometry, the electron is strongly localized on one anion site and it polarizes the H centre (Br_2^-) strongly if close (<1 Å) (Song and Baetzold 1992). As the formula above for D_{so} was derived for the on-centre symmetry, we are not using it. Instead, we try to estimate it from those of KBr and RbBr assuming that we have reasonable values for the D_{ss} for these bromides. Indeed, earlier calculations as well as a semiempirical fit of the triplet π band lifetimes as a function of the distance between the F and H centres give a good correlation (Song and Chen 1989). We use those values of d_{H-F} for KBr and RbBr (5 and 6 Å respectively) to arrive at D_{ss} of -400 and -220 mT respectively (d_{H-F} is the distance between the centre of the F centre and the midpoint of the Br_2^- molecule). From the experimental values of D, $+265$ and $+185$ mT for KBr and RbBr respectively, one obtains D_{so}: 665 and 405 mT. By extrapolating these data, we assume that D_{so} of NaBr, in the off-centre geometry is in the range of 800 to 1000 mT. From the measured $|D|$ value of 23 mT, we can deduce the range of d_{H-F}: 1.5–3.0 Å with which we can fit D_{ss}. These data are assembled in table 1.

Table 1. Comparison of experimental zero-field splitting parameters with theoretical estimates for three alkali bromides.

	d_{H-F} (Å)	D (mT)	D_{so}	D_{ss}
NaBr	1.5–3.1	|23|	1000–800	−1020 to −780
KBr	5	+265	665	−400
RbBr	6	+185	405	−220

From the above discussion, it appears that both models are capable of accounting for the observed $|D|$ value of 23 mT, much smaller than in KBr and RbBr. However, when the lifetime of the π band in NaBr of 4.8×10^{-7} s is compared to those in the other two of 1.3×10^{-4} s and 1.8×10^{-4} s, respectively, it becomes clear that the very diffuse on-centre electron wavefunction is incompatible with such a short lifetime. An estimate of the lifetime of the π band as a function of α_e of the excited electron yields that for a value of $\alpha_e = 0.002$ a value of $\tau = 10^{-3}$ s is expected, while for $\alpha_e = 0.01$ τ becomes 10^{-5} s. We, therefore, conclude here on the basis of the D value analysis, although it was semiquantitative, that the triplet STE in NaBr is probably of C_{2v} symmetry with a relatively small shift of $Q_2 \approx 1$ Å from the on-centre position, where $Q_2 = d_{H-F} - a/\sqrt{2}$, a being the nearest-neighbour distance (Song and Williams 1993, ch 5).

4.2. Hyperfine structure

A dominant contribution to the HF interaction parameter A_{zz} will be due to the V_k centre part of the STE. For the V_k centre in NaBr itself $A_{zz} = 44$ mT (Shoemaker 1973). Since the spin

Hamiltonian of equation (1) refers here to an $S = 1$ system, the HF parameters of electron and hole are scaled by one half, i.e. the V_k contribution alone would be 22 mT, assuming that the two Br nuclei are equivalent. If we assume that the two Br nuclei are inequivalent, the situation is similar to that in the fluorides, such as in CaF_2. Indeed, according to theoretical calculations on NaBr (Song and Williams 1993, ch 5), at the off-centre shift of about 1.5 Å ($d_{H-F} \cong 3.6$ Å), the hole charge is distributed as 60 against 40%. If we scale the HF parameters of the V_k centre according to this weight and scale again by $\frac{1}{2}$, then one obtains 26 and 18 mT, which can be compared to 31 and 24 mT obtained above as a possible fit. The discrepancy can be attributed in part to the contribution of the F centre which is very close to one Br atom. If, on the other hand, we assume a hole distribution of 55 against 45%, then the A_{zz} are 24 mT and 20 mT. One should note that the wavefunction of the excited electron localized on the anion site is strongly distorted according to *ab initio* calculations and the contribution of the F centre to the HF point contact term may not follow from that of a simple exponential decay.

The HF interaction parameter estimate requires careful consideration of the details of the electron wavefunction at an ionic site, e.g. the amplification factor (Seidel and Wolf 1968). Beside, the electron wavefunction is quite distorted compared to that of a regular F centre.

On the other hand, if we assume that the STE in NaBr is on-centre with the symmetry of D_{2h} point group, then A_{zz} is fitted to be 28 mT which is larger than half the V_k value by about 6 mT. This discrepancy cannot be explained by a diffuse excited electron. The HF contribution of a diffuse electron with $\alpha_e = 0.002$ (see section 4.1) is very small. From a crude approximation, it can be estimated to be two or three orders of magnitude smaller than for the Br^- (second-nearest neighbour) of an F centre, which in NaBr is estimated to be about 2.5 to 3 mT by extrapolation from the known values in KBr and RbBr (Seidel and Wolf 1968).

Thus, we conclude, although a number of parameters are not quantitatively known and had to be estimated crudely, that our overall analysis explains the observed zero-field splitting and HF interaction reasonably well with an off-centre model and an off-centre shift Q_2 by about 1 Å. Not only can the on-centre model not explain D and A_{zz}, but it also fails to account for the lifetime of the π luminescence.

Thus, the conclusion is that the type I STE is not truly of on-centre geometry, but of split electron–hole geometry as in types II and III. The magnitude of axial shift is much smaller, however.

Acknowledgments

We would like to thank the Deutsche Forschungsgemeinschaft for financial support (UR) and Dr F Koschnick for his help with the experiments and for fruitful discussions.

References

Baetzold R C and Song K S 1993 *Phys. Rev.* B **97** 1199
Fowler W B, Marrone M J and Kabler M N 1973 *Phys. Rev.* B **8** 5909
Hirota S, Edamatsu K and Hirai M 1991 *Phys. Rev. Lett.* **67** 3283
Kan'no K, Tanaka K and Hayhashi T 1990 *Rev. Solid State Sci.* **4** 383
Marrone M J, Patten F W and Kabler M N 1973 *Phys. Rev. Lett.* **31** 47
Meise W, Rogulis U, Koschnick F K, Song K S and Spaeth J M 1994 *J. Phys.: Condens. Matter* **6** 1801
Seidel H and Wolf H C 1968 *Physics of Color Centers* ed W B Fowler (New York: Academic) ch 8
Shluger A L, Itoh N, Puchin V E and Heifets E N 1991 *Phys. Rev.* B **44** 1499
Shoemaker D 1973 *Phys. Rev.* B **7** 786

Song K S and Baetzold R C 1992 *Phys. Rev.* B **46** 1960
Song K S and Chen L F 1989 *J. Phys. Soc. Japan* **58** 3022
Song K S and Leung C H 1989 *J. Phys.: Condens. Matter* **1** 8425
Song K S, Leung C H and Spaeth J M 1990 *J. Phys.: Condens. Matter* **2** 6373
Song K S, Leung C H and Williams R T 1989 *J. Phys.: Condens. Matter* **1** 683
Song K S and Williams R T 1993 *Self-trapped Excitons (Springer Series in Solid State Sciences 105)* (Berlin: Springer) ch 5
Suzuki T, Tanimura K and Itoh N 1994 *Phys. Rev.* **49** 7233
Tokizaki T, Makimura T, Akiyama H, Nakamura A, Tanimura K and Itoh N 1991 *Phys. Rev. Lett.* **67** 2701
Wasiela A, Ascarelli G and Merle d'Aubigné Y 1973a *Phys. Rev. Lett.* **31** 993
——1973b *J. Physique Coll.* **34** C9 123

J Phys.: Condens. Matter 9 (1997) 1–13. Printed in the UK PII: S0953-8984(97)83917-3

Zero-field splitting and line shape of the ODMR of self-trapped excitons in NaBr

U Rogulis†§, F K Koschnick†, J-M Spaeth† and K S Song‡

† Universität-Gesamthochschule Paderborn, Fachbereich Physik, Warburger Strasse 100, D-33098 Paderborn, Germany

‡ Department of Physics, University of Ottawa, Ottawa, Ontario K1N 6N5, Canada

Received 30 April 1997, in final form 23 July 1997

Abstract. The optically detected electron paramagnetic resonance (ODMR) spectrum of self-trapped excitons (STEs) in NaBr was measured using a microwave frequency of 25.9 GHz and compared with that measured previously at 24.0 GHz. In lock-in detected ODMR only one structureless non-Gaussian line was observed for each frequency. From the field positions of the lines obtained in the previous and new measurements a zero-field splitting of $D = 1.7$ T was derived. On the basis of transient ODMR measurements in KBr it is shown that the shape of the ODMR line does not follow the V_K-centre nuclear spin statistics of the STE because of the dependence of the lifetimes on the nuclear spin states. Similar effects seem to occur in all alkali bromides.

1. Introduction

Recent work has considerably clarified the structure of the self-trapped exciton (STE) in a number of alkali halides. There are now good reasons to classify the STEs into the so-called type II (weakly off centre) and type III (strongly off centre) STEs, that is to be primitive and possibly nearest-neighbour Frenkel defect pairs, respectively. Concerning the so-called type I STEs, which include those in NaBr and NaI, both calculations and optical transition studies are not clearly conclusive as to the symmetry of the system (strictly on centre versus marginally off centre without a centre of inversion) (Song and Williams 1996).

In order to clarify this situation concerning the type I STEs, the first electron paramagnetic resonance (EPR) study of the triplet state of the STE (Song and Williams 1996) using optical detection via luminescence had been made in NaBr (Rogulis *et al* 1995). The microwave frequency used was 24 GHz (K band), the detection mode was the standard lock-in technique, and the spectrum consisted of a structureless non-Gaussian line centred at $g = 2$ with a halfwidth of about 135 mT. The spectrum showed a different structure compared to those in KCl or KBr, and that seemed not surprising. In the latter cases clearly resolved hyperfine (hf) structures, typical for V_K centres, were obtained. In NaBr, the observed ODMR line shape, which was 'flat' at the centre, was interpreted as being the result of a closely separated pair of Gaussian lines, and the small separation was attributed to the zero-field splitting. The D parameter was estimated to be about 23 mT (Rogulis *et al* 1995).

§ Permanent address: Institute of Solid State Physics, University of Latvia, 8, Kengaraga Street, LV-1063 Riga, Latvia.

0953-8984/97/010001+13$19.50

In a more recent work, Kan'no *et al* (1996) have studied the EPR of the STE in NaBr using a pulse technique and microwaves of 9 GHz (X band). They obtained a single line with somewhat less flattened top, which was centred at 1.45 T. Kan'no *et al* failed to observe the second line expected for a fine-structure split triplet spectrum within their available magnetic field range. This seemed to indicate a possibly very large D value. In an attempt to estimate the D value, Kan'no *et al* (1996) combined their line with the one obtained by Rogulis *et al* (1995) and thus estimated the D parameter to be about 1.7 T, much larger than in other bromides (265 mT in KBr and 185 mT in RbBr). However, Kan'no *et al* (1996) had to assume a g value, which was taken to be $g = 2$.

In this report, we present new results obtained with two different microwave frequencies in the K-band (24 GHz and 25.9 GHz). Based on our new studies, we also obtained a large D value of 1.68 T, which is close to that proposed by Kan'no *et al* (1996) as described above.

In view of the proposal of Kan'no *et al*, we undertook to investigate the reason for having observed an apparent 'double' line with the standard ODMR technique, which has previously lead to the determination of a small D value. Previous experiments on KBr (Marrone *et al* 1973, Wasiela *et al* 1973) indicated that also there the line shape does not follow the expectation from the hf structure. We, therefore, undertook transient ODMR experiments in order to find the reason for the non-Gaussian line shapes. They were performed on KBr because of the better signal-to-noise ratio compared to NaBr. It turned out that the lifetimes of the different nuclear spin states of the V_K centre are different. In ODMR experiments with lock-in detection at audio-frequency between a few hertz and 100 kHz, these lifetime differences influence the ODMR line intensities.

In summary, we have found that in our previous work (Rogulis *et al* 1995) and in the work of Kan'no *et al* (1996) only one fine-structure component of the STE ODMR spectrum was observed due to the unusually large D value.

2. Experimental details

The pure NaBr crystals were grown with the Czochralski method. The NaBr powder was treated before crystal growth with Br_2 to avoid oxygen contamination. The extremely pure KBr crystal was provided by G McDugle (Eastman Kodak). The optically detected electron paramagnetic resonance was measured as a microwave induced change of the luminescence intensity in a computer controlled custom built K-band spectrometer (24–25.9 GHz). The details of the stationary lock-in detected ODMR for the x-ray induced luminescence have been described previously (Rogulis *et al* 1995).

The time resolved ODMR measurements were performed with a PC controlled transient recording board triggered by the microwave switch controller. As a microwave switch a p–i–n diode was used with a response time of 50 ns. The ODMR effect was monitored with a time resolution switching the microwave power on and off. 65 000 scans for each cycle (switching on and off the microwave power) were measured.

3. Experimental results

3.1. Lock-in detected ODMR

The ODMR spectra of the STEs in NaBr are shown in figure 1, for two different microwave frequencies—at 24 GHz (figure 1(a), reported earlier by Rogulis *et al* (1995)) and 25.9 GHz (figure 1(b)). We observe a shift of the broad resonance line to lower magnetic fields by

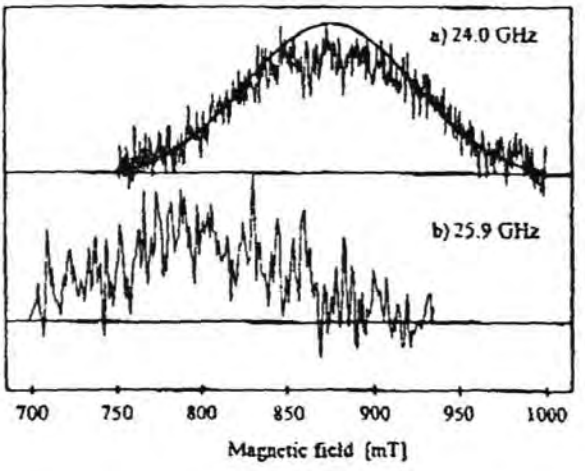

Figure 1. Optically detected EPR spectra of the triplet STE in NaBr for $B \parallel [110]$, $T = 1.6$ K. (a) $\nu_{EPR} = 24.0$ GHz. The solid line is a calculated Gaussian single line. The experimental line shape appears as a Gaussian line with a 'flattened' top. (b) $\nu_{EPR} = 25.9$ GHz.

76 mT when the microwave frequency increases. If this shift was determined by the Zeeman splitting, then the line shift would be expected to higher magnetic fields upon increase of the microwave frequency.

The obtained shift to lower field could be explained by a very large value of the zero-field splitting D. From the determination of the resonance fields from figure 1(a) and (b), we obtained the following spin Hamiltonian parameters:

$$g = 1.80 \pm 0.2 \qquad D = 1.66 \pm 0.2 \text{ T}.$$

We obtained a higher precision in the determination of the parameters when taking into account our resonance fields together with the resonance field obtained by Kan'no *et al* (1996):

$$g = 1.87 \pm 0.05 \qquad D = 1.68 \pm 0.05 \text{ T}.$$

Further, in figure 1(a), we evaluated the halfwidth of our ODMR spectrum, under the assumption that there is one Gaussian-like spectrum with a 'flattened' (depressed) central part. In such a way we obtained a halfwidth of 122 mT. This value is close to that found by Kan'no *et al* (1996). We tried to find the reason for the flattened lineshape measured with our conventional lock-in technique.

Because of the low signal to noise of the ODMR spectrum no full angular dependence could be measured; from this in principle, the zero field splitting could also have been determined.

3.2. Transient ODMR experiments in KBr

We used transient ODMR experiments to follow the dynamical relations between the relaxation times in different hf transitions of the ODMR spectra. We had to use the ODMR of the STE of a KBr crystal for the transient ODMR experiments instead of our NaBr crystal, since the signal-to-noise ratio in NaBr was too bad.

In figure 2, the spectrum of the lock-in detected ODMR is shown for the KBr crystal for $B_0 \parallel [110]$, the axis of the STE. Similar to earlier observations by Marrone *et al* (1973)

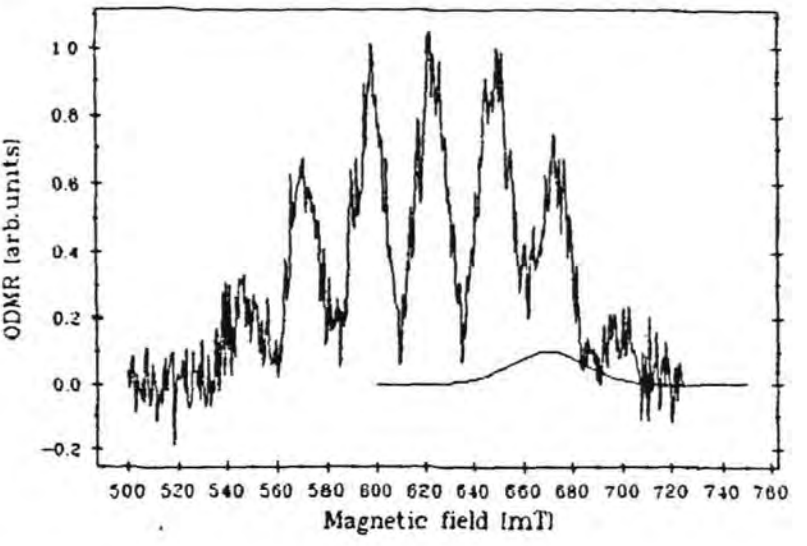

Figure 2. The optically detected EPR spectrum of the triplet STE in KBr for $B \parallel [110]$, $T = 1.6$ K. ($\nu_{EPR} = 25.5$ GHz). The solid line centred at 670 mT is the calculated EPR spectrum of STEs in perpendicular orientation.

and Wasiela *et al* (1973) we observe in figure 2 that all three 'middle' components have about the same relative intensities (middle line depression) rather than the statistical relation 3:4:3, as could be expected. At the higher-magnetic-field side of the spectrum in figure 2 also the resonances from the other perpendicular STE orientations appear (simulated with parameters taken from Wasiela *et al* (1973). In KBr the 'flattened' central part is seen more clearly than in NaBr where the signal-to-noise ratio is much worse. However, the line shape in NaBr is clearly non-Gaussian (see figure 1(a)).

In figure 3, the transient ODMR spectra are shown for the middle line and two adjacent ones. We have analysed the decay relations of these three spectra. We obtained these by switching microwaves 'on'; the amplitude of the middle line is somewhat higher than that for the adjacent ones, but the subsequent decay of the middle line is faster than for the other lines. The ratios of the initial amplitudes of the middle line to the two other lines in figure 3 are 1.33:1 (which is close to the expected 4:3 for the statistical distribution of the hf lines) and 1.15:1 (not exactly 4:3, but higher than 1:1).

We therefore observed experimentally that the lifetimes of the different ODMR components are different and depend on the nuclear spin states. In the conventional lock-in technique the averaged values of the ODMR line intensities are measured. Numerical integration of our time resolved patterns in figure 3 leads to the same final intensity of all the three middle lines: this is what is observed in lock-in technique experiments. Thus, the lock-in technique gives 'wrong' intensities of the ODMR lines and the total lineshape of the ODMR is determined by lifetime effects of transitions in different nuclear spin states.

3.3. Simulation of the transient ODMR experiments

In order to understand the common feature observed for most of the STEs in alkali halides that the hf split ODMR transitions do not have the intensity ratio expected from the statistical distribution of the occupation of the m_I states, we have to analyse the ODMR effect

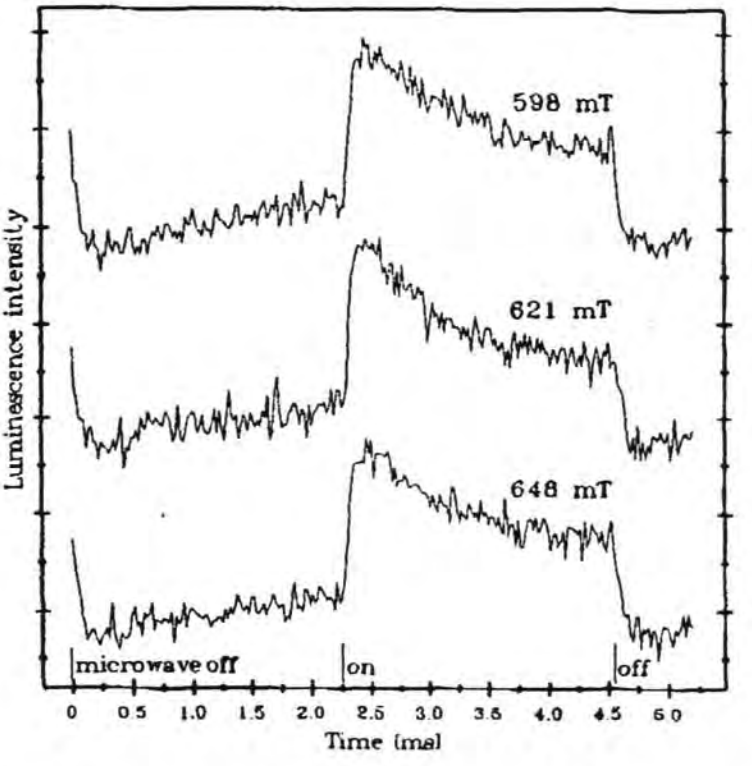

Figure 3. Time resolved ODMR spectra of KBr for $B \parallel [110]$ for the middle line (621 mT) and two adjacent ones (598 mT and 648 mT).

quantitatively. The intensity of the $m_I = 0$ transition is usually depressed and does not have the predicted ratio of 4:3 in comparison with the neighbouring $m_I = \pm 1$ transitions. The only exception is the STE in KCl, having much smaller hf interactions with the two central nuclei of the molecule. In order to calculate the ODMR effect and to analyse its transients we solved a rate equation system. Since we ignored coherence effects, we do not need to use the density matrix formalism.

We made four simplifications. (i) We neglect the influence of the spin–lattice relaxation. This is justified because the lifetimes of the excited triplet states are much smaller than the spin–lattice relaxation time at the measurement temperature of 1.5 K. This can also be seen directly from the decay of the ODMR, which can be described by the difference of two exponentials, each reflecting the lifetime of the excited state involved in the ODMR transition (Chan 1982) (see figure 4; see below for an explanation). (ii) We only take into account the two triplet levels which are connected by the microwave transition. The third level does not influence the ODMR effect as it is decoupled from the two other states because of the neglect of the spin–lattice relaxation. (iii) We consider the hf levels separately. In other words, we solve the rate equations, consisting of only two states for the different m_I sublevels with different lifetimes, each of which are estimated by a fit to the measured transients. (iv) We assume that all triplet levels are optically pumped at the same rate. This means that we introduce only one parameter P for the pumping probability. With these simplifications, one hf subsystem of the triplet can be described with the following rate

equations:

$$\frac{dN_{f,s}}{dt} = P(N - N_f - N_s) \pm \mu(N_s - N_f) - \frac{1}{\tau_{f,s}} N_{f,s} \tag{1}$$

with N_f the population of the fast excited state, N_s the population of the slow excited state (bottleneck), N the population of the ground state, P the optical pumping probability, μ the transition probability induced by the microwaves, τ_f the lifetime of the fast excited state, and τ_s the lifetime of the slow excited state.

After Barry (1992) the solution of the rate equations (1) is

$$N_{f,s}(t) = A_{f,s} + B_{f,s}\exp(\lambda_1 t) + C_{f,s}\exp(\lambda_2 t) \tag{2}$$

with

$$\lambda_{1,2} = -P - \mu - \frac{1}{2}\left(\frac{1}{\tau_f} + \frac{1}{\tau_s}\right) \pm \sqrt{(P-\mu)^2 + \left(\frac{1}{\tau_f} - \frac{1}{\tau_s}\right)^2}. \tag{3}$$

$A_{f,s}$, $B_{f,s}$, and $C_{f,s}$ are functions of the pumping probability, the microwave transition probability, the lifetimes, and the initial conditions N_f^0 and N_s^0:

$$\begin{aligned}
A_{f,s} &= \frac{PN(2\mu + 1/\tau_{s,f})}{\lambda_1\lambda_2} \\
B_{f,s} &= \frac{PN(2\mu + 1/\tau_{s,f})}{\lambda_1(\lambda_1 - \lambda_2)} + \frac{PN + (\mu - P)N_{f,s}^0 + (\lambda_1 + P + \mu + 1/\tau_{s,f})N_{f,s}^0}{\lambda_1 - \lambda_2} \\
C_{f,s} &= -\frac{PN(2\mu + 1/\tau_{s,f})}{\lambda_2(\lambda_1 - \lambda_2)} - \frac{PN + (\mu - P)N_{f,s}^0 + (\lambda_2 + P + \mu + 1/\tau_{s,f})N_{f,s}^0}{\lambda_1 - \lambda_2}.
\end{aligned} \tag{4}$$

The transient ODMR signal can be calculated as

$$\mathrm{ODMR}(t) = \frac{1}{\tau_f} N_f(t) + \frac{1}{\tau_s} N_s(t) \tag{5}$$

In the following, using KBr as an example, we analyse the ODMR effect of the STE using the solution of the rate equations as derived above.

Table 1. Parameters of the fit of the transient ODMR measurements

m_I	P (s^{-1})	μ (s^{-1})	τ_f (ms)	τ_s (ms)
+1	1.5	450	0.06 ± 0.01	1.9 ± 0.06
−1	1.5	450	0.06 ± 0.01	1.9 ± 0.1
0	1.5	450	0.06 ± 0.015	1.5 ± 0.1

Figure 4 illustrates a fit of equation (5) to the measured transients for the $m_I = 0$ and +1 transitions. To improve the accuracy of the fitting procedure, solutions were calculated for both cases, microwaves on and off ($\mu > 0$ and $\mu = 0$, respectively). The initial conditions, in other words the actual populations N_s^0 and N_f^0 at the beginning of each period (microwaves on and off, respectively), depend on what happened in the previous period and what happened in all periods prior thereto. These populations were calculated iteratively. After optimization of the parameters for the pumping probability P and the microwave transition probability μ, they were kept constant for all three transitions ($m_I = 0, \pm 1$). Calculations showed that variations in μ are negligible for the different hf sublevels. For the transition $m_I = 0$ the measured transient used for the fit was scaled down by a factor

7

Figure 5

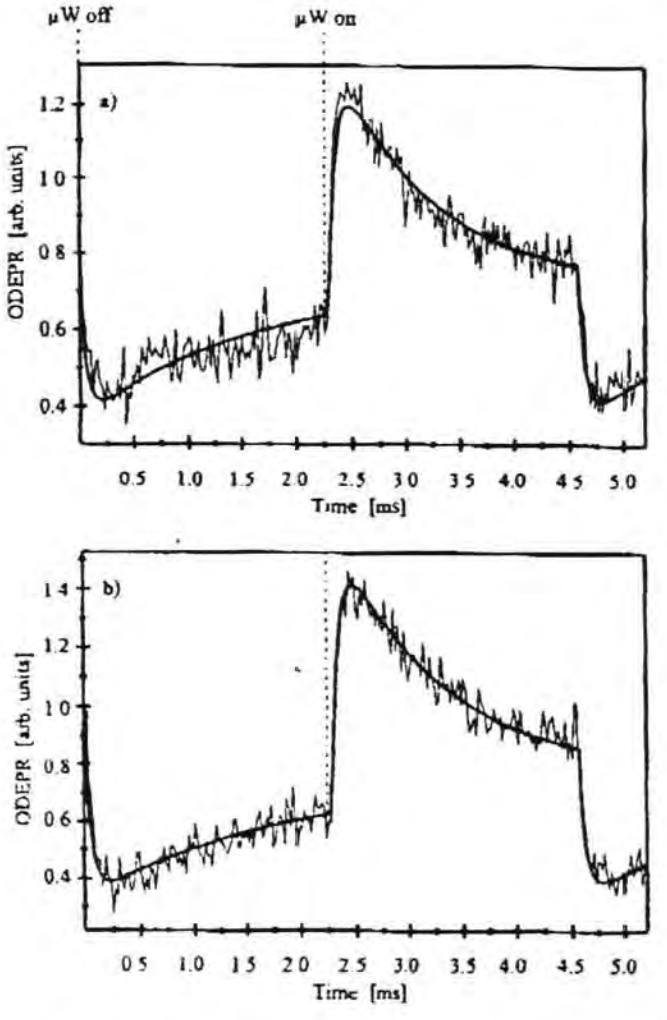

Figure 4. Simulation of the transient ODMR experiments of the STE in KBr (a) for the middle hf line at 621 mT ($m_I = 0$) and (b) for the side line at 598 mT ($m_I = 1$).

of $\frac{3}{4}$ to compensate for the statistics of coupling of the two nuclear spins which do not enter the rate equations. The parameters obtained by the fit are listed in table 1. The agreement between this fit and the measured transients of the ODMR is excellent. The fit could reproduce the fact that the ODMR effect of the $m_I = 0$ transition is smaller if the gain due to the statistics of nuclear spin coupling (factor $\frac{4}{3}$ with respect to the $m_I = \pm 1$ transitions) is taken into account. One important result is that the lifetimes of the bottlenecks (slow component, τ_s) of the hf subsystems are different while the fast component (τ_f) does not change within experimental error. The lifetimes of the bottlenecks of the $m_I = \pm 1$ subsystems are both equal to 1.9 ms within experimental error, whereas the lifetime of the $m_I = 0$ transition is 1.5 ms. Because of the 'faster' bottleneck of the $m_I = 0$ hf subsystem with respect to the other hf subsystems, the ODMR effect is smaller. This results in a depression of the stationary ODMR spectrum for the $m_I = 0$ line. To demonstrate this we calculated the total area of the ODMR transients, being a measure of the signal obtained

with lock-in detection. The ratio of the areas of the transients follows exactly the ratio of the ODMR lines measured with lock-in detection in ordinary stationary ODMR experiment.

Below, we discuss the reason for the faster decay of the bottleneck for the $m_I = 0$ situation. It is shown that the mixing of the spin wavefunctions of the triplet levels is the maximum for this hf subsystem and that this mixing reduces the lifetime of the bottleneck.

Now, we discuss some limiting cases. In our experiments, we excited optically the STE with an x-ray tube. The intensity and thus the pumping rate of the x-rays is very low. Therefore, the following conditions are certainly valid for our experiments:

$$P \ll \frac{1}{\tau_f}, \frac{1}{\tau_s}$$

and therefore

$$N \gg N_f, N_s. \tag{6}$$

Then, if the microwave power is switched off ($\mu = 0$), the time behaviour of the ODMR transients simply reflects the lifetimes τ_f and τ_s of the involved excited states, if the spin–lattice relaxation is negligible. Under this condition the difference between the exponentials of the fast decay (with τ_f) and the slow recovery (with τ_s) of the photoluminescence is measured. The fast decay results in a lowering of the photoluminescence intensity to a level lower than the stationary value without microwave transitions. The slow recovery to this stationary state without microwave excitation occurs with τ_s, the lifetime of the bottleneck. For this simple case the rate equations (1) can be simplified:

$$\frac{dN_{f,s}}{dt} = PN - \frac{1}{\tau_{f,s}} N_{f,s}. \tag{7}$$

The solutions are

$$N_{f,s} = PN\tau_{f,s} + (N^0_{f,s} - PN\tau_{f,s}) \exp\left(-\frac{t}{\tau_{f,s}}\right) \tag{8}$$

and the transient ODMR signal is

$$\mathrm{ODMR}(t) = 2PN + \frac{1}{\tau_s}(N^0_s - PN\tau_s) \exp\left(-\frac{t}{\tau_s}\right) + \frac{1}{\tau_f}(N^0_f - PN\tau_f) \exp\left(-\frac{t}{\tau_f}\right). \tag{9}$$

At $t = 0$ the microwaves induce transitions between both levels. Therefore, the population of the slow level is smaller than the stationary value for $\mu = 0$ ($N^0_s < PN\tau_s$) and that of the fast level is larger ($N^0_f > PN\tau_f$). Thus, the prefactor of the exponential with the fast lifetime is positive, while for the slow lifetime it is negative, resulting in a difference of exponentials as mentioned above. If spin–lattice relaxation were important, the ODMR transients would be more complicated than the simple difference of exponentials with the fast and the slow lifetime.

The lifetimes we estimated from such decay experiments are consistent with the values we obtained from the fit of (2) to the whole ODMR transient, consisting of periods where the microwaves are switched on and off. Moreover, we found that the rise time of the photoluminescence after switching on the microwaves is equal to the lifetime of the fast excited states. From equation (3) it can be easily seen that this can only happen if the microwave transition probability μ is small in comparison to the lifetime τ_f of the fast levels. This is not the case for the slow levels. Here μ is of the order of $1/\tau_s$ (from the fit, $\mu = 450\ \mathrm{s}^{-1}$ and $1/\tau_s \approx 670\ \mathrm{s}^{-1}$ and $530\ \mathrm{s}^{-1}$, for the $m_I = 0$ and ± 1 transition, respectively). This can be seen in the different recovery times after switching off the microwaves in comparison to the decay of the ODMR transient to the stationary value

after switching on (recovery time = τ_s = 1.5 ms for $m_I = 0$ and 2 ms for $m_I = \pm 1$ in comparison to the decay times of the ODMR transients of 0.9 and 1.0 ms, respectively). For the conditions in our experiments ($P \ll 1/\tau_{f,s}$, $\mu \ll 1/\tau_f$, $\mu \sim 1/\tau_s$) the time behaviour of the ODMR effect after switching on the microwaves is

$$\lambda_1 = -\mu - \frac{1}{\tau_s} \qquad \lambda_1 = -\frac{1}{\tau_f}. \tag{10}$$

Under saturating microwave transitions the decay time of the ODMR transient to a stationary value after switching on would be $\frac{1}{2}(1/\tau_f + 1/\tau_s)$ (Barry 1992) which can be easily seen from (3). With our estimated lifetimes this decay would be of the order of 0.1 ms, which was not measured.

4. Discussion

4.1. Line shape of the ODMR of the STEs

Our observations and their analysis in KBr are thought to have the same reason as the observations made with stationary ODMR in NaBr. We propose the same reason for the 'flattened' lineshape of the STEs in NaBr and KBr seen with the lock-in technique. We found that the lifetimes of the STE hf lines are different for the different nuclear spin states. We note that at the first moment of the switching 'on' of the microwaves the ratio of the amplitudes of the ODMR effect for different hf lines is close to the ratios, which are expected from the V_K-centre nuclear spin statistics. In the ODMR experiments with a pulse technique (Kan'no *et al* 1996) less depression of the ODMR lineshape has been observed.

We note that the same 'flattened' lineshape has been found in all of the other conventional lock-in measurements on STEs in alkali bromides with NaCl-type structure—KBr (Wasiela *et al* 1973, Marrone *et al* 1973) as well as RbBr (Mori *et al* 1978) (in hf line groups for the 0° oriented STEs, where the overlaps with the 90° oriented STEs have not significantly influenced the middle lines of the hf spectrum). Such 'flattened' lineshapes of the ODMR spectra of the STE seem to occur in bromides, but not in the chlorides (e.g. KCl (Block *et al* 1978)). The hf interaction parameters for V_K centres are much larger in bromides than in chlorides, which may lead to a larger influence of the nuclear spin states on the lifetimes of the STE hf components. We have performed some experiments with probably not so pure KBr crystals where the amplitude of the middle hf line became even lower than that of the two adjacent ones. The ODMR measurements presented in figures 2, 3 and 4 were performed on extremely pure KBr crystals.

(...figures 2,3 and 4...)

4.2. Lifetimes of different nuclear spin states

We found that the lifetimes for the fast and slow components in KBr are very close to those published by Mukai *et al* (1989). Let us discuss the reason for the observed lifetime shortening of the middle hf line of the ODMR of the STE in the slow decay component (bottleneck). Our explanation is based on the idea that the radiative lifetimes of the hf sublevels are changed when mixing with other hf sublevels belonging to the nearby triplet sublevels.

The hf Hamiltonian term considered here is

$$H_{hf} = a(I_z S_z + (S_+ I_- + S_- I_+)/2). \tag{11}$$

The second term of the hf interaction is the term mixing the various m_I levels between the three sublevels of m_s. Thus it raises or lowers m_I by unity as follows:

$$I_+|I, m_I\rangle = \sqrt{I(I+1) - m_I(m_I+1)}|I, m_I + 1\rangle \tag{12}$$

$$I_-|I, m_I\rangle = \sqrt{I(I+1) - m_I(m_I-1)}|I, m_I - 1\rangle. \tag{13}$$

The $m_s = 0$ state is purely a triplet in the absence of a magnetic field. The long-lifetime component of the triplet originates from this state. We estimated the lifetimes of the sublevels through perturbation theory. We found that in our present model the lifetimes of the long-lifetime component have a trend to increase from the central to the side lines, which is in agreement with the experimental fit shown in table 1. We analysed in the present model also the lifetimes of the short-lifetime components arising in our experiment from the $m_s = +1$ state. In this case the perturbation contributes only a small change in the wavefunction. The mixing term of the hf interaction Hamiltonian does not modify the lifetimes within experimental precision. This is what we observed by the experimental fit shown in table 1.

4.3. Analysis of the D value of the STE in NaBr

The main point which sets NaBr apart from the other two bromides is the magnitude of the D parameter. It is 1.7 T in NaBr compared with 0.265 and 0.185 T, respectively, in KBr and RbBr. There is therefore almost an order of magnitude difference. The case of KBr and RbBr has been satisfactorily understood in terms of the large off-centre geometry of the STE which makes the STE more like a second-nearest-neighbour F–H pair. One of the principal points of interest is whether an STE in NaBr is in the strictly on-centre geometry, with the point group D_{2h} symmetry, or slightly off centre with C_{2v} symmetry. Several aspects are well established regarding these geometries. First, in the on-centre case the hole distribution is equal on the two bromide ions while it is strongly polarized when it is weakly off centre (Song and Williams 1996). The bromide ion, which is closer to the localized electron, carries more hole. The other point is that the electron wavefunction is quite different in the two geometries. In the on-centre case the wavefunction is very extended (Song and Williams 1996), while in the off-centre case the wavefunction is much more compact, similar to that of the ground state of an F centre.

The zero-field splitting parameter D is made up of two contributions, D_{ss} and D_{so}, representing the dipole–dipole and spin–orbit interactions, respectively. The first term can be estimated from an approximate knowledge of the wavefunctions of the electron and hole as well as their separation in the lattice. In the NaCl lattice along the ⟨110⟩ axis, D_{ss} is negative (Song *et al* 1990). For large separation it varies as d^{-3} where d is the separation of the two dipoles. D_{so} has been derived by Fowler *et al* (1973) for the on-centre case:

$$D_{so} = \xi^2 \Delta / 4E_\perp^2 \tag{14}$$

where ξ is the spin–orbit splitting, Δ the exchange energy and $E_\perp$ the energy difference between σ_u and π_u states. This formula has been derived for the on-centre geometry, the only model of the STE at the time. On the other hand, it is reasonable to apply it to the strongly off-centre STE such as in KBr and RbBr. Indeed, in those STEs the hole centre of the STE is a more or less well formed H centre occupying a single cation site. In such cases, the hole population is found equally distributed on the two halide ions (Song and Williams, 1996).

The problem is that this formula has not been tested for a weakly off-centre geometry STE such as might be the case in NaBr. Based on this information we attempt to estimate

the two contributions to D and determine the nature of the STE in NaBr as indicated by the ODMR.

(i) *The on-centre STE.* Using the 14 above and values of the parameters ($\xi = 0.306$ eV, $\beta = 0.04$ eV, $E_\perp = 1.95$ eV for the V_K centre), D_{10} is found to be $\cong$2000 mT. From a theoretical estimation of $D_{11} = -20$ to -160 mT, we obtain $D \cong 1980$ to 1840 mT. These values are close to the new value obtained here, 1.7 T, if we assume that $D > 0$. As we argued already in our previous paper (Rogulis *et al* 1995) the wavefunction of the electron which was used ($\alpha = 0.002$ to 0.01 in units of Bohr radius squared) in obtaining D_{11} seems incompatible with the short triplet lifetime in NaBr.

(ii) *The off-centre STE.* Instead of estimating D_{10} directly from the above equation, we attempt to find 'reasonable' values of D_{10}, which can give acceptable values of D_{11} and d_{H-F}. We have examined a range of D_{10} between 1000 and 3000 mT. We assumed that D is positive, following Kawata *et al* (1992). When we accept that the off-centre shift can only be very moderate in NaBr, we found that the set $D_{11} \cong -1300$ mT and $D_{10} \cong +3000$ mT is most reasonable. Corresponding to this D_{11} value the separation between the electron and hole centres is estimated to be small, about 1 Å. These data are shown in table 2.

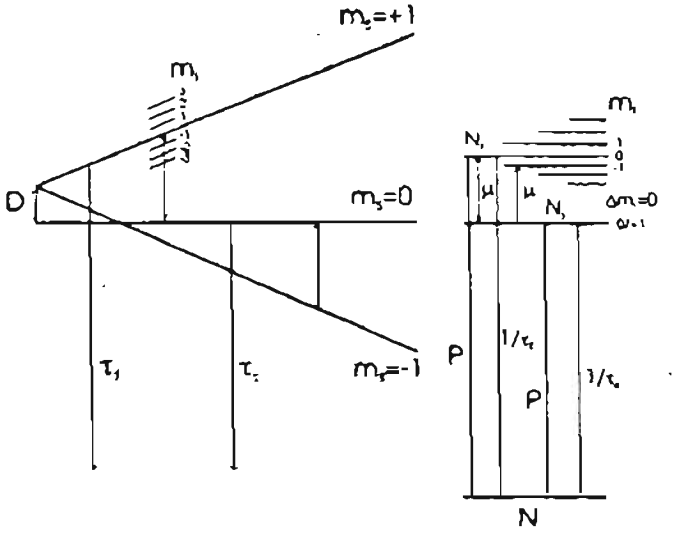

Figure 5. A schematic illustration of the parameters for the simulation of the transient ODMR experiments.

Table 2. A comparison of experimental zero-field splitting parameters with theoretical estimates for three alkali bromides.

	d_{N-F} (Å)	D (mT)	D_{10} (mT)	D_{11} (mT)
NaBr	~1	1700	3000	−1300
KBr	5	+265	665	−400
RbBr	6	+185	405	−220

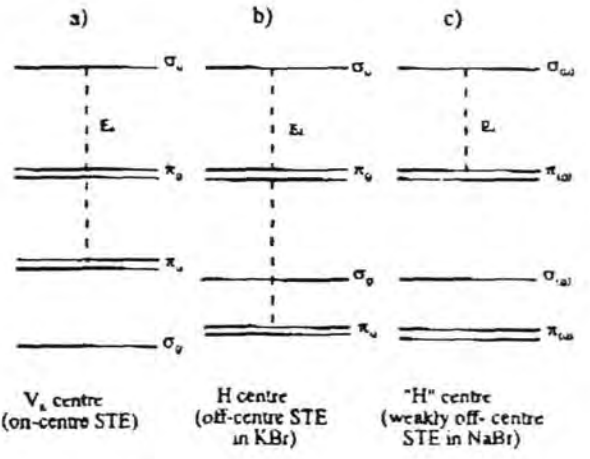

Figure 6. X_2^- energy levels. Broken lines indicate the spin–orbit coupling of the levels. (a) V_K centres (on-centre STE). (b) H centre (after Stoneham (1975)) (off-centre STE). (c) 'H' centre (weakly off-centre STE) in NaBr.

As we can see the most uncertain element is D_{zo} for NaBr in the weakly off-centre geometry. Equation (14) is valid for both the on-centre and the strongly off-centre case. The main difference between an H centre and a V_K centre (of an on-centre STE) is in the hf interacting level difference $E_\perp$ between the σ_u and π_u states. $E_\perp$ is considerably larger in an H centre (see figure 6) (Stoneham 1975). In the absence of a suitable theory to treat a polarized H centre, we will rely on the general relationship between D_{zo} and other parameters contained in (14) to understand the reason for the much larger D_{zo} value in NaBr compared to those in KBr and RbBr. As we stated above, the hole centre of a weakly off-centred STE is strongly polarized and it should not be considered to be a regular H centre. The centre of inversion is lost in such a case and as a result σ_u and σ_g as well as π_u and π_g are substantially mixed. This situation is schematically shown in figure 6(c). The mixing pairs of levels repel in energy to some extent. One principal effect of this mixing is in the contribution to D_{zo}. Not only the original pair, $\sigma_{(u)}$–$\pi_{(u)}$, contribute, but also the pair $\sigma_{(u)}$–$\pi_{(g)}$ could contribute to D_{zo}. Indeed, the latter could be dominant, because of the smaller energy difference. This could explain the much larger value of D_{zo} for NaBr which we chose above.

5. Conclusion

Our new measurements with the frequency of 25.9 GHz together with the previous measurement using 24.0 GHz have shown that the zero-field splitting of the STE in NaBr is indeed very large in agreement with the recent results of Kan'no *et al* and not small as we had concluded from our previous measurement at 24 GHz. The non-Gaussian line shape with a depression in the middle has been reinterpreted. The line originates in one fine-structure transition only, but its shape deviates from the Gaussian line form expected from unresolved hf interactions with the two Br nuclei of the V_K centre. The depression in the middle is a consequence of the different radiative lifetimes of the nuclear spin sublevels together with the lock-in technique used to observe the ODMR spectrum. The $m_I = 0$ sublevel of the bottleneck state ($m_s = 0$) experiences a relative shortening in the radiative

lifetime compared to the other m_I sublevels. This shortening occurs because of larger admixtures of nuclear sublevels in the $m_s = \pm 1$ manifold into the $m_s = 0$, $m_I = 0$ state compared to the other m_I, $m_s = 0$ levels because of the large Br hf interactions. This effect was demonstrated by transient measurements of the ODMR of the STE in KBr. The shortened lifetime of the m_I sublevels leads to a 'weakening' of the bottleneck condition and therefore to a reduced signal measured in the lock-in technique. This effect occurs in all bromides, with a large hf interaction as seen from the ODMR line shapes and not in the chlorides, with a smaller hf interaction. The large D value is interpreted to be due to a STE in an off-centre configuration, where the separation between the electron and the hole centre is small, estimated to be approximately 1 Å.

References

Barry W A 1992 *PhD Thesis* Lehigh University

Block D, Wasiela A and Merle d'Aubigne Y 1978 *J. Phys. C: Solid State Phys.* 11 4201

Chan I Y 1982 *Triplet State ODMR Spectroscopy* ed R H Clark — publisher? (New York: Willey)

Fowler W B, Marrone M J and Kabler M N 1973 *Phys. Rev.* B 8 5909

Kan'no K, Shirai M, Matsumoto M and Akimoto I 1996 *Proc. 13th ICDIM (Wake Forest, 1996)*

Kawata T, Mukai T, Matsumoto T and Kan'no K 1992 *Defects in Insulating Materials, Proc. 12th ICDIM (Schloss Nordkirchen)* vol 2, p 1232

Marrone M J, Patten F W and Kabler M N 1973 *Phys. Rev. Lett.* 31 467

Mon Y, von der Weid J P and Aegerter M 1978 *Solid State Commun.* 26 181

Mukai T, Kan'no K and Nakai Y 1989 *J. Phys. Soc. Japan* 58 1838

Rogulis U, Spaeth J M and Song K S 1995 *J. Phys.: Condens. Matter* 7 4939

Song K S, Leung C H and Spaeth J M 1990 *J. Phys.: Condens. Matter* 2 6373

Song K S and Williams R T 1996 *Self-Trapped Excitons (Springer Series in Solid State Sciences, 105)* 2nd ed (Berlin: Springer) ch 5

Stoneham A M 1975 *Theory of Defects in Solids* (Oxford: Oxford University Press)

Wasiela A, Ascarelli G and Merle d'Aubigne Y 1973 *Phys. Rev. Lett.* 31 993

year held? editors? publishers? ed. O. Kanert and J.-M. Spaeth (World Scientific, Singapore 1993)

Materials Science Forum Vols. 239-241 (1997) pp. 577-580

ODMR of Triplet States of Self-Trapped Excitons in Li_2GeO_3 Crystals

U. Rogulis[1], A. Trukhin[1], J.-M. Spaeth[2] and M. Springis[1]

[1] Institute of Solid State Physics, University of Latvia, Kengaraga 8, LV-1063 Riga, Latvia

[2] Fachbereich Physik, University of Paderborn, Warburger Str. 100, D-33095 Paderborn, Germany

Keywords: ODMR, Self-Trapped Excitons, Li_2GeO_3 Crystal

Abstract. In the X-ray-induced broad luminescence band of the self trapped excitons (STE) at 2.7eV an optically detected paramagnetic resonance (ODMR) spectrum was measured at 24GHz (K-band) and 1.5 K. The sets of the ODMR lines can be understood as originating from triplet spin systems (S=1) with orthorhombic fine structure (FS) tensors (E≠0). We obtained two different triplet states with somewhat different FS interaction parameters, but very similar orientations of the principal axes (within 5 degrees). The principal axis z of each of the FS tensors makes an angle of about 25 degrees with the a- axis in the c-a plane. This direction is close to the Ge-O nonbridging bond direction. The nearly isotropic g value g=2.2 may be explained as being due to an unpaired spin of the electron component of the triplet state localized on Ge as Ge^{3+} ($4s^1$).

Introduction.

Li_2GeO_3 belongs to the oxide crystals, the structure of which involves MeO_4 (Me=Si,Ge,..) tetrahedra. The structure of the Li_2GeO_3 crystal (Cmc2$_1$ symmetry [1]) consists of chains of GeO_4 tetrahedra, located in the c-b plane along the c-axis. Li-containing c-b planes are situated between the planes of GeO_4 chains. This structure in the plane a-b is shown in Fig.1.

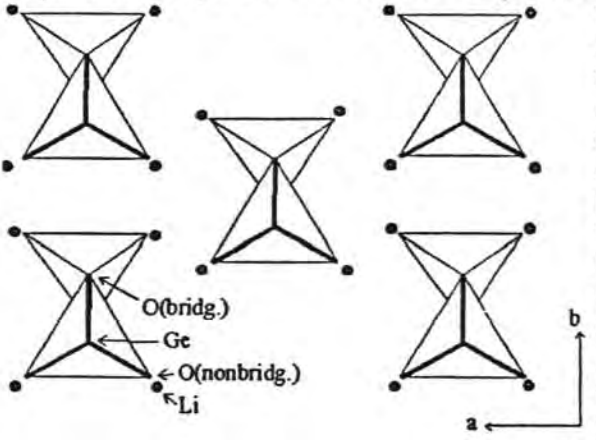

Fig. 1. Li_2GeO_3 structure in a-b plane (after [1])

The X-ray induced luminescence of the Li_2GeO_3 crystal consists of a broad band at 2.7eV. The proposed triplet nature from measurements of the photoluminescence decay kinetics predicted the existence of optically detected magnetic resonance (ODMR) for the luminescence center [2]. There are only few ODMR data on STE's in oxide crystals. From the ODMR data the spin-Hamiltonian parameters were obtained for SiO_2 and SiO_2-Ge crystals [3,4]. Fisher et. al. [5] presented the attempt to interprete these ODMR data in a charge transfer model within the Me-O bond with the corresponding relaxation effects.

The aim of the present investigation was to carry out ODMR measurements of the STE in Li_2GeO_3 and to obtain more information about the structure of the luminescence center.

Experimental.

The direction of the optical axis of the crystal was determined by use of a polarization microscope. The ODMR was measured as a change in X-ray luminescence intensity upon inducing EPR transitions with a custom built, computer controlled spectrometer working in K-band (24GHz). For details see, for example [6]. Additional magnetic shielding was used to avoid the influence of the magnetic field on the X-ray tube. The integral luminescence was measured at a temperature of about of 1.5K. The microwave modulation frequency was 270 Hz.

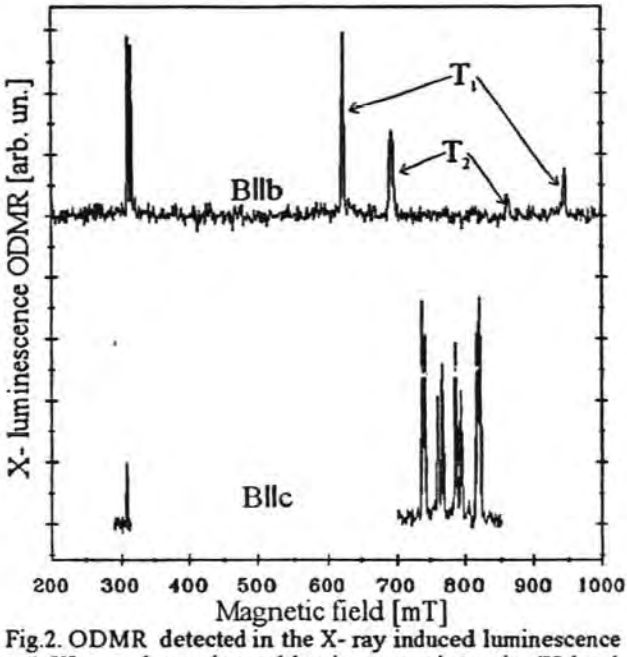

Fig.2. ODMR detected in the X- ray induced luminescence at 1.5K as a change in total luminescence intensity (K-band, 24 GHz). T_1 and T_2 denote the 2 triplet systems.

Results.

The ODMR spectra of the Li_2GeO_3 crystal measured during the X-ray excitation are shown in Fig.2 for the magnetic field orientations Bllc- and Bllb- axes of the crystal. The spectrum consists of an anisotropic group of lines centered about 770 mT and a nearly isotropic line at about 310 mT. We have measured the angular dependence in two perpendicular planes: B varied in the a-c and b-c planes. The full angular dependence in the plane a-c is shown in Fig.3.

We used the spin-Hamiltonian of a triplet spin (S=1) system with an orthorhombic fine structure tensor (E≠0) to analyse our ODMR lines:

$$H=\mu_B BgS+D[S_z^2-1/3S(S+1)]+ +E(S_x^2-S_y^2)$$

From the type of angular dependence in Fig.3 we conclude that here we measured indeed triplet state ODMR.

The anisotropic group of lines can be explained by the allowed ($\Delta m_s=\pm1$) transitions and the nearly

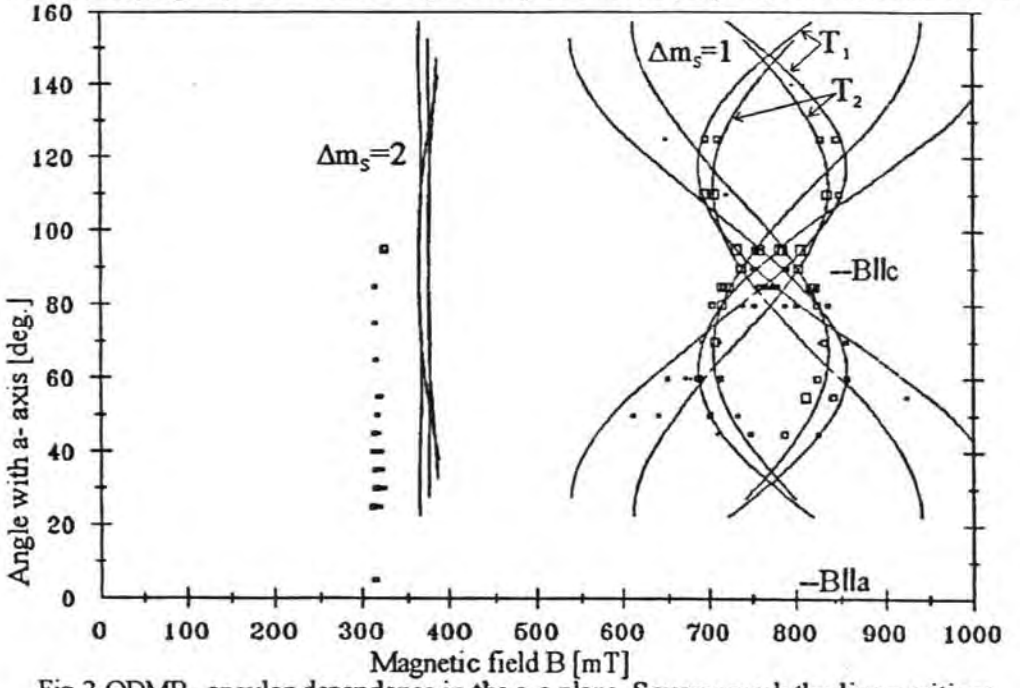

Fig.3 ODMR- angular dependence in the a-c plane. Squares mark the line positions, solid lines are calculated for two parameter sets T_1 and T_2

isotropic line is attributed to forbidden ($\Delta m_s=\pm 2$) transitions.

The allowed ODMR lines appear in pairs of lines with a splitting of up to about 60mT, while the forbidden transitions do not show a splitting more than about 10mT.

There are two possibilities to explain such a splitting. Either there are two triplet states (centers) with different D and E values of the FS tensor, however, with a very similar orientation of the principal axes (within 5 degrees). From the analysis of the spectra we obtain:

T_1: g=2.2; $|D_1|$=7.5 GHz; $|E_1|$=0.8 GHz; angle α=27.5° with a- axis in a-c plane;

T_2: g=2.2; $|D_2|$=5.1 GHz; $|E_2|$=0.35 GHz; angle α=22.5° with a- axis in a-c plane

(see solid lines in Fig.3).

The other possibility, which we think is less likely, would be to assume some unknown anisotropic interaction which causes the additional splitting. However, in this case, the forbidden transitions should also be split, but splittings of such a magnitude were not observed.

Moreover, in the latter case approximately the same line intensity for the corresponding interaction split lines would be expected. We find the line intensities not to be in pairs. We found the ratio of the intensities between the outer pair of allowed lines to be 4:1, the same for the inner pair (Fig.2, upper spectrum). The outer pair corresponds to one triplet system T_1, the inner to the other one T_2.

Further, we see, that in the direction Bllb, where the largest line splitting for the allowed lines occurs, the low field allowed lines are higher in intensity. This situation is shown in Fig.4 for the one set of FS parameters assuming D>0, Bllb and B being perpendicular to the principal axis z of the FS tensor.

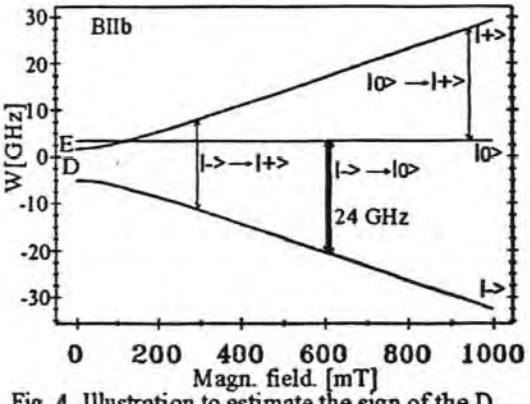

Fig. 4. Illustration to estimate the sign of the D parameter of the FS tensor. The principal axis of the tensor is perpendicular to the magnetic field B

Since at low temperatures the |-> state is more populated than the |0> state, we expect a higher line intensity. The observation of Fig.2 confirms that D>0. The discrepancy between the $\Delta m_s=\pm 2$ lines may be due to higher order effects.

The principal axes of the FS tensor make an angle of about 25 degrees with the a-axis in the c-a plane. The direction of the principal axis of the FS tensor is close to the Ge-O nonbridging bond direction. This feature is supported by measurements of the linear polarization of the emission. There are three possibilities to explain the data of the linear polarization measurements.

In one possibility the polarization is very close to the angular position of the principal axis of the FS [2]. There the dominating polarization axis z makes an angle of about 60° with the c axis of the crystal and is directed parallel to the Ge-O nonbridging bond direction nearly in the a-c plane of the crystal (deviation from the a-c plane of about 15°). The angular positions of the FS tensor orientations and the polarization axis z are shown in Fig.5 for the planes a-c and a-b.

The intensities of the allowed ODMR lines decrease if the external magnetic field is parallel to the principal axis of the FS tensor. The reason is that ODMR operates on the linearly polarized luminescence transitions of which a radiation is observed if the angle between B, along which we observe, becomes large with respect to the orientation of the electrical vector of the polarization transitions (~30° with the a- axis in a-c plane). This confirms that the principal axis z of the FS tensor and the polarization main axis are nearly parallel.

If we assume the angular position of the principal axis of the FS tensor to correspond to the direction of the spatially separated unpaired spins, we can deal with the Ge-O nonbridging bond direction. We

must stress, that the principal axis of the FS tensor cannot be associated with Ge-O bridging directions in the b-c plane, because the principal axis (z) makes an angle of more than 60° with the b-c plane. It is also not possible to associate the ODMR data with the Li-O bond directions, because then we should have obtained many more orientations of the principal axes of the FS tensor.

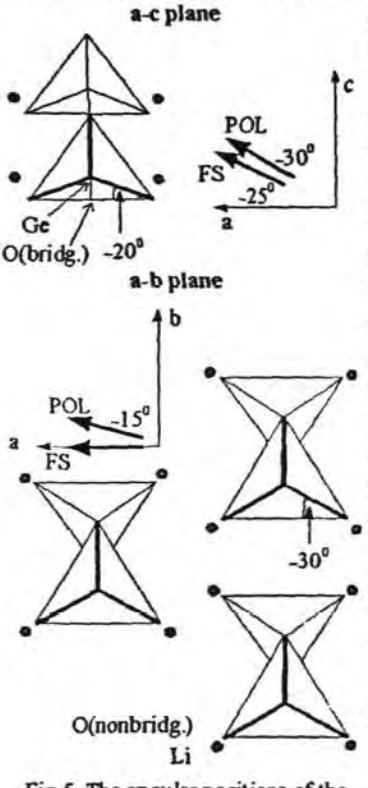

Fig.5. The angular positions of the FS and polarization axes in the a-c and a-b planes.

The second feature, which could help us to get additional information about the model, is the nearly isotropic g- factor g=2.2. The deviation from the free electron g value is significant and should limit the possible explanations. We find, that the isotropic g factor is characteristic for s^1 electron configurations and particularly also for Ge^{3+} ions [7]. Therefore a very probable position of the electron component of the STE would be located on the Ge site. The oxygen site is the most likely site for the hole location [8], also in the triplet state in SiO_2 tetrahedra- type structures [3,4]. In the case of the Li_2GeO_3, the measurements of the transient absorption spectra give evidence that the oxygen site could be involved in the STE [2].

It seems that the reason for the two different triplet states in the Li_2GeO_3 crystal could lie in the Li surrounding of the nonbridging oxygen ion. After [1] there are about 3 different positions of the nearest neighbour Li ions and may be, there exist different relaxation pathways of the exited triplet state of the STE in the Li_2GeO_3 crystal structure.

We suggest the excited state of the STE to be the electron configuration $(Ge)4s^1(O)2p^5$. The positive sign of the D parameter of the FS tensor may be understood by assuming that the spin- orbit contribution to D is larger than the spin- spin contribution [9,10].

We propose in conclusion that the X- ray induced luminescence is a triplet luminescence from two slightly different triplet states. We associate the the triplets with a charge transfer state along the Ge- O nonbridging bond and assume the unpaired electron to be on a Ge^{3+} centre and the hole on the nonbridging oxygen. Further work is needed to understand the full details of the observed ODMR data.

References.

[1] H. Wöllenkle, A. Wittmann, Monatshefte fur Chemie **99**, 244 (1968).
[2] A. Trukhin, Proceedings of the ICDIM'96, Wake Forest (USA).
[3] W. Hayes, M.J. Kane, O. Salminen, R.L. et.al., J. Phys. C: Solid State Phys. **17**, 2943 (1984).
[4] W. Hayes and T.J.L. Jenkin, J. Phys. C: Solid State Phys., **21**, 2391 (1988).
[5] A.J. Fisher, W. Hayes and A.M. Stoneham, Phys. Rev. Lett. **64**, 2667 (1990).
[6] J.-M. Spaeth, J.R. Niklas and B.H. Bartram, *Structural Analysis of Point Defects in Solids* (Springer Series in Solid State Sciences 43) (Springer, Berlin, Heidelberg) 1992.
[7] S.V. Nistor, D. Schoemaker and I. Ursu, phys. stat. sol. (b) **185**, 9 (1994).
[8] D.L. Griscom, Phys. Rev. B **40**, 4224 (1989).
[9] A.M. Stoneham, *Theory of Defects in Solids* (Oxford Univ. Press, Oxford, 1975) pp.450-455.
[10] K.S. Song and R.T. Williams, Self- Trapped Excitons (Springer Series in Solid State Sciences 105) (Springer, Berlin) 1993.

ELSEVIER

Journal of Luminescence 72–74 (1997) 890–892

JOURNAL OF LUMINESCENCE

Self-trapped exciton in Li_2GeO_3

Anatoly N. Trukhin*, Uldis Rogulis, Maris Spingis

University of Latvia, Solid State Physics Institute, 8 Kengaraga St., LV-1063, Riga, Latvia

Abstract

Self-trapped excitons (STE) are discovered in Li_2GeO_3 crystal. The PL band at 2.7 eV with a strong Stoke's shift is excited in the intrinsic absorption range of Li_2GeO_3 crystal, in which the optical gap is situated at 6 eV. The activation energy of the STE luminescence thermal quenching is not monoenergetic and is situated in the range 40–100 meV. The luminescence is strongly polarized. The decay kinetics can be characterized by $\tau = 0.9$ ms at 45 K. At 5 K it can be approximated by fast (0.6 ms) and slow (4–2.5 ms) components. Decay kinetics is determined by triplet state of STE splits in zero magnetic field. Two different excited triplet states (centers) have the average ODMR parameters $[D] = 6.3$ GHz and $[E] = 0.6$ GHz. The transient absorption of STE shows two bands at 3.7 and 4.7 eV, similar to transient absorption of STE in GeO_2 crystal with the structure of α-quartz.

Keywords: Self-trapped exciton; Li_2GeO_3; Luminescence

1. Introduction

The Li_2GeO_3 crystal belongs to a family of tetrahedrally structured materials [1] and its orthorhombic structure consists of an infinite chain of tetrahedra $[Ge_2O_6]_\infty$ with lithium ions between them. Space group symmetry is C_{mc2_1}–C_{2v}.

The existence of STE in Li_2GeO_3 crystal was predicted in Ref. [2] after studying the intrinsic absorption threshold in Li_2GeO_3 and hexagonal GeO_2 crystals. The STE for h-GeO_2 was discovered in Ref. [3]. It was observed that intrinsic absorption thresholds obey the Urbach–Toyozawa rule with parameters coinciding within experimental errors in both the crystals. Therefore, it was concluded that the lowest energy states absorbing photons belong to GeO_4 tetrahedral network and the states of lithium oxide should be at a higher energy. Guided by these data, we realized a complex of experimental investigation of the properties of Li_2GeO_3 crystal analogous to those made previously in Refs. [2–5].

The Li_2GeO_3 samples of a good optical quality were studied. The optical axis direction was determined by using a polarizing microscope. The photoluminescence excitation was done by a grating vacuum monochromator with discharge lamps in hydrogen atmosphere. An X-ray tube with W anticathod (15 mA, 40 kV) was used to study luminescence under ionizing radiation. A pulsed electron beam (250 kV, 270 kA, 20 ns) was used for measuring the transient absorption spectra. The X-ray excited luminescence intensities I_a, I_b, I_c, polarized parallel to the corresponding crystallographic axis

* Corresponding author. Fax: 371-2-711 2883; e-mail: truhins@acad.latnet.lv.

PII S0022-2313(96)00418-8

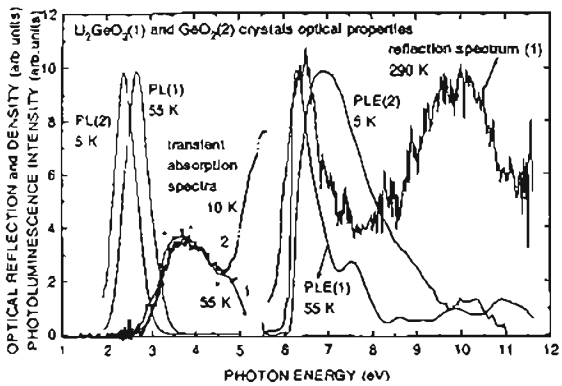

Fig. 1. Photoluminescence (PL) and PL excitation (PLE) as well as transient absorption spectra of Li_2GeO_3 crystal compared with those of h-GeO_2 crystal. The reflection spectrum of lithium germanate is also presented. GeO_2 transient absorption spectra was taken from [7].

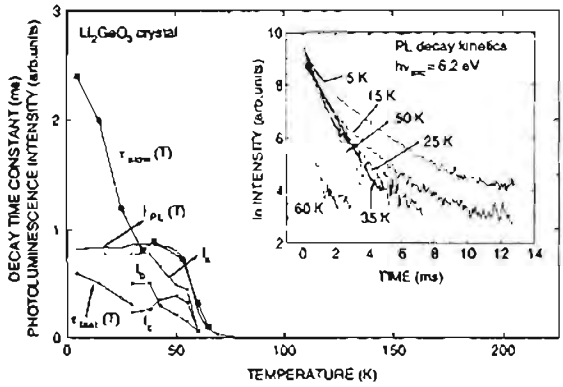

Fig. 2. Temperature dependencies of PL decay-time constant and PL intensity of Li_2GeO_3 crystal. The intensities I_a, I_b, I_c polarized parallel to the corresponding crystallographic axis a, b, c were measured under X-ray excitation. Inset shows the PL decay kinetics curves.

a, b, c, respectively, were measured by a Polaroid analyzer. Other details of equipments are described in Refs. [2–6].

In Fig. 1 the main measured spectra are shown. The broad photoluminescence (PL) band is situated at 2.7 eV. Its excitation starts from 6 eV at higher energies. The PL yield of non-quenched luminescence is 0.15 ± 0.05. The energetic yield of the luminescence excited by X-ray or electron beam is about 2%. This luminescence is not seen in pure electron–hole recombination process in such phenomena as thermostimulated luminescence and long duration (minutes and hours) afterglow. The excitation band at 6 eV corresponds well with a band in reflectivity spectrum at 6.5 eV. The Li_2GeO_3 crystal's spectra are compared with the spectra of GeO_2 crystal from Ref. [3].

The activation energy of the luminescence thermal quenching is not monoenergetic and is situated in the range 40–100 meV.

In Fig. 2 (inset) the PL decay kinetics at different temperatures are presented. It is seen that decay kinetics can well be approximated by exponentially (Fig. 2 main picture), where $\tau = 0.9$ ms for 45 K. The decay is sufficiently long and we can conclude that the luminescence is due to the forbidden transitions. Starting from 35 K the decay kinetic curves become non-exponential and its decay time increases with decrease in the temperature. At the beginning of the decay a fast component can be extracted. The temperature dependencies of the fast and slow components are presented in Fig. 2 by points. Such a behavior is usually observed for triplet states split in the zero magnetic field.

For long-living excited state we find the corresponding in-living time a transient absorption whose spectrum is presented in Fig. 1, curve 1. The spectrum contains two absorption bands at 3.7 and 4.7 eV, which correspond well with those of h-GeO_2 [7].

The ODMR spectra gave two sets of data, proposing two kinds of luminescence centers [6]. These two excited triplet states (centers) have different D and E values of the fine structure (FS) tensors, however, they have very similar orientations of the principal axes (within 5°). The g-factor is $g = 2.2$, and the average FS interaction parameters are $[D] = 6.3$ GHz, $[E] = 0.6$ GHz [6]. The principal axes of the FS tensors make an angle of about 25° with the a-axis in the c–a-plane, this direction is close to the Ge–O (non-bridging) bond direction.

2. Discussion

The fact that the luminescence band observed at 2.7 eV can only be excited with high yield in the intrinsic range shows that this is a host material

luminescence. The strong Stoke's shift on the one hand, and the lack of this luminescence in pure electron–hole recombination process on the other shows that this is a self-trapped exciton (STE) luminescence. From the spectroscopic and ODMR data we conclude that the luminescence is due to the transition from triplet state of the orthorhombic center. The luminescence intensities I_a, I_b, I_c, being dependent on the orientation of transition moment of the center, can be calculated by summation over all the possible equivalent orientations of transition moments, which are composed in the actual case of three moments (x, y, z), oriented along the highest symmetry axis of center (z) and perpendicular to it (x, y). Based on the orthorhombic symmetry of Li_2GeO_3 crystal lattice mutual ratio and temperature dependence of I_a, I_b, I_c (Fig. 2) can be explained with three differently oriented sets of moments (x, y, z), having various temperature-dependent contribution rates of x, y, z: (1) z directed towards the middle length Ge–O bond nearly in the ac-plane of the crystal; (2) z directed towards the long Ge–O bond in the bc plane; (3) two z directions along the short and long Ge–O bonds in the bc plane.

The STE model can be described to Ge–O bond rupture, as in the case of GeO_2 [3]. The hole component of the STE is related mainly to oxygen and that makes the STE similar to Li_2GeO_3 and h-GeO_2 crystals.

Acknowledgements

This work was supported by the Latvian Scientific Counsil, Grant 96.0665.

References

[1] A.N. Lasarev and A.P. Mirgorodsky, Neorg. Mater. (Sov.) 12 (1973) 2159.
[2] A.N. Trukhin and P.A. Külis, J. Non-Cryst. Solids 188 (1995) 125.
[3] A.N. Trukhin, Solid State Commun. 85 (1993) 723.
[4] A.N. Trukhin, Non-Cryst. Solids. 149 (1992) 32.
[5] A.N. Trukhin, Solid State Commun. 90 (1994) 761.
[6] U. Rogulis, A.N. Trukhin, J.M. Spaeth and M. Springis, Abstracts ICDIM'96 (USA), p. 264.
[7] C. Itoh and K. Tanimura, private communication.